Title

Increasing Crumb Rubber Usage by Adding Small Amounts of Crumb Rubber Modifier in Hot-Mix Asphalt. Phase 1: Laboratory Tests and CalME Simulations

Authors

Liang, Yanlong
Jones, David
Buscheck, Jeffrey
et al.

Publication Date

2021-10-01

DOI

10.7922/G2MG7MTK

October 2021
Research Report: UCPRC-RR-2020-06

Increasing Crumb Rubber Usage by Adding Small Amounts of Crumb Rubber Modifier in Hot-Mix Asphalt. Phase 1: Laboratory Tests and CalME Simulations

Authors:
Yanlong Liang, David Jones, Jeffrey Buscheck, John Harvey, Rongzong Wu, and Liya Jiao

Partnered Pavement Research Center (PPRC) Project 4.61 and 4.62 (DRISI Tasks 3024 and 3190):
CRM Asphalt Binder in DGAC Mixes

PREPARED FOR:

California Department of Transportation
Division of Research, Innovation, and System Information
Office of Materials and Infrastructure

PREPARED BY:

University of California
Pavement Research Center
UC Davis and UC Berkeley

Blank page

TECHNICAL REPORT DOCUMENTATION PAGE

1. REPORT NUMBER UCPRC-RR-2020-06	2. GOVERNMENT ASSOCIATION NUMBER	3. RECIPIENT'S CATALOG NUMBER
4. TITLE AND SUBTITLE Increasing Crumb Rubber Usage by Adding Small Amounts of Crumb Rubber Modifier in Hot-Mix Asphalt. Phase 1: Laboratory Tests and CalME Simulations		5. REPORT PUBLICATION DATE February 2022 6. PERFORMING ORGANIZATION CODE
7. AUTHOR(S) Yanlong Liang (ORCID: 0000-0002-7538-9757) David Jones (ORCID: 0000-0002-2938-076X) Jeffrey Buscheck (ORCID: 0000-0002-8924-6212) John Harvey (ORCID: 0000-0002-8924-6212) Rongzong Wu (ORCID: 0000-0001-7364-7583) Liya Jiao (ORCID: 0000-0003-0648-693X)		8. PERFORMING ORGANIZATION REPORT NO. UCPRC-RR-2020-06 UCD-ITS-RR-22-31
9. PERFORMING ORGANIZATION NAME AND ADDRESS University of California Pavement Research Center Department of Civil and Environmental Engineering, UC Davis 1 Shields Avenue Davis, CA 95616		10. WORK UNIT NUMBER 11. CONTRACT OR GRANT NUMBER 65A0628
12. SPONSORING AGENCY AND ADDRESS California Department of Transportation Division of Research, Innovation, and System Information P.O. Box 942873, Sacramento, CA 95814		13. TYPE OF REPORT AND PERIOD COVERED Research Report 14. SPONSORING AGENCY CODE
15. SUPPLEMENTAL NOTES doi:10.7922/G2MG7MTK		

16. ABSTRACT

In 2015, Caltrans expressed interest in studying the addition of small amounts of crumb rubber (CRM) in dense-graded asphalt mixes to increase the total amount of recycled tire rubber used. Small amounts were defined as 5% to 10% CRM by weight of the binder or approximately 0.25% to 0.5% CRM by weight of the aggregate. In this report, the terms "CRM binder" and "CRM mix" are used to denote the modified mixes. Four approaches for adding the rubber were proposed: 1) Addition of 5% to 10% CRM particles smaller than 250 µm to the asphalt binder, not resulting in a change to the PG of the base binder, achieved by blending softer base binders and/or polymers with the rubber at the refinery/terminal; 2) Addition of 5% to 10% CRM particles smaller than 2.36 mm to the asphalt binder, with allowable changes to the PG of the base binder, and produced using a field-blending process similar to that used for producing asphalt rubber binders with between 18% and 22% CRM; 3) Adding 0.25% to 0.5% CRM by weight of the aggregate directly into the mix using a dry-process; and 4) Addition of 5% to 10% CRM with particles smaller than 250 µm to the asphalt binder, with allowable changes to the PG of the base binder, and produced using a field-blending process.

Laboratory test results and mechanistic-empirical performance simulations both indicate that dense-graded mixes produced with binders containing between 5% and 10% crumb rubber modifier (CRM) by weight of the binder will generally have equal or better performance to dense-graded mixes produced with unmodified binders. Finer CRM gradations (i.e., smaller than 250 µm) in wet process approaches allow binder testing with standard Superpave performance grading tests and appear to provide more consistent results. Based on literature reviews, adding between 0.25% and 0.5% CRM with particles sizes smaller than 500 µm in dry process mixes will also provide equal or better performance to mixes that contain no CRM. If any of the approaches are adopted, more scrap tires would be recycled into pavement applications. The following recommendations are proposed based on the findings from this study:

- Additional mechanistic-empirical performance simulations followed by pilot studies should be carried out to confirm the findings discussed in this report, to better quantify the benefits, to expand the *CalME* materials library, and to identify the most appropriate applications in pavement structures in the different California climate zones.
- Some relaxation of the solubility requirements in the PG-M specification should be considered to allow more use of Approach-4 binders. Laboratory test results and performance simulations did not indicate that a relaxation in solubility requirements would have a detrimental effect on performance.
- Given that dry process approaches are the simplest and cheapest method of incorporating CRM into mixes, limited additional testing with finer CRM particles, along with performance simulations, should be conducted to confirm that findings from research conducted in other states and countries are applicable to California applications.

17. KEYWORDS Rubber modified binder, crumb rubber modifier, CRM, *CalME* simulation	18. DISTRIBUTION STATEMENT No restrictions. This document is available to the public through the National Technical Information Service, Springfield, VA 22161

19. SECURITY CLASSIFICATION (of this report) Unclassified	20. NUMBER OF PAGES 267	21. PRICE None

UCPRC ADDITIONAL INFORMATION

1. DRAFT STAGE Final	2. VERSION NUMBER 1
3. PARTNERED PAVEMENT RESEARCH CENTER STRATEGIC PLAN ELEMENT NUMBER 4.61 and 4.62	4. DRISI TASK NUMBER 3024 and 3190
5. CALTRANS TECHNICAL LEAD AND REVIEWER(S) T. Pyle and C. Barros	6. FHWA NUMBER CA223190A

7. PROPOSALS FOR IMPLEMENTATION
None

8. RELATED DOCUMENTS
None

9. LABORATORY ACCREDITATION
The UCPRC laboratory is accredited by AASHTO re:source for the tests listed in this report

10. SIGNATURES

D. Jones **FIRST AUTHOR**	J. Harvey **TECHNICAL REVIEW**	C. Fink **EDITOR**	J. Harvey **PRINCIPAL INVESTIGATOR**	C. Barros **CALTRANS TECH. LEAD**	T.J. Holland **CALTRANS CONTRACT MANAGER**

DISCLAIMER STATEMENT

This document is disseminated in the interest of information exchange. The contents of this report reflect the views of the authors who are responsible for the facts and accuracy of the data presented herein. The contents do not necessarily reflect the official views or policies of the State of California or the Federal Highway Administration. This publication does not constitute a standard, specification, or regulation. This report does not constitute an endorsement by the Department of any product described herein.

For individuals with sensory disabilities, this document is available in alternate formats. For information, call (916) 654-8899, TTY 711, or write to California Department of Transportation, Division of Research, Innovation and System Information, MS-83, P.O. Box 942873, Sacramento, CA 94273-0001.

PROJECT OBJECTIVES

The objective of this project is to provide the information needed for Caltrans to decide whether and how to move forward with each of four approaches for adding small amounts of crumb rubber modifier (CRM) to dense-graded hot-mix asphalt, and the technologies required to follow these approaches. This goal will be achieved through completion of the following tasks:

1. Identification of various types of materials that may fall within each of the four categories.
2. Review of available literature regarding past or present technologies identified, including specifications, reports, and any other information (written or oral) that can be gathered.
3. Identification of any issues regarding specification testing.
4. Testing and analysis of example materials to determine their capability of meeting Superpave performance grading (PG) specifications; comparison with currently specified materials in terms of expected performance; and, if a material cannot meet all specifications, information regarding the likely effect on performance. This will include asphalt binder and mix testing.
5. Evaluation of effects of mix properties on pavement performance in different thicknesses of overlays and new/reconstructed asphalt pavements using *CalME* software for different levels of traffic and different climate regions.

6. A life cycle cost analysis (LCCA) that includes identification of cost and performance data, and analysis of net present value, with sensitivity analysis, for materials within each category (not funded in this phase of the study).
7. A life cycle analysis (LCA) that includes development of environmental flow data, calculation of impacts, and interpretation and reporting of the results (not funded in this phase of the study).
8. Assistance with development of test methods, methods of determining CRM content, specification language, and guidelines (not funded in this phase of the study).
9. Reporting of all results.

This report covers Tasks 1 through 5.

ACKNOWLEDGMENTS

The University of California Pavement Research Center (UCPRC) acknowledges the California Department of Resources Recycling and Recovery (CalRecycle) for partial funding of this study. The UCPRC also acknowledges the assistance provided by individuals at the following agencies, companies, and universities:

- A. Teichert and Son, Inc.
- APS (American Pavement Systems)
- Alon Asphalt, Inc.
- Wright Asphalt, Inc.
- US Polyco, Inc.
- VSSI International and George Reed Construction, Inc.
- Full Circle Technologies, Inc.
- Owens Corning, Inc.
- CRM Rubber, Inc.
- University of Nevada, Reno
- California Department of Transportation
- UC Pavement Research Center Laboratory Staff

Blank page

EXECUTIVE SUMMARY

In 2015, Caltrans expressed interest in studying the addition of small amounts of crumb rubber (CRM) in dense-graded asphalt mixes to increase the total amount of recycled tire rubber used. Small amounts were defined as 5% to 10% CRM by weight of the binder or approximately 0.25% to 0.5% CRM by weight of the aggregate. In this report, the terms "CRM binder" and "CRM mix" are used to denote the modified mixes.

The following four approaches for adding the rubber were proposed:

1. Approach-1: Addition of 5% to 10% CRM particles smaller than 250 µm to the asphalt binder by weight of the binder, not resulting in a change to the PG of the base binder, achieved by blending softer base binders and/or polymers with the rubber at the refinery/terminal.
2. Approach-2: Addition of 5% to 10% CRM particles smaller than 2.36 mm to the asphalt binder, with allowable changes to the PG of the base binder, and produced using a field-blending process similar to that used for producing asphalt rubber binders with between 18% and 22% CRM by weight of the binder. Two gradations (passing a 2.36 mm [#8] and a 1.18 mm [#16] sieve) were assessed in this study.
3. Approach-3: Adding 0.25% to 0.5% CRM by weight of the aggregate directly into the mix using a dry-process. Particles passing a 2.36 mm (#8) sieve were used in this study; however, most dry process mixes in the United States use particles smaller than 500 µm (passing the #30 sieve).
4. Approach-4: Addition of 5% to 10% CRM with particles smaller than 250 µm to the asphalt binder, with allowable changes to the PG of the base binder, and produced using a field-blending process.

This project included a literature review, development of a comprehensive workplan, laboratory testing based on a partial factorial experimental design, and a series of mechanistic-empirical performance simulations.

A total of 26 binders (6 control [base] binders, 18 CRM binders, and 2 styrene-butadiene-styrene [SBS] binders) and 19 mixes (5 control mixes and 14 CRM mixes) were tested. Binder tests included performance grading, multiple stress creep recovery, stiffness frequency sweeps, solubility, ductility, viscosity, and Fourier-Transform Infrared Spectroscopy. Mix tests included dynamic and flexural modulus to assess stiffness, repeated load triaxial to assess rutting

performance, Hamburg wheel track to assess moisture resistance, flexural beam fatigue to assess fatigue and reflective cracking resistance, semicircular bending to assess fracture cracking resistance, and uniaxial thermal stress and strain tests to assess low temperature cracking resistance.

Since laboratory tests only reveal material performance under a specific set of controlled testing conditions and may not be representative of actual field performance where layer thicknesses, climate, traffic loading, and other factors all play a role, particularly for bottom-up fatigue cracking performance, laboratory test results were used as inputs in mechanistic-empirical simulations, using *CalME* software, to predict likely field responses for several typical application scenarios.

Test Result Summary

Laboratory binder and mix test results revealed that CRM binders and CRM mixes had equal or better performance to their control (base) binders and mixes in terms of potential rutting and cracking performance in most cases, based on the following observations:

- Approach-1 binders met project specific performance grading criteria, including solubility.
- Approach-2 binders had higher high-temperature performance gradings than their base binders in the unaged- and rolling thin film oven (RTFO)-aged conditions, and lower intermediate-temperature performance gradings after pressure vessel aging. Bending beam rheometer (BBR) tests indicated that these CRM binders had the same low-temperature performance grade as their base binders, with decreasing creep stiffness with increasing CRM content. Adding CRM also lowered the non-recoverable creep compliance and increased the percentage recovery in the multiple stress creep recovery (MSCR) test.
- Approach-4 CRM binders showed performance grade changes that were proportional to the CRM content. These binders met the Caltrans PG-M specification criteria, except for solubility, and showed better performance than their base binders at high, intermediate, and low temperatures.
- Binder test results indicate that CRM binders will potentially be more resistant to rutting and to low-temperature cracking. CRM binders generally developed fewer carbonyl components than the control binders after PAV-aging, indicating that they will potentially age at a slower rate than their base binders.
- The Approach-1, Approach-2, and Approach-4 CRM binders were found to be suitable for use in dense-graded mixes. Mixes produced with binders containing CRM particles smaller

than 250 µm met volumetric design criteria at the same binder content as the control base binder. Mixes produced with binders containing larger CRM particles (up to 2.36 mm) required higher optimum binder contents than the control mix to meet volumetric criteria. Dry process mixes produced with 0.25% and 0.5% coarse CRM (<2.36 mm) by weight of the aggregate also needed higher optimum binder contents than the control mix to account for the CRM. Although no adjustments were made to aggregate gradations to accommodate the CRM, the mixes with wet-process binders (Approaches-1, 2 and 4) and the mix with 0.25% dry-process CRM all passed the volumetric criteria for Caltrans Type-A HMA. The dry process mix with 0.5% CRM failed some of the voids in mineral aggregate (VMA) criteria.

- Approach-1 and Approach-4 mixes had higher stiffnesses (determined with dynamic and flexural modulus tests) at high temperatures than the control mixes, indicating potentially better rutting performance, but only a marginal stiffness difference at intermediate temperatures, indicating potentially similar cracking resistance at a given tensile strain (fatigue performance in the field depends on the structure type and is an interaction of stiffness and fatigue at a given strain). They also showed the potential for equal or better rutting and moisture resistance than the control mixes in repeated load triaxial and Hamburg wheel track tests, and potentially longer fatigue lives than the control mixes in beam fatigue tests at strain levels below 400 µstrain. Mixes produced with binders containing 5% CRM showed potential for better low-temperature cracking performance in the uniaxial thermal stress and strain test.
- Approach-2 CRM mixes had higher stiffnesses (dynamic and flexural modulus) and better rutting and moisture resistance (repeated load triaxial and Hamburg wheel track) than the control mix. Fatigue results were inconsistent across the range of strains, with the control mix performance generally falling between the 5% CRM content mix (longer fatigue life than the control) and the 10% CRM content mix (shorter fatigue life than the control). Low-temperature cracking resistance tests were not conducted on these mixes.
- Approach-3 mixes had poorer rutting, moisture and thermal cracking resistance than the control mix, but better fatigue performance at strains higher than 600 µstrain. It should be noted that most dry mixes produced in the United States are now prepared with CRM particles smaller than 500 µm (passing the #30 sieve), considerably smaller than the 2.36 mm maximum size tested in this study. Poor performance in this round of testing was mostly attributed to the relatively large CRM particles used, which were not satisfactorily accommodated in the dense gradation.
- Semicircular bend (SCB) test results had high variability between replicate specimens. Taking this into consideration, SCB test results indicated that the CRM mixes had similar fracture resistance to their control mixes.

Mechanistic-empirical performance simulation results indicated that field performance of the CRM mixes in different pavement structures varied on a case-by-case basis, depending on the scenario. As with any other pavement design, appropriate applications of CRM mixes need to be determined based on an analysis of project-specific mix properties, pavement structure, traffic, and climate. However, general trends indicated that mixes produced with Approach-1, Approach-2, and Approach-4 binders had similar or better performance than their control binders in most of the scenarios that were assessed. The dry process mixes did not perform well, as expected, because of the larger CRM particles used in the study. Different results are expected if finer CRM gradations are used.

Conclusions

Laboratory test results and mechanistic-empirical performance simulations both indicate that dense-graded mixes produced with binders containing between 5% and 10% CRM by weight of the binder will generally have equal or better performance to dense-graded mixes produced with unmodified binders. Finer CRM gradations (i.e., smaller than 250 µm, used in Approach-1 and Approach-4 binders) allow binder testing with standard Superpave performance grading tests and appear to provide more consistent results. Based on literature reviews, adding between 0.25% and 0.5% CRM with particles sizes smaller than 500 µm in dry process mixes will also provide equal or better performance to mixes that contain no CRM. If any of the approaches are adopted, more scrap tires would be recycled into pavement applications.

Recommendations

The following recommendations are proposed based on the findings from this study:

- Laboratory test results and mechanistic-empirical performance simulations support the use of small quantities of CRM in dense-graded mixes, both as a means of recycling more waste tires, and for improving pavement layer performance under a given set of conditions. Pilot studies should be considered to confirm these findings, to better quantify the benefits, and to expand the *CalME* materials library.
- Preliminary mechanistic-empirical performance simulation results indicate that dense-graded mixes produced with rubber-modified binders meeting the current Caltrans PG-M specification could be beneficially used in a wide range of pavement layer applications. These findings are supported by literature from other state departments of transportation

that have implemented similar specifications. Additional mechanistic-empirical performance simulations should be carried out to confirm these findings and to identify the most appropriate applications in pavement structures in the different California climate zones.

- Some relaxation of the solubility requirements in the PG-M specification should be considered to allow more use of Approach-4 binders. Laboratory test results and performance simulations did not indicate that a relaxation in solubility requirements would have a detrimental effect on performance.
- Given that dry process approaches are the simplest and cheapest method of incorporating CRM into mixes, limited additional testing with finer CRM particles, along with performance simulations, should be conducted to confirm that findings from research conducted in other states and countries are applicable to California applications.

Blank page

TABLE OF CONTENTS

EXECUTIVE SUMMARY ..... **vii**
LIST OF TABLES ..... **xvii**
LIST OF FIGURES ..... **xix**
LIST OF ABBREVIATIONS ..... **xxiii**
TEST METHODS CITED IN THE TEXT ..... **xxv**
CONVERSION FACTORS ..... **xxvii**
1. INTRODUCTION **1**
1.1 Background to the Study 1
1.2 Proposed Approaches 2
1.3 Problem Statements 3
1.4 Study Objective/Goal 3
1.5 Report Structure 4
1.6 Measurement Units 5
2. MATERIALS AND PROCESSES FOR CRM BINDER AND MIX APPROACHES **7**
2.1 Introduction 7
2.2 Materials and Processes for Approach-1 7
2.3 Materials and Processes for Approach-2 7
2.4 Materials and Processes for Approach-3 8
2.4.1 Materials and Processes for Approach-4 8
3. LITERATURE REVIEW **9**
3.1 Introduction 9
3.2 Background 9
3.3 States Permitting the Use of Recycled Tire Rubber in Binder Modification 10
3.4 Factors Effecting Binder Rheology Specific to CRM Binders 12
3.4.1 Effect of Rubber Grinding Method 12
3.4.2 Effect of CRM Content on Binder Properties 12
3.4.3 Effect of CRM Particle Size on Binder Properties 12
3.5 Dry Process Rubberized Asphalt Mixes 13
3.6 Engineered Rubber Products 14
3.7 Binder Testing Issues 14
3.8 Mix Testing Issues 15
3.9 Pavement Performance Simulation Issues 15
3.10 Literature Review Summary 17
4. MATERIAL PREPARATION AND EXPERIMENTAL DESIGN **19**
4.1 Introduction 19
4.2 Materials 19
4.2.1 Approach-1 Binders 19
4.2.2 Approach-2 Binders 20
4.2.3 Approach-4 Binders 20
4.2.4 Aggregates 21
4.3 Experiment Design 23
4.4 Asphalt Binder Testing Experimental Design 23

4.4.1 Performance-Grading 23
4.4.2 Multiple-Stress Creep Recovery 26
4.4.3 Frequency Sweep 26
4.4.4 Solubility and Ductility 27
4.4.5 Viscosity 27
4.4.6 Fourier-Transform Infrared Spectroscopy 28
4.5 Asphalt Mix Testing Experimental Design 29
4.5.1 Volumetric Mix Design 31
4.5.2 Dynamic Modulus 31
4.5.3 Flexural Modulus 32
4.5.4 Rutting Resistance (AMPT) 32
4.5.5 Rutting and Moisture Resistance (HWTT) 33
4.5.6 Fatigue Cracking Resistance 33
4.5.7 Fracture Cracking Resistance (SCB) 34
4.5.8 Low-Temperature Cracking Resistance (UTSST) 34
4.6 Pavement Performance Simulations Using CalME Software 35
5. EVALUATION OF APPROACH-1 BINDERS AND MIXES 37
5.1 Introduction 37
5.2 Approach-1 Binder Test Results 37
5.2.1 Introduction 37
5.2.2 High-Temperature Grading 37
5.2.3 Intermediate-Temperature Grading 41
5.2.4 Low-Temperature Grading 42
5.2.5 Multiple Stress Creep Recovery 45
5.2.6 Frequency Sweep 45
5.2.7 Solubility 48
5.2.8 Ductility 48
5.2.9 FTIR Testing 48
5.3 Approach-1 Mix Test Results 52
5.3.1 Volumetric Mix Design 52
5.3.2 Mix Stiffness: Dynamic and Flexural Modulus 53
5.3.3 Rutting Resistance: Unconfined Repeated Load Triaxial Test 56
5.3.4 Rutting and Moisture Resistance: Hamburg Wheel Track Test 58
5.3.5 Fatigue/Reflective Cracking Resistance: Four-Point Beam Test 59
5.3.6 Fracture Cracking Resistance: Semicircular Bend Test 61
5.3.7 Low-Temperature Cracking: Uniaxial Thermal Stress and Strain Test 62
5.4 Approach-1 Test Result Summary 63
6. EVALUATION OF APPROACH-2 BINDERS AND MIXES 65
6.1 Introduction 65
6.2 Approach-2 Binder Test Results 65
6.2.1 Introduction 65
6.2.2 High-Temperature Grading 65
6.2.3 Intermediate-Temperature Grading 69
6.2.4 Low-Temperature Grading 70
6.2.5 Multiple Stress Creep Recovery 72

6.2.6 Frequency Sweep 73
6.2.7 Solubility and Ductility 73
6.2.8 FTIR Testing 73
6.3 Approach-2 Mix Test Results 77
6.3.1 Volumetric Mix Design 77
6.3.2 Mix Stiffness: Dynamic and Flexural Modulus 80
6.3.3 Rutting Resistance: Unconfined Repeated Load Triaxial Test 83
6.3.4 Rutting and Moisture Resistance: Hamburg Wheel Track Test 85
6.3.5 Fatigue/Reflective Cracking Resistance: Four-Point Beam Test 85
6.3.6 Fracture Cracking Resistance: Semicircular Bend Test 87
6.3.7 Low-Temperature Cracking: Uniaxial Thermal Stress and Strain Test 89
6.4 Approach-2 Test Result Summary 89
7. EVALUATION OF APPROACH-3 MIXES 91
7.1 Introduction 91
7.2 Approach-3 Mix Test Results 91
7.2.1 Volumetric Mix Design 91
7.2.2 Mix Stiffness: Dynamic and Flexural Modulus 92
7.2.3 Rutting Resistance: Unconfined Repeated Load Triaxial Test 93
7.2.4 Rutting and Moisture Resistance: Hamburg Wheel Track Test 96
7.2.5 Fatigue/Reflective Cracking Resistance: Four-Point Beam Test 97
7.2.6 Fracture Cracking Resistance: Semicircular Bend Test 97
7.2.7 Low-Temperature Cracking: Uniaxial Thermal Stress and Strain Test 99
7.3 Approach-3 Test Result Summary 100
8. EVALUATION OF APPROACH-4 BINDERS AND MIXES 101
8.1 Introduction 101
8.2 Approach-4 Binder Test Results 101
8.2.1 Introduction 101
8.2.2 High-Temperature Grading 101
8.2.3 Intermediate-Temperature Grading 104
8.2.4 Low-Temperature Grading 105
8.2.5 Multiple Stress Creep Recovery 107
8.2.6 Frequency Sweep 107
8.2.7 Solubility 109
8.2.8 Ductility 109
8.2.9 FTIR Testing 110
8.3 Approach-4 Mix Test Results 110
8.3.1 Volumetric Mix Design 112
8.3.2 Mix Stiffness: Dynamic and Flexural Modulus 113
8.3.3 Rutting Resistance: Unconfined Repeated Load Triaxial Test 115
8.3.4 Rutting and Moisture Resistance: Hamburg Wheel Track Test 117
8.3.5 Fatigue/Reflective Cracking Resistance: Four-Point Beam Test 117
8.3.6 Fracture Cracking Resistance: Semicircular Bend Test 118
8.3.7 Low-Temperature Cracking: Uniaxial Thermal Stress and Strain 118
8.4 Approach-4 Test Result Summary 120

9. PRELIMINARY PAVEMENT PERFORMANCE SIMULATIONS 123
9.1 Introduction 123
9.2 CalME Simulation Input 123
9.3 CalME Simulation Results 125
9.3.1 Asphalt Concrete Overlay on Cracked Asphalt Concrete 125
9.3.2 Asphalt Concrete Overlay on Cracked Portland Cement Concrete 127
9.4 CalME Simulation Summary 129
10. CONCLUSIONS AND RECOMMENDATIONS 131
10.1 Study Summary 131
10.2 Test Result Summary 132
10.3 Conclusions 134
10.4 Recommendations 134
REFERENCES 137
APPENDIX A: TEST RESULTS FOR APPROACH-1 BINDERS AND MIXES 143
APPENDIX B: TEST RESULTS FOR APPROACH-2 BINDERS AND MIXES 169
APPENDIX C: TEST RESULTS FOR APPROACH-3 MIXES 197
APPENDIX D: TEST RESULTS FOR APPROACH-4 BINDERS AND MIXES 209
APPENDIX E: CalME SIMULATION RESULTS 223

LIST OF TABLES

Table 4.1: Aggregate Gradation Distribution....21
Table 4.2: Aggregate Bulk Specific Gravity....22
Table 4.3: Aggregate Gradations....22
Table 4.4: Summary of Binder and Mix Testing....24
Table 4.5: Approach-1 Binders: Factors and Factorial Levels....25
Table 4.6: Approach-2 Binders: Factors and Factorial Levels....25
Table 4.7: Approach-4 Binders: Factors and Factorial Levels....25
Table 4.8: FTIR Wavenumber Limits of Chemical Area Indices....29
Table 4.9: Approach-1 Mixes: Factors and Factorial Levels....30
Table 4.10: Approach-2 Mixes: Factors and Factorial Levels....30
Table 4.11: Approach-3 Mixes: Factors and Factorial Levels....31
Table 4.12: Approach-4 Mixes: Factors and Factorial Levels....31
Table 4.13: Summary of Mix Test Factors....32
Table 5.1: App-1: Continuous Grades....38
Table 5.2: App-1: Low-Temperature Test Results....44
Table 5.3: App-1/Ref-A: Mixing and Compaction Settings....52
Table 5.4: App-1/Ref-A: Mix-A Mix Design Summary....53
Table 5.5: App-1/Ref-A: Summary of Superpave Mix Design Parameters....53
Table 5.6: App-1: Semicircular Bend Test Results....62
Table 6.1: App-2: Continuous Grades....69
Table 6.2: App-2: Low-Temperature Test Results....70
Table 6.3: App-2: Mixing and Compaction Settings....79
Table 6.4: App-2: Mix Design Summary....80
Table 6.5: App-2: Semicircular Bend Test Results....87
Table 7.1: App-3: Mixing and Compaction Settings....92
Table 7.2: App-3: Mix Design Summary....92
Table 7.3: App-3: Semicircular Bend Test Results....99
Table 8.1: App-4: Continuous Grades....103
Table 8.2: App-4: Low Temperature Test Results....106
Table 8.3: App-4: Mixing and Compaction Settings....113
Table 8.4: App-4: Mix Design Summary....113
Table 8.5: App-4: SCB Test Results....118
Table 9.1: CalME Climate Inputs....124
Table 9.2: Asphalt Concrete Overlay on Cracked Asphalt Concrete....124
Table 9.3: Asphalt Concrete Overlay on Cracked Portland Cement Concrete....124
Table 9.4: RHMA-G Mix Parameters....125
Table 9.5: CalME Traffic Inputs....125
Table 9.6: Performance Ranking of Overlay Applications on Cracked Asphalt Concrete....126
Table 9.7: Performance Ranking of Overlays on Cracked Portland Cement Concrete....128

Blank page

LIST OF FIGURES

Figure 3.1: CRM application by Caltrans *(3)*. 11
Figure 3.2: General rules of fatigue resistance and stiffness *(54)*..... 16
Figure 4.1: Sieve analyses of the CRM samples from Supplier-D..... 20
Figure 4.2: Plot of aggregate gradation. 22
Figure 4.3: Example of modulus master curves: Plotted by frequency at tested temperature. .. 28
Figure 4.4: Example of modulus master curves: Plotted by shifted frequency. 28
Figure 4.5: Example of normalized FTIR absorbance spectrum. 30
Figure 5.1: App-1/Ref-A: G*/sin(δ) of unaged and RTFO-aged PG 64 binders at 64°C. 39
Figure 5.2: App-1/Ref-A: G*/sin(δ) of unaged and RTFO-aged PG 70 binders at 70°C. 39
Figure 5.3: App-1/Ref-B: G*/sin(δ) of unaged and RTFO-aged PG 64 binders at 64°C. 39
Figure 5.4: App-1/Ref-B: G*/sin(δ) of unaged and RTFO-aged PG 70 binders at 70°C. 39
Figure 5.5: App-1/Ref-A: Phase angles of unaged and RTFO-agedP G 64 binders at 64°C..... 40
Figure 5.6: App-1/Ref-A: Phase angles of unaged and RTFO-aged PG 70 binders at 70°C..... 40
Figure 5.7: App-1/Ref-B: Phase angles of unaged and RTFO-aged PG 64 binders at 64°C..... 40
Figure 5.8: App-1/Ref-B: Phase angles of unaged and RTFO-aged PG 70 binders at 70°C..... 40
Figure 5.9: App-1/Ref-A: G*×sin(δ) of PAV-aged binders at 25°C..... 42
Figure 5.10: App-1/Ref-B: G*×sin(δ) of PAV-aged binders at 25°C..... 42
Figure 5.11: App-1/Ref-A: Low-temperature creep stiffness and m-value. 43
Figure 5.12: App-1/Ref-B: Low-temperature creep stiffness and m-value. 43
Figure 5.13: App-1/Ref-A: Jnr values of RTFO-aged binders at 64°C. 46
Figure 5.14: App-1/Ref-A: Percentage recovery of RTFO-aged binders at 64°C. 46
Figure 5.15: App-1/Ref-B: Jnr values of RTFO-aged binders at 64°C. 46
Figure 5.16: App-1/Ref-B: Percentage recovery of RTFO-aged binders at 64°C. 46
Figure 5.17: App-1/Ref-A: RTFO-aged binder master curves at 20°C. 47
Figure 5.18: App-1/Ref-A: Normalized RTFO-aged binder master curves at 20°C. 47
Figure 5.19: App-1/Ref-B: RTFO-aged binder master curves at 20°C. 47
Figure 5.20: App-1/Ref-B: Normalized RTFO-aged binder master curves at 20°C. 47
Figure 5.21: App-1/Ref-A: Solubility of unaged binders. 50
Figure 5.22: App-1/Ref-B: Solubility of unaged binders. 50
Figure 5.23: App-1/Ref-A: Ductility of RTFO-aged binders at 25°C. 50
Figure 5.24: App-1/Ref-B: Ductility of RTFO-aged binders at 25°C. 50
Figure 5.25: App-1/Ref-A: Carbonyl area index changes after aging. 51
Figure 5.26: App-1/Ref-B: Carbonyl area index changes after aging. 51
Figure 5.27: App-1/Ref-A: Sulfoxide area index changes after aging. 51
Figure 5.28: App-1/Ref-B: Sulfoxide area index changes after aging. 51
Figure 5.29: App-1/Mix-A: Air-void content vs. asphalt binder content. 54
Figure 5.30: App-1/Mix-A: VMA vs. asphalt binder content. 54
Figure 5.31: App-1/Mix-A: Dust proportion vs. asphalt binder content. 54
Figure 5.32: App-1/Mix-A: VFA vs. asphalt binder content. 54
Figure 5.33: App-1/Ref-A: Dynamic modulus master curves at 20°C. 55
Figure 5.34: App-1/Ref-A: Normalized dynamic modulus master curves at 20°C. 55
Figure 5.35: App-1/Ref-A: Flexural modulus master curves at 20°C. 55

Figure 5.36: App-1/Ref-A: Normalized flexural modulus master curves at 20°C. 55
Figure 5.37: App-1/Ref-A: Black diagram of dynamic modulus results. 57
Figure 5.38: App-1/Ref-A: Black diagram of flexural modulus results. 57
Figure 5.39: App-1/Ref-A: Flow number at 50°C. 57
Figure 5.40: App-1/Ref-A: Average permanent strain vs. load cycle at 50°C. 57
Figure 5.41: App-1/Ref-A: Hamburg Wheel Track rutting at 50°C. 58
Figure 5.42: App-1/Ref-A: Beam fatigue at 20°C and 10 Hz for PG 64-16 mixes. 60
Figure 5.43: App-1/Ref-A: Beam fatigue at 20°C and 10 Hz for PG 70-10 mixes. 60
Figure 5.44: App-1/Ref-A: Calculated fatigue life of PG 64 mixes. 60
Figure 5.45: App-1/Ref-A: Calculated fatigue life of PG 70 mixes. 60
Figure 5.46: App-1/Ref-A: SCB fracture energy and tensile strength at 25°C. 61
Figure 5.47: App-1/Ref-A: SCB flexibility index at 25°C. 61
Figure 5.48: App-1/Ref-A: Uniaxial thermal stress and strain. 63
Figure 6.1: App-2/Supp-D: G*/sin(δ) of unaged binders at 70°C. 66
Figure 6.2: App-2/Supp-F: G*/sin(δ) of unaged binders at 70°C. 66
Figure 6.3: App-2/Supp-D: G*/sin(δ) of RTFO-aged binders at 70°C. 66
Figure 6.4: App-2/Supp-F: G*/sin(δ) of RTFO-aged binders at 70°C. 66
Figure 6.5: App-2/Supp-D: Phase angles at 70°C. 67
Figure 6.6: App-2/Supp-F: Phase angles at 70°C. 67
Figure 6.7: App-2/Supp-D: G*×sin (δ) of PAV-aged binders at 25°C. 71
Figure 6.8: App-2/Supp-F: G*×sin (δ) of PAV-aged binders at 25°C. 71
Figure 6.9: App-2/Supp-D: Low-temperature creep stiffness and m-value. 71
Figure 6.10: App-2/Supp-F: Low-temperature creep stiffness and m-value. 71
Figure 6.11: App-2/Supp-D: Jnr values of RTFO-aged binders at 64°C. 74
Figure 6.12: App-2/Supp-D: Percentage recovery of RTFO-aged binders at 64°C. 74
Figure 6.13: App-2/Supp-F: Jnr values of RTFO-aged binders at 64°C. 74
Figure 6.14: App-2/Supp-F: Percentage recovery of RTFO-aged binders at 64°C. 74
Figure 6.15: App-2/Supp-D: RTFO-aged binder master curves at 40°C. 75
Figure 6.16: App-2/Supp-D: Normalized RTFO-aged binder master curves at 40°C. 75
Figure 6.17: App-2/Supp-F: RTFO-aged binder master curves at 40°C. 75
Figure 6.18: App-2/Supp-F: Normalized RTFO-aged binder master curves at 40°C. 75
Figure 6.19: App-2/Supp-D: Carbonyl area index changes after aging. 76
Figure 6.20: App-2/Supp-F: Carbonyl area index changes after aging. 76
Figure 6.21: App-2/Supp-D: Sulfoxide area index changes after aging. 76
Figure 6.22: App-2/Supp-F: Sulfoxide area index changes after aging. 76
Figure 6.23: App-2/Supp-D: Rotational viscosity. 78
Figure 6.24: App-2/Supp-F: Rotational viscosity. 78
Figure 6.25: App-2/Supp-D: Dynamic modulus master curves at 20°C. 81
Figure 6.26: App-2/Supp-D: Normalized dynamic modulus master curves at 20°C. 81
Figure 6.27: App-2/Supp-F: Dynamic modulus master curves at 20°C. 81
Figure 6.28: App-2/Supp-F: Normalized dynamic modulus master curves at 20°C. 81
Figure 6.29: App-2/Supp-D: Flexural modulus master curves at 20°C. 82
Figure 6.30: App-2/Supp-D: Normalized flexural modulus master curves at 20°C. 82
Figure 6.31: App-2/Supp-D: Black diagram of dynamic modulus results. 82
Figure 6.32: App-2/Supp-F: Black diagram of dynamic modulus results. 82

Figure 6.33: App-2/Supp-D: Black diagram of flexural modulus results. 83
Figure 6.34: App-2/Supp-D: Flow number at 50°C. 84
Figure 6.35: App-2/Supp-F: Flow number at 50°C. 84
Figure 6.36: App-2/Supp-D: Average permanent strain versus load cycle at 50°C. 84
Figure 6.37: App-2/Supp-F: Average permanent strain versus load cycle at 50°C. 84
Figure 6.38: App-2/Supp-D: Hamburg Wheel Track rutting at 50°C. 86
Figure 6.39: App-2/Supp-F: Hamburg Wheel Track rutting at 50°C. 86
Figure 6.40: App-2/Supp-D: Beam fatigue at 20°C and 10 Hz. 86
Figure 6.41: App-2/Supp-D: Calculated fatigue life. 86
Figure 6.42: App-2/Supp-D: SCB fracture energy and tensile strength at 25°C. 88
Figure 6.43: App-2/Supp-D: SCB flexibility index at 25°C. 88
Figure 6.44: App-2/Supp-F: SCB fracture energy and tensile strength at 25°C. 88
Figure 6.45: App-2/Supp-F: SCB flexibility index at 25°C. 88
Figure 7.1: App-3: Dynamic modulus master curves at 20°C. 94
Figure 7.2: App-3: Normalized dynamic modulus master curves at 20°C. 94
Figure 7.3: App-3: Flexural modulus master curves at 20°C. 94
Figure 7.4: App-3: Normalized flexural modulus master curves at 20°C. 94
Figure 7.5: App-3: Black diagram of dynamic modulus results. 95
Figure 7.6: App-3: Black diagram of flexural modulus results. 95
Figure 7.7: App-3: Flow number at 50°C. 95
Figure 7.8: App-3: Average permanent strain vs. load cycle at 50°C. 95
Figure 7.9: App-3: Hamburg Wheel Track rutting at 50°C. 96
Figure 7.10: App-3: Beam fatigue at 20°C and 10 Hz. 98
Figure 7.11: App-3: Calculated fatigue life. 98
Figure 7.12: App-3: SCB fracture energy and tensile strength at 25°C. 98
Figure 7.13: App-3: SCB flexibility index at 25°C. 98
Figure 7.14: App-3: Uniaxial thermal stress and strain. 99
Figure 8.1: App-4/Supp-C: G*/sin(δ) of unaged and RTFO-aged binders. 102
Figure 8.2: App-4/Supp-D: G*/sin(δ) of unaged and RTFO-aged binders. 102
Figure 8.3: App-4/Supp-C: Phase angles of unaged and RTFO-aged binders. 102
Figure 8.4: App-4/Supp-D: Phase angles of unaged and RTFO-aged binders. 102
Figure 8.5: App-4: G*×sin (δ) of PAV-aged binders at 25°C. 104
Figure 8.6: App-4: Low temperature creep stiffness and m-value. 105
Figure 8.7: App-4: Jnr values of RTFO-aged binders at 64°C. 108
Figure 8.8: App-4: Percentage recovery of RTFO-aged binders at 64°C. 108
Figure 8.9: App-4: RTFO-aged binder master curves at 20°C. 108
Figure 8.10: App-4: Normalized RTFO-aged binder master curves at 20°C. 108
Figure 8.11: App-4: Solubility of unaged binders. 111
Figure 8.12: App-4: Ductility of RTFO-aged binders at 25°C. 111
Figure 8.13: App-4: Carbonyl area index changes after aging. 111
Figure 8.14: App-4: Sulfoxide area index changes after aging. 111
Figure 8.15: App-4: Rotational viscosity. 112
Figure 8.16: App-4/Supp-C: Dynamic modulus master curves at 20°C. 114
Figure 8.17: App-4/Supp-C: Normalized dynamic modulus master curves at 20°C. 114
Figure 8.18: App-4/Supp-C: Flexural modulus master curves at 20°C. 114

Figure 8.19: App-4/Supp-C: Normalized flexural modulus master curves at 20°C. 114
Figure 8.20: App-4/Supp-C: Black diagram of dynamic modulus results. 116
Figure 8.21: App-4/Supp-C: Black diagram of flexural modulus results. 116
Figure 8.22: App-4/Supp-C: Flow number at 50°C. 116
Figure 8.23: App-4/Supp-C: Average permanent strain vs. load cycles at 50°C. 116
Figure 8.24: App-4/Supp-C: Hamburg wheel track rutting at 50°C. 117
Figure 8.25: App-4/Supp-C: Beam fatigue at 20°C and 10 Hz. 119
Figure 8.26: App-4/Supp-C: Calculated fatigue life. 119
Figure 8.27: App-4/Supp-C: SCB fracture energy and tensile strength at 25°C. 119
Figure 8.28: App-4/Supp-C: SCB flexibility index at 25°C. 119
Figure 8.29: App-4/Supp-C: Uniaxial thermal stress and strain. 120
Figure 9.1: AC on AC: Simulation results for 0.15 ft. overlays of Mix-A, -B, and -C. 126
Figure 9.2: AC on PCC: Simulation results for 0.15 ft. overlays of Mix-A, -B, and -C. 129

LIST OF ABBREVIATIONS

AASHTO	American Association of State Highway and Transportation officials
AC	Asphalt concrete
AMPT	Asphalt mixture performance tester
ARB	Asphalt rubber binder
ASTM	American Society for Testing and Materials
AV	Air void
BBR	Bending beam rheometer
CA	Carbonyl area index
CalME	California Mechanistic-Empirical Design Software
CalRecycle	California Department of Resources, Recycling, and Recovery
Caltrans	California Department of Transportation
CoV	Coefficient of variation
CRI	Cracking resistance index
CRM	Crumb rubber modifier
DM	Dynamic modulus
DOT	Department of Transport/Department of Transportation
DP	Dust proportion
DSR	Dynamic shear rheometer
DWA	Dry weight of aggregate
ESAL	Equivalent single axle loads
FAT	Beam fatigue test
FHWA	Federal Highway Administration
FI	Flexibility index
FS	Frequency sweep
FTIR	Fourier transform infrared
FTIR-ATR	Fourier-transform infrared spectroscopy with attenuated total reflection
G*	Dynamic shear modulus
Gmb	Bulk specific gravity
Gmm	Theoretical maximum specific gravity
GTR	Ground tire rubber
HMA	Hot-mix asphalt
HWT	Hamburg wheel track
HWTT	Hamburg wheel track test
JMF	Job mix formula
Jnr	Non-recoverable creep compliance
LCA	Life cycle assessment
LCCA	Life cycle cost assessment
MSCR	Multiple stress creep recovery
NMAS	Nominal maximum aggregate size
OBC	Optimal binder content
PAS	Permanent axial strain
PAV	Pressure aging vessel
PCC	Portland cement concrete
PG	Performance rade
PG-AR	Performance grade of asphalt rubber binders (California)
PG-ARB	Performance grade of asphalt rubber binders (Florida)

PG-CRM	Performance grade of crumb rubber modified binders (Louisiana)
PG-M	Performance grade of modified binders (California)
RAP	Reclaimed asphalt pavement
RHMA	Rubberized hot-mix asphalt
RHMA-G	Gap-graded rubberized hot-mix asphalt
RHMA-O	Open-graded rubberized hot-mix asphalt
RLT	Repeated load triaxial
RTFO	Rolling thin-film oven
SBS	Styrene-butadiene-styrene
SCB	Semicircular bending test
SSD	Saturated surface dry
SUL	Sulfoxide area index
Superpave	SUperior PERforming asphalt PAVEment
UCPRC	University of California Pavement Research Center
UTSST	Uniaxial thermal stress and strain test
VFA	Voids filled with asphalt
VMA	Voids in mineral aggregate

TEST METHODS CITED IN THE TEXT

AASHTO

M 320 Standard Specification for Performance-Graded Asphalt Binder

M 323 Standard Specification for Superpave Volumetric Mix Design

PP 3 Standard Practice for Preparing Hot-Mix Asphalt (HMA) Specimens by Means of the Rolling Wheel Compactor

R 28 Standard Practice for Accelerated Aging of Asphalt Binder Using a Pressurized Aging Vessel (PAV)

R 30 Standard Practice for Mixture Conditioning of Hot-Mix Asphalt (HMA)

T 51 Standard Method of Test for Ductility of Asphalt Materials

T 84 Standard Method of Test for Specific Gravity and Absorption of Fine Aggregate

T 85 Standard Method of Test for Specific Gravity and Absorption of Coarse Aggregate

T 44 Standard Method of Test for Solubility of Bituminous Materials

T 164 Standard Method of Test for Quantitative Extraction of Asphalt Binder from Hot-Mix Asphalt (HMA)

T 166 Standard Method of Test for Bulk Specific Gravity (Gmb) of Compacted Hot-Mix Asphalt (HMA) Using Saturated Surface-Dry Specimens

T 209 Standard Method of Test for Theoretical Maximum Specific Gravity (Gmm) and Density of Hot-Mix Asphalt (HMA)

T 240 Standard Method of Test for Effect of Heat and Air on a Moving Film of Asphalt Binder (Rolling Thin-Film Oven Test)

T 308 Standard Method of Test for Determining the Asphalt Binder Content of Hot-Mix Asphalt (HMA) by the Ignition Method

T 312 Standard Method of Test for Preparing and Determining the Density of Asphalt Mix Specimens by Means of the Superpave Gyratory Compactor

T 313 Standard Method of Test for Determining the Flexural Creep Stiffness of Asphalt Binder Using the Bending Beam Rheometer

T 315 Standard Method of Test for Determining the Rheological Properties of Asphalt Binder Using a Dynamic Shear Rheometer

T 316 Standard Method of Test for Viscosity Determination of Asphalt Binder Using Rotational Viscometer

T 321 Standard Method of Test for Determining the Fatigue Life of Compacted Asphalt Mixtures Subjected to Repeated Flexural Bending

T 324 Standard Method of Test for Hamburg Wheel-Track Testing of Compacted Hot-MixAsphalt

T 331 Bulk Specific Gravity (Gmb) and Density of Compacted Hot-Mix Asphalt (HMA) Using Automatic Vacuum Sealing Method

T 350 Standard Method of Test for Multiple Stress Creep Recovery (MSCR) Test of Asphalt Binder Using a Dynamic Shear Rheometer (DSR)

T 378 Standard Method of Test for Determining the Dynamic Modulus and Flow Number for Asphalt Mixtures Using the Asphalt Mixture Performance Tester (AMPT)

TP 124 Provisional Standard Method of Test for Determining the Fracture Potential of Asphalt Mixtures Using Semicircular Bend Geometry (SCB) at Intermediate Temperature

ASTM

D 8303 Standard Test Method for Determining Thermal Cracking Properties of Asphalt Mixtures Through Measurement of Thermally Induced Stress and Strain

CONVERSION FACTORS

APPROXIMATE CONVERSIONS TO SI UNITS				
Symbol	**When You Know**	**Multiply By**	**To Find**	**Symbol**
LENGTH				
in.	inches	25.40	millimeters	mm
ft.	feet	0.3048	meters	m
yd.	yards	0.9144	meters	m
mi.	miles	1.609	kilometers	km
AREA				
in^2	square inches	645.2	square millimeters	mm^2
ft^2	square feet	0.09290	square meters	m^2
yd^2	square yards	0.8361	square meters	m^2
ac.	acres	0.4047	hectares	ha
mi^2	square miles	2.590	square kilometers	km^2
VOLUME				
fl. oz.	fluid ounces	29.57	milliliters	mL
gal.	gallons	3.785	liters	L
ft^3	cubic feet	0.02832	cubic meters	m^3
yd^3	cubic yards	0.7646	cubic meters	m^3
MASS				
oz.	ounces	28.35	grams	g
lb.	pounds	0.4536	kilograms	kg
T	short tons (2000 pounds)	0.9072	metric tons	t
TEMPERATURE (exact degrees)				
°F	Fahrenheit	(F-32)/1.8	Celsius	°C
FORCE and PRESSURE or STRESS				
lbf	pound-force	4.448	newtons	N
lbf/in^2	pound-force per square inch	6.895	kilopascals	kPa
APPROXIMATE CONVERSIONS FROM SI UNITS				
Symbol	**When You Know**	**Multiply By**	**To Find**	**Symbol**
LENGTH				
mm	millimeters	0.03937	inches	in.
m	meters	3.281	feet	ft.
m	meters	1.094	yards	yd.
km	kilometers	0.6214	miles	mi.
AREA				
mm^2	square millimeters	0.001550	square inches	in^2
m^2	square meters	10.76	square feet	ft^2
m^2	square meters	1.196	square yards	yd^2
ha	hectares	2.471	acres	ac.
km^2	square kilometers	0.3861	square miles	mi^2
VOLUME				
mL	milliliters	0.03381	fluid ounces	fl. oz.
L	liters	0.2642	gallons	gal.
m^3	cubic meters	35.31	cubic feet	ft^3
m^3	cubic meters	1.308	cubic yards	yd^3
MASS				
g	grams	0.03527	ounces	oz.
kg	kilograms	2.205	pounds	lb.
t	metric tons	1.102	short tons (2000 pounds)	T
TEMPERATURE (exact degrees)				
°C	Celsius	1.8C + 32	Fahrenheit	°F
FORCE and PRESSURE or STRESS				
N	newtons	0.2248	pound-force	lbf
kPa	kilopascals	0.1450	pound-force per square inch	lbf/in^2

* SI is the abbreviation for the International System of Units. Appropriate rounding should be made to comply with Section 4 of ASTM E380. (Revised April 2021)

Blank page

1. INTRODUCTION

1.1 Background to the Study

California continues to face the challenge of diverting more than 40 million scrap tires from landfills annually. The California Department of Resources Recycling and Recovery (CalRecycle) is responsible for finding new uses for waste tires. In recent years, CalRecycle has estimated that about 33 million (81%) of the approximately 40 million waste tires generated each year were diverted through various alternatives, including reuse, retreading, and combustion.

In 2005, the California Legislature passed, and the governor signed, Assembly Bill 338, which requires the California Department of Transportation (Caltrans) to use a specific percentage of crumb rubber per metric ton of the total amount of asphalt paving materials placed. As of 2013, Caltrans has been required to use, on an annual average, 11.58 lb. (5.2 kg) of crumb rubber per metric ton of the total amount of asphalt paving materials used in construction, maintenance, and rehabilitation of the state highway system.

In 2006, the Federal Highway Administration (FHWA) Recycled Materials Policy was established. This policy states that recycled materials should get first consideration in materials selection. The determination of the use of recycled materials should include an initial review of engineering and environmental suitability, followed by an assessment of economic benefit. Any restriction that prohibits the use of recycled materials without a technical basis should be removed from specifications.

In 2015, Caltrans changed its mission statement to include sustainability, with the goal of sustainability and stewardship to preserve and enhance California's resources and assets. As part of this mission, Caltrans initiated an investigation into the potential for further reducing landfill disposal of scrap tires by requiring that, in addition to the use of gap- and open-graded rubberized hot-mix asphalt overlays, consideration be given to using a relatively small amount of crumb rubber modifier (CRM) in dense-graded mixes. Small amounts are defined as between 5% and 10% by weight of the asphalt binder or between 0.25% and 0.5% by weight of the aggregate if dry CRM is used. This proposed expanded use of CRM was driven primarily by environmental

considerations and not enhanced performance, as has been the historical approach when considering new materials. The terms “CRM binder” and “CRM mix” are used in this report to describe binders and mixes modified with these small amounts of rubber.

1.2 Proposed Approaches

In 2015, Caltrans and industry identified the following four approaches for using small amounts of CRM in dense-graded asphalt concrete meeting current Caltrans specifications:

Approach-1: Wet Process with No Agitation, Complete Digestion

CRM binders meeting all current Superpave (SUperior PERforming asphalt PAVEments) performance grade (PG) specifications, with the addition of 5% to 10% CRM combined with other adjustments to the binder as needed so that there is no change to the project-specified PG of the unmodified binder (i.e., if the project specifications called for a PG 64-16 binder, the PG of the CRM binder needed to be PG 64-16). This could be achieved by blending softer base binders and/or polymers. It was anticipated that binders that already meet the current Caltrans modified performance grade specification (PG-M) would fall into this category.

Approach-2: Wet Process with Agitation, Incomplete Digestion

CRM binders meeting anticipated performance grade specifications for asphalt rubber binders (PG-AR) with changes to some components of the specification (e.g., solubility). It was anticipated that binders prepared using the same approach currently being used to prepare asphalt rubber binders used in gap- and open-graded mixes (i.e., CRM particles <2.36 mm [passing the #8 sieve]) and in chip seals (i.e., CRM particles <1.41 mm [passing the #14 sieve]), but with lower CRM contents (5% to 10% by weight of the binder) and potentially smaller CRM particles, would fall into this category. Some positive changes to the project-specified PG of the unmodified binder would be permitted (e.g., a CRM binder graded as PG 70-16, if the project specifications called for a PG 64-16 binder, would be acceptable, but a CRM binder graded as PG 70-10 or PG 58-16 would not be acceptable).

Approach-3: Dry process

Addition of between 0.25% and 0.5% CRM per ton of the aggregate (≈5 to 10 lb./ton [2.3 to 4.5 kg/ton]) using a dry process. Mixes containing this CRM would still need to meet all Caltrans specifications. The PG of the binder should not change if this approach is followed.

Approach-4: Wet Process with Agitation, Complete Digestion

Same as Approach-2, but using other recycled tire rubber formulations, typically with a finer CRM particle size, such as ground devulcanized tire rubber, which can be field-blended to achieve a binder containing between 5% and 10% CRM (by weight of the binder) that still meets PG specifications, but with potentially some relaxation (e.g., solubility and/or separation). Positive changes to the project-specified PG of the unmodified binder would be permitted.

1.3 Problem Statements

The following problem statements were identified in preparation for conducting the CRM binder study:

- In 2015, Caltrans did not have a clear identification of all materials, past and current, that may fall into each of the four categories listed in Section 1.2.
- The literature had not been reviewed to gather information regarding properties, performance, variability, and potential issues with specific reference to these four approaches.
- Apart from mixes produced with binders meeting the Caltrans PGM specification for modified binders, Caltrans had limited performance-related laboratory test results and field performance data covering binders and dense-graded mixes containing small amounts of CRM.
- Apart from mixes produced with binders meeting the Caltrans PGM specification, Caltrans had limited field construction experience with these specific approaches but did have extensive experience in all aspects of using CRM in gap- and open-graded mixes.

1.4 Study Objective/Goal

In 2015, Caltrans requested the University of California Pavement Research Center (UCPRC) evaluate the technical feasibility, life cycle cost analysis (LCCA), and environmental life cycle

assessment (LCA) of each of the four potential CRM binder/CRM mix approaches. The goal of the project was to provide the information needed for Caltrans to decide whether and how to move forward with each of the approaches and the technologies that fall within them. This goal was anticipated to be achieved through the completion of the following tasks:

1. Identification of various types of materials that may fall within each of the four categories.
2. Review of available literature regarding past or present technologies identified, including specifications, reports, and any other information (written or oral).
3. Testing and analysis of example materials to determine their capability of meeting current Superpave PG specifications, including comparison with currently specified materials in terms of expected performance. This includes binder and mix testing. It should be noted that the primary focus of laboratory testing was on accommodating additional CRM in binder/mixes and not on improving performance of the binder and mix, in line with the terms of reference provided to the UCPRC.
4. Mechanistic simulation/evaluation, using *CalME* mechanistic-empirical design software, of the effects of CRM mix properties on pavement performance in overlays with different thicknesses and new/reconstructed asphalt pavements for different levels of traffic in different climate regions.
5. An LCCA that includes identification of cost and performance data, and analysis of net present value, with sensitivity analysis, for materials within each category (not funded in this phase of the study).
6. An LCA that includes the development of environmental flow data, calculation of impacts, and interpretation and reporting of the results (not funded in this phase of the study).
7. Performance monitoring of pilot studies (not funded in this phase of the study).
8. Assistance with the development of test methods, methods of determining CRM content, specification language, and guidelines (not funded in this phase of the study).
9. Reporting of all results.

This report provides an update on work completed to date in Task 1 through Task 4.

1.5 Report Structure

This report includes the following chapters and appendices, which address the tasks discussed in Section 1.4:

- Chapter 2 covers materials and processes for CRM binder and CRM mix Approaches, addressing Task 1.
- Chapter 3 summarizes the literature relevant to CRM binder and CRM mix initiatives, addressing Task 2.

- Chapter 4 details the material sampling and preparation procedures and experimental designs that were followed to address Task 3.
- Chapters 5 through 8 discuss the evaluation of each approach in terms of binder and mix performance, addressing Task 3.
- Chapter 9 covers the *CalME* simulations using the results presented in Chapters 5 through 8, addressing Task 4.
- Chapter 10 provides conclusions and recommendations.
- Appendix A through Appendix E include testing and simulation results, supporting Chapters 5 through 8.

1.6 Measurement Units

Although Caltrans recently returned to the use of US standard measurement units, metric units have always been used by the UCPRC for laboratory, Heavy Vehicle Simulator, and field measurements and data storage. In this report, both English and metric units (provided in parentheses after the English units) are provided in general discussion. In keeping with convention, metric units are used in laboratory data analyses and reporting. Note that Superpave asphalt binder performance grading procedures all use metric units as standard. A conversion table is provided on page xxvii.

Blank page

2. MATERIALS AND PROCESSES FOR CRM BINDER AND MIX APPROACHES

2.1 Introduction

This chapter addresses Task 1 of the study focusing on identification of various types of materials that may fall within each of the four CRM binder and CRM mix approaches.

2.2 Materials and Processes for Approach-1

Based on the California Asphalt Rubber Usage Guideline *(1)*, a CRM binder for Approach-1 would be produced using a "wet process with no agitation" method. In this process, hot asphalt binder and crumb rubber modifier (CRM, typically passing the #60 [250 µm] or finer sieve) would be blended in the refinery or at an asphalt binder terminal. No subsequent agitation with a special auger or paddles would be required to disperse the CRM particles in the binder phase because CRM particles are usually digested or dispersed uniformly by circulation of the binder within the storage tank. This approach typically requires that the CRM particles be smaller than 250 µm and fully digested in the binder to be able to pass the solubility test at the 99% minimum. Approach-1 materials would be subject to meeting both performance grade binder and dense-graded mix design testing specifications.

PG tests can be performed on this type of binder following the specified procedure in the AASHTO or ASTM standards for conventional asphalt binder without any modification of testing equipment, methods, or grading criteria.

2.3 Materials and Processes for Approach-2

According to the California Asphalt Rubber Usage Guideline, Approach-2 CRM binders would be categorized as "wet process, field-blended binder with agitation." This binder would be produced following the same methods used to produce asphalt rubber binders that are currently used in gap- and open-graded rubberized asphalt concrete mixes and in rubberized chip seals. The apparent main difference from current asphalt rubber binder specifications would be that the CRM content is between 5% and 10% by weight of the binder, instead of the currently specified 18% to 22%. Approach-2 materials would be subject to meeting both performance grade binder (with the possible relaxation of solubility requirements) and dense-graded mix design testing

specifications. Any proposed PG binder-type grading specifications would need to factor in the presence of larger, incompletely digested CRM particles and higher mix production temperatures, which will require adjustments to dynamic shear rheometer (DSR), rolling thin film oven (RTFO), pressure-aging vessel (PAV), and bending beam rheometer (BBR) testing procedures.

Performance grading tests and procedures for testing asphalt rubber binders with particle sizes up to 2.36 mm in size (i.e., passing the #8 sieve) are currently being finalized at the UCPRC *(2)* and were used for this study.

2.4 Materials and Processes for Approach-3

Based on the California Asphalt Binder Usage Guideline, CRM used in this approach would act as a portion of the aggregate structure when used in the dry process. The CRM content in the standard dry process is normally between 1% and 3% by total weight of the mix; however, CRM mixes would typically only contain between 0.25% and 0.5% CRM by total weight of the mix. Consequently, the need to alter the gradation of the mix to accommodate the CRM particles, which have significantly lower densities than the granular aggregates, is unlikely. Different sizes of CRM can be used. Given that the CRM is not being used to modify the binder, Approach-3 materials would be subject to meeting dense-graded mix design testing specifications only.

2.4.1 Materials and Processes for Approach-4

According to the California Asphalt Rubber Usage Guideline, Approach-4 CRM binders would also be categorized as “wet process, field-blended binder with agitation.” However, these binders would differ from Approach-2 binders in that finer gradation CRM particles would be used to reduce reaction time and to provide a more homogenous binder with full digestion of the particles. Devulcanized and other commercially available recycled tire products were considered in this study as Approach-4 materials. Approach-4 materials would be subject to meeting both performance grade binder and dense-graded mix design testing specifications but with some relaxation for certain attributes (e.g., solubility in binder tests).

3. LITERATURE REVIEW

3.1 Introduction

This literature review, addressing Task 2 of the project workplan, is based on a search of relevant available reports, journals, specifications, and other written documentation identified through search engines and information databases, and in the older paper documents available in the UCPRC library.

Although there is considerable published information on the modification of asphalt binders and mixes using recycled tire rubber, the literature review found very limited information specifically relevant to the goals of the CRM initiative (i.e., adding small amounts of CRM to asphalt binder). Key issues that may be relevant in terms of identifying testing procedures and interpreting test results are summarized below.

3.2 Background

Recycled tire rubber modifier used in pavement applications is known as either crumb rubber modifier (CRM, used in this report) or ground tire rubber (GTR), which is produced from scrap tires and some other waste rubber materials. Rubber modifiers have been widely used in the pavement industry because of their engineering and environmental benefits.

In California, binder used in rubberized hot-mix asphalt (RHMA) must contain between 18% and 22% CRM by weight of the binder. RHMA generally has a longer service life than conventional hot-mix asphalt (HMA) in thin overlays (i.e., ≤0.2 ft. [60 mm]), which is credited to its improved resistance to the initiation and propagation of fatigue and reflective cracks. RHMA typically requires less maintenance during its service life cycle, which usually results in lower life cycle costs than conventional HMA in thin overlay applications.

Using RHMA also has environmental benefits. In California, the use of CRM in RHMA diverted more than 5.5 million waste tires from landfills or tire stockpiles in 2018 *(3)*. Open-graded RHMA (RHMA-O) surface layers also generate less traffic noise than surfaces paved with conventional HMA and retain the noise reduction longer than conventional open-graded mixes (OGFC) *(4-6)*.

Several states use rubberized asphalt in pavements, including Arizona, Arkansas, California, Florida, Georgia, Kansas, Louisiana, Michigan, Mississippi, New Jersey, Texas, and Wisconsin. According to the US Environmental Protection Agency, California and Arizona were the leaders in CRM use in 2016, followed by Florida. Approximately 12 million tires are recycled and used in paving applications annually in the United States *(7)*.

In California, typical applications of CRM in pavement engineering include chip seals, stress absorbing membrane interlayers, gap-graded rubberized hot-mix asphalt (RHMA-G), and open-graded rubberized hot-mix asphalt (RHMA-O). Field observations on pavement experiments starting in the late 1970s followed by comprehensive laboratory and accelerated pavement testing by the UCPRC starting in the early 1990s *(8)* showed that the use of RHMA significantly prolonged service life and improved reflective cracking resistance. RHMA-O provided good surface friction and better durability than conventional OGFC *(5,6)*. RHMA-G was found to be a cost-effective overlay, allowing for a 50% thickness reduction compared to conventional HMA overlays with respect to reflective cracking *(9,10)*. Later laboratory and field studies showed that newly paved RHMA-G and RHMA-O could reduce traffic noise by 1.0 dBA and 1.9 dBA, respectively, over a 10-year service life compared to conventional HMA *(5,6)*.

Given these benefits, Caltrans expressed interest in 2015 in investigating potential additional applications to increase CRM use to help meet legislative requirements. According to the California Public Resource Code section 42703(a), Caltrans must use an average of 11.58 lb. of CRM per metric ton of asphalt concrete placed, which equates to about 35% of the total amount of asphalt concrete placed by the agency *(3)*. Figure 3.1 illustrates this rubber use objective and actual use up to 2018 *(3)*. Usage in 2018 was 46.4%, notably higher than the 35% target.

3.3 States Permitting the Use of Recycled Tire Rubber in Binder Modification

Published information documenting research on the use of recycled tire rubber in asphalt binders and mixes was sourced from numerous states, including Arizona, Arkansas, California, Florida, Georgia, Kansas, Louisiana, Massachusetts, Michigan, Mississippi, New Jersey, Texas, and Wisconsin. Most recent research has focused on mixes prepared with terminal blend (i.e., Approach-1) binders.

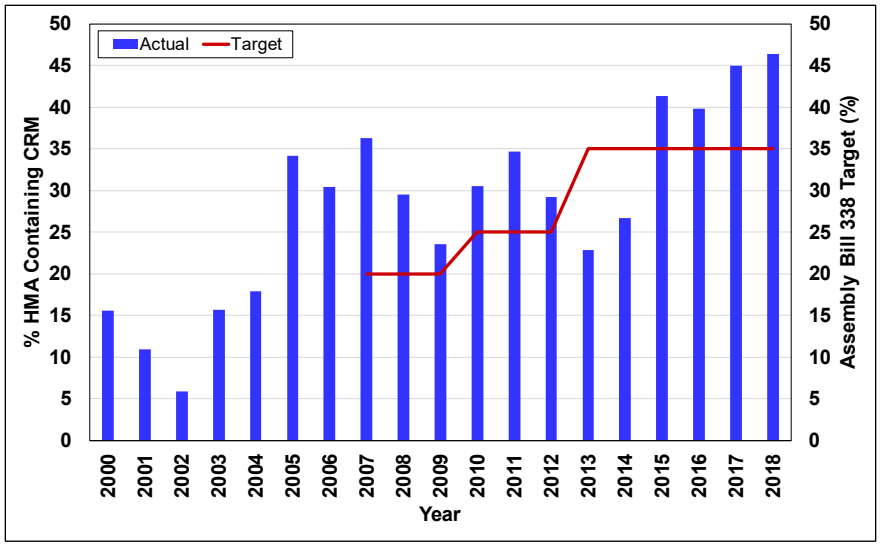

Figure 3.1: CRM application by Caltrans *(3)*.

The experience of transportation departments in Florida and Louisiana that are applicable to Approach-1 and potentially applicable to Approach-4 CRM binders are summarized as follows:

- The Florida Department of Transportation (DOT) started using rubber-modified binders in the late 1990s. Up to 5% CRM with particles smaller than 300 µm (passing the #50 sieve) is permitted in binders used in dense-graded mixes, and up to 12% CRM with particles smaller than 600 µm (passing the #30 sieve) is permitted in binders used in open-graded mixes. Long-term monitoring of pavement sections showed that these mixes produced with tire rubber-modified binders exhibited a better friction index, better rutting resistance, and better durability *(11,10)*. In 2015, Florida DOT published a PG 76-22 asphalt rubber binder (ARB) specification, which required a minimum of 7% CRM by weight of the binder. This PG 76-22 binder is required to meet all criteria specified in AASHTO M 320 except for solubility, which has been removed as a requirement. Laboratory and accelerated wheel load test results indicated that dense-graded mixes containing this PG 76-22 ARB binder provided similar rutting and cracking resistance to the same mix produced with PG 76-22 modified with styrene-butadiene-styrene (SBS) modified binder *(9,12)*.
- The Louisiana DOT investigated adding up to 9% CRM in unmodified PG 64-22 binders using a terminal-blending process to produce PG 76-22 rubber-modified binders. Laboratory and accelerated wheel load test results indicated that this rubber-modified binder provided comparable performance to PG 76-22 SBS-modified binders *(13)*. The Louisiana DOT does not have a solubility requirement for rubber-modified binders.

3.4 Factors Effecting Binder Rheology Specific to CRM Binders

3.4.1 Effect of Rubber Grinding Method

All states using recycled tire rubber as an asphalt modifier appear to require ambient-ground CRM.

3.4.2 Effect of CRM Content on Binder Properties

Considerable published research has been conducted on the effect of CRM content on binder properties. However, only the literature focusing on CRM contents below 10% by weight of the binder was reviewed *(14-26)*. All of these studies noted clear changes in binder rheology after the addition of as little as 3% CRM by weight of the binder, with the degree of change increasing with increasing CRM content. Key rheological properties affected include higher viscosity, increased stiffness, reduced phase angle, lower creep stiffness, and reduced storage stability when compared to the unmodified control base binder. The low-temperature m-value property did not appear to be influenced by increasing the CRM content by up to 10%.

3.4.3 Effect of CRM Particle Size on Binder Properties

The surface area of CRM particles increases with decreasing particle size. Consequently, smaller particles are likely to interact with the base binder more effectively than larger particles, leading to potentially shorter reaction times at lower blending temperatures, and to improve storage stability (i.e., the period before separation of the CRM particles from the asphalt begins). Larger particle surface areas also facilitate absorption of the light oils in the base binder, which promotes digestion of the CRM. Several published studies have focused on evaluating the impact of CRM particle size on the properties of asphalt rubber binders *(27-33)*. Unfortunately, there was little standardization of the sizes of CRM particles assessed (passing the #200 [75 µm] up to #8 [2.36 mm] sieves) with no clear distinction of the boundary between what was considered to be fine and coarse. However, the studies generally concluded that digestion times, phase angle, and fatigue cracking resistance decreased with decreasing particle size, while stability, viscosity, stiffness, and rutting resistance all increased with decreasing particle size. Low-temperature creep stiffness did not appear to be significantly influenced by CRM particle size. Binder contents in mixes also tended to decrease with decreasing CRM particle size used in the binder given that gaps in the aggregate gradation can be smaller.

3.5 Dry Process Rubberized Asphalt Mixes

Most published research on dry process rubberized asphalt mixes has focused on comparisons of performance between dry and wet processes, based on expectations of performance improvement rather than initiatives that use small amounts of CRM primarily as a means of using more waste tires. Most studies used higher percentages of CRM than those proposed by Caltrans for this study (i.e., typically higher than an equivalent of 0.5% by weight of the mix). Key findings that were documented in studies *(15,26,34–39)* comparing dry and wet processes are summarized below. It should be noted that comprehensive research to improve dry process rubberized asphalt mix performance is currently being undertaken in a number of states and that some of the issues identified below may have been addressed through improved asphalt plant production procedures.

- The dry CRM did not effectively react with the asphalt binder.
- Dry process mixes had poorer compaction (i.e., higher air void contents).
- Dry process mixes had poor distribution of the CRM through the mix.
- Dry process mixes exhibited poorer cohesion between the binder and the aggregate leading to increased moisture sensitivity.
- Dry process mixes generally had poorer rutting and fatigue cracking resistance, and higher variability in performance parameters.
- The differences in performance between the two processes lessened in significance with decreasing CRM content and decreasing CRM particle size.
- Dry process mixes were considerably cheaper to produce than wet process mixes given the ease of adding it to the mix and the absence of a need for any significant plant modifications.

One study *(40)* investigated adding 0.5% CRM by total weight of the mix in a dry process to a mix produced with terminal blend rubber-modified binder with the objective of increasing total CRM content. The CRM particles used in the tests were smaller than 1.18 mm (i.e., passing the #16 sieve) and were treated with extender oils before being added to the mix. Tests were carried out to compare rutting and cracking performance of the mixes with and without addition of the dry process CRM. The results indicated that the rutting performance of the dry process mix diminished but the fatigue cracking resistance improved.

3.6 Engineered Rubber Products

Engineered rubber projects include devulcanized tire rubber as well as a number of proprietary formulations made from waste tires that can be used to modify asphalt. Simplification of the blending process is usually the primary reason for their use *(41–43)*. A number of published studies have compared devulcanized rubber-modified binders with conventional asphalt rubber binders and with SBS-modified binders *(44–46)*. Findings from these studies indicate that devulcanized rubber-modified binders can be prepared at lower temperatures than conventional binders and that they generally have lower high-temperature viscosities. No differences in rutting and cracking performance or in moisture resistance were noted between the three binder types.

3.7 Binder Testing Issues

The overall rubber-binder interaction in the rubber-modified binder is complex. It is generally accepted that the evaluation criteria of rubber-modified binders should focus on physical properties rather than on chemical properties *(15)*.

The UCPRC is currently finalizing the development of a Superpave-type performance grading testing procedure for asphalt rubber binders *(2)*. The standard AASHTO M 320 procedure is not considered appropriate given that the maximum CRM particle size permitted in the Caltrans specifications (i.e., 100% passing the #8 [2.36 mm] sieve) exceeds by a considerable margin the maximum recommended size for testing with a 25 mm diameter parallel plate with 1 or 2 mm gap geometry in a DSR. The gap size should be a minimum of four times the size of the maximum particle size *(47,48)*. Removal of larger incompletely digested CRM particles (i.e., >500 µm) to allow testing with 2 mm gap parallel plate geometry, and testing in a concentric cylinder geometry with a 6 mm gap, based on initial work by the FHWA *(49)*, are currently being investigated. Modified procedures for RTFO- and PAV-aging, and modified BBR specimen preparation procedures, are also being developed to better represent plant production and field conditions.

A parallel study by a Caltrans task group investigated using 25 mm parallel plate geometry with a 3 mm gap *(50)*. However, this study focused primarily on asphalt rubber binders used in chip

seals, where the maximum CRM particle size is limited to 1.0 mm (i.e., passing the #14 [1.4 mm] sieve) to prevent spray nozzle blockages. The study did not compare other procedures.

In this study, the standard Superpave PG method was used to test Approach-1 and Approach-4 CRM binders containing CRM particles smaller than 250 µm. The modified Superpave PG method discussed in the UCPRC report *(2)* was used to grade Approach-2 CRM binders containing CRM particles smaller than 2.36 mm.

3.8 Mix Testing Issues

No references to any significant potential issues with regard to testing mixes prepared using any of the proposed CRM binder and CRM mix approaches were found during the literature review and none were anticipated. However, based on a general discussion in the literature, the following factors would need to be taken into consideration during any future mix testing:

- A hold time, as used for RHMA-G mixes, may still be required after compacting specimens (gyratory or rolling wheel) prepared with rubber-modified binders with smaller rubber contents, given the tendency of the CRM in the specimens to continue swelling while still hot. A similar hold time to that listed in the current Caltrans specifications for RHMA-G was proposed as an interim measure.
- At least three replicates should be tested in any procedure given that the very small amounts of CRM being added may have little to no effect on some test results. Test results and comparisons of results of control and modified specimens need to be interpreted with care given that the variation in results may be within the precision and bias range of a given test (i.e., what appears to be a difference in performance between a control specimen and a specimen prepared with a rubber-modified binder may be attributable to the expected variability in results for that test).
- Adding between 0.25% and 0.5% dry CRM by total weight of the mix to the dry mix ingredients prepared for compacting laboratory test specifications may not be representative of production-scale mixes. Between 18 and 37 g of CRM is added to the 7.0 kg of aggregate typically required to prepare gyratory-compacted specimens. The very small amount of dry rubber, small specimen sizes, and random CRM distribution in the specimen may result in some variability in laboratory test results.

3.9 Pavement Performance Simulation Issues

Incorporation of CRM into asphalt binder changes the rheological properties, which in turn can influence mix stiffness. Over the service life, rubber-modified mixes appear to age more slowly

than conventional asphalt mixes, which also affects mix stiffness. These changes in mix stiffness influence pavement performance over time.

Recent studies showed that oxidative aging might occur deeper than the top 20 mm (0.75 in.) of the pavement surface *(51,52)*, which in turn can have a greater effect on pavement performance. The aged binder is stiffer than the original unaged binder, which can have either a positive or negative affect on performance depending on layer thickness and location of the layer in the pavement structure *(53)*, given that traffic loading, mix stiffness, and relationships between stiffness, fatigue life, and tensile strain all affect bottom-up fatigue cracking. Although stiffer mixes are generally better for thicker pavements and softer mixes are generally better for thinner pavements, mechanistic analyses are required to determine the optimal application for mixes with different stiffness and fatigue properties at different strain scenarios. This concept is illustrated in Figure 3.2 *(54)*.

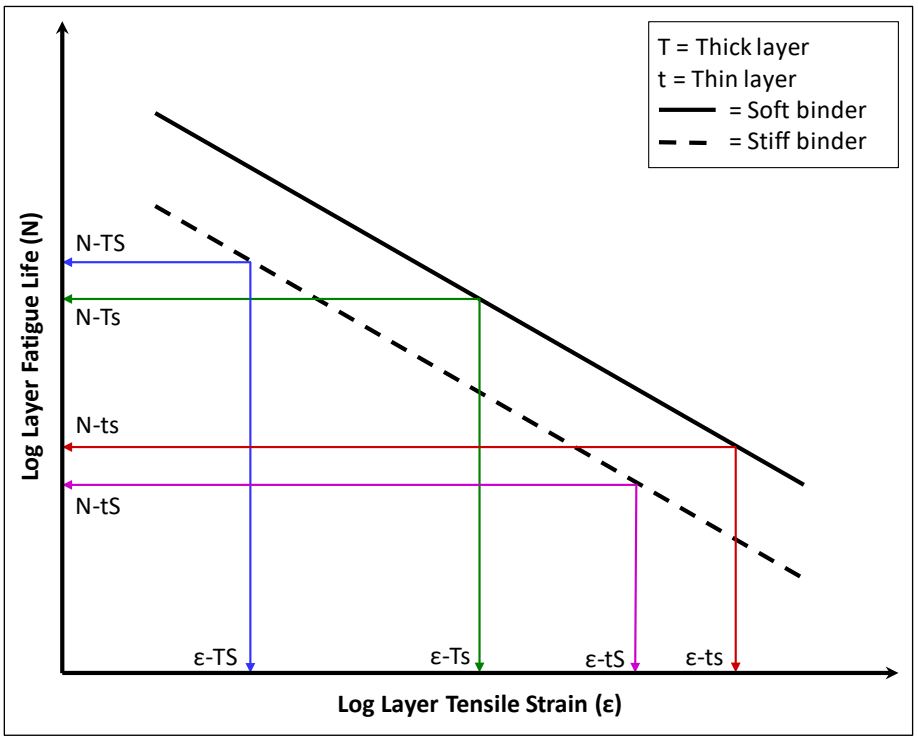

Figure 3.2: General rules of fatigue resistance and stiffness *(54)*.

In general, a relatively thin pavement layer (i.e., ≤0.2 ft. [60 mm]) is strain controlled. Stiffening of the binder generates more dissipated energy in the mix caused by strains from traffic and environmental loading (i.e., daily temperature fluctuations cause thermal stresses), but because

the layer is thin the increased stiffness does not decrease the strains from traffic. This decreases the time to failure for reflective cracking and bottom-up fatigue cracking. Stiffer mixes also have a lower strain-at-break caused by extreme cold temperatures resulting in top-down thermal-cracking. Conversely, thicker asphalt layers (i.e., >0.2 ft. [60 mm]) are primarily stress-controlled. Stiffening of the binder can reduce layer bending and associated tensile strains, which have a greater influence than the decreased fatigue life at a given strain, with the net effect of reducing the risk of reflective and fatigue cracking.

Rubber-modified binders appear to have a slower rate of aging than unmodified binders, indicating that rubber-modified mixes will have a slower increase in stiffening caused by oxidation. In Figure 3.2, rubber-modified binder performance after long-term oxidative aging is plotted as the solid line and conventional unmodified binder is plotted as a dashed line, which is beneficial when used in thin layers *(13,55)*.

The performance of rubber-modified mixes in other pavement structures, such as thick surface layers, is not well understood and will require project-specific mechanistic-empirical simulations to identify suitable applications.

3.10 Literature Review Summary

Many states have specifications that allow tire rubber as a substitution for SBS modification (e.g., California [PG-M], Florida [PG-ARB], and Louisiana [PG-CRM]), and their properties are similar to Approach-1 discussed in this study. Limited published research on Approach-2, Approach-3, and Approach-4 modification was found.

Although considerable research has been undertaken to understand the advantages and disadvantages of using recycled tire rubber to modify asphalt binders, no published information was found on initiatives focusing on adding small amounts of CRM to hot-mix asphalt as a means of disposing of scrap tires rather than for binder modification to improve performance.

Preliminary indications from this literature review include the following:

- Binders modified using Approach-1, Approach-2, and Approach-4 will be influenced by the CRM content and CRM particle size. Mix properties prepared using Approach-3 are also likely to be influenced by CRM content and particle size.

- It is unlikely that the performance grade of CRM binders prepared using Approach-2 and Approach-4 will be the same as that of the base binder. A one-grade bump in the high-temperature grade can be expected if 5% CRM by weight of the binder is added, and a two-grade bump is likely when between 5% and 10% CRM is added.
- The use of smaller CRM particles (i.e., less than 1.4 mm) in Approach-2 and Approach-3 binders will probably have less effect on the binder and mix properties than larger CRM particles (i.e., up to 2.36 mm).
- Although the objective of this investigation is to use more recycled tire rubber in asphalt pavement, some benefits, including improved moisture resistance and improved rutting and fatigue cracking resistance, are still likely despite the small quantities of CRM used.

4. MATERIAL PREPARATION AND EXPERIMENTAL DESIGN

4.1 Introduction

This chapter discusses the material collection and experimental design for addressing the study objectives. The selected CRM technologies were commercially available, and there was agreement with Caltrans on which ones to include in the study as examples for their group before any testing was started. Industry suppliers were asked to review the study plan and agree to it prior to providing their technologies for testing. All binder samples provided to the UCPRC were guaranteed by the suppliers to meet the requirements for the respective approach. The UCPRC did not witness the preparation of any of the CRM binders.

4.2 Materials

Binders for the study were received from six different sources. Where applicable, the unmodified base binders were also obtained for control purposes. All binders were stored at the UCPRC in a temperature-controlled room maintained at 25°C (≈77°F).

4.2.1 Approach-1 Binders

Approach-1 binders were supplied by two refineries (Refinery-A and Refinery-B in this report), and both met the Caltrans PG-M specification. Refinery-B provided an incomplete set of binders, which prevented any detailed comparisons between binders. Binder test results for this supplier are included for informational purposes. No mixes were produced with Refinery-B binders.

During binder production, unmodified base binders were blended with CRM particles, reported by both suppliers to be smaller than 250 µm (passing the #60 sieve), into a 25% concentrate by weight of the binder. Base binder performance grade (PG) was selected by the supplier to ensure that the CRM binder met the target PG. The concentrated rubber-modified binders were then blended with additional softer binders (PG 58-28) and/or additives (e.g., styrene-butadiene-styrene [SBS] and/or other polymers) to achieve the final 5% and 10% CRM content by weight of the binder.

Samples of the base binders were supplied for use as control binders in the study. The PG 64-16 control binder from Refinery-A was also used in Approach-3 mixes with dry-process CRM.

4.2.2 Approach-2 Binders

Approach-2 binders were produced at two Sacramento asphalt plants (Supplier-D and Supplier-F in this report) following standard asphalt rubber field-blending procedures, but with target CRM contents of 5% and 10% that are lower than the 18% to 22% used in standard asphalt rubber binders.

Supplier-D provided two modified binders, one produced with a maximum CRM particle size of 2.0 mm (i.e., passing the 2.36 mm [#8] sieve] and one produced with a maximum CRM particle size of 1.0 mm (i.e., passing the 1.18 mm [#16] sieve]). A PG 64-22 base binder was used for both.

Supplier-F provided one modified binder produced with the coarser (i.e., passing 2.36 mm) CRM and an unmodified PG 64-22 binder from a different source to that used by Supplier-D.

Both suppliers reported that they did not use extender oils and that blending temperature was 190°C (≈375°F). CRM gradations from Supplier-D are shown in Figure 4.1.

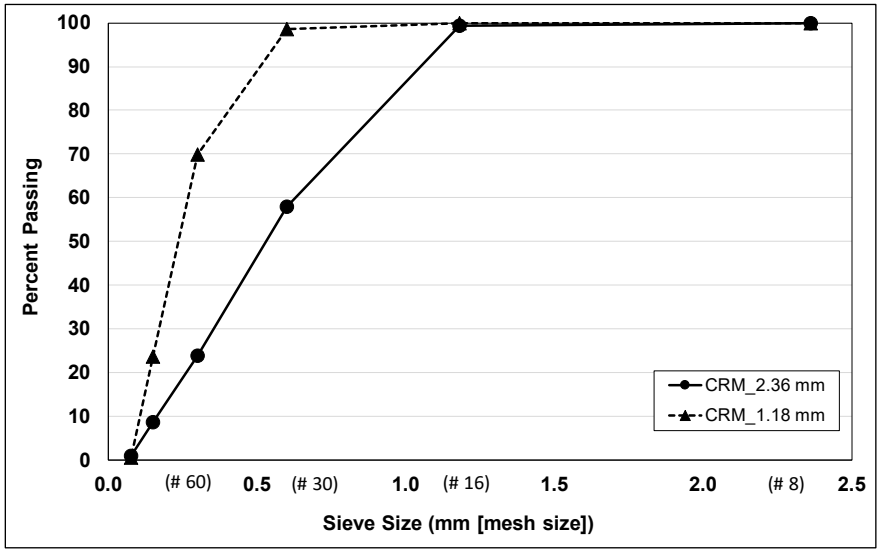

Figure 4.1: Sieve analyses of the CRM samples from Supplier-D.

4.2.3 Approach-4 Binders

Approach-4 binders were provided by two suppliers (Supplier-C and Supplier-D in this report). The unmodified PG 64-22 base binder sourced from Refinery-A and used as the control for the Approach-1 binders and mixes from that refinery was provided to both suppliers to produce their binders.

Supplier-C produced a concentrated binder with 25% devulcanized rubber by weight of the binder. CRM particles used were <250 µm (passing the #60 sieve) and were supplied in a soluble pellet form. This concentrated binder was then diluted at the UCPRC using the same PG 64-22 base binder to achieve the target 5% and 10% CRM content.

Supplier-D followed a similar process to Supplier-C, but used untreated but finer, ambient-ground CRM particles (passing a 180 µm [#80] sieve).

4.2.4 Aggregates

All mixes were prepared using a single aggregate source (crushed alluvial) sampled from an asphalt plant in Sacramento. Reclaimed asphalt pavement (RAP) was sampled from the same plant. Mix designs were based on a Caltrans-approved Type-A hot-mix asphalt (HMA) job mix formula (JMF) provided by the asphalt plant.

The virgin aggregates included five bins: 3/4 in., 1/2 in., 3/8 in., 1/4 in. dust, and natural sand. RAP was added at a rate of 15% by weight of the virgin aggregate. Bin gradations and percentage of each bin used in the mix provided by the aggregate supplier are provided in Table 4.1.

Table 4.1: Aggregate Gradation Distribution

Sieve Size (mm [in./#])	3/4 in. (% passing)	1/2 in. (% passing)	3/8 in. (% passing)	1/4'' Dust (% passing)	Sand (% passing)	3/8'' RAP (% passing)
25 (1)	100.0	100.0	100.0	100.0	100.0	100.0
19 (3/4)	95.3	100.0	100.0	100.0	100.0	100.0
12.5 (1/2)	41.7	86.7	100.0	100.0	100.0	99.9
9.5 (3/8)	20.2	31.7	96.4	100.0	100.0	97.2
4.75 (#4)	7.5	1.1	29.0	95.7	99.8	64.9
2.36 (#8)	4.1	1.0	7.8	66.1	89.8	40.6
1.18 (#16)	2.8	1.0	4.9	46.3	76.8	28.0
0.60 (#30)	2.1	1.0	4.2	34.6	50.0	20.2
0.30 (#50)	1.7	1.0	3.5	25.7	20.0	12.8
0.15 (#100)	1.3	1.0	3.0	18.8	8.2	6.8
0.075 (#200)	1.3	0.7	2.8	12.9	2.8	2.3
% of mix gradation	15	12	27	22	9	15

Sampled aggregates and RAP were dried at 110°C (230°F) and 60°C (140°F), respectively for 24 hours and then stored in sealed buckets until batching. Batched samples were prepared using the same bin percentages listed in the supplied JMF.

The bulk specific gravity (Gmb) and the absorption of aggregates were calculated by the saturated-surface-dry method following AASHTO T 84 and T 85. Table 4.2 summarizes the bulk specific gravities of the coarse, fine, and combined portions of the batched aggregates.

Table 4.2: Aggregate Bulk Specific Gravity

Bulk Specific Gravity						
Virgin Aggregate			RAP Aggregate			Combined
Coarse	Fine	Combined	Coarse	Fine	Combined	Virgin & RAP
2.76	2.65	2.71	2.70	2.63	2.65	2.70

Table 4.3 and Figure 4.2 show that both the original mix design gradation from the supplier and the laboratory gradation produced by the UCPRC met the Caltrans 3/4 in. nominal maximum aggregate size (NMAS) gradation specifications for Type-A HMA. The UCPRC laboratory gradation was slightly finer than the supplier's JMF gradation.

Table 4.3: Aggregate Gradations

Testing Laboratory	Aggregate Gradation (% passing)					
	3/4 in. (19 mm)	1/2 in. (12.5 mm)	#4 (4.75 mm)	#8 (2.36 mm)	#30 (0.6 mm)	#200 (0.075 mm)
Supplier	98.5	84.1	46.2	30.6	16.3	4.2
UCPRC	99.3	89.6	48.8	31.5	16.6	4.5

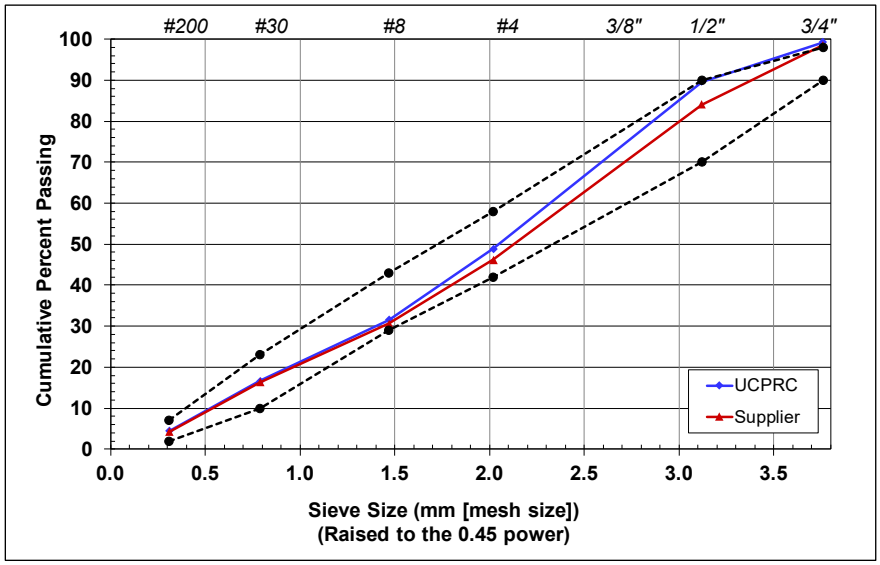

Figure 4.2: Plot of aggregate gradation.

Binder content in the RAP was determined by chemical extraction (AASHTO T 164) in accordance with Caltrans specifications. The test results indicated a binder content of 4.0% by dry weight of

the aggregate (DWA), which is close to the value (4.39%) listed in the supplied JMF. The aggregate gradation in the RAP was determined after ignition of the RAP binder (AASHTO T 308).

An optimum binder content (OBC) was determined for each CRM mix following the Superpave mix design method to account for any differences in the supplied binders. Mix designs are discussed separately for each approach in Chapters 5 through 8.

4.3 Experiment Design

All of the binders prepared for each Approach were tested. However, due to time and funding constraints, mix testing was carried out following a partial factorial that tested at least one group of mixes (control, 5% CRM and 10% CRM) in each approach. Table 4.4 summarizes the binders and mixes that were tested in each Approach. Binder identification codes include the following information:

Source_Base binder PG_CRM content_CRM size_(SBS content if applicable)

4.4 Asphalt Binder Testing Experimental Design

The following binder tests were conducted to evaluate and characterize the properties of the CRM binders:

- Performance grading of the binders.
- Multiple stress creep and recovery (MSCR) tests on Approach-1, Approach-2, and Approach-4 binders to characterize permanent deformation resistance.
- Frequency sweep (FS) tests on Approach-1, Approach-2, and Approach-4 binders to evaluate binder stiffness.
- Solubility and ductility tests on Approach-1 and Approach-4 binders to evaluate CRM particle digestion and binder ductility.
- Fourier Transform Infrared (FTIR) spectroscopy tests on Approach-1, Approach-2, and Approach-4 binders to track any changes in binder chemistry after aging.

Table 4.5 through Table 4.7 summarize the binder test factors and factor levels used in this study.

4.4.1 Performance-Grading

A dynamic shear rheometer (DSR) was used to determine the binder PG following AASHTO T 315. The standard Superpave PG method was used to evaluate the control and the Approach-1 and Approach-4 CRM binders (CRM size <250 µm). A modified Superpave PG method (concentric

cylinder geometry) currently being developed by the UCPRC *(2)* for asphalt rubber binders (PG-AR) was used to evaluate the Approach-2 CRM binders (CRM size <2.36 mm). All Approach-2 binders were tested as-produced (i.e., incompletely digested CRM particles >500 µm were not removed prior to testing) and consequently the results may have been influenced by the presence of these particles given that asphalt binder and CRM particles age differently.

Table 4.4: Summary of Binder and Mix Testing

Approach	Refinery/ Supplier Code	Blending Method	CRM Content (%)	Maximum CRM Size (mm)	SBS Content (%)	Binder Identification Code[a]	Mix ID
1	A	Control	0	N/A	0	A_64-16	A
		Terminal	5	0.25	N/A	A_64-16_5_0.25	B
		Terminal	10	0.25	N/A	A_64-16_10_0.25	C
		Control	0	N/A	0	A_70-10	D
		Terminal	5	0.25	N/A	A_70-10_5_0.25	E
		Terminal	10	0.25	N/A	A_70-10_10_0.25	F
	B	Control	0	N/A	0	B_64-16	-
		Terminal	5	0.25	0	B_64-22_5_0.25	-
		Terminal	10	0.25	0	B_70-16_10_0.25	-
		Terminal	5	0.25	3.5	B_64-28_5_0.25_3.5SBS	-
		Terminal	10	0.25	3.5	B_70-22_10_0.25_3.5SBS	-
		Terminal	0	N/A	3.5	B_64-22_3.5SBS	-
		Terminal	0	N/A	3.5	B_70-22_3.5SBS	-
2	D	Control	0	N/A	0	D_64-22	S
		Field	5	2.36	0	D_64-22_5_2.36	T
		Field	10	2.36	0	D_64-22_10_2.36	U
		Field	5	1.18	0	D_64-22_5_1.18	V
		Field	10	1.18	0	D_64-22_10_1.18	W
	F	Control	0	N/A	0	F_64-22	P
		Field	5	2.36	0	F_64-22_5_2.36	Q
		Field	10	2.36	0	F_64-22_10_2.36	R
3	A	Dry	5	2.36	0	A_64-16_5_2.36_DRY	G
		Dry	10	2.36	0	A_64-16_10_2.36_DRY	H
4	C	Control	0	N/A	0	A_64-22	J
		Field	5	0.25	0	C_64-22_5_0.25	K
		Field	10	0.25	0	C_64-22_10_0.25	L
	D	Control	0	N/A	0	A_64-22	J
		Field	5	0.18	0	D_64-22_5_0.18	-
		Field	10	0.18	0	D_64-22_10_0.18	-

[a] Binder ID format: binder source_PG_CRM content in percentage_maximum CRM particle size in mm.

Table 4.5: Approach-1 Binders: Factors and Factorial Levels

Factor	Factorial Levels	Details
Binder source	2	Two refineries, one from California
Modified binder PG	2	PG 64-16 and PG 70-10
CRM content	3	0%, 5%, and 10% by total weight of the binder
CRM size	1	<250 µm (passing #60 sieve)
SBS polymer content	2	0% and 3.5% by total weight of the binder in select binders
Total number of binders tested: 13		

Table 4.6: Approach-2 Binders: Factors and Factorial Levels

Factor	Factorial Levels	Details
Binder source	2	Supplier-D and Supplier-F
Base binder PG	1	64-22
CRM content	3	0%, 5%, and 10% by total weight of the binder
CRM size	2	<2.36 mm (passing #8 sieve) & <1.18 mm (passing #16 sieve)
Total number of binders: 8		

Table 4.7: Approach-4 Binders: Factors and Factorial Levels

Factor	Factorial Levels	Details
Base binder source	1	Refinery-A
Base binder PG	1	64-22
CRM source	2	Supplier-C and Supplier-D
CRM content	3	0%, 5%, and 10 % by total weight of the binder
CRM size	2	<250 µm (passing #60 sieve) and <180 µm (passing #80 sieve)
Total number of binders: 5		

Short-term aging of the binders was simulated by RTFO-aging following AASHTO T 240. For the control and the Approach-1 and Approach-4 CRM binders, the RTFO-aging was conducted at the standard 163°C with 35 g of binder in each RTFO bottle. Approach-2 binders were RTFO-aged at 190°C using 37 g and 39 g specimens for 5% and 10% CRM contents respectively, in line with the proposed PG-AR testing procedures *(2)*.

Long-term aging of the binder was simulated by PAV-aging following AASHTO R 28. Specimen weight for the control and the Approach-1 and Approach-4 CRM binders was 50 g per pan. Specimen weights were increased to 53 g and 56 g for Approach-2 binders with 5% and 10% CRM contents, respectively, in line with the proposed PG-AR testing procedures *(2)*.

The low-temperature PGs were determined on PAV-aged binders using a bending beam rheometer (BBR) following AASHTO T 313. Specimens of the control and the Approach-1 and Approach-4 binders were prepared using a standard BBR mold. Approach-2 binder specimens

were prepared using the proposed PG-AR modified BBR mold *(2)*, which allows pouring of the binder in the width-dimension instead of the thickness-dimension.

4.4.2 Multiple-Stress Creep Recovery

Multiple-stress creep recovery tests were performed on RTFO-aged binders following AASHTO T 350. The test temperature was universally set to 64°C based on the high temperature PG of the control (base) binders. Parallel plate geometry was used for testing the control and the Approach-1 and Approach-4 binders, and concentric cylinder geometry was used for Approach-2 binders. The non-recoverable creep compliance was calculated as an indicator of the rutting resistance, and the average percent recovery was used to evaluate the effects of rubber modification.

4.4.3 Frequency Sweep

Frequency sweep tests were performed on RTFO-aged control and the Appoach-1 and Approach-4 binders using an 8 mm parallel plate geometry in a DSR at temperatures of 4, 20, and 40°C, and frequencies between 25.1 and 0.1 radians/second. A constant 0.1% strain was applied to prevent any nonlinear viscoelastic behavior in the binder.

Frequency sweep tests on Approach-2 binders were conducted with a concentric cylinder geometry with a 10 mm bob and 9.5 mm gap at intermediate temperatures of 20, 40, and 50°C. Tests could not be run at 4°C because the concentric cylinder geometry used has not been calibrated at this low temperature *(2)*. The test strain was maintained at 0.01% to avoid any non-linear viscoelastic behavior in the binder.

A symmetric sigmoidal fit function was used to convert the frequency sweep data into a master curve at the reference temperature using the fit function in Equation 4.1 *(56)*. The midpoint of the temperature testing range was selected as the reference temperature (i.e., 20°C for Approach-1 and Approach-4 binders and 40°C for Approach-2 binders):

$$log|E^*| = \delta + \frac{\alpha}{1+e^{\beta+\gamma log\omega f_r}} \quad \textbf{(4.1)}$$

Where:

$|E^*|$: magnitude of complex modulus (kPa)

α: fitting parameter (the high asymptote of the master curve)

δ: fitting parameter (the lower asymptote of the master curve)
β, γ: fitting parameters (the slope of the transition region of the master curve)
ω: frequency (Hz)
f_r: reduced frequency, which is the shifted frequency at the reference temperature from the frequency at the test temperature (Hz)

Equation 4.1 can be used to generate a binder master curve by substituting the complex modulus (E^*) with the shear complex modulus (G^*). The reduced frequency can be calculated using the Arrhenius equations (Equations 4.2 and 4.3), which are based on the time-temperature superposition *(56)*:

$$logf_r = logf + log\alpha_T \quad \textbf{(4.2)}$$

$$log\alpha_T = \frac{E_a}{R(ln10)}\left(\frac{1}{T} - \frac{1}{T_r}\right) \quad \textbf{(4.3)}$$

Where:
f: frequency sweep test loading frequency (Hz)
α_T: shift factor as a function of temperature in Kelvin (°K)
E_α: activation energy (Jol/Molar)
T: test temperature (°K)
T_r: reference temperature (°K)
R: ideal gas constant, 8.314 J/ (°K molar)

Measured dynamic moduli can be horizontally shifted into a single master curve at the reference temperature using the above equations. The shift factor (α_T) can be determined using the solver function by minimizing the sum of squares error between the predicted and measured dynamic moduli in Microsoft Excel®. Figure 4.3 and Figure 4.4 show examples of the fitting procedure.

4.4.4 Solubility and Ductility

The solubility test was conducted on unaged binders following AASHTO T 44, and the ductility test was run on RTFO-aged binders following AASHTO T 51. These two tests were completed by a contract testing laboratory, with binders provided by the UCPRC.

4.4.5 Viscosity

Rotational viscometer tests were used to determine the mixing and compaction temperatures for field-blended CRM binders (Approach-2 and Approach-4) following AASHTO T 316. The mixing

and compaction temperatures for Approach-1 binders were reported by the suppliers based on results using the same test procedure.

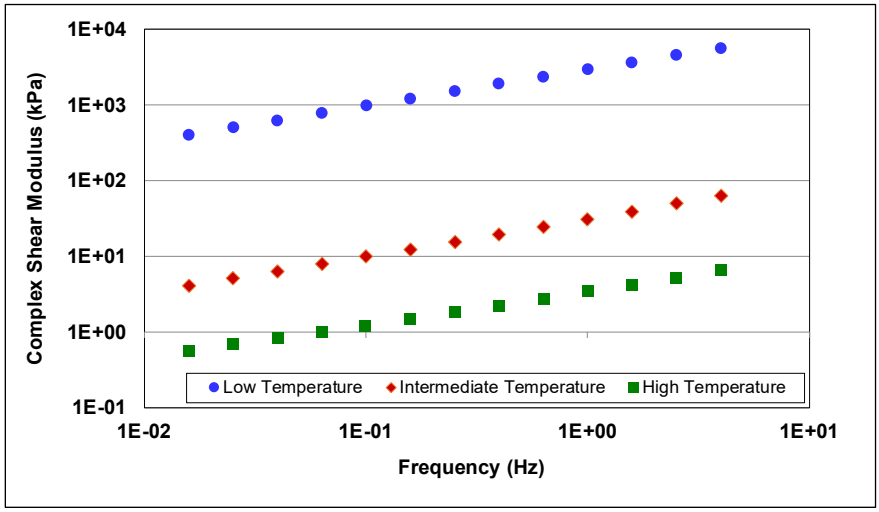

Figure 4.3: Example of modulus master curves: Plotted by frequency at tested temperature.

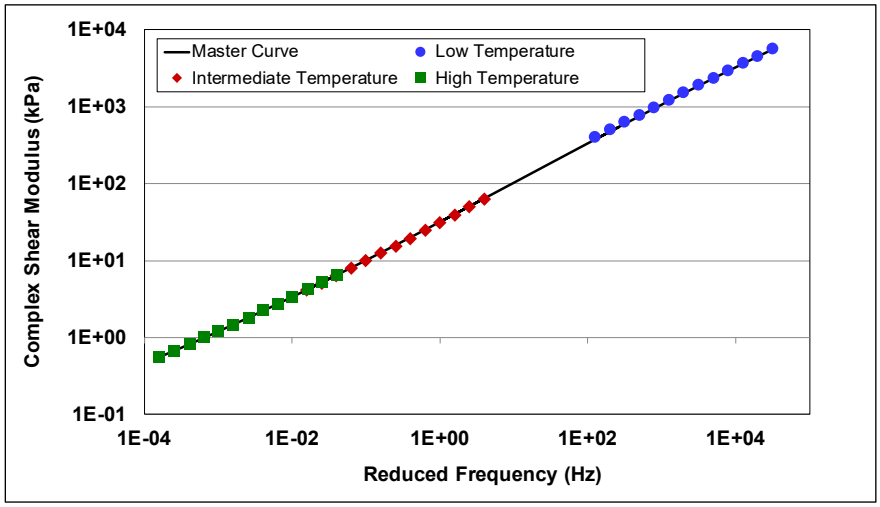

Figure 4.4: Example of modulus master curves: Plotted by shifted frequency.

Tests were conducted at 135°C and 165°C. A viscosity chart was plotted based on the measured binder viscosities at these two temperatures to determine the mixing and compaction temperatures where the viscosities were 0.17 and 0.28 Pa s, respectively.

4.4.6 Fourier-Transform Infrared Spectroscopy

Chemical component changes in the unaged, RTFO-aged, and PAV-aged binders were evaluated using Fourier-transform infrared spectroscopy with attenuated total reflection (FTIR-ATR).

The spectra measured by the FTIR are recorded in a reflective mode, from 4,000 to 400 cm^{-1}, at a resolution of 4 cm^{-1}. Each measurement entails 24 scans, and an average value is recorded. Nine replicate measurements were taken to ensure that representative measurements of each binder sample were collected. The carbonyl and sulfoxide components were used to track oxidative aging, which are usually defined by the peaks at 1,680 cm^{-1} and 1,030 cm^{-1} *(52,57-59)*. The tangential integration of the component area index was calculated between the upper and lower wavenumbers. Table 4.8 lists the wavenumbers used in this study.

Table 4.8: FTIR Wavenumber Limits of Chemical Area Indices

Component Index	Lower Wave Number (cm^{-1})	Upper Wave Number (cm^{-1})
Carbonyl	1,675	1,750
Sulfoxide	982	1,050

The spectra were normalized using the aliphatic band at 2,923 cm^{-1} to eliminate any variability introduced by the operator and any background impacts between repeat measurements. This aliphatic band structure is not affected by aging over time *(59,60)*. The chemical component area index was then integrated from the normalized spectra using Equation 4.4 *(59)*. Figure 4.5 shows an example of a spectrum and the respective component.

$$I_i = \int_{w_{l,i}}^{w_{u,i}} a(w)dw - \frac{a(w_{u,i})+a(w_{l,i})}{2} \times (w_{u,i} - w_{l,i}) \quad \textbf{(4.4)}$$

Where:

I_i: index of area *i*

$w_{l,i}$: lower wavenumber integral limit of area *i*

$w_{u,i}$: upper wave number integral limit of area *i*

$a(w)$: absorbance as a function of wavenumber

4.5 Asphalt Mix Testing Experimental Design

The following asphalt mix tests were conducted to evaluate the laboratory performance of CRM mixes:

- Volumetric mix design of CRM mixes following Caltrans specifications.
- Asphalt mixture performance tester (AMPT) dynamic modulus (DM) and flexural modulus frequency sweep (FS) testing to evaluate mix stiffness at various temperatures and frequencies.
- AMPT repeated load triaxial (RLT) testing to evaluate permanent deformation resistance.
- Hamburg wheel track testing (HWTT) to evaluate moisture damage resistance.

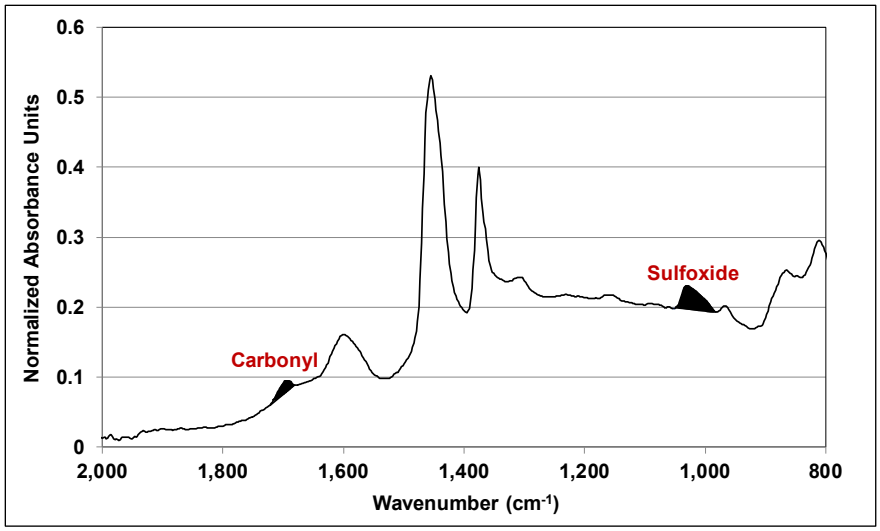

Figure 4.5: Example of normalized FTIR absorbance spectrum.
Plot shows tangential integration with carbonyl and sulfoxide areas.

- Flexural beam fatigue (FAT) testing to characterize fatigue performance under strain-controlled conditions.
- Semicircular bending (SCB) testing to evaluate fracture cracking resistance.
- Uniaxial thermal stress and strain testing (UTSST) to evaluate low-temperature cracking resistance. This test was not conducted on Approach-2 CRM mixes. All testing was performed at the University of Nevada, Reno.

Table 4.9 through Table 4.12 summarize the mix test factors and factor levels used in this study.

Table 4.9: Approach-1 Mixes: Factors and Factorial Levels

Factor	Factorial Levels	Details
Binder source	1	Refinery-A
Modified binder PG	2	PG 64-16 and PG 70-10
CRM content	3	0%, 5%, and 10% by total weight of the binder
CRM size	1	<250 µm (passing #60 sieve)
Aggregate source	1	Crushed alluvial with 15% RAP
Total number of mixes: 6		

Table 4.10: Approach-2 Mixes: Factors and Factorial Levels

Factor	Factorial Levels	Details
Binder source	2	Supplier-D and Supplier-F
Base binder PG		64-22
CRM content	3	0%,5%, and 10% by total weight of the binder
CRM size	2	<2.36 mm (passing #8 sieve) and <1.18 mm (passing #16 sieve)
Aggregate source	1	Crushed alluvial with 15% RAP
Total number of mixes: 8		

Table 4.11: Approach-3 Mixes: Factors and Factorial Levels

Factor	Factorial Levels	Details
Binder source	1	Refinery-A
Binder PG	1	64-16
CRM content	2	0.25% and 0.5% by total weight of the aggregate
CRM size	1	<2.36 mm (passing #8 sieve)
Aggregate source	1	Crushed alluvial with 15% RAP
Total number of mixes: 2		

Table 4.12: Approach-4 Mixes: Factors and Factorial Levels

Factor	Factorial Levels	Details
Base binder source	1	Refinery A
Base binder PG	1	PG 64-22
CRM source	1	Supplier-C
CRM content	3	0%, 5% and 10% by total weight of the binder
CRM size	1	<250 µm (#60 sieve)
Aggregate source	1	Crushed alluvial with 15% RAP
Total number of mixes: 3		

4.5.1 Volumetric Mix Design

A Superpave mix design was completed for each binder following AASHTO M 323 using the job mix formula provided by the asphalt plant (aggregate supplier) as a baseline. Mix designs are discussed for each Approach in Chapters 5 through 8.

After determining the optimum binder content, mix testing specimens were produced at the target air-void contents. Table 4.13 summarizes the factors for these tests. The air-void contents of the HWTT, beam, and SCB specimens were determined according to AASHTO T 166 (saturated surface-dry [SSD] method). The air-void contents of AMPT and UTSST specimens were determined according to AASHTO T 331 (CoreLok). Theoretical maximum specific gravity (Gmm) was determined according to AASHTO T 209.

After completing the mix design, specimens were prepared for testing according to AASHTO T 312 (AMPT, HWTT, SCB, and UTSST) or AASHTO PP 3 (beam fatigue).

4.5.2 Dynamic Modulus

Dynamic modulus testing followed AASHTO T 378 using an AMPT with specimens prepared in a gyratory compactor.

Specimens were tested at 4, 21, 38, and 54°C at frequencies between 25 and 0.1 Hz. Measured dynamic moduli and phase angles were horizontally shifted into a master curve at 20°C using Equations 4.2, 4.3, and the Williams-Landel-Ferry shift function *(61)* in Equation 4.5.

Table 4.13: Summary of Mix Test Factors

Test	Air-Void Content (%)	Temperature (°C)	Testing Parameters	Replicates
DM	7.0±0.5	4, 21, 38, 54	Strain controlled (100 µstrain) at 0.1-25 Hz	3
FS	7.0±1.0	10, 20, 30	Strain controlled (100 µstrain) at 0.01-15 Hz	3
RLT	7.0±0.5	50	Unconfined specimen	4
HWTT	7.0±1.0	50	Submerged specimen	4
FAT	7.0±1.0	20	3 strain levels (200, 300, 400 µstrain) at 10 Hz	3/strain level
SCB	7.0±1.0	25	Loading rate of 50 mm/min	4
UTSST	7.0±1.0	-Δ10/hour	Unconfined specimen	4

$$log(\alpha_T) = \frac{-C_1(T-T_r)}{C_2+(T-T_r)} \quad \textbf{(4.5)}$$

Where:

α_T: shift factor as a function of temperature T

T: test temperature in Kelvin (°K)

T_r: reference temperature in Kelvin (°K)

C1 and *C2*: fitting parameters

4.5.3 Flexural Modulus

Flexural beam frequency sweep testing followed AASHTO T 321 using a beam fatigue apparatus and beams prepared using a rolling wheel compactor.

Specimens were tested at 10, 20, and 30°C at frequencies between 15 and 0.01 Hz. A sinewave frequency was applied to produce a tensile strain of 100 µstrain on the longitudinal surface of the beam. The measured stiffnesses and phase angles were horizontally shifted into master curves at 20°C using Equations 4.2 and 4.5. Flexural stiffnesses were used in the *CalME* simulations discussed in Chapter 9.

4.5.4 Rutting Resistance (AMPT)

Permanent deformation resistance testing followed AASHTO T 378 using an AMPT with specimens prepared in a gyratory compactor. The repeated load triaxial parameters assessed included flow number and the number of cycles to reach 5% permanent axial strain (PAS). Specimens were tested with no confinement under a deviator stress of 483 kPa *(62–64)*.

4.5.5 Rutting and Moisture Resistance (HWTT)

Rutting and moisture resistance testing was done using a Hamburg wheel tracking (HWT) device following AASHTO T 324 with specimens prepared in a gyratory compactor. Water temperatures were maintained at 50°C.

4.5.6 Fatigue Cracking Resistance

Fatigue cracking resistance testing followed AASHTO T 321 on beams prepared using a rolling wheel compactor. Beam specimens are subjected to four-point bending by applying sinusoidal loading at three different strain levels (high, intermediate, and low) at a frequency of 10 Hz and temperature of 20°C. The fatigue life for each strain level was selected as the maximum value of the product of stiffness at each number of cycles multiplied by the number of cycles.

In this study, the testing approach currently specified in AASHTO T 321 was modified to optimize the quantity and quality of the data collected. Replicate specimens were first tested at high and medium strain levels to develop an initial regression relationship between fatigue life and strain (Equation 4.6). Strain levels were selected, based on experience, to achieve fatigue lives between 10,000 and 100,000 load cycles and between 300,000 and 500,000 load cycles for high and medium strains, respectively. Additional specimens were then tested at lower strain levels estimated to achieve a fatigue life of about 1 million load repetitions based on linear extrapolation of the log-log relationship between strain and fatigue lives from the first two strain levels. The final linear regression relationship between fatigue life and strain was then updated using the measured fatigue life at the lowest strain level.

$$LnN = A + B \times \varepsilon \quad \textbf{(4.6)}$$

Where:

N: fatigue life (number of cycles)

ε: strain level (μstrain)

A and B: model parameters

Test results were also used to generate the material fatigue response in the *CalME* simulations, discussed in Chapter 9, taking into consideration that ranking of mixes for fatigue life based on controlled-strain laboratory test results will generally correspond with field fatigue or reflective cracking performance for overlays thinner than about 75 mm (0.25 ft.) but may not correspond

with expected field performance for thicker layers of asphalt. For thicker layers, the interaction of the pavement structure, traffic loading, temperature, and mix stiffness with the controlled-strain beam fatigue results needs to be simulated using mechanistic analysis to rank mixes for expected field performance.

4.5.7 Fracture Cracking Resistance (SCB)

Fracture cracking resistance was assessed in terms of fracture energy, strength, and flexibility index (FI) determined from the semicircular bending test following AASHTO TP 124 on gyratory-compacted specimens.

Tests were run at 25°C with four replicates. Fracture energy, strength, and flexibility index were determined using Equations 4.7 through 4.9, respectively. Potential differences in notch properties in the specimen (i.e., notch ending in the mastic, fine aggregate matrix, against a large aggregate, or within a large aggregate) were taken into consideration when assessing variability between replicate test results *(65)*.

$$G_f = \frac{W_f}{Area_{lig.}} \times 10^6 \quad \textbf{(4.7)}$$

$$\sigma = \frac{\mathrm{Lp}}{2rt} \quad \textbf{(4.8)}$$

$$FI = A \times \frac{G_f}{|Spp|} \quad \textbf{(4.9)}$$

Where:

G_f: fracture energy (Joule/m^2)
W_f : work of fracture (Joule)
$Area_{lig}$: ligament area (mm^2)
σ: strength of the SCB specimen
Lp: peak load applied during the test
r: radius of the SCB specimen
t: thickness of the SCB specimen
FI: flexibility index
A: correlation parameter, a typical value is 0.01
Spp: post-peak slope

4.5.8 Low-Temperature Cracking Resistance (UTSST)

Low-temperature cracking resistance testing followed ASTM D8303 on gyratory compacted specimens. Compacted specimens were oven-aged according to AASHTO R 30 at 85°C for

120 hours to simulate long-term aging. Specimens were prepared at the UCPRC and testing was done at the University of Nevada, Reno.

Aged specimens were conditioned at 20°C. An initial tensile load of 20±10 N was applied, followed by cooling at a rate of 10°C per hour until the restrained specimen failed. The fracture temperature was defined as the temperature at which the applied loading reduced by 25%, or a global fracture was observed. Behavior was evaluated in terms of the cracking resistance index (CRI_{Env}) and environmental adjustment factor (F_{Env}), determined with Equations 4.10 and 4.11, respectively *(66)*.

$$CRI_{Env} = \frac{A_V + A_i\left(1 + \frac{A_V}{A_V + A_i} + \frac{A_p}{A_p + A_i}\right)}{\left(\sigma_{vgt}/\sigma_f\right)} \times F_{Env} \quad \textbf{(4.10)}$$

$$F_{Env} = \frac{A_{vgt-F}}{A_{vgt-crit}} \quad \textbf{(4.11)}$$

Where:

AV: area of viscous behavior
Ai: area of crack initiation
AP: area of crack propagation
σvgt: thermal stress at viscous glassy transition (kPa)
σf: thermal stress at fracture (kPa)
Avgt-F: area under the thermal stress-strain plot between the viscous glassy transition temperature and the fracture temperature of the restrained UTSST specimen
Avgt-crit: area under the thermal stress-strain plot between the viscous glassy transition temperature and the required environmental temperature at a given location

4.6 Pavement Performance Simulations Using CalME Software

In addition to the laboratory evaluation, expected performance of CRM mixes was simulated under a range of pavement structures, climate conditions, and traffic using the *CalME* software.

CalME uses incremental-recursive functions to account for fatigue damage using the entire damage curve. The cracking effect is described as a layer stiffness reduction during the simulation. The damage rate is correlated to the strain energy in the material throughout the simulation period, which changes continuously with changes in loading frequency and temperature gradient. The simulation result is obtained from an empirical function based on field observations of the correlation between visual surface cracks and mix stiffness. The critical

location for fatigue damage is calculated at the bottom of the asphalt layer(s) based on tensile strains under the vehicle loading stress, temperature gradient stress, and material stiffnesses determined from the frequency sweep test.

CalME simulations were used to predict likely CRM mix performance in the field and to compare it to that of conventional dense-graded mixes. This simulation was expected to provide information for identifying where CRM materials can be effectively used.

Simulation results are presented in terms of reflective cracking in overlays on asphalt concrete and portland cement concrete. No rutting simulations were conducted in this phase of the study.

5. EVALUATION OF APPROACH-1 BINDERS AND MIXES

5.1 Introduction

This chapter discusses the test results for Approach-1 CRM binders and mixes. Binder test results are presented first, followed by mix test results. Summary plots are presented in the text, while more detailed, tabulated results are provided in Appendix A. Details on the binders tested and the binder and mix testing details are discussed in Chapter 4 and are not repeated in this chapter.

Approach-1 binders (i.e., control, and with 5% and 10% CRM) provided by the two refineries were prepared to meet target performance grades. To do this, suppliers needed to adjust base binders, blend binders, and/or use additives. Consequently, direct comparisons between the control and modified binders and between binders modified with 5% and 10% CRM should be done with caution, given that the adjustments and/or additives may have also influenced behavior beyond that of the CRM content alone. Refinery-B did not supply a complete set of binders, and consequently detailed comparisons between these binders were not feasible.

5.2 Approach-1 Binder Test Results

5.2.1 Introduction

Unmodified and CRM binders were grouped by binder performance grade (PG) as follows. Performance parameters evaluated included binder PG at high, intermediate, and low temperatures; multiple stress creep recovery (MSCR); stiffness master curves from frequency sweeps; solubility; ductility; and aging resistance potential. The control and CRM binders are compared within each PG group, but not between groups:

- Refinery-A binders were grouped into PG 64-16 and PG 70-10 sets with each set containing an unmodified control, binder with 5% CRM, and binder with 10% CRM.
- Refinery-B binders were grouped into similar PG 64-XX and PG 70-XX sets but with only a PG 64-16 control binder. Note that Refinery-B did not provide a complete set of binders.

5.2.2 High-Temperature Grading

High-temperature grading results are listed in Table A.1 (unaged) and Table A.2 (RTFO-aged) in Appendix A. Figure 5.1 through Figure 5.4 show the average high temperature testing results for the unaged and RTFO-aged binders from both refineries. Dashed lines on the plot indicate the

1.00 kPa and 2.20 kPa test thresholds for unaged binders and RTFO-aged binders, respectively. The results show that:

- All Refinery-A binders met the PG requirements (>1.0 kPa for unaged binders and >2.20 kPa for RTFO-aged binders) at their respective grading temperatures.
- All Refinery-B PG 64 binders passed the high-temperature criteria under unaged and RTFO-aged conditions. All PG 70 binders passed in the unaged condition, while two of the three passed under RTFO-aged conditions. The B_70-22_10_0.25_3.5SBS binder failed marginally at 0.04 kPa lower than the required minimum. This indicates that some part of the hybrid modification of the binder using 10% CRM and 3.5% SBS likely decreased the rate of age-hardening during RTFO-aging.

Figure 5.5 through Figure 5.8 show the phase angles for the unaged and RTFO-aged binders from both refineries. The results show that:

- The phase angles of the RTFO-aged binders were lower than those of the unaged binders, as expected, indicating that RTFO-aging stiffened the binder.
- Adding 5% and 10% CRM had limited effect on phase angle but adding SBS had a significant effect, indicating that this additive changed the elastic properties of the binder.

Table 5.1 summarizes the continuous grades for the binders. The continuous grade is defined as the temperature where the unaged binder's G*/sin(δ) value equals 1.00 kPa and the RTFO-aged binder's G*/sin(δ) value equals 2.20 kPa.

Table 5.1: App-1: Continuous Grades

Refinery	Binder ID	Unaged Binder (°C)		RTFO-Aged Binder (°C)		Hardening Ratio
		G*/sin(δ) =1.00 kPa	Grade change	G*/sin(δ) =2.20 kPa	Grade change	G*/sin(δ)(RTFO) / G*/sin(δ) (Unaged) at 64°C
A	A_64-16	67.1	N/A	66.5	N/A	2.07
	A_64-16_5_0.25	67.0	-0.1	67.6	+1.1	2.44
	A_64-16_10_0.25	68.3	+1.2	68.5	+2.0	2.33
	A_70-10	71.4	N/A	70.8	N/A	2.11
	A_70-10_5_0.25	71.9	+0.5	72.2	+1.4	2.49
	A_70-10_10_0.25	72.7	+1.3	72.6	+1.6	2.30
B	B_64-16	69.8	N/A	69.8	N/A	2.27
	B_64-22_5_0.25	67.0	-2.8	66.5	-3.3	2.11
	B_64-22_3.5SBS	69.4	-0.4	66.7	-3.1	1.77
	B_64-28_5_0.25_3.5SBS	66.2	-3.6	64.5	-5.3	1.94
	B_70-16_10_0.25	70.9	+1.1	72.2	+2.4	2.77
	B_70-22_3.5SBS	74.5	+4.7	72.7	+2.9	2.00
	B_70-22_10_0.25_3.5SBS	72.5	+2.7	69.8	+0.0	1.85

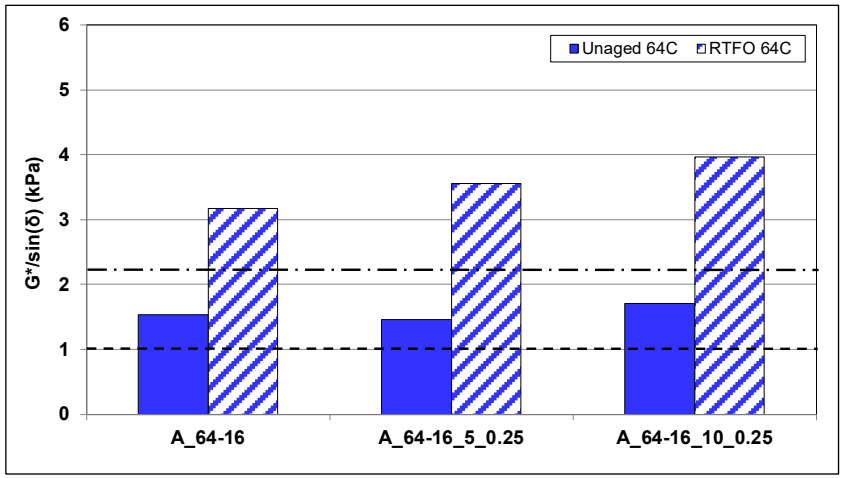

Figure 5.1: App-1/Ref-A: G*/sin(δ) of unaged and RTFO-aged PG 64 binders at 64°C.

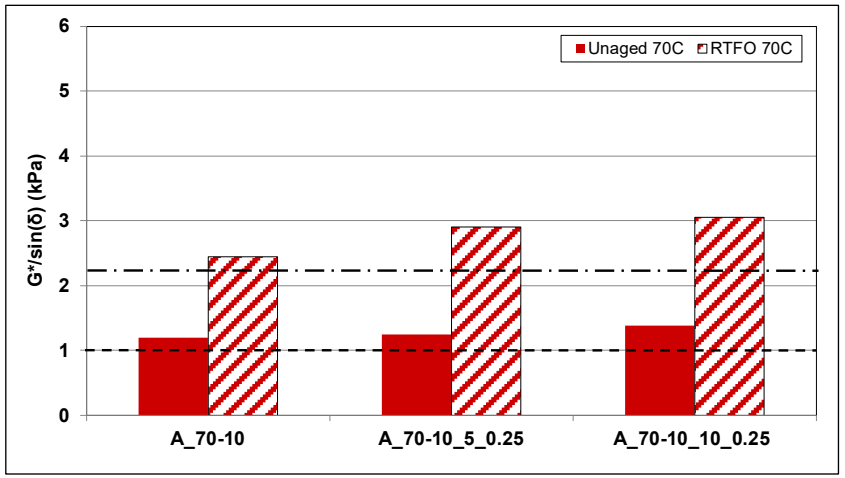

Figure 5.2: App-1/Ref-A: G*/sin(δ) of unaged and RTFO-aged PG 70 binders at 70°C.

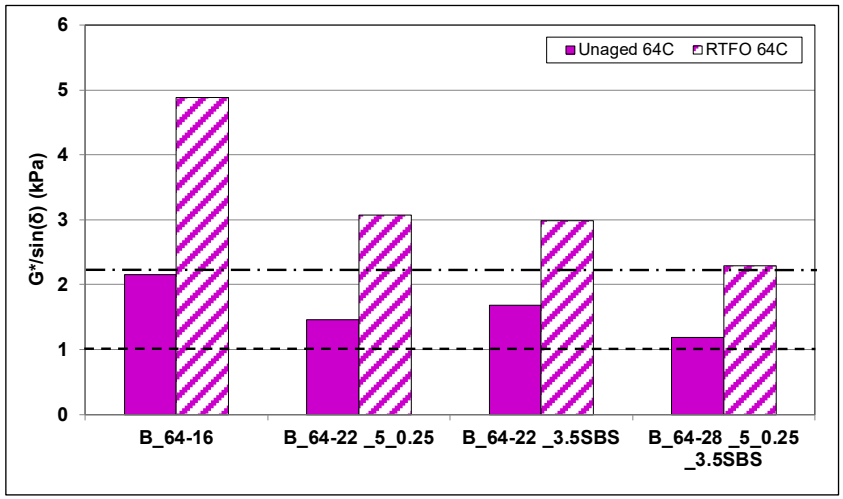

Figure 5.3: App-1/Ref-B: G*/sin(δ) of unaged and RTFO-aged PG 64 binders at 64°C.

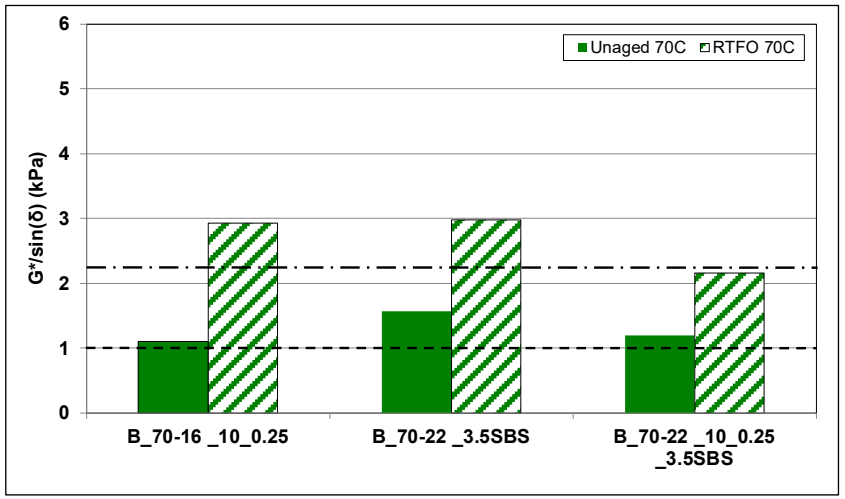

Figure 5.4: App-1/Ref-B: G*/sin(δ) of unaged and RTFO-aged PG 70 binders at 70°C.

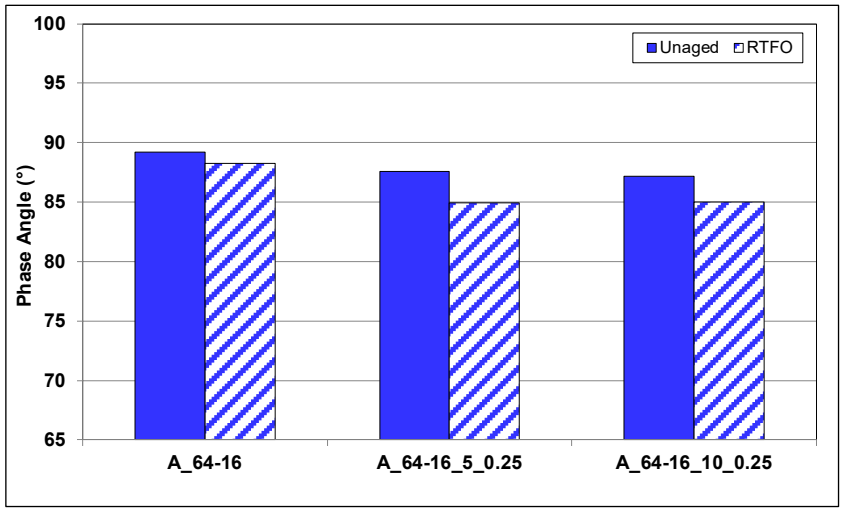

Figure 5.5: App-1/Ref-A: Phase angles of unaged and RTFO-agedP G 64 binders at 64°C.

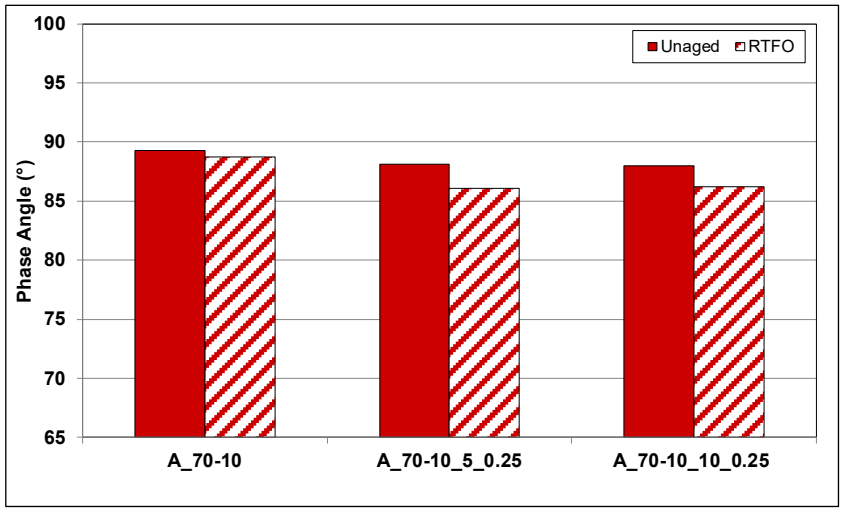

Figure 5.6: App-1/Ref-A: Phase angles of unaged and RTFO-aged PG 70 binders at 70°C.

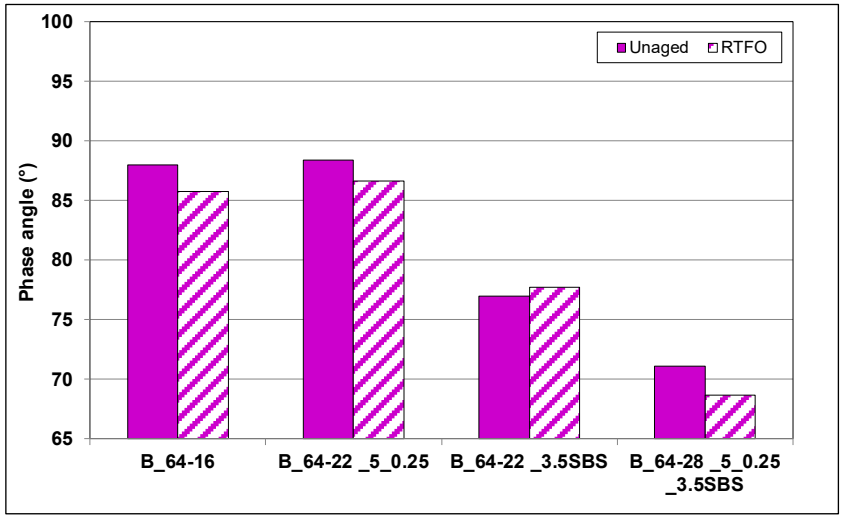

Figure 5.7: App-1/Ref-B: Phase angles of unaged and RTFO-aged PG 64 binders at 64°C.

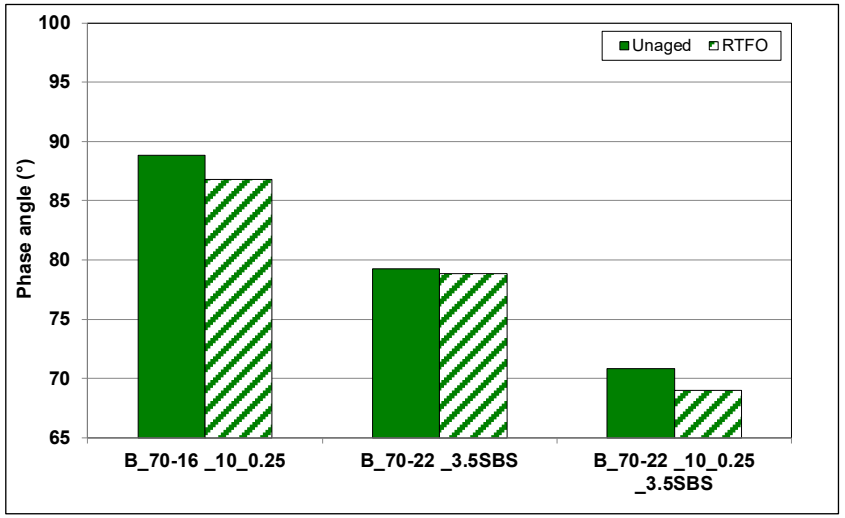

Figure 5.8: App-1/Ref-B: Phase angles of unaged and RTFO-aged PG 70 binders at 70°C.

The results show that:

- In the unaged condition, the continuous grades of the control and the CRM binders were similar, while the SBS-modified binders had notably higher grades.
- After RTFO aging, the continuous grades of the Refinery-A CRM binders were marginally higher than the control, while those of the Refinery-B CRM binders were lower. These differences indicate that the binder formulations used by different suppliers to meet PG requirements may have influenced some properties of the binder. Adding SBS led to a notable reduction in the continuous grade of the PG 64 binders, but a notable increase for the PG 70 binders, with differences dominated by differences in phase angle.

The G*/sin(δ) values of the RTFO-aged binders were divided by the corresponding values of the unaged binders to determine an age-hardening ratio. Although this ratio is not considered to be a performance indicator, it is a useful parameter for further assessing the effects of short-term aging on binder properties. A hardening ratio of 2.2 implies that the unaged and RTFO-aged binders would have the same high-PG. The results show that:

- The hardening ratios of the control binders were less than 2.2 with the exception of the Refinery-B PG 64 control, which was marginally higher with a ratio of 2.27.
- All of the CRM binders had hardening ratios higher than 2.2.
- The four Refinery-B binders containing SBS had notably lower hardening ratios than the other binders, with ratios ranging between 1.77 and 2.00.

5.2.3 Intermediate-Temperature Grading

Intermediate-temperature grading results are listed in Table A.3 in Appendix A. Figure 5.9 and Figure 5.10 respectively show the average intermediate temperature test results for Refinery-A and Refinery-B PAV-aged binders. In the figures, the histograms represent the G*×sin(δ) values at 25°C, and the dot points show the continuous grades at the temperature where the binder G*×sin(δ) values equal 5,000 kPa, as specified in AASHTO M 320. The results show that:

- The CRM binders were softer than their control binders in each PG group after PAV-aging, which indicated potentially better fatigue cracking resistance in a thin overlay application where cracking behavior would be strain-controlled.
- CRM binders with 10% CRM were stiffer than those with 5% CRM in the same PG group.
- The Refinery-B binders had lower intermediate temperatures and lower stiffnesses at 25°C than the Refinery-A binders, supporting the observation that different binder and additive formulations had been used to meet the PG targets.
- Binders with SBS had the lowest continuous grades and stiffnesses of all the binders tested.

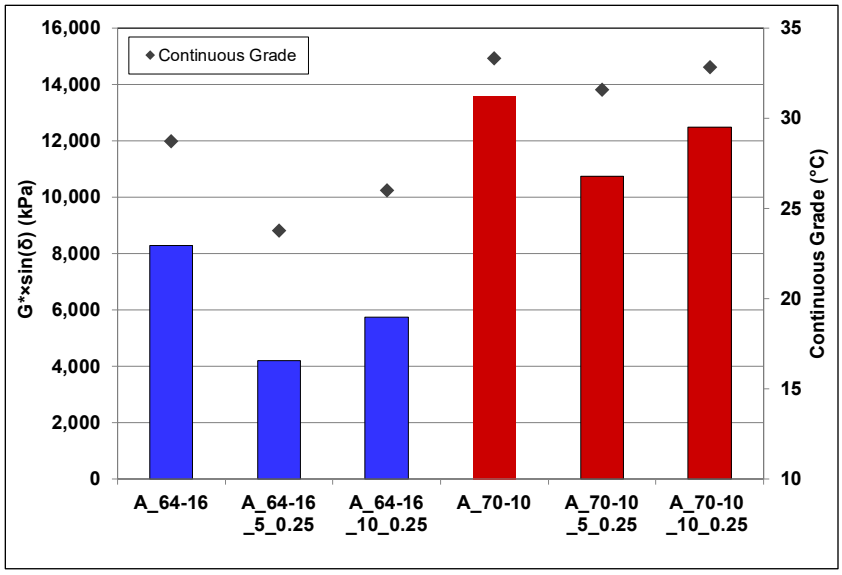

Figure 5.9: App-1/Ref-A: G*×sin(δ) of PAV-aged binders at 25°C.

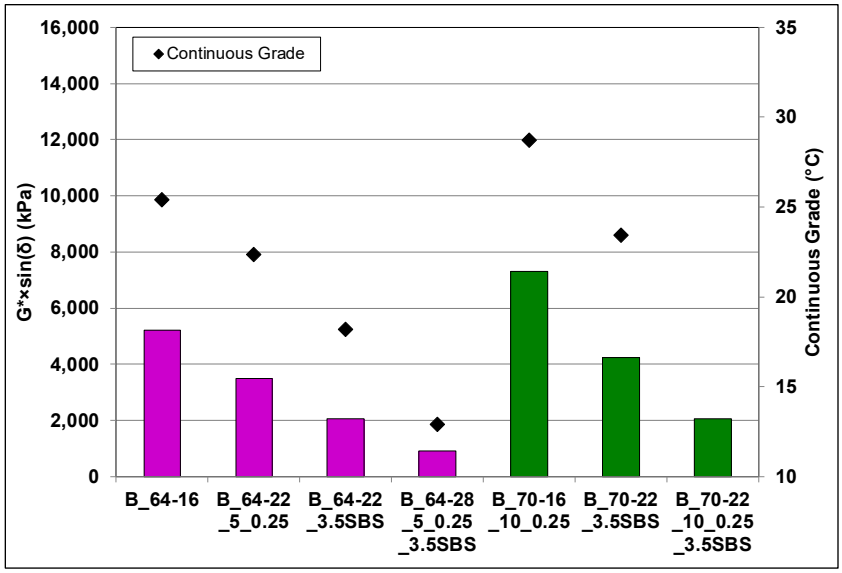

Figure 5.10: App-1/Ref-B: G*×sin(δ) of PAV-aged binders at 25°C.

5.2.4 Low-Temperature Grading

Bending beam rheometer test results are listed in Table A.4 in Appendix A. Figure 5.11 and Figure 5.12 show selected average bending beam rheometer results for the Refinery-A and Refinery-B PAV-aged binders. Only one test temperature is shown for each binder (i.e., -6°C for PG 64-16, -12°C for PG 64-22, -18°C for PG 64-28, and 0°C for PG 70-10). The maximum allowable creep stiffness (300 MPa) and lowest minimum allowable m-value (0.300) limits at the selected measuring temperature are shown as dashed lines on the plots.

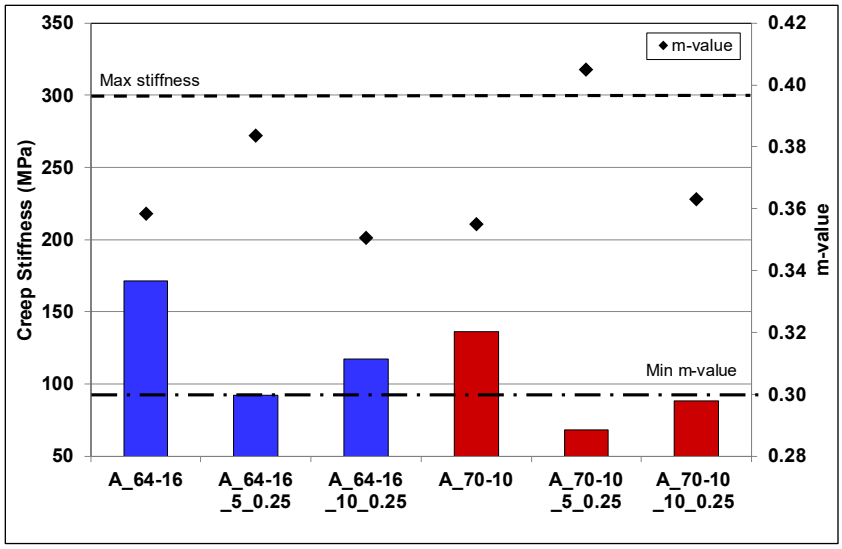

Figure 5.11: App-1/Ref-A: Low-temperature creep stiffness and m-value.

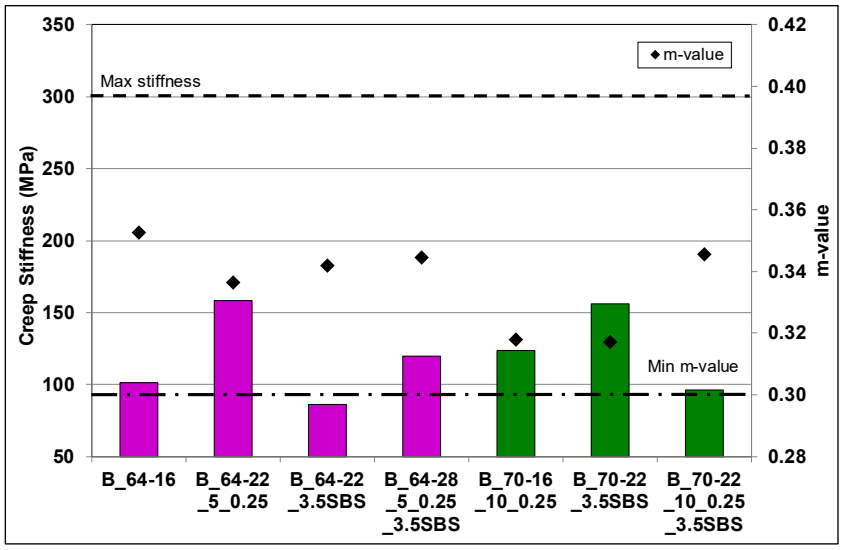

Figure 5.12: App-1/Ref-B: Low-temperature creep stiffness and m-value.

The results show that:

- All binders passed the low-temperature stiffness and m-value criteria at the minimum measuring temperatures.
- When comparing results in the same PG group, Refinery-A CRM binders had lower creep stiffnesses and m-values that were equal to or greater than the corresponding control binders. This implies that the CRM binders would likely have better low-temperature cracking performance than the control binders.
- Refinery-A CRM binders with 5% CRM had better low-temperature performance than binders with 10% CRM.

- The results for the Refinery-B binders are inconclusive given that an incomplete set of binders was provided for testing.

Additional BBR tests were run at lower temperatures (i.e., -18°C and -24°C) to calculate critical temperatures for the binders (i.e., where stiffness equals 300 MPa or m-value equals 0.300). The results are summarized in Table 5.2. The difference between the critical temperatures calculated by stiffness and m-value (delta T_c or ΔT_c) is an indicator of the binder stress relaxation *(67)*. Less negative or positive differences in ΔT_c indicate better resistance to thermal cracking. Less negative or positive differences in ΔT_c occur when the critical parameter for meeting the specification is the m-value, or if the critical value is stiffness then the m-value temperature is similar.

Table 5.2: App-1: Low-Temperature Test Results

Refinery	Binder ID	$T_{c\text{-stiffness}}$ (°C)	$T_{c\text{-m value}}$ (°C)	ΔT_c (°C)
A	A_64-16	-11.0	-14.5	3.4
	A_64-16_5_0.25	-15.1	-15.3	0.3
	A_64-16_10_0.25	-12.9	-17.2	4.3
	A_70-10	-10.0	-21.9	11.9
	A_70-10_5_0.25	-10.3	-9.7	-0.6
	A_70-10_10_0.25	-8.1	-10.6	2.6
B	B_64-16	-13.7	-12.3	-1.3
	B_64-22_5_0.25	-16.7	-15.6	-1.1
	B_64-22_3.5SBS	-20.1	-17.3	-2.8
	B_64-28_5_0.25_3.5SBS	-25.4	-23.9	-1.5
	B_70-16_10_0.25	-13.1	-7.9	-5.2
	B_70-22_3.5SBS	-18.2	-13.2	-5.0
	B_70-22_10_0.25_3.5SBS	-21.1	-17.9	-3.1

The results show that:

- The critical temperatures of the Refinery-A binders were dominated by m-value, while those of the Refinery-B binders were dominated by creep stiffness.
- All but one of the Refinery-A binders had a positive ΔT_c value, while all of the Refinery-B binders had negative ΔT_c values.
- Adding 5% CRM to Refinery-A binders had little impact on ΔT_c, while adding 10% CRM showed a distinct increase in ΔT_c.
- Adding SBS to the Refinery-B binders had a notable effect on ΔT_c.

5.2.5 Multiple Stress Creep Recovery

Multiple stress creep recovery test results are listed in Table A.5 in Appendix A. Figure 5.13 through Figure 5.16 respectively show the average MSCR test results at 64°C for the RTFO-aged binders from Refinery-A and Refinery-B. The results show that:

- Adding CRM to the Refinery-A PG 64 binders lowered the non-recoverable creep compliance (Jnr), with 10% CRM having a larger effect than 5% CRM. The opposite was observed for the PG 70 binders, with CRM binders showing higher Jnr values, and lower CRM contents having a larger effect than higher contents. This is attributed in part to the supplier having to adjust the constituents of the CRM binders to meet the target PG. The results from the PG 64 binders were consistent with MSCR tests on asphalt rubber binders, which typically show lower Jnr values than the corresponding base binder from which it was produced.
- Adding CRM to binders, regardless of source, increased the percent recovery of the binder, as expected, with increasing CRM content having a corresponding increase in percent recovery.
- Adding 3.5% SBS to select Refinery-B binders resulted in a significant decrease in Jnr values and a significant increase in elastic recoveries, indicating that SBS had a different influence on binder properties compared to CRM. This implies that SBS modification would potentially result in better rutting performance than modification with CRM, despite the lower age-hardening of the SBS modified binders after RTFO-aging as shown in Table 5.1.
- The results for the Refinery-B binders were inconclusive given that an incomplete set of binders was provided for testing.

5.2.6 Frequency Sweep

Figure 5.17 and Figure 5.19 show the master curves for Refinery-A and Refinery-B RTFO-aged binders, and Figure 5.18 and Figure 5.20 show the curves normalized to the control binders to facilitate comparison. The master curves were developed at 20°C using measured dynamic moduli and phase angles from the frequency sweep tests. The following observations were made:

- The results for Refinery-A show that the master curves for binders within the same PG group were not significantly different. The results for the Refinery-B binders are inconclusive given that an incomplete set of binders was provided for testing.
- At 20°C and 1E-05 Hz, which corresponds to 64°C and 10 Hz on a trafficked pavement based on the time-temperature superposition principle, the normalized moduli of the CRM binders were between 0.3 and 1.8 times those of the control binders.

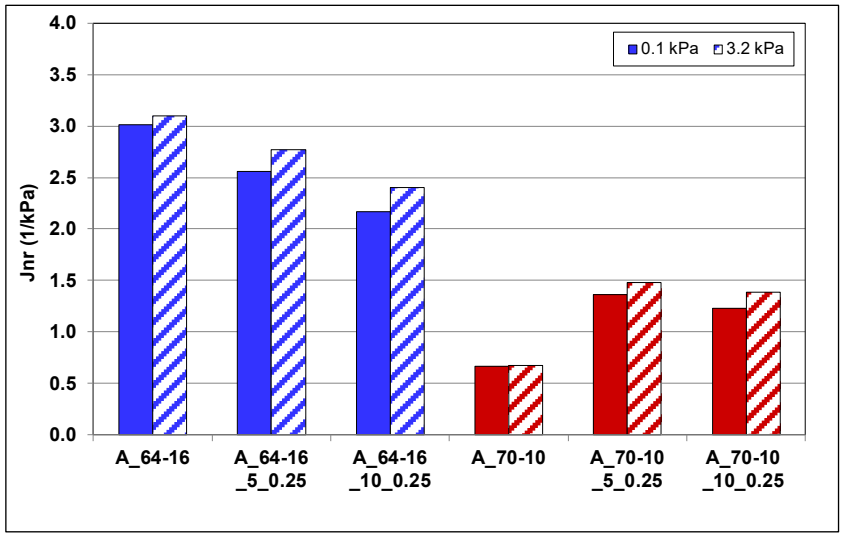

Figure 5.13: App-1/Ref-A: Jnr values of RTFO-aged binders at 64°C.

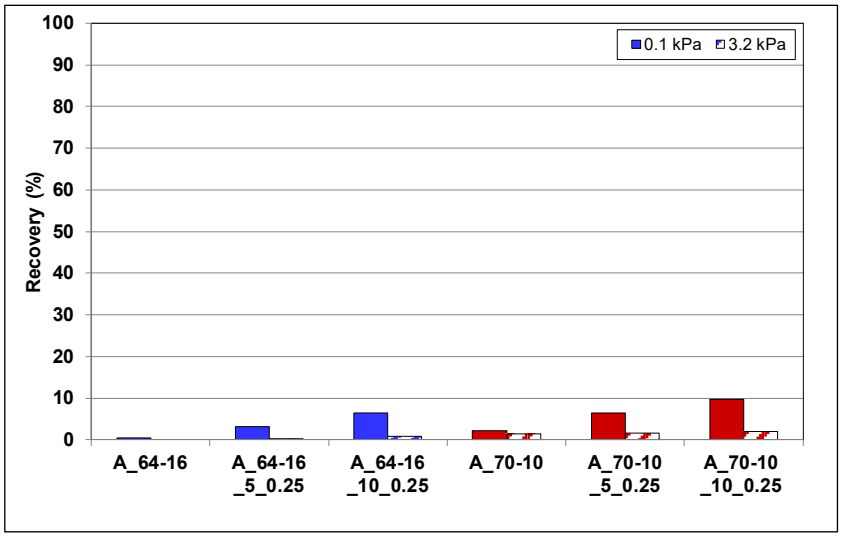

Figure 5.14: App-1/Ref-A: Percentage recovery of RTFO-aged binders at 64°C.

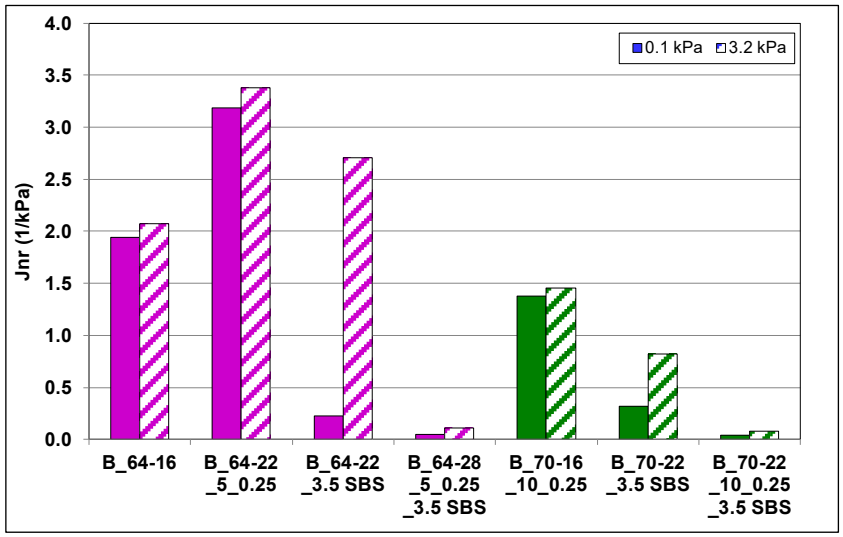

Figure 5.15: App-1/Ref-B: Jnr values of RTFO-aged binders at 64°C.

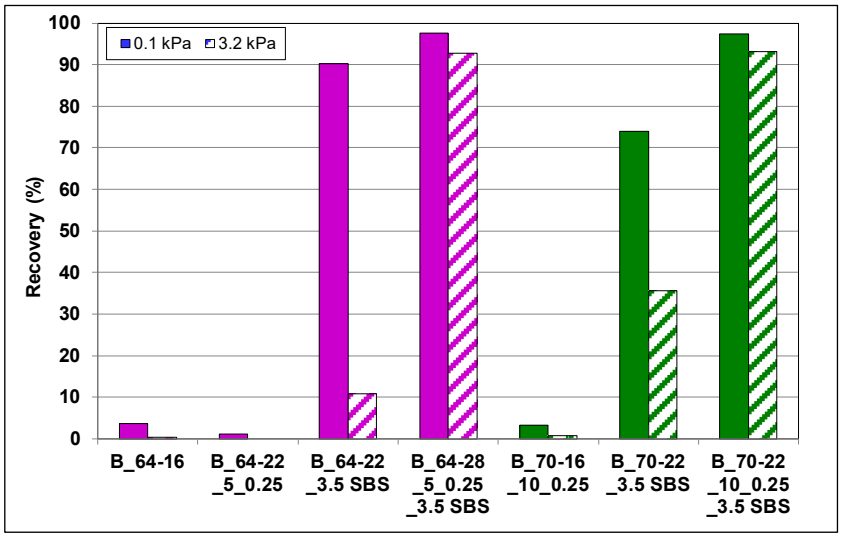

Figure 5.16: App-1/Ref-B: Percentage recovery of RTFO-aged binders at 64°C.

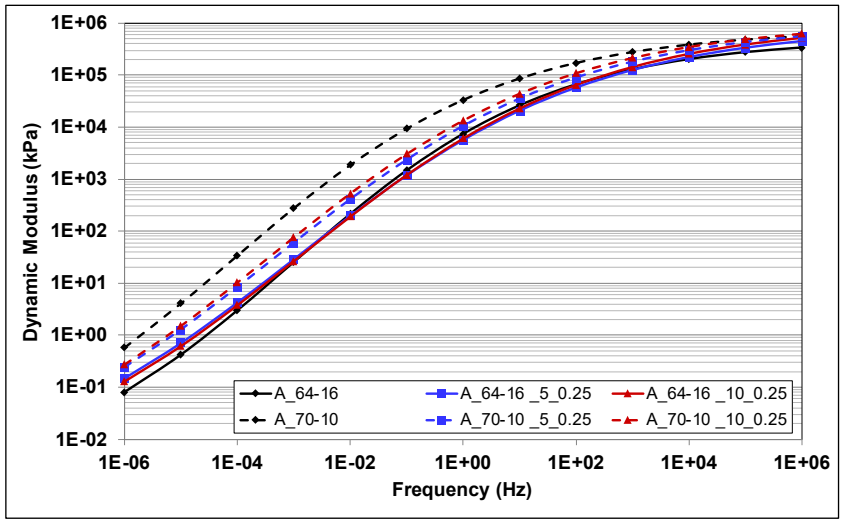

Figure 5.17: App-1/Ref-A: RTFO-aged binder master curves at 20°C.

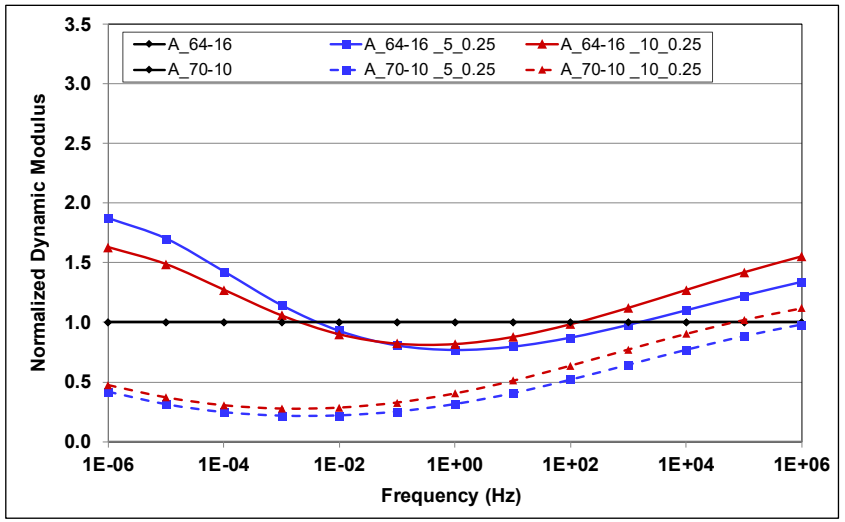

Figure 5.18: App-1/Ref-A: Normalized RTFO-aged binder master curves at 20°C.

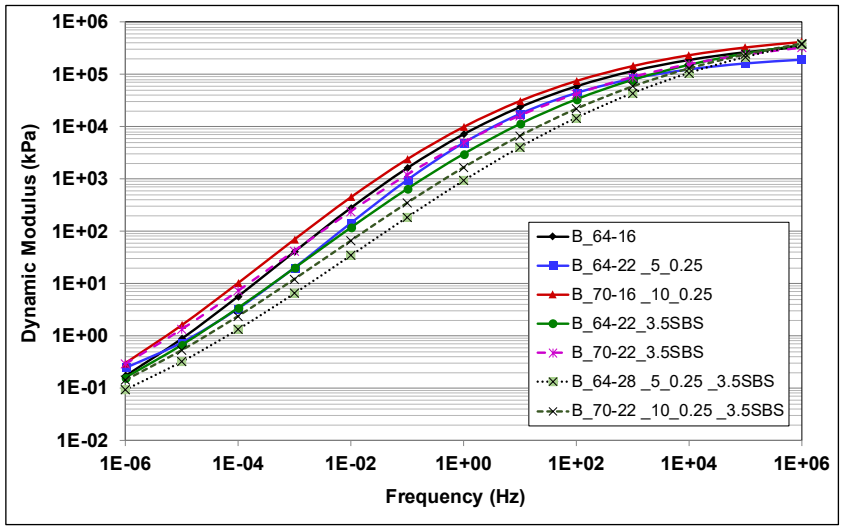

Figure 5.19: App-1/Ref-B: RTFO-aged binder master curves at 20°C.

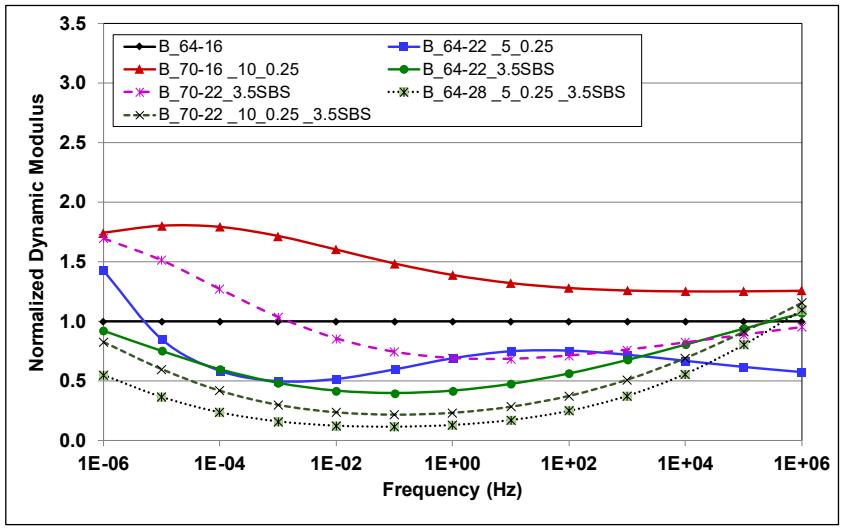

Figure 5.20: App-1/Ref-B: Normalized RTFO-aged binder master curves at 20°C.

- At 20°C and 10 Hz, at which binder fatigue tests were conducted, the CRM binders had lower dynamic moduli than their control binders in the same PG group (except for the Refinery-B PG 70-10 CRM binder with 10% CRM), indicating that most CRM binders were softer than the control binders and would therefore be expected to have better fatigue performance in strain-controlled fatigue tests.
- Dynamic modulus at higher frequencies (>1E+04 Hz at 20°C) can be used as an indicator of low-temperature performance. However, the master curve regression model is often not precise at these higher frequencies, as previous studies have suggested *(68,69)*, and consequently the BBR test is considered to be a more appropriate indicator of low-temperature performance than the master curve.

5.2.7 Solubility

Figure 5.21 and Figure 5.22 show the solubility test results for the unaged Refinery-A and Refinery-B binders, respectively. The results show that:

- All binders passed the Caltrans PG-M specification requirement for solubility (i.e., ≥97.5%).
- The small CRM particles were well digested.
- Solubility decreased with increasing CRM.
- Adding SBS to Refinery-B binders did not change the solubility.

5.2.8 Ductility

Figure 5.23 and Figure 5.24 show the ductility test results at 25°C for the RTFO-aged Refinery-A and Refinery-B binders, respectively. Caltrans specifications (Section 92) specify a minimum ductility of 75 cm for unmodified binders but do not specify any requirements for modified binders. The results of tests on the CRM binders (the control binders were not tested) show that:

- The Refinery-A CRM binders all exceeded the test limit of 150 cm, indicating good tensile properties.
- The Refinery-B CRM binders with no SBS modifiers exceeded the 75 cm ductility limit for unmodified binders. The two CRM binders with SBS modifiers had ductilities lower than 75 cm. Given that an incomplete set of binders was provided for testing, the effects of potential key influencing factors (i.e., PG and CRM content) on ductility could not be determined.

5.2.9 FTIR Testing

Binders were tested in unaged, RTFO-aged, and PAV-aged condition. Given that suppliers needed to make adjustments to base binders and/or used additives to meet the target PG, and that an incomplete set of binders was provided by Refinery-B, direct comparisons of carbonyl (CA) and

sulfoxide (SUL) indices between the different binders cannot be made. However, a preliminary analysis was made based on the information provided by the suppliers.

Figure 5.25 and Figure 5.26 show the CA indices of the Refinery-A and Refinery-B binders. The results show that:

- CA indices increased after RTFO-aging and again after PAV-aging, confirming that CA indices are sensitive to the level of aging and can be used to track oxidative aging in the binder.
- Unaged Refinery-A binders had negative CA indices attributed to the concave curve over the CA peak in the FTIR spectra. This concave curve resulted in a negative integration of the CA index, indicating that no carbonyl components were identified.
- Unaged Refinery-B binders all indicated CA indices, which implies that some aging had occurred during the blending process at the refinery.
- Increasing the CRM content from 5% to 10% in the Refinery-A CRM binders decreased the CA indices after RTFO- and PAV-aging, with the exception of the PG 70-10 binders after PAV-aging, where the binder with 10% CRM had a marginally higher index. These inconsistencies are attributed in part to the supplier having to adjust the constituents of the CRM binders to meet the target PG.
- Results for the Refinery-B binders were inconclusive, as expected, given that a complete set of binders was not compared.

Figure 5.27 and Figure 5.28 show the SUL indices for the Refinery-A and Refinery-B binders. The results show that:

- SUL indices increased after RTFO- and PAV-aging, as expected.
- Adding CRM did not result in a consistent increase or decrease in the SUL indices at the same aging condition. This is again attributed to the suppliers having to adjust the constituents of the binders containing CRM to meet the target PG. However, adding 10% CRM appeared to result in a reduction in SUL in the Refinery-A binders compared to binders with 5% CRM.
- Results for the Refinery-B binders were inconclusive, as expected, given that a complete set of binders could not be compared.

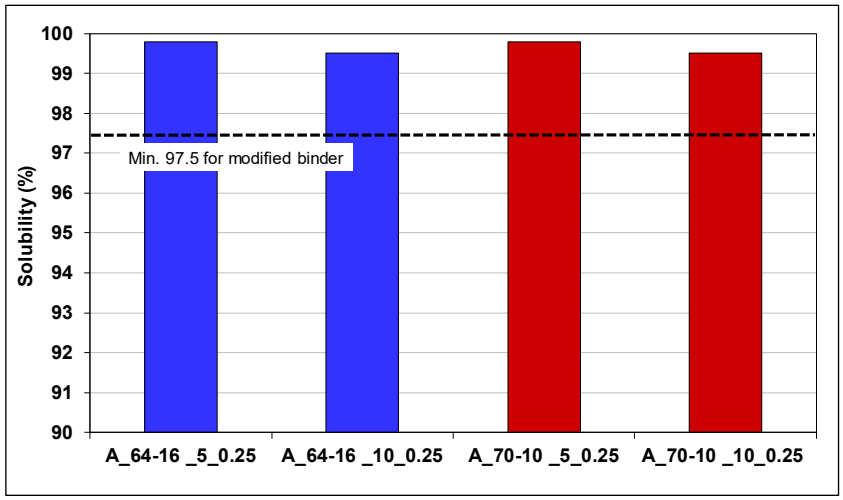

Figure 5.21: App-1/Ref-A: Solubility of unaged binders.

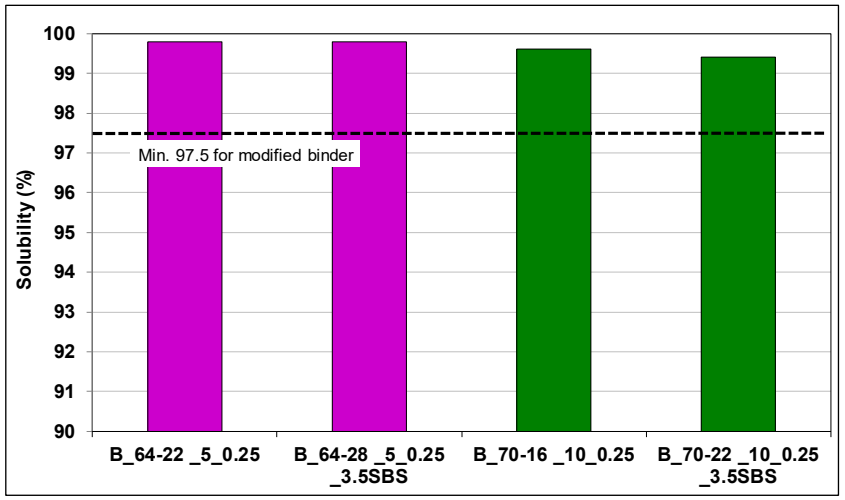

Figure 5.22: App-1/Ref-B: Solubility of unaged binders.

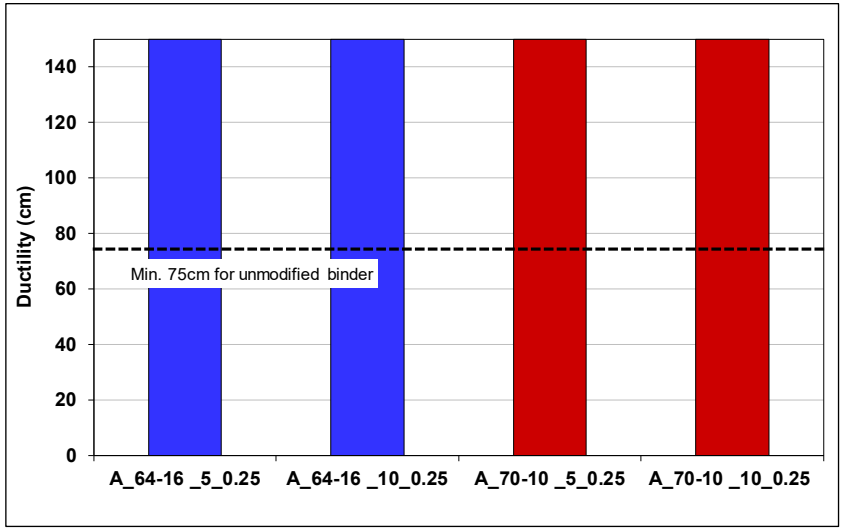

Figure 5.23: App-1/Ref-A: Ductility of RTFO-aged binders at 25°C.

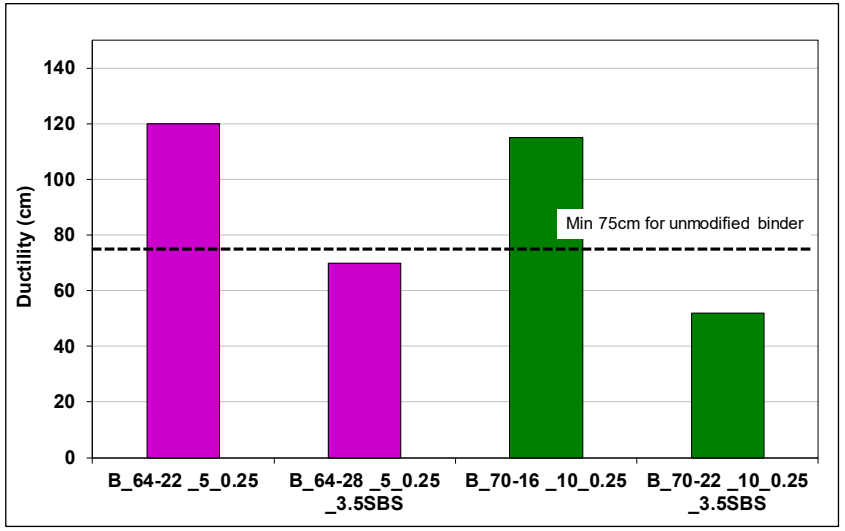

Figure 5.24: App-1/Ref-B: Ductility of RTFO-aged binders at 25°C.

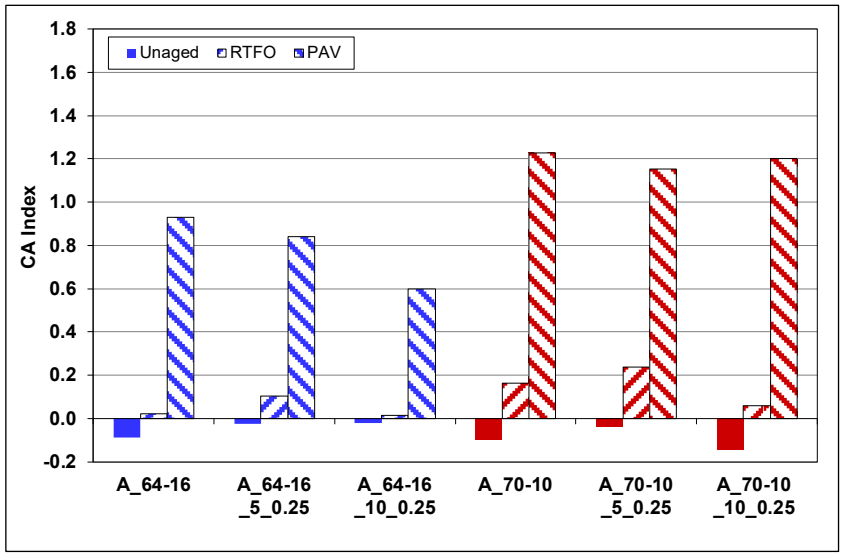

Figure 5.25: App-1/Ref-A: Carbonyl area index changes after aging.

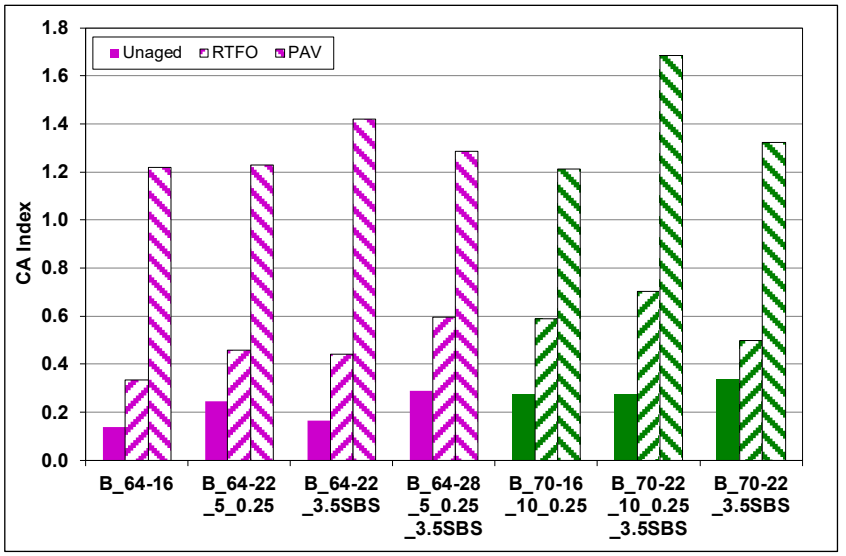

Figure 5.26: App-1/Ref-B: Carbonyl area index changes after aging.

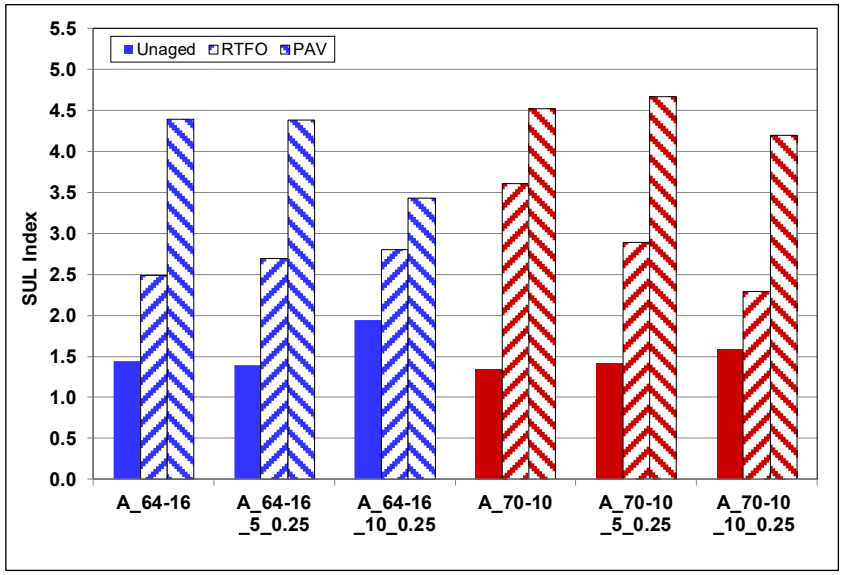

Figure 5.27: App-1/Ref-A: Sulfoxide area index changes after aging.

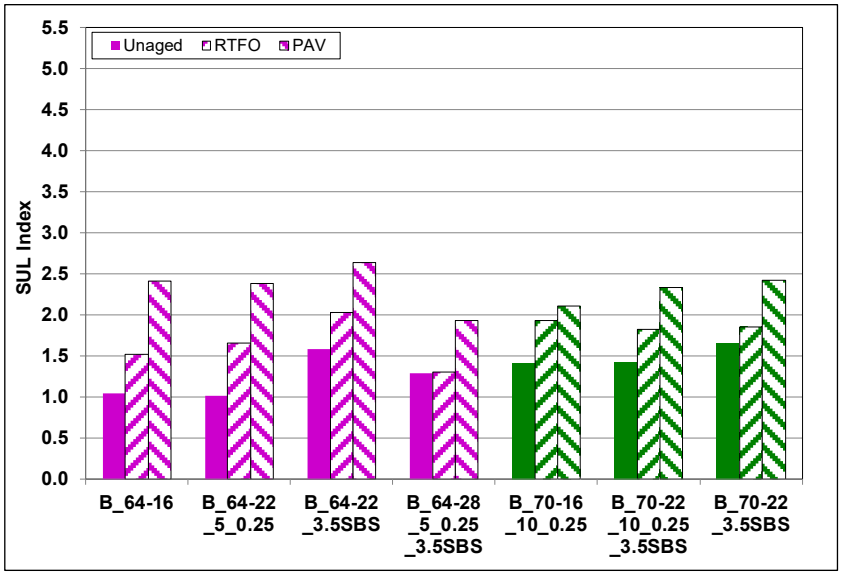

Figure 5.28: App-1/Ref-B: Sulfoxide area index changes after aging.

5.3 Approach-1 Mix Test Results

Mix testing was done on specimens prepared with binders from Refinery-A only. Note that direct comparisons between the control mix and mixes with CRM were not possible given that the supplier needed to make adjustments to the base binder and/or use additives to meet the target PG of the CRM binders.

5.3.1 Volumetric Mix Design

The Superpave volumetric mix design method (AASHTO M 323) was followed to select the optimum binder content (OBC) to meet Caltrans Type-A HMA specifications. Key parameters of the mix design included the following:

- Target air-void (AV) content at N_{design} (85 gyrations) of 4%±0.5%
- Voids in mineral aggregate (VMA) between 13.5% and 16.5% for 3/4 in. nominal maximum aggregate size (NMAS) mixes
- Dust proportion (DP) between 0.6 and 1.3
- Although not specified, voids filled with asphalt (VFA) was also calculated (the recommended VFA range is between 65% and 75%)

Mix-A, produced with the unmodified base binder supplied by Refinery-A, was used for the mix design confirmation. Once completed, the remaining mixes (B through F) were verified at the design optimum binder content and adjustments were made where necessary if the volumetric parameters did not meet the above stated requirements.

Table 5.3 summarizes the mixing and compaction temperatures and the gyratory compaction pressures. The mixing and compaction temperatures followed the binder profiles provided by Refinery-A. Table 5.4 summarizes the mix design results for Mix-A. Total binder content is by percent of the dry weight of the aggregate and includes both virgin and RAP binder.

Table 5.3: App-1/Ref-A: Mixing and Compaction Settings

Mix ID	Binder ID	Mixing Temp. (°C)	Compact Temp. (°C)	Compact Pressure (kPa)	Hold Time (Minutes)
A	A_64-16	150/165	140	600	0
B	A_64-16_5_0.25	150/165	140	600	0
C	A_64-16_10_0.25	150/165	140	600	0
D	A_70-10	170/185	155	600	0
E	A_70-10_5_0.25	170/185	155	600	0
F	A_70-10_10_0.25	170/185	155	600	0

Table 5.4: App-1/Ref-A: Mix-A Mix Design Summary

Binder Content (%)	Max. Specific Gravity (g/cm^3)	Air-Void Content (%)	VMA (%)	DP	VFA (%)
4.3	2.612	7.9	14.6	1.6	46.2
4.8	2.580	5.5	13.9	1.3	60.8
5.2	2.558	4.1	13.7	1.1	70.0
5.3 (OBC)	2.556	4.0	13.7	1.1	71.1
5.7	2.535	3.0	13.9	1.0	78.7

Figure 5.29 through Figure 5.32 plot air-void content, VMA, dust proportion, and VFA for Mix-A. The optimum binder content of 5.3% by dry weight of the aggregate was determined through interpolation using the air-void content plot. VMA, DP, and VFA were verified at this binder content. After verification, Mix-B through Mix-F were all verified at the 5.3% binder content. The results from these verifications are summarized in Table 5.5. All mixes met the specification requirements at this optimum binder content.

Table 5.5: App-1/Ref-A: Summary of Superpave Mix Design Parameters

Mix ID	Optimum Binder Content (%)	Air-Void Content at N_{design} (%)	VMA (%)	DP	VFA (%)
A	5.3	4.0	13.7	1.1	71.1
B	5.3	4.2	13.9	1.1	70.1
C	5.3	4.3	14.1	1.1	69.5
D	5.3	4.4	14.3	1.1	69.3
E	5.3	3.9	13.7	1.1	71.3
F	5.3	4.3	14.2	1.1	69.3

Using a fixed binder content of 5.3% for all mixes implies that adding 5% and 10% CRM would have decreased the actual base asphalt binder content in those mixes. However, the results in Table 5.5 show that this slight reduction in the actual base binder content did not appear to have any notable effect on the mix volumetric parameters.

5.3.2 Mix Stiffness: Dynamic and Flexural Modulus

Dynamic and flexural modulus test results are listed in Table A.4 and Table A.5 in Appendix A. Dynamic and flexural modulus master curves for the six mixes at a 20°C reference temperature are shown in Figure 5.17 and Figure 5.19, respectively. Master curves normalized to the unmodified base binder are shown in Figure 5.18 and Figure 5.20, respectively. Dynamic modulus master curves were developed from frequency sweep testing in an AMPT at 4, 21, 38, and 54°C, while flexural frequency sweep testing was done in a beam fatigue apparatus at 10, 20, and 30°C.

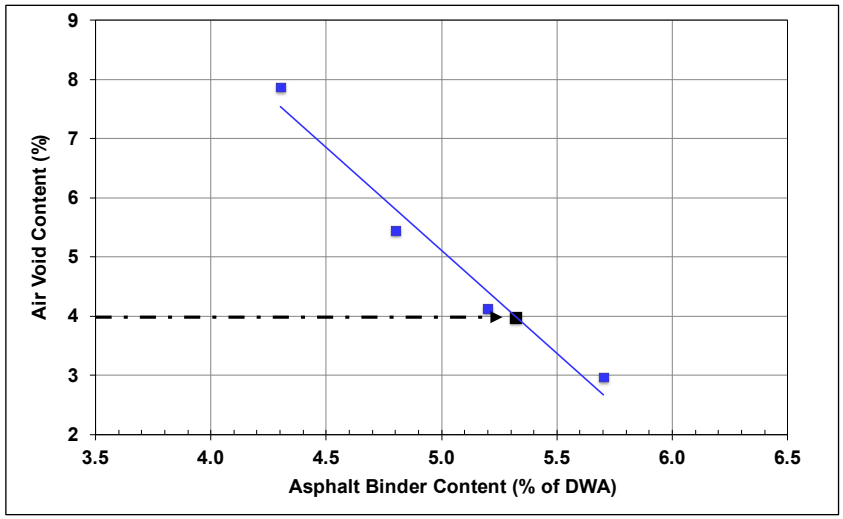

Figure 5.29: App-1/Mix-A: Air-void content vs. asphalt binder content.

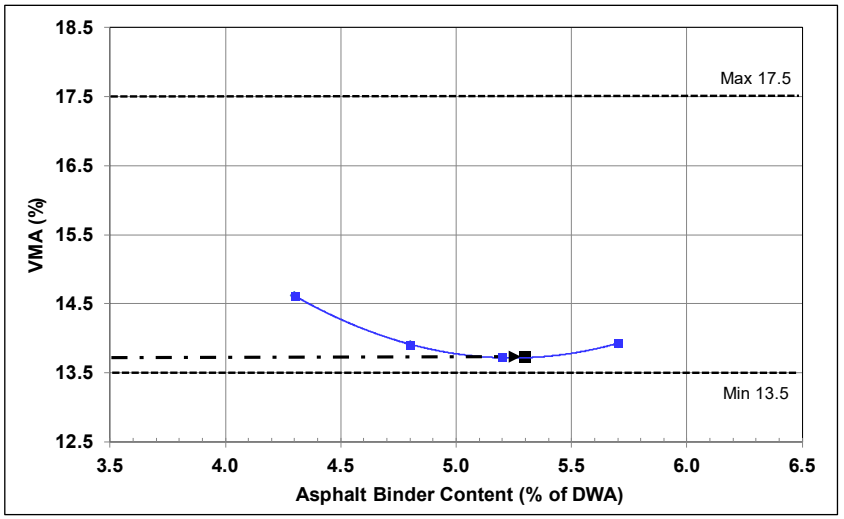

Figure 5.30: App-1/Mix-A: VMA vs. asphalt binder content.

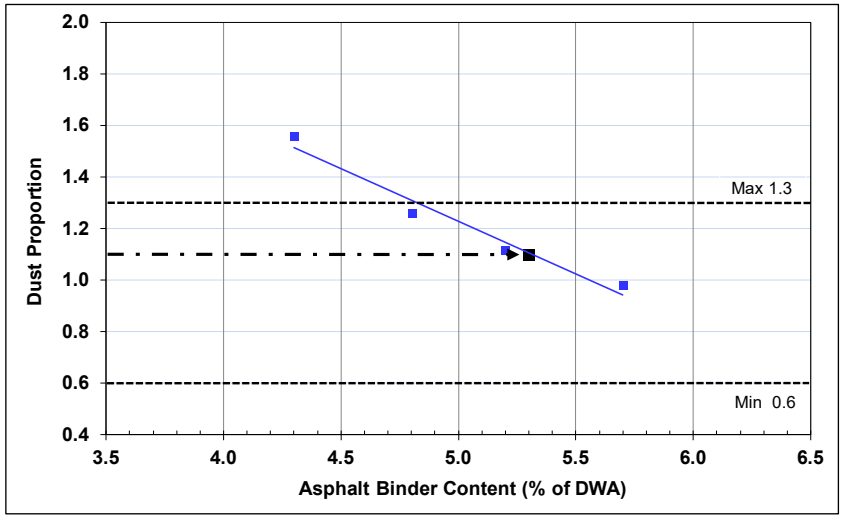

Figure 5.31: App-1/Mix-A: Dust proportion vs. asphalt binder content.

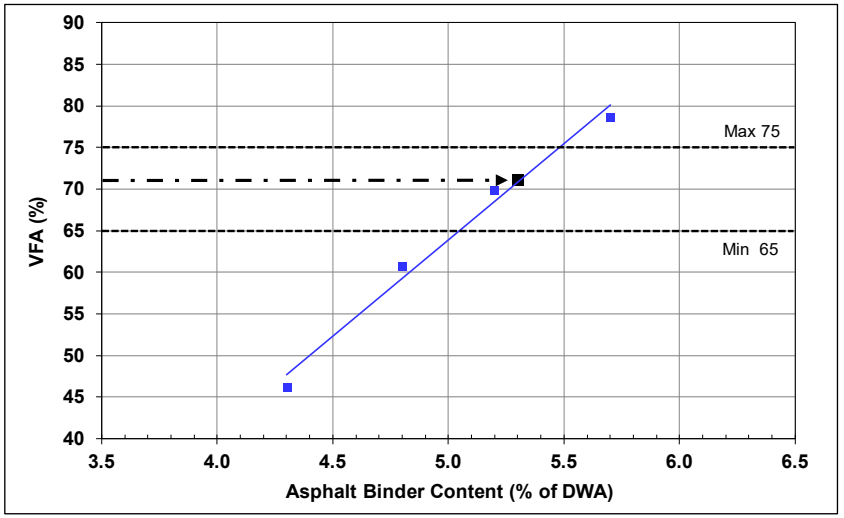

Figure 5.32: App-1/Mix-A: VFA vs. asphalt binder content.

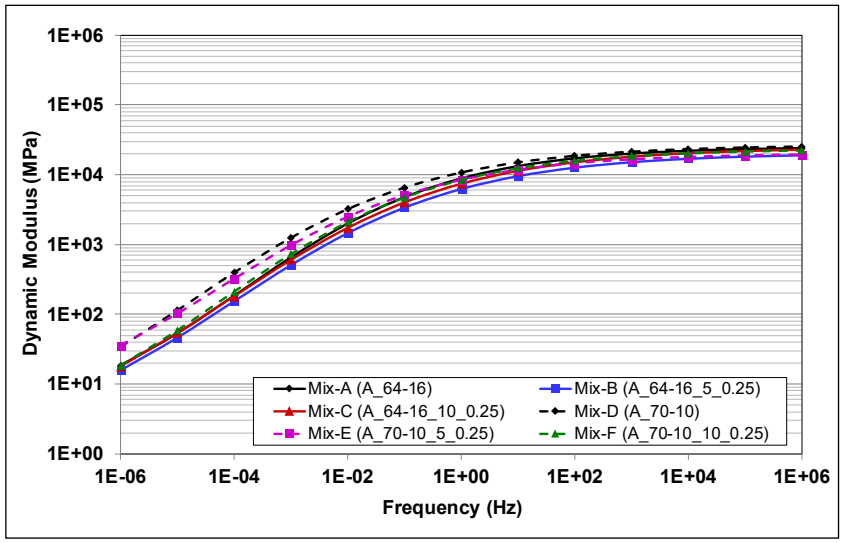

Figure 5.33: App-1/Ref-A: Dynamic modulus master curves at 20°C.

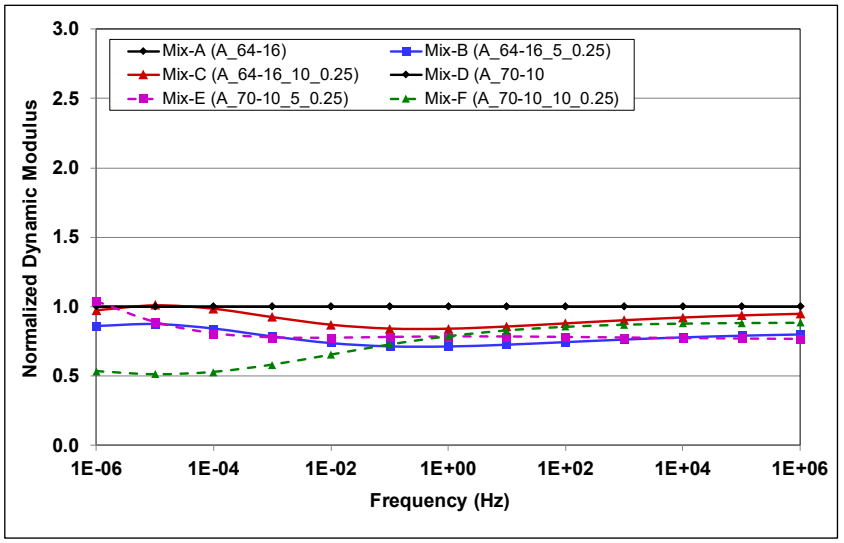

Figure 5.34: App-1/Ref-A: Normalized dynamic modulus master curves at 20°C.

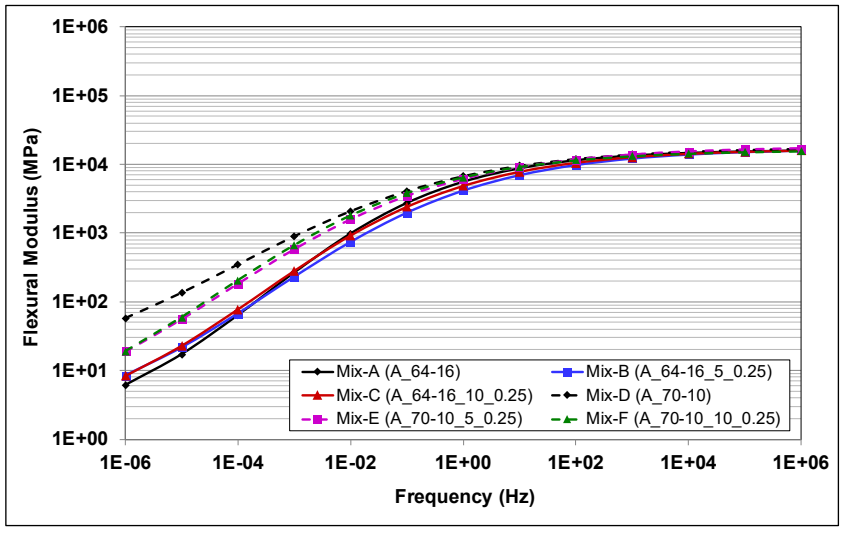

Figure 5.35: App-1/Ref-A: Flexural modulus master curves at 20°C.

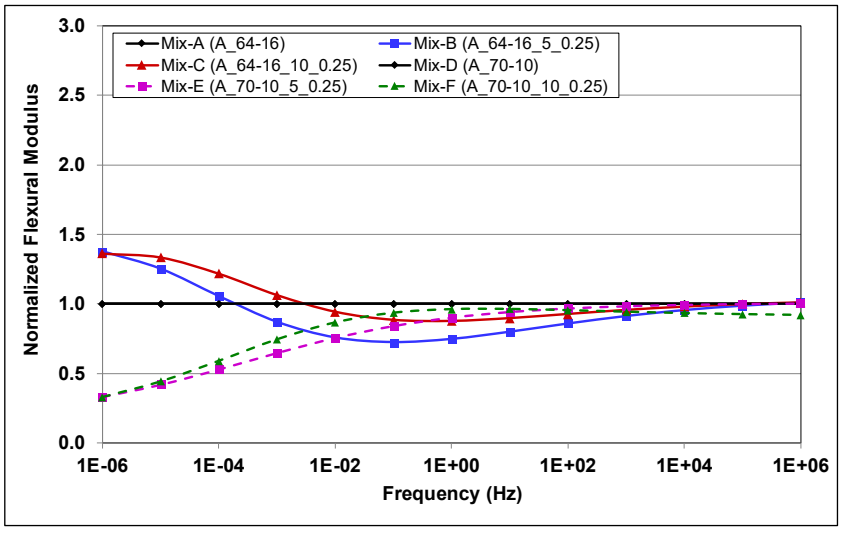

Figure 5.36: App-1/Ref-A: Normalized flexural modulus master curves at 20°C.

The plots show that:

- The dynamic and flexural modulus master curves showed similar trends to each other and to the binder master curves, as expected.
- The PG 70-10 mixes were stiffer than the PG 64-16 mixes at low- and mid-range frequencies, as expected.
- On the standard master curves, the PG 64-16 mixes all appear to have similar dynamic and flexural moduli across the full range of frequencies tested. However, the normalized plots indicate that the CRM mixes had marginally lower stiffnesses than the control mixes in the mid- and upper range of frequencies, indicating that the CRM affected stiffness, consistent with published experience. Flexural moduli of the CRM mixes were marginally higher than the control mix at the lower frequencies. However, it should be noted that direct comparisons between the control and CRM mixes are not possible given that the supplier needed to make adjustments to the base binder and/or use additives to meet the target PG of the CRM binders.
- At lower frequencies, the PG 70-10 CRM mixes had lower stiffnesses than the control mix, with stiffness decreasing with increasing CRM content, indicating that the CRM would likely have some influence on these mixes at higher pavement temperatures. At mid- and upper-frequency ranges, the CRM mixes had marginally lower stiffnesses with little difference between the two CRM contents. Any comparisons between the control and CRM mixes need to considered with caution.

Figure 5.37 and Figure 5.38 show black diagrams (complex modulus versus phase angle) derived from the dynamic and flexural modulus test results. These black diagrams show that there were no significant differences between the control mixes and mixes with CRM. These observations and the results from the dynamic and flexural modulus tests imply that mixes produced with these CRM binders should have similar, or marginally better, rutting and cracking performance to the control mixes.

5.3.3 Rutting Resistance: Unconfined Repeated Load Triaxial Test

Repeated load triaxial test results are listed in Table A.6 in Appendix A. Figure 5.39 and Figure 5.40 respectively plot the average unconfined RLT and average permanent strain against load cycle test results at 50°C. Whiskers on the data indicate the lowest and highest flow numbers of the five replicates in each mix.

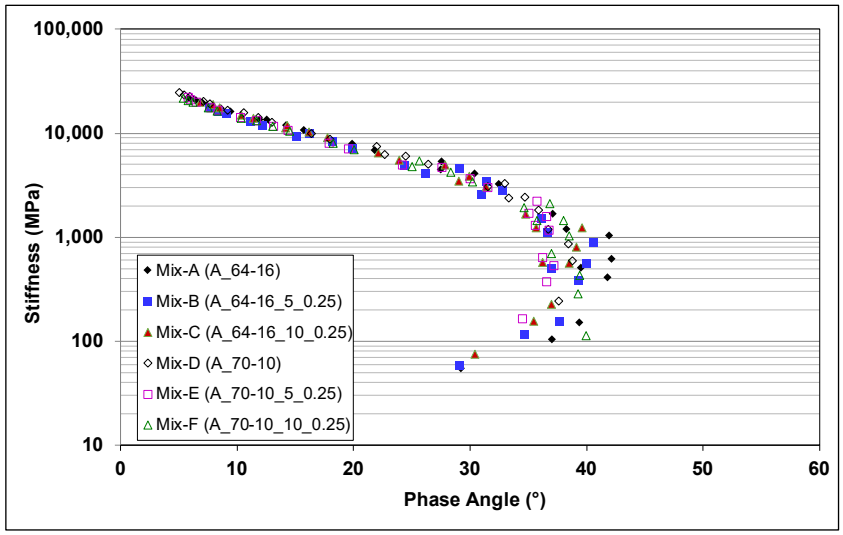

Figure 5.37: App-1/Ref-A: Black diagram of dynamic modulus results.

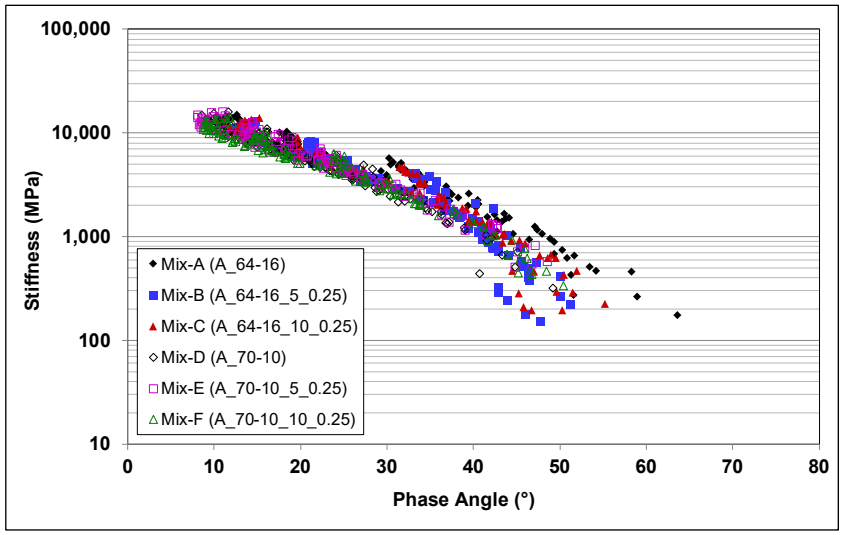

Figure 5.38: App-1/Ref-A: Black diagram of flexural modulus results.

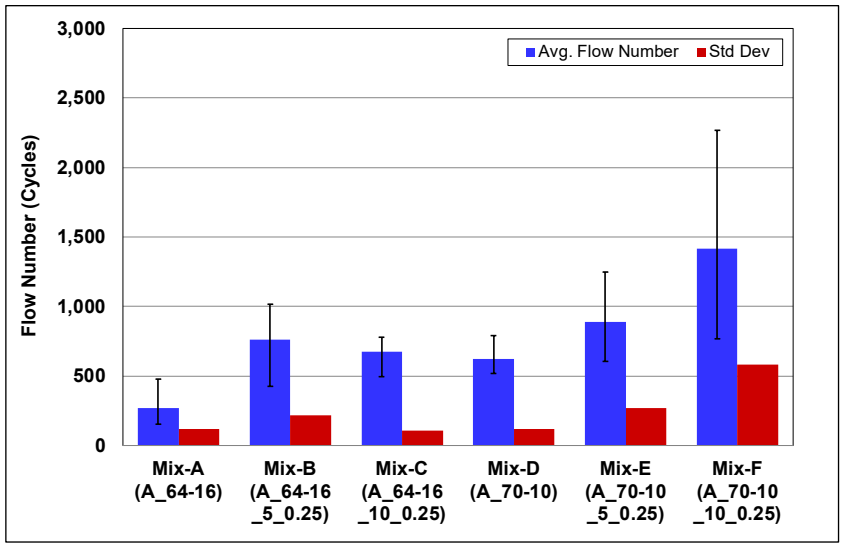

Figure 5.39: App-1/Ref-A: Flow number at 50°C.

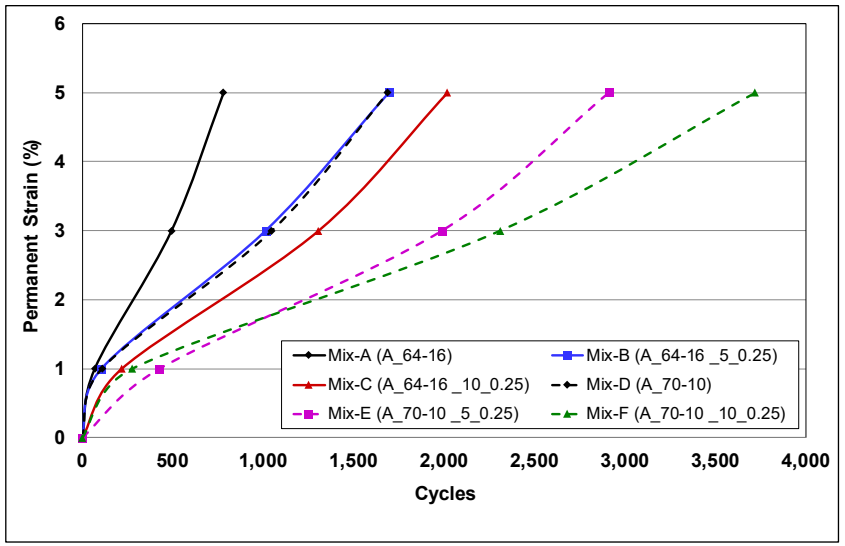

Figure 5.40: App-1/Ref-A: Average permanent strain vs. load cycle at 50°C.

The results show that:

- There was considerable variability across the replicate test results. However, the AASHTO T 378 maximum coefficient of variation for a single operator testing 19 mm (3/4 in.) NMAS mixes of 58.5% was not exceeded for any of the mixes.
- Taking the variability into consideration, the PG 70-10 binders, with and without CRM, showed better rutting resistance than the PG 64-16 binders, as expected.
- CRM binders had better rutting resistance than the unmodified control binders. Increasing the CRM content from 5% to 10% further improved the rutting resistance.
- Trends observed for the number of cycles to 1%, 3%, and 5% permanent axial strain were similar to those observed for the flow number results. At lower strain levels, the difference in the number of cycles required to reach the selected strain level was much closer between the mixes, with the rankings of some of the mixes different from those for the higher strain levels.
- Although the mix master curves discussed in Section 5.3.2 suggest that the PG 70-10 CRM mixes were less stiff than the control mix at low frequencies (corresponding to high temperatures based on the time-temperature superposition principle), the RLT test results indicate equal or better rutting resistance. This is supported by the binder MSCR test results discussed in Section 5.2.5, which suggests a higher percentage recovery of the CRM binders when the load is removed.

5.3.4 Rutting and Moisture Resistance: Hamburg Wheel Track Test

Hamburg wheel track test results are listed in Table A.7 in Appendix A. Figure 5.41 shows the HWTT results for all mixes at 50°C. The rut depth shown is the average of the left and right wheel track.

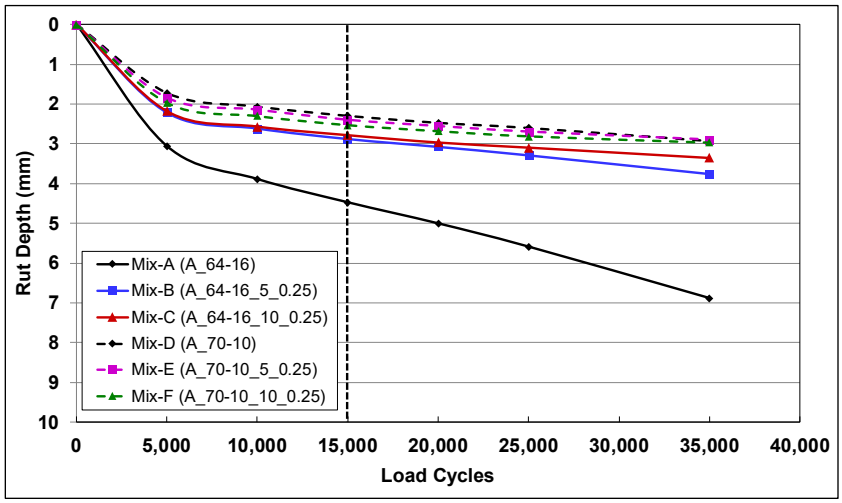

Figure 5.41: App-1/Ref-A: Hamburg Wheel Track rutting at 50°C.

The results indicate that:

- All mixes performed well within the specified limits (average maximum rut depth may not exceed 0.5 in. [≈12.5 mm] at 15,000 load cycles) and indicate that no mixes were moisture sensitive. Inflection points indicating stripping were not observed for any of the mixes.
- An embedment phase was observed in the first 5,000 load repetitions for all mixes, after which the rate of rut-depth increase slowed considerably.
- The PG 64-16 control mix had the deepest rut at the end of the test (35,000 load repetitions) and the fastest rate of rut-depth increase.
- The PG 64-16 CRM mixes were notably more rut and moisture resistant than the control mix. There was essentially no difference in rut depth between the mix with 5% CRM and the mix with 10% CRM.
- There was essentially no difference in rut depth between the three PG 70-10 mixes, and they were all marginally more rut resistant than the PG 64-16 mixes with CRM.

5.3.5 Fatigue/Reflective Cracking Resistance: Four-Point Beam Test

Four-point beam test results are listed in Table A.8 in Appendix A. Figure 5.42 and Figure 5.43 respectively show the flexural beam fatigue test results for the PG 64-16 and PG 70-10 mixes at 20°C and 10 Hz. The plots show the regression results from the data for predicted fatigue life against the applied peak-to-peak strain in a log-log plot. Calculated fatigue lives at 200, 300, 400, and 600 µstrain are compared in Figure 5.44 and Figure 5.45. The results show that:

- The models were generally appropriate based on the high R-squared values of the model fitting and the repeatability of the test results at each strain level.
- CRM mixes had longer fatigue lives than their control mixes, with the mixes with 5% CRM showing better performance than the mixes with 10% CRM. The exception was the PG 64-16 mix with 10% CRM, which appeared to have a shorter fatigue life than the control mix at high strain levels.
- The performance differences between mixes reduced with increasing strain level.
- The CRM mixes were more strain-sensitive than their control mixes, which may influence how they are best used in pavement applications. The potential implications of this are discussed in Chapter 9.

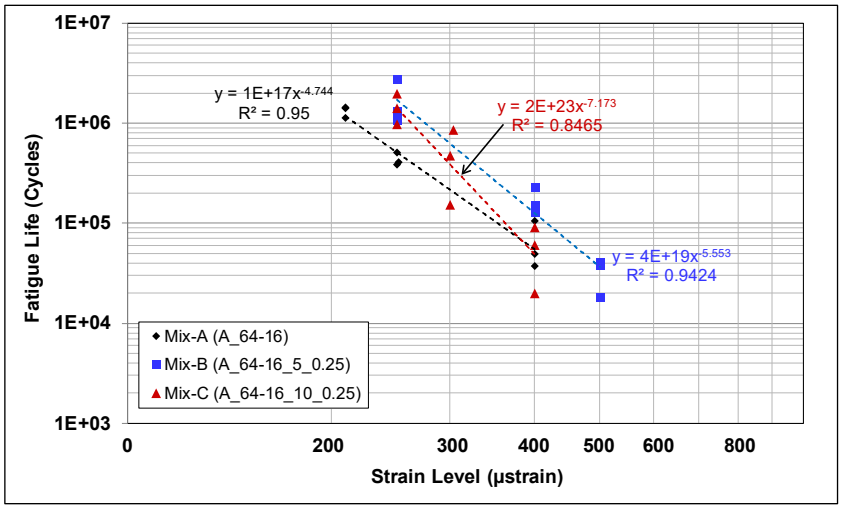

Figure 5.42: App-1/Ref-A: Beam fatigue at 20°C and 10 Hz for PG 64-16 mixes.

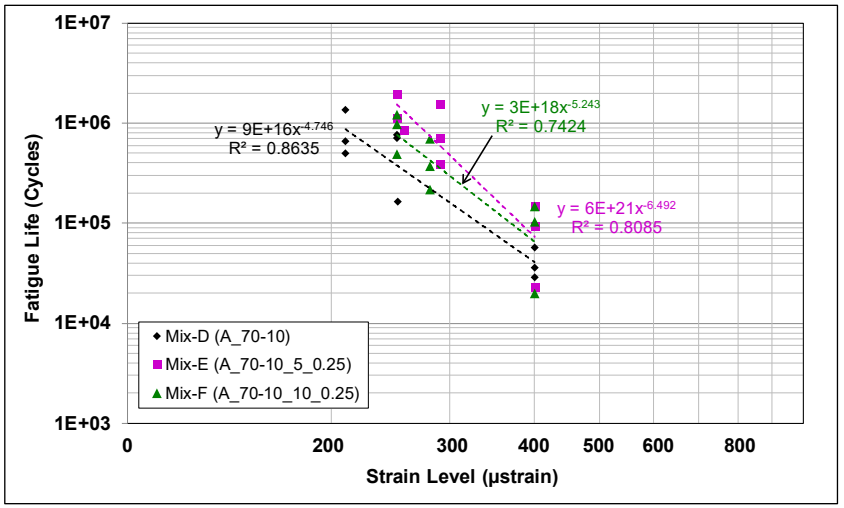

Figure 5.43: App-1/Ref-A: Beam fatigue at 20°C and 10 Hz for PG 70-10 mixes.

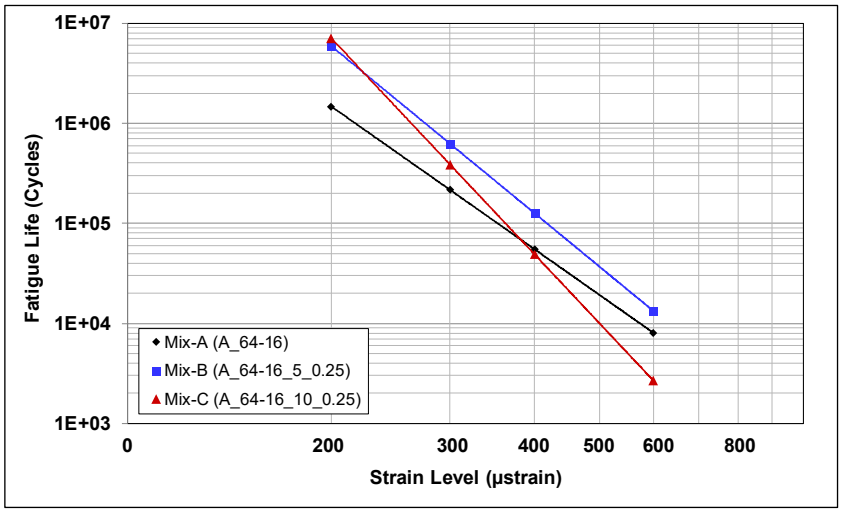

Figure 5.44: App-1/Ref-A: Calculated fatigue life of PG 64 mixes.

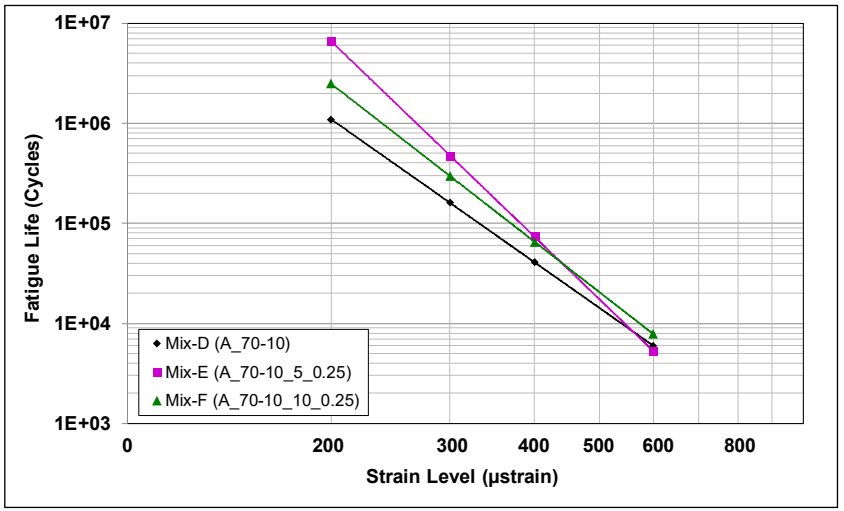

Figure 5.45: App-1/Ref-A: Calculated fatigue life of PG 70 mixes.

5.3.6 Fracture Cracking Resistance: Semicircular Bend Test

Semicircular bend test results are listed in Table A.9 in Appendix A. Figure 5.46 and Figure 5.47 respectively show the average fracture energy and strength, and flexibility index results. Whiskers on the data show the lowest and highest fracture energies and flexibility indices for the four replicates tested for each mix.

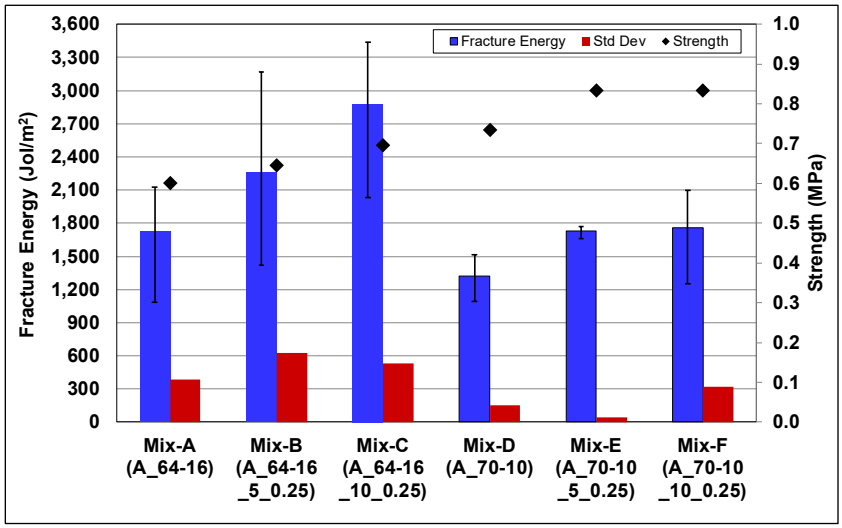

Figure 5.46: App-1/Ref-A: SCB fracture energy and tensile strength at 25°C.

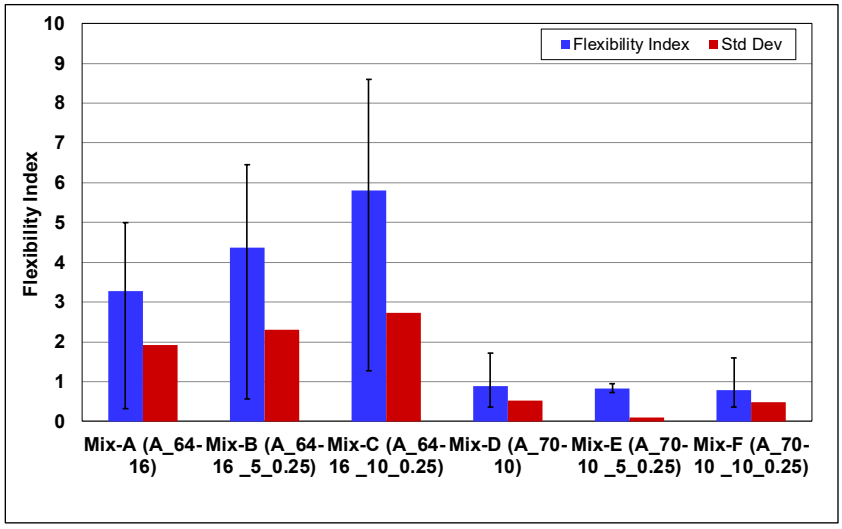

Figure 5.47: App-1/Ref-A: SCB flexibility index at 25°C.

The results show that:

- Fracture energy and flexibility index results had similar trends, as expected.
- Adding CRM resulted in a marginal strength increase over the control mixes. The PG 70 mixes had slightly higher strengths than the PG 64 mixes.

- There was considerable variability in the results of the replicate tests for each mix. This observation is consistent with previous studies and reports in the literature *(70)*. Table 5.6 provides a statistical analysis of the SCB test results. The coefficients of variation (CoV) of the flexibility index values were notably higher than the fracture energy values and strength. This should be taken into consideration when interpreting the results.

Table 5.6: App-1: Semicircular Bend Test Results

Mix ID	Binder ID	Fracture Energy (Jol/m^2)	CoV[a] (%)	Flexibility Index	CoV (%)	Strength (MPa)	CoV (%)
A	A_64-16	1,714	22.7	3.27	58.8	0.60	10.8
B	A_64-16_5_0.25	2,226	28.0	4.34	52.6	0.65	14.9
C	A_64-16_10_0.25	2,781	19.0	5.81	47.1	0.70	9.7
D	A_70-10	1,305	11.8	0.88	60.1	0.74	5.9
E	A_70-10_5_0.25	1,689	2.8	0.87	11.4	0.81	0.5
F	A_70-10_10_0.25	1,739	18.5	0.80	60.6	0.83	4.5

[a] CoV: coefficient of variation

- The PG 64-16 mixes had significantly higher fracture energies and flexibility index values than the PG 70-10 mixes.
- Results were consistent with the binder intermediate temperature PG results at 25°C (shown in Figure 5.9 and Figure 5.10), indicating that using softer binders can improve the fracture cracking resistance, as expected.
- The CRM mixes provided better cracking resistance than the control mixes. This was less evident in the PG 70-10 mixes, which was attributed in part to supplier-made adjustments to the base binder and/or the use of additives to meet the target PG of the CRM binders.
- Fracture cracking resistance increased with increasing CRM content.
- The ranking of flexibility index results matched the ranking of flexural fatigue life at low strain levels (<400 µstrain). However, the SCB results did not correlate well with fatigue life, confirming observations from other studies *(70)*.

5.3.7 Low-Temperature Cracking: Uniaxial Thermal Stress and Strain Test

Uniaxial thermal stress and strain test (UTSST) results are listed in Table A.10 in Appendix A and summarized in Figure 5.48. The results show that:

- The CRM mixes had equivalent or better thermal cracking resistance than the control mixes.
- Mixes with 5% CRM had higher cracking resistance (CRI_{Env}) values and lower fracture temperatures than those with 10% CRM.

- The UTSST results were consistent with the binder low-temperature test results discussed in Section 5.2.4, where the binders with 5% CRM had the lowest stiffness and the highest m-value in their PG groups.
- The mixes with 5% CRM exceeded the recommended minimum cracking resistance index of 17°C *(66)*. All other mixes were below this value.

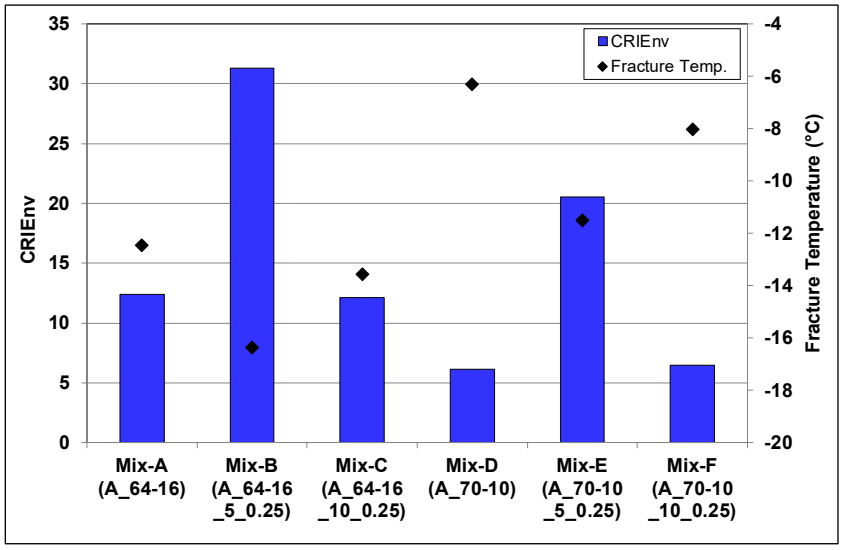

Figure 5.48: App-1/Ref-A: Uniaxial thermal stress and strain.

5.4 Approach-1 Test Result Summary

This chapter covers the evaluation of Approach-1 CRM binders (5% and 10% CRM by weight of the binder, with CRM particles <250 µm) produced using a terminal-blend process. The following important observations were made from the test results:

- The CRM binders tested in this part of the study met the specified PG, but this required binder blending and/or the use of additives, which limited the ability to compare properties and performance between the supplied base binder and the CRM binders, and between the binders with different CRM contents. Results of the binders from Refinery-B could not be compared given that an incomplete set of binders was provided by the refinery.
- All of the binders tested met the Caltrans PG-M specifications.
- The multiple stress creep recovery test results indicated that adding CRM decreased the non-recoverable compliance and increased the percentage recovery at high temperatures (64°C in this test) when compared to the control binders with the same PG.
- The low-temperature test results indicated that adding CRM resulted in lower creep stiffnesses at low temperatures (<0°C) than the control binders with the same PG.
- Adding 5% or 10% CRM together with 3.5% SBS resulted in much lower binder stiffnesses after RTFO- and PAV-aging than those measured on the binders with only CRM.

Modification with CRM and SBS therefore also resulted in improved intermediate- and low-temperature performance and multiple stress creep recovery compared to binders with only CRM.

- Approach-1 CRM binders could be accommodated in a dense-graded aggregate structure at the same binder content as the control mix and still meet all mix design requirements.
- Stiffness master curves of the mixes showed that using CRM binders did not result in significant stiffness changes compared to the control mix.
- Mixes produced with CRM binders had equivalent or better rutting and moisture resistance than their control mixes.
- Mixes produced with CRM binders generally had longer fatigue lives than their control mixes at low strains (<400 µstrain) but shorter fatigue lives at higher strains. Fatigue performance of the mixes produced with CRM binders were more strain sensitive than the control mixes.
- Mixes produced with CRM binders had better fracture cracking resistance than their control mixes. Despite high variability between replicate specimens of the same mix, fracture energies and flexibility indices provided a reasonable indication of expected fatigue performance at low strain levels (<400 µstrain) and that use of CRM binders would likely result in improved cracking resistance compared to the control mixes.
- Mixes produced with CRM binders had better low-temperature cracking resistance and lower fracture temperatures than their control mixes. A CRM content of 5% appeared to provide the best performance of the mixes tested. Results were consistent with the binder low-temperature test results, indicating that low-temperature performance is dominated by the binder properties. As noted previously, producers made changes in addition to the CRM content for their 5% and 10% CRM binders.

6. EVALUATION OF APPROACH-2 BINDERS AND MIXES

6.1 Introduction

This chapter discusses the performance of Approach-2 CRM binders and mixes. Binder test results are presented first, followed by mix test results. Summary plots are presented with the text, while more detailed, tabulated results are provided in Appendix B. Details on the binders tested and testing details are discussed in Chapter 4 and are not repeated in this chapter.

6.2 Approach-2 Binder Test Results

6.2.1 Introduction

Approach-2 CRM binders were prepared with the same base binders provided by each supplier for control testing purposes. The base binders were field blended with CRM at the asphalt plant at 190°C. No additional additives or extender oils were used. Blending of the binders containing 5% and 10% CRM took 30 and 60 minutes, respectively.

Supplier-D and Supplier-F used PG 64-22 base binders from different sources to produce their CRM binders. In the following analyses, Approach-2 CRM binders and control binders are grouped and compared by supplier.

6.2.2 High-Temperature Grading

High-temperature grading results are listed in Table B.1 (unaged) and Table B.2 (RTFO-aged) in Appendix B. Figure 6.1 through Figure 6.4 show the average high temperature testing results at 70°C for the unaged and RTFO-aged binders from both suppliers. Figure 6.5 and Figure 6.6 show the phase angles for unaged and RTFO-aged binders for Supplier-D and Supplier-G, respectively. The results show that:

- The base binder used by Supplier-D did not meet the PG requirements for a PG 64-22 unaged binder (i.e., >1.0 kPa, indicated by a dashed line on Figure 6.1 and Figure 6.3) and only just met the requirement for RTFO-aged binders (i.e., >2.2 kPa, indicated by a dashed line on Figure 6.2 and Figure 6.4). The binders with CRM all exceeded the minimum requirements, indicating that adding CRM had a notable stiffening effect.

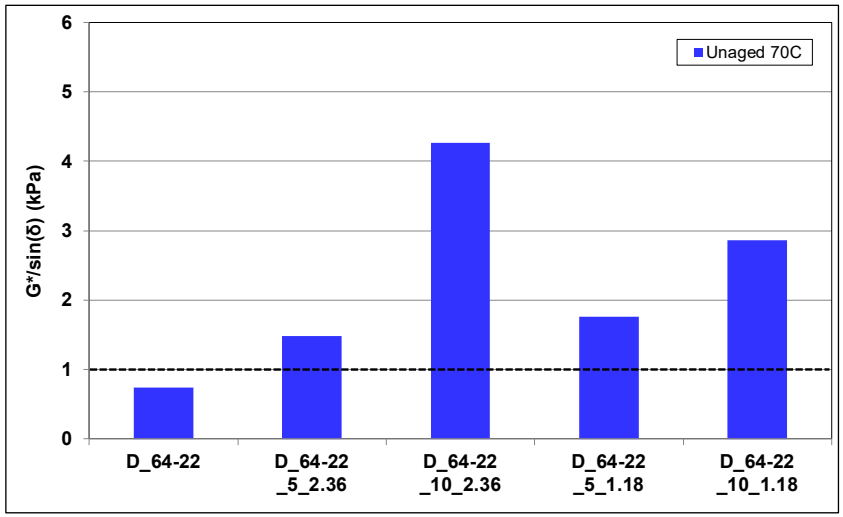

Figure 6.1: App-2/Supp-D: G*/sin(δ) of unaged binders at 70°C.

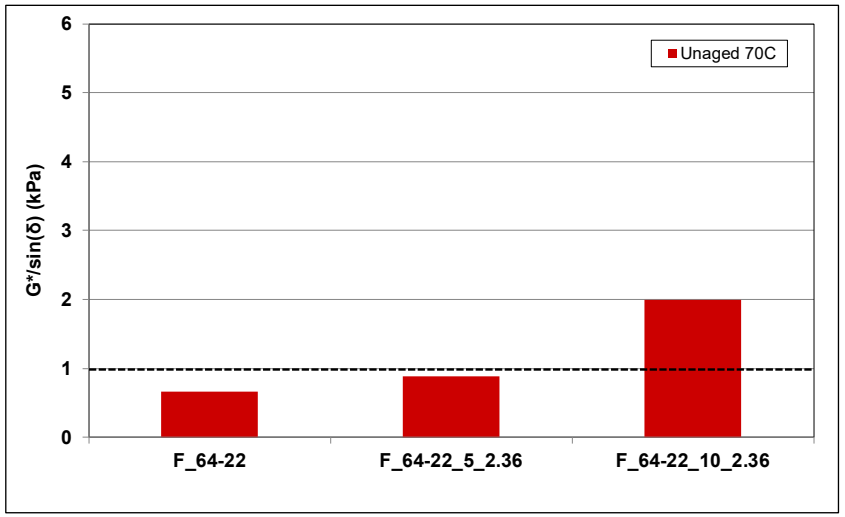

Figure 6.2: App-2/Supp-F: G*/sin(δ) of unaged binders at 70°C.

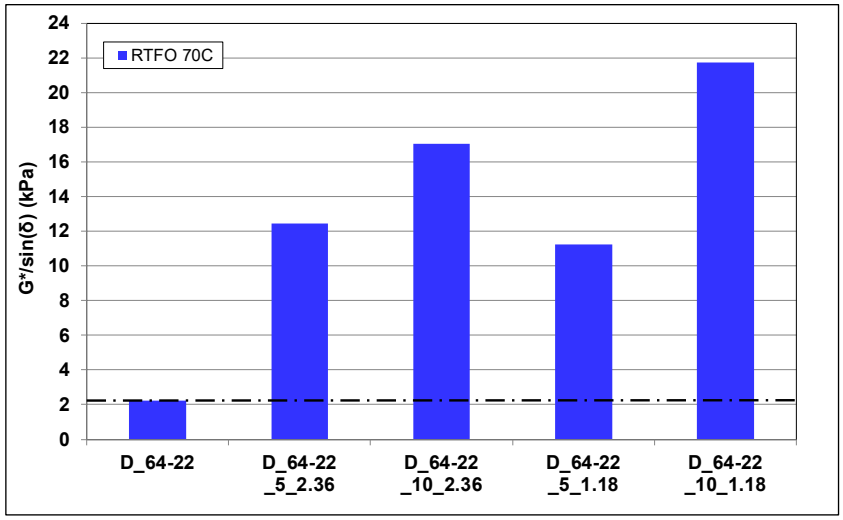

Figure 6.3: App-2/Supp-D: G*/sin(δ) of RTFO-aged binders at 70°C.

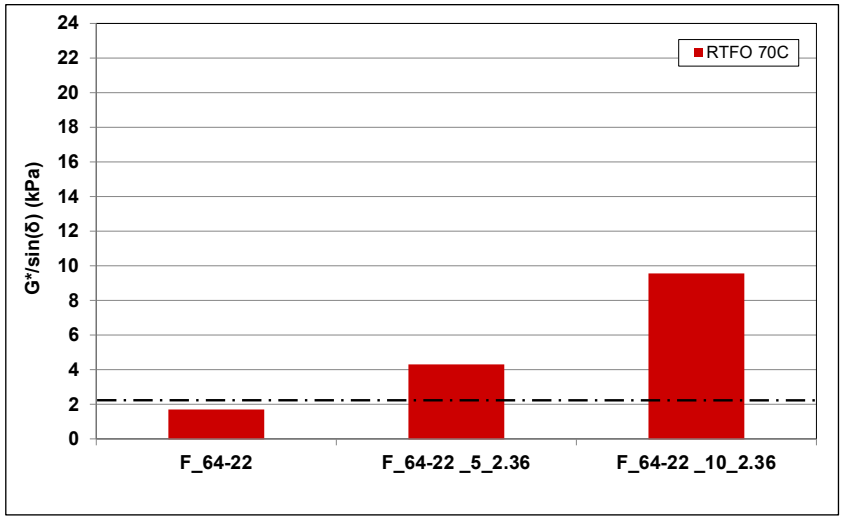

Figure 6.4: App-2/Supp-F: G*/sin(δ) of RTFO-aged binders at 70°C.

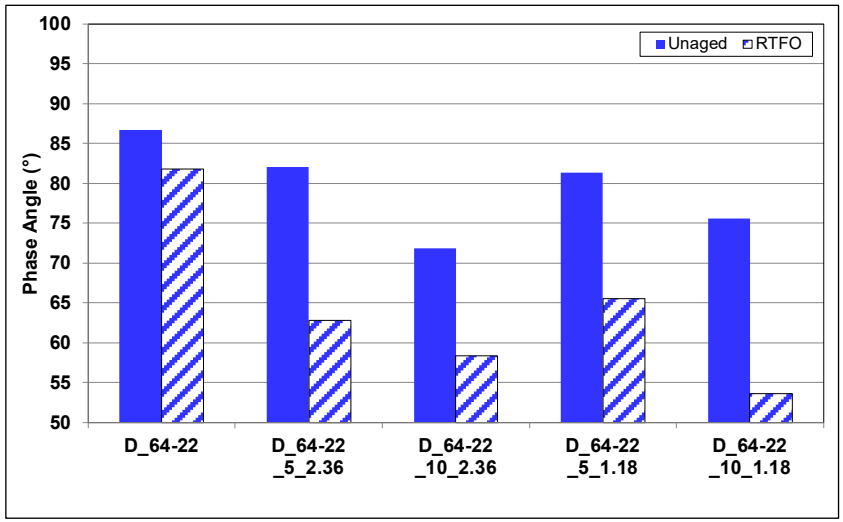

Figure 6.5: App-2/Supp-D: Phase angles at 70°C.

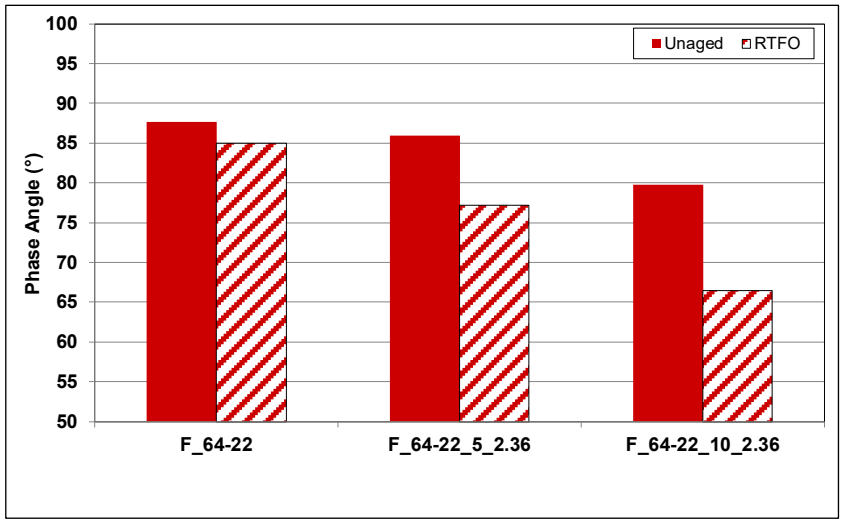

Figure 6.6: App-2/Supp-F: Phase angles at 70°C.

- The base binder used by Supplier-F did not meet the minimum PG requirements for PG 64-22 unaged or RTFO-aged binders. The binder with 5% CRM did not meet the unaged requirement but did meet the RTFO-aged requirement. The binder with 10% CRM met all requirements, but the difference between the base and modified binder was less significant than that observed in the binders from Supplier-D.
- Increasing the maximum CRM particle size from 1.18 mm to 2.36 mm had no observed effect when 5% CRM was added. However, when 10% CRM was added, the binder with the larger particles had a higher stiffness than the binder with smaller CRM particles. The differences were attributed in part to the degree of digestion, with the larger, incompletely digested particles potentially affecting the results. The issues associated with measuring the performance properties of binders with incompletely digested rubber particles, which age differently to the asphalt, are being investigated in a separate UCPRC study *(2)*.
- The phase angles of the RTFO-aged binders were lower than those of the unaged binders, as expected, indicating that RTFO aging increased the elastic behavior and decreased the viscous behavior of the binder.
- Adding CRM resulted in a drop in phase angle. The decrease in phase angle was larger for higher percentages of CRM for both the unaged and aged binders, indicating that addition of the CRM influenced the elastic properties of the binder. CRM maximum particle size did not appear to have a significant effect on phase angle, although the trends observed between the different binders were consistent with those observed in the high temperature tests.

Table 6.1 summarizes the continuous grades for the Approach-2 binders. The continuous grade is defined as the temperature where the unaged binder's G*/sin(δ) value equals 1.00 kPa and the RTFO-aged binder's G*/sin(δ) value equals 2.20 kPa The results show that:

- Adding CRM increased the continuous grades in all instances, as expected, with grade increasing with increasing CRM content.
- Particle size had limited effect on continuous grade when 5% CRM was added, but a more notable but inconsistent effect when 10% CRM was added. Adding 10% of the smaller CRM particles resulted in a lower continuous grade in the unaged condition but a higher continuous grade after RTFO aging, which supports the observation that the smaller particles digested more effectively in the binder with additional exposure to high temperatures and agitation.
- The age-hardening ratios calculated for each binder were consistent with the above observations. All binders had an age-hardening ratio greater than 2.2.
- Binders from Supplier-G had notably lower age-hardening ratios that those from Supplier-D. Although the base binder used by Supplier-G had a lower hardening ratio than

the one used by Supplier-D, the difference in hardening ratios for the CRM binders show a much greater difference.

Table 6.1: App-2: Continuous Grades

Supplier	Binder ID	Unaged Binder (°C)		RTFO-Aged Binder (°C)		Hardening Ratio
		G*/sin(δ) =1.00 kPa	Grade Change	G*/sin(δ) =2.20 kPa	Grade Change	G*/sin(δ)(RTFO) / G*/sin(δ) (Unaged) at 70°C
D	D_64-22	67.7	N/A	70.1	N/A	2.98
	D_64-22_5_2.36	73.7	+6.0	86.7	+16.6	8.63
	D_64-22_10_2.36	84.4	+16.7	90.9	+20.8	4.06
	D_64-22_5_1.18	74.6	+6.9	85.2	+15.1	6.82
	D_64-22_10_1.18	80.1	+12.4	93.1	+23.0	8.17
F	F_64-22	66.8	N/A	68.0	N/A	2.54
	F_64-22_5_2.36	68.9	+2.1	75.8	+7.8	2.42
	F_64-22_10_2.36	76.7	+9.9	83.9	+15.9	4.79

6.2.3 Intermediate-Temperature Grading

Intermediate-temperature grading results are listed in Table B.3 in Appendix B. Figure 6.7 and Figure 6.8 respectively show the average intermediate temperature test results for Supplier-D and Supplier-G PAV-aged binders. In the figures, the histograms represent the G*×sin(δ) values at 25°C, and the dot points show the continuous grades at the temperature where the binder G*×sin(δ) values equal 5,000 kPa, as specified in AASHTO M 320. The results show that:

- The CRM binders were softer than their control binders in each PG group after PAV aging, which indicated potentially better fatigue cracking resistance in thin overlay applications where cracking behavior would be strain controlled.
- The CRM binders with 10% CRM were marginally stiffer than the binders with 5% CRM with the exception of the Supplier-D binder with 10% CRM produced with particle sizes up to 2.36 mm, which had the lowest stiffness of all the binders tested.
- Binders produced with the smaller CRM particles had higher stiffnesses than those produced with the larger CRM particles.
- The Supplier-G binders had higher intermediate temperatures and higher stiffnesses at 25°C than the equivalent Supplier-D binders with larger rubber particles.
- The results imply that mixes produced with the CRM binders should have marginally better fatigue cracking resistance than mixes produced with the unmodified base binders when used in thin overlays. The results also indicate that base binder source could be an important factor in CRM binder performance.

6.2.4 Low-Temperature Grading

Bending beam rheometer test results are listed in Table B.4 in Appendix B. Figure 6.9 and Figure 6.10 show selected average results for the Supplier-D and Supplier-G PAV-aged binders.

One test temperature (-12°C) is shown for each binder. The maximum allowable creep stiffness (300 MPa) and lowest minimum allowable m-value (0.300) limits at the selected measuring temperature are shown as dashed lines on the plots. The results show that:

- All binders passed the low-temperature stiffness and m-value criteria at the minimum measuring temperatures. However, three of the Supplier-D CRM binders had m-values that were close to the minimum limit.
- The CRM binders had lower stiffnesses and lower m-values than their control binders. Stiffnesses decreased with increasing CRM content. This implies that mixes produced with Approach-2 CRM binders could have potentially better low-temperature cracking resistance than mixes produced with the control binders.
- Supplier-D CRM binders produced with smaller CRM particles had higher stiffnesses than the equivalent binders produced with larger CRM particles. Particle size did not appear to have a notable effect on m-value.

Additional BBR tests were run at -24°C to calculate the critical temperatures for these binders (i.e., where stiffness equals 300 MPa or m-value equals 0.300). The results are summarized in Table 6.2. The difference between the critical temperatures calculated by stiffness and m-value (ΔT_C) is an indicator of the binder stress relaxation *(67)*. As noted previously, less negative or positive differences in ΔT_c indicate better resistance to thermal cracking. Less negative or positive differences in ΔT_c occur when the critical parameter for meeting the specification is the m-value, or if the critical value is stiffness, then the m-value temperature is similar.

Table 6.2: App-2: Low-Temperature Test Results

Supplier	Binder ID	$T_{C\text{-stiffness}}$ (°C)	$T_{C\text{-m value}}$ (°C)	ΔT_C (°C)
D	D_64-22	-17.3	-14.6	-2.6
	D_64-22_5_2.36	-19.8	-12.2	-7.5
	D_64-22_10_2.36	-24.7	-12.5	-12.2
	D_64-22_5_1.18	-17.9	-12.3	-5.6
	D_64-22_10_1.18	-22.4	-12.3	-10.1
F	F_64-22	-17.8	-14.7	-3.1
	F_64-22_5_2.36	-18.5	-14.1	-4.3
	F_64-22_10_2.36	-20.1	-12.6	-7.5

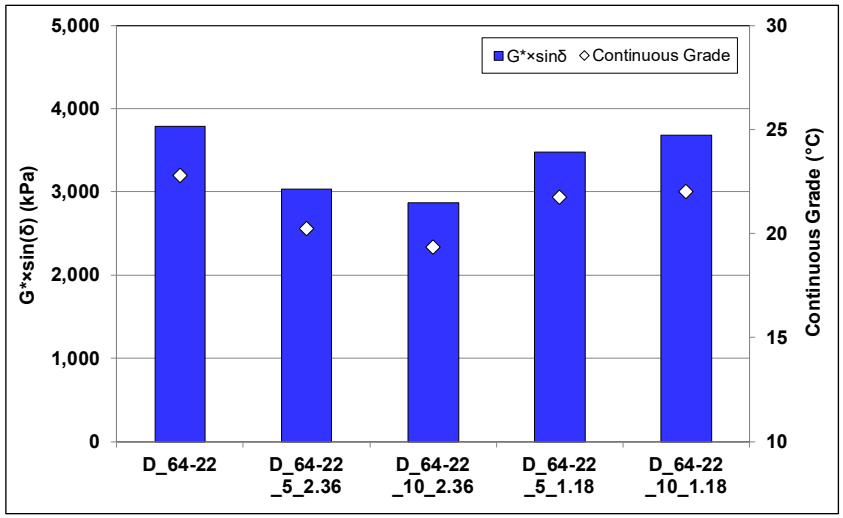

Figure 6.7: App-2/Supp-D: G*×sin (δ) of PAV-aged binders at 25°C.

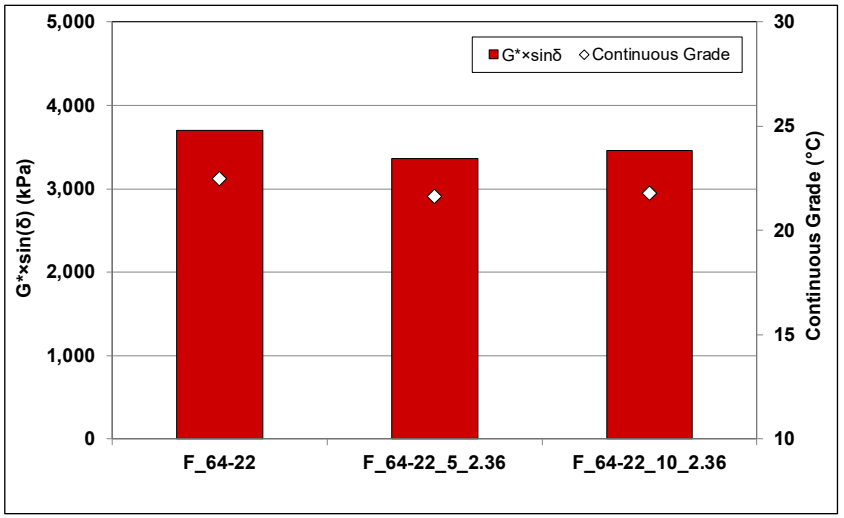

Figure 6.8: App-2/Supp-F: G*×sin (δ) of PAV-aged binders at 25°C.

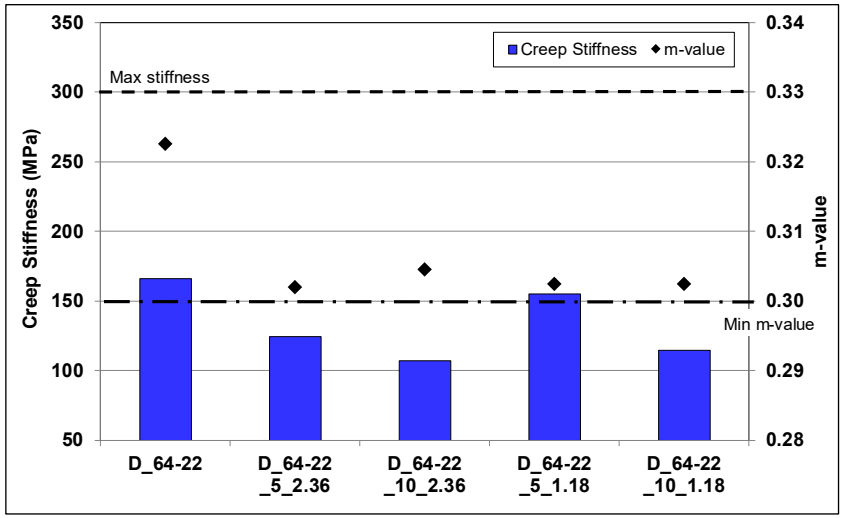

Figure 6.9: App-2/Supp-D: Low-temperature creep stiffness and m-value.

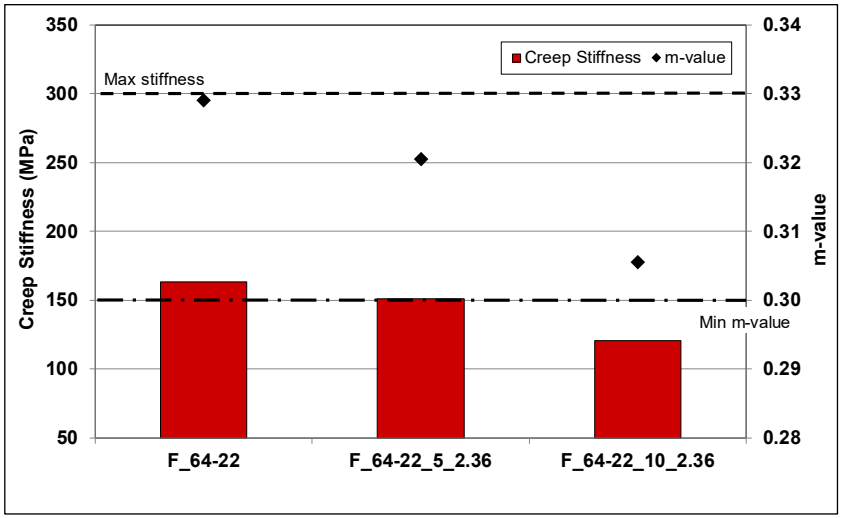

Figure 6.10: App-2/Supp-F: Low-temperature creep stiffness and m-value.

The results show that:

- The critical temperatures of the binders from both suppliers were dominated by creep stiffness, with all binders having negative ΔT_C values. However, the differences between the binders from Supplier-F were less significant than the differences between the binders from Supplier-D, indicating that the base binder source potentially influenced the results.
- Adding CRM had a notable effect on the ΔT_C values, with increasing CRM content resulting in increasingly lower values.
- For the CRM binders from Supplier-D, binders with smaller rubber particles had higher ΔT_C values than the equivalent binders with larger rubber particles.
- The results show similar trends to testing results from standard asphalt rubber binders (i.e., containing between 18% and 22% CRM) *(2)*.

6.2.5 Multiple Stress Creep Recovery

Multiple stress creep recovery test results are listed in Table B.5 in Appendix B. Figure 6.11 through Figure 6.14 show the MSCR test results at 64°C for the RTFO-aged binders. The results show that:

- There was a notable difference in the Jnr values for the two base binders, which clearly influenced the non-recoverable creep compliance (Jnr) values in the CRM binders.
- Adding CRM to both base binders lowered the Jnr for the unaged specimens, with 10% CRM having a larger effect than 5% CRM. The differences in Jnr between the base and CRM binders from Supplier-F were larger than those from Supplier-D.
- The difference in Jnr between 5% and 10% CRM in the Supplier-D binders was negligible, but more apparent in the Supplier-F binders.
- CRM particle size had a negligible effect on the Supplier-D Jnr values, indicating that the base binder influenced multiple stress creep recovery more than CRM particle size when small amounts of CRM were added.
- The differences in results between tests conducted at 0.1 kPa and 3.2 kPa were small, but consistent across the different binders.
- Adding CRM to binders, regardless of source, increased the percent recovery of the binder, as expected, with increasing CRM content having a corresponding increase in percent recovery.
- The effect of particle size on percent recovery was inconsistent. The binders with 5% CRM with larger particles had a higher percentage recovery than the binder produced with smaller particles. The opposite was observed when 10% CRM was added. These trends are consistent with the other PG tests discussed in previous sections.

- The results suggest that mixes produced with these Approach-2 CRM binders would be less susceptible to permanent deformation than mixes produced with the base binders.

6.2.6 Frequency Sweep

Figure 6.15 and Figure 6.17 show the master curves for Supplier-D and Supplier-F RTFO-aged binders and Figure 6.16 and Figure 6.18 show the curves normalized to the control binders to facilitate comparison.

The master curves were developed at 40°C using dynamic moduli and phase angles from frequency sweep tests (test temperatures of 20°C, 40°C, and 50°C). The results show that:

- The master curves of the CRM binders were flatter than the control binder, indicating that adding CRM reduced the temperature susceptibility of the binder.
- At frequency ranges below 1E-02 Hz at 40°C, which corresponds to 64°C and 10 Hz on a trafficked pavement, the normalized moduli of the CRM binders were significantly higher than the control binders. This further supports previous observations that mixes produced with the CRM binders would be expected to have better permanent deformation resistance than mixes produced with the unmodified control binders.
- At frequency ranges around 1E+03 at 40°C, which corresponds to intermediate temperatures on a trafficked pavement (i.e., 25°C and 10 Hz), the CRM binders had lower dynamic moduli than their control binders. This observation indicated that Approach-2 CRM binders were softer than the control binders. This further supports previous observations that mixes produced with the CRM binders would likely have better fatigue cracking performance in thin overlays (≤0.2 ft. [60 mm]) than mixes produced with the unmodified control binders.

6.2.7 Solubility and Ductility

Approach-2 binders were not tested for solubility and ductility.

6.2.8 FTIR Testing

Binders were tested in unaged, RTFO-aged, and PAV-aged condition. Figure 6.19 and Figure 6.20 show the carbonyl (CA) indices and Figure 6.21 and Figure 6.22 show the sulfoxide (SUL) indices of the Supplier-D and Supplier-F binders, respectively. The results show that:

- CA indices increased after RTFO-aging and again after PAV-aging, confirming that CA indices are sensitive to the level of aging in these binders and can be used to track oxidative aging.

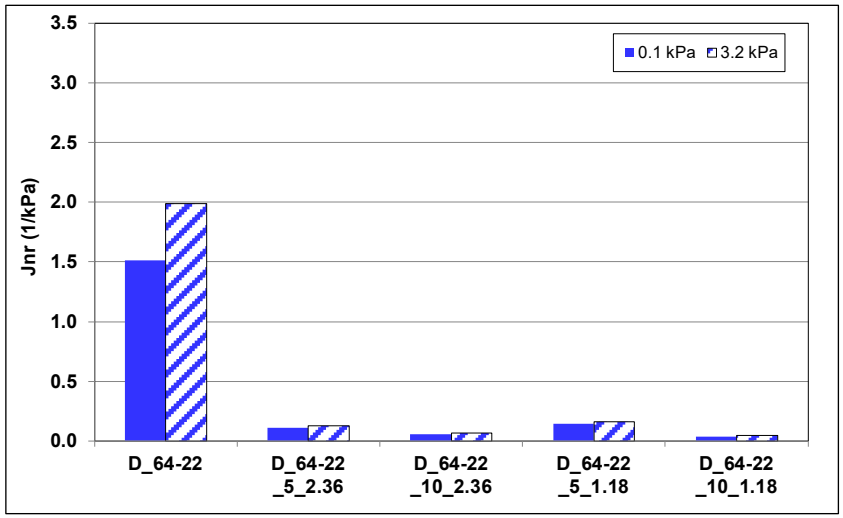

Figure 6.11: App-2/Supp-D: Jnr values of RTFO-aged binders at 64°C.

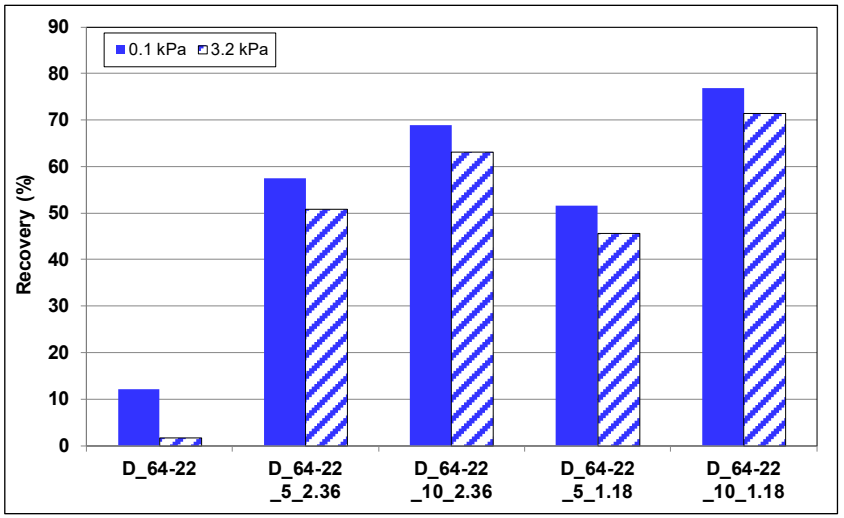

Figure 6.12: App-2/Supp-D: Percentage recovery of RTFO-aged binders at 64°C.

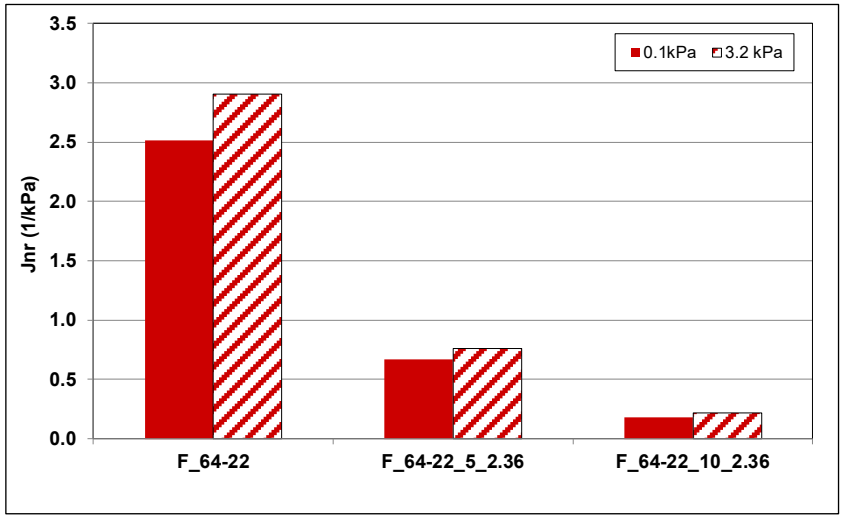

Figure 6.13: App-2/Supp-F: Jnr values of RTFO-aged binders at 64°C.

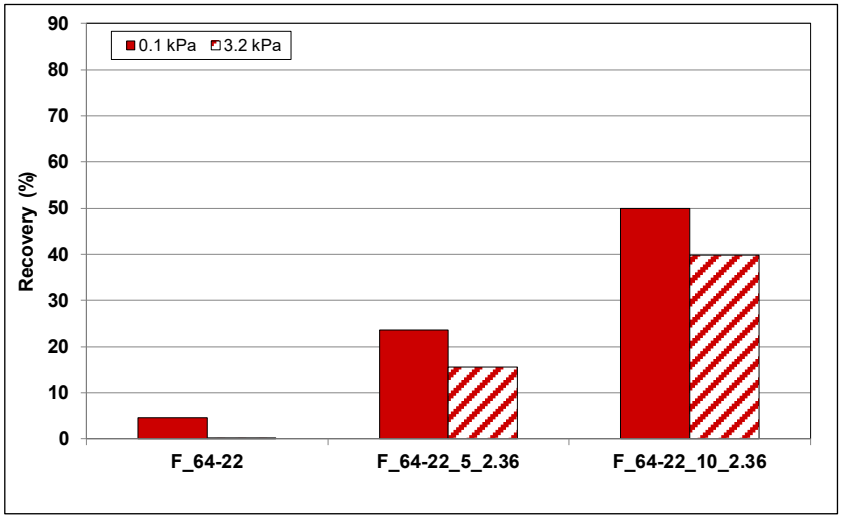

Figure 6.14: App-2/Supp-F: Percentage recovery of RTFO-aged binders at 64°C.

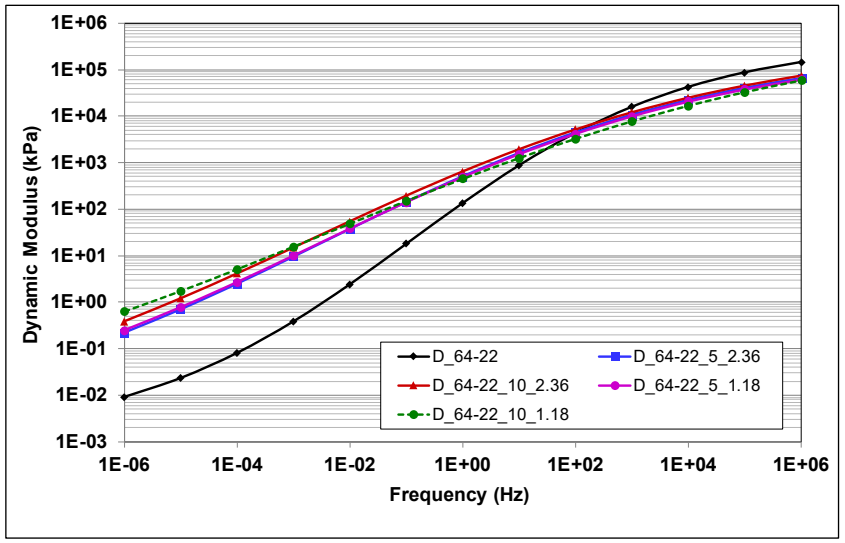

Figure 6.15: App-2/Supp-D: RTFO-aged binder master curves at 40°C.

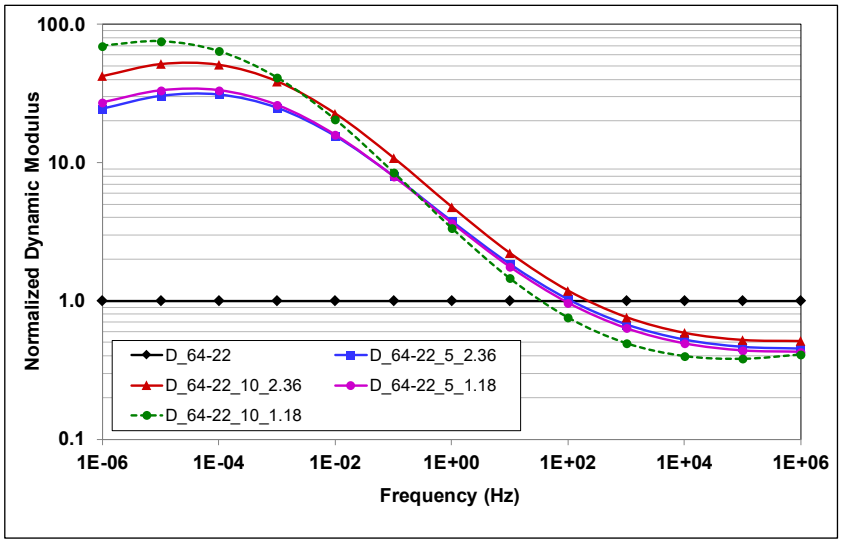

Figure 6.16: App-2/Supp-D: Normalized RTFO-aged binder master curves at 40°C.

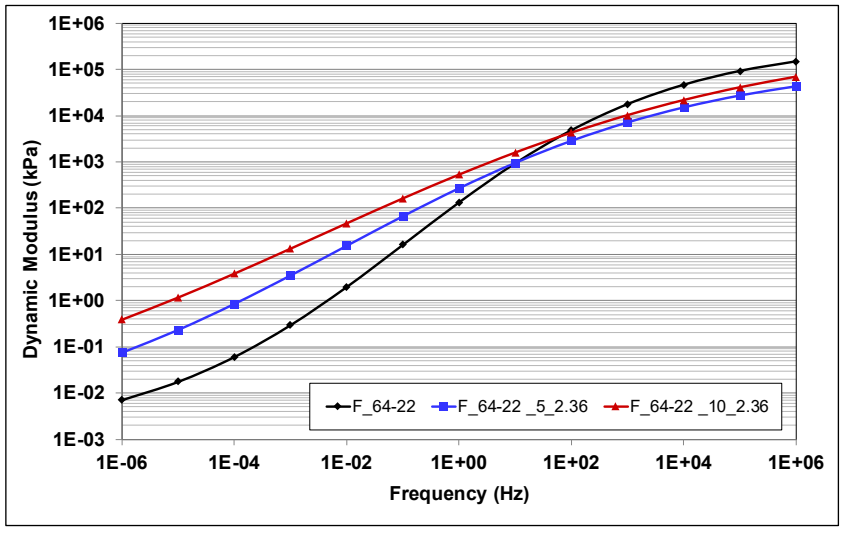

Figure 6.17: App-2/Supp-F: RTFO-aged binder master curves at 40°C.

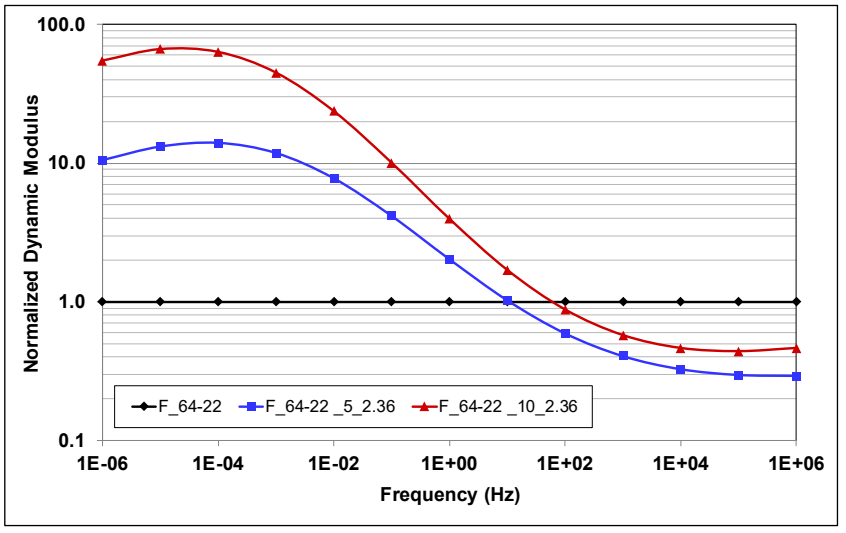

Figure 6.18: App-2/Supp-F: Normalized RTFO-aged binder master curves at 40°C.

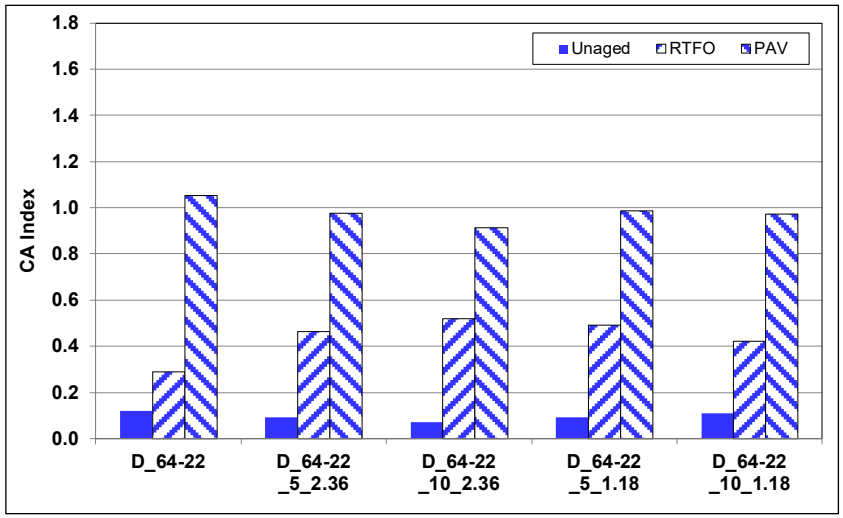

Figure 6.19: App-2/Supp-D: Carbonyl area index changes after aging.

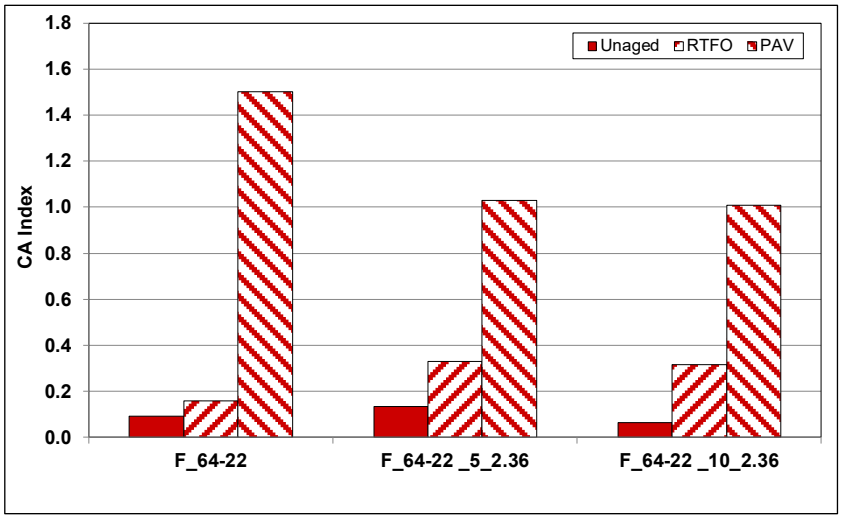

Figure 6.20: App-2/Supp-F: Carbonyl area index changes after aging.

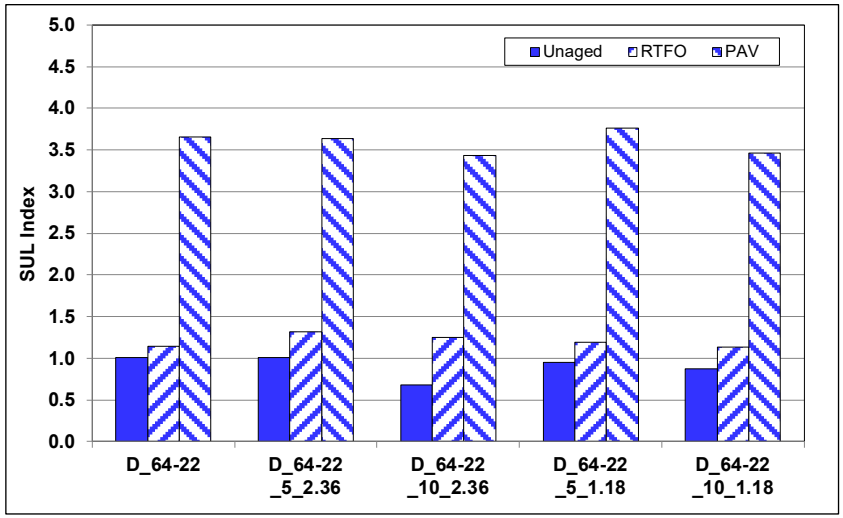

Figure 6.21: App-2/Supp-D: Sulfoxide area index changes after aging.

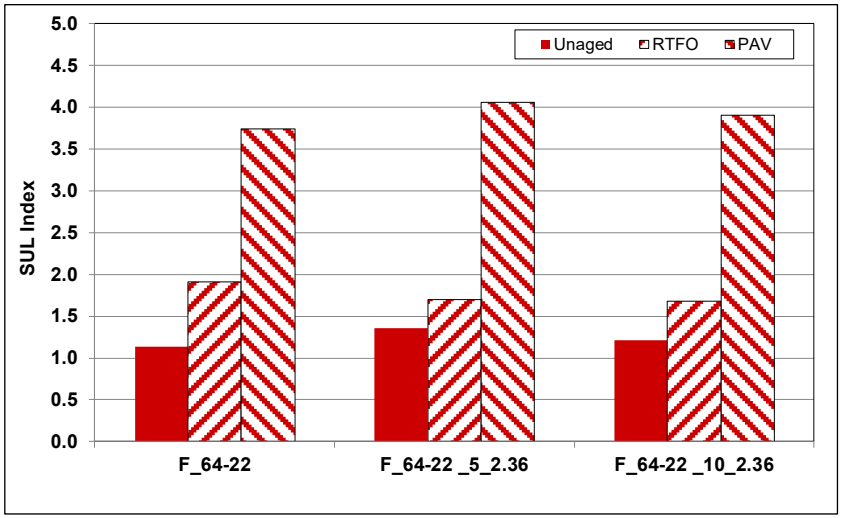

Figure 6.22: App-2/Supp-F: Sulfoxide area index changes after aging.

- Adding CRM resulted in higher CA indices after RTFO-aging compared to the base binder. The amount of CRM added and the CRM particle size did not have notable effects on the results.
- After PAV aging, the CA indices of the Supplier-D CRM binders were similar to those of the base binder, while those of the Supplier-F binders were notably lower than the base binder, indicating that this base binder was more sensitive to aging that the base binder used by Supplier-D. The amount of CRM added and the CRM particle size did not have notable effects on the PAV-aged binder results.
- SUL indices increased after RTFO- and PAV-aging, as expected, with PAV-aging have a larger effect than RTFO-aging.
- Adding CRM did not appear to have any significant effect on the SUL indices.

6.3 Approach-2 Mix Test Results

Mix testing was done on specimens prepared with binders from both suppliers. However, due to time and resource constraints, flexural modulus and fatigue/reflective cracking performance tests were carried out on select mixes produced with Supplier-D binders and coarse (<2.36 mm) CRM particles only.

6.3.1 Volumetric Mix Design

The Superpave volumetric design method (AASHTO M 323) was followed to select the optimum binder content (OBC) to meet Caltrans Type-A HMA specifications. Key parameters of the mix design include the following:

- Target air-void (AV) content at N_{design} (85 gyrations) of 4%±0.5%.
- Voids in mineral aggregate (VMA) between 13.5% and 16.5% for 3/4 in. nominal maximum aggregate size (NMAS) mixes.
- Dust proportion (DP) between 0.6 and 1.3.
- Although not specified, voids filled with asphalt (VFA) was also calculated. The recommended VFA range is between 65% and 75%.

Mixing and compaction temperatures were determined from binder temperature-viscosity curves at 135 and 165°C using a 10-mm diameter spindle. No tests were run above 165°C due to the limitations of the testing geometry. Since viscosity at higher temperatures (>165°C) is lower than the minimum viscosity that can be measured using the 10 mm spindle (i.e., approximate measuring range between 250 and 5,000,000 cPa·s), a larger 15 mm spindle, with an

approximate measuring range between 50 and 1,000,000 cPa·s would be required. However, given that the testing cup diameter is 18 mm and the coarser CRM particles had a maximum size of about 2 mm, the remaining gap of approximately 1 mm was considered too small to produce accurate results.

The mixing and compaction temperatures were determined at the temperatures where the binder viscosity reached 0.17±0.02 Pa·s and 0.28±0.03 Pa·s, respectively. Figure 6.23 and Figure 6.24 show the temperature-viscosity curves for the binders from Supplier-D and Supplier-F, respectively.

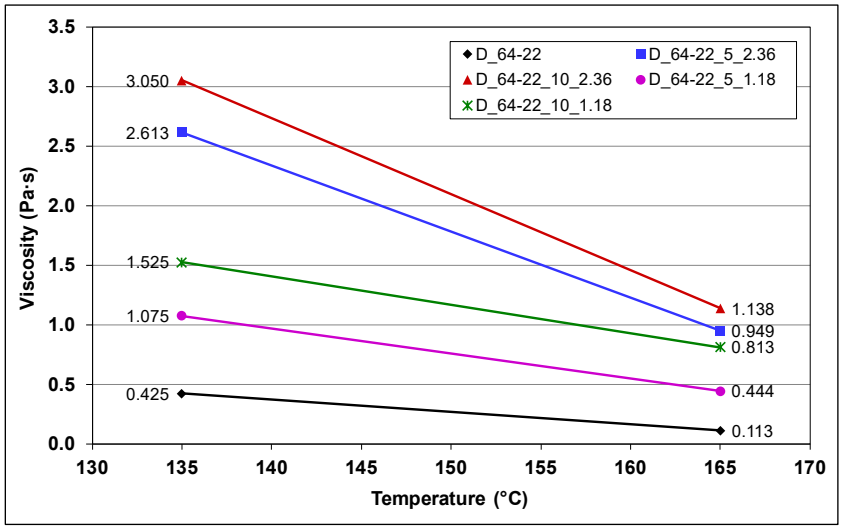

Figure 6.23: App-2/Supp-D: Rotational viscosity.

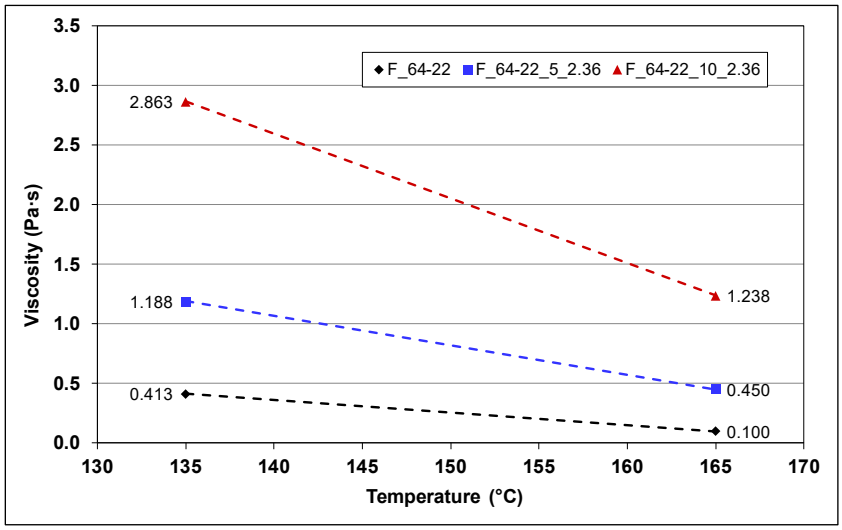

Figure 6.24: App-2/Supp-F: Rotational viscosity.

Table 6.3 summarizes the mixing and compaction temperatures and the gyratory compaction pressure. The required mixing and compaction temperatures increased with increasing CRM content and approached the lower boundary of typical mixing temperatures (i.e., 190°C to 200°C) used for traditional RHMA-G mixes. CRM particle size effected mixing and compaction temperatures, with CRM binders with 10% smaller particles requiring notably higher temperatures than the CRM binder produced with larger particles. The gyratory compactor was set to 600 kPa, which is the standard pressure used for conventional dense-graded mixes and lower than that used for RHMA-G mixes (i.e., 825 kPa).

Table 6.3: App-2: Mixing and Compaction Settings

Mix ID	Binder ID	Mixing Temp. (°C)	Compact Temp. (°C)	Compact Pressure (kPa)	Hold Time (Minutes)
S	D_64-22	160	149	600	0
T	D_64-22_5_2.36	178	176	600	0
U	D_64-22_10_2.36	180	178	600	0
V	D_64-22_5_1.18	175	172	600	0
W	D_64-22_10_1.18	192	188	600	0
P	F_64-22	160	149	600	0
Q	F_64-22_5_2.36	176	172	600	0
R	F_64-22_10_2.36	185	182	600	0

The optimum binder content of Mix-A (5.3% binder by dry weight of the aggregate), tested with the Approach-1 binders and discussed in Chapter 5, was used as the baseline, with air-void contents at N_{design} (4.0%±0.5%), VMA, DP, and VFA all verified at this binder content. The two control mixes produced with the base binders from Supplier-D and Supplier-F (Mix-P and Mix-S) both passed the Type-A HMA design requirements using the 5.3% binder content. However, the mixes produced with CRM binders required higher binder contents, consistent with the higher CRM contents, to meet the volumetric design criteria. The volumetric plots for the mixes produced with the CRM binders are presented in Figure B.1 through Figure B.6 in Appendix B. Table 6.4 summarizes the mix design results.

The optimum binder content increased 0.3% by dry weight of the aggregate when adding 5% CRM and by 0.6% when adding 10% CRM, which resulted in a similar amount of virgin asphalt to that used in the control mixes, after the weight of the CRM particles were taken into consideration. The volumetric design results show that the Approach-2 CRM binders can be used in dense-graded mixes at these CRM contents, despite the relatively large particle sizes.

Table 6.4: App-2: Mix Design Summary

Mix ID	Binder ID	Optimum Binder Content (%)	Air-Void Content at N_{design} (%)	VMA (%)	DP	VFA (%)
S	D_64-22	5.3	4.3	14.6	1.0	70.5
T	D_64-22_5_2.36	5.6	4.5	15.0	1.0	69.9
U	D_64-22_10_2.36	5.9	3.8	15.2	0.9	74.8
V	D_64-22_5_1.18	5.6	3.9	14.1	1.0	72.5
W	D_64-22_10_1.18	5.6	3.8	14.5	1.0	73.9
P	F_64-22	5.3	4.4	14.1	1.1	68.2
Q	F_64-22_5_2.36	5.6	4.1	14.8	1.0	72.6
R	F_64-22_10_2.36	6.1	4.3	15.8	0.9	72.6

6.3.2 Mix Stiffness: Dynamic and Flexural Modulus

Dynamic and flexural modulus test results are listed in Table B.4 and Table B.5 in Appendix B. Dynamic modulus master curves representing a 20°C reference temperature (developed from AMPT frequency sweep tests at 4, 21, 38, and 54°C) for the eight mixes tested are shown in Figure 6.25 and Figure 6.27. Master curves normalized to the unmodified base binder are shown in Figure 6.26 and Figure 6.28 for comparison purposes. Flexural modulus master curves for the mixes produced with Supplier-D binders and representing a 20°C reference temperature are shown in Figure 6.29, with the normalized master curve shown in Figure 6.30. These master curves were developed from beam frequency sweep tests at 10, 20, and 30°C. Figure 6.31 through Figure 6.33 show black diagrams (complex modulus versus phase angle) derived from the dynamic and flexural modulus test results.

The results show that:

- The dynamic and flexural modulus master curves showed similar trends to each other and to the binder master curves, as expected. However, the flexural master curves show a bigger difference between the control and CRM mixes at mid and lower frequencies, and between the mixes with 5% and 10% CRM.
- Mixes produced with binders from Supplier-D had marginally higher stiffnesses than the mixes produced with binders from Supplier-F. The differences in stiffness between the different Supplier-F binder mixes were less distinct than the differences between the Supplier-D binder mixes.
- Mix stiffnesses were similar when the frequency was higher than 10 Hz at 20°C. The CRM mixes were stiffer than the control mix when the frequency was less than 10 Hz at 20°C, indicating that these CRM mixes could potentially be more resistant to rutting at high temperatures than the control mix.

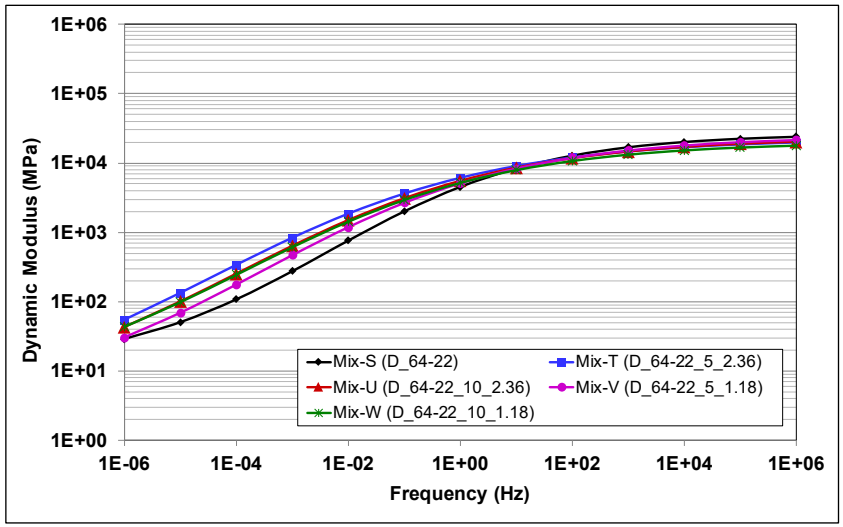

Figure 6.25: App-2/Supp-D: Dynamic modulus master curves at 20°C.

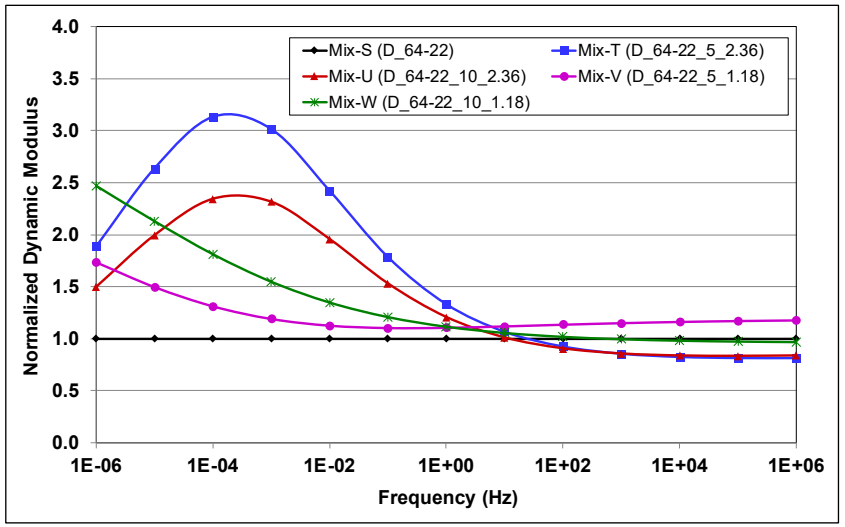

Figure 6.26: App-2/Supp-D: Normalized dynamic modulus master curves at 20°C.

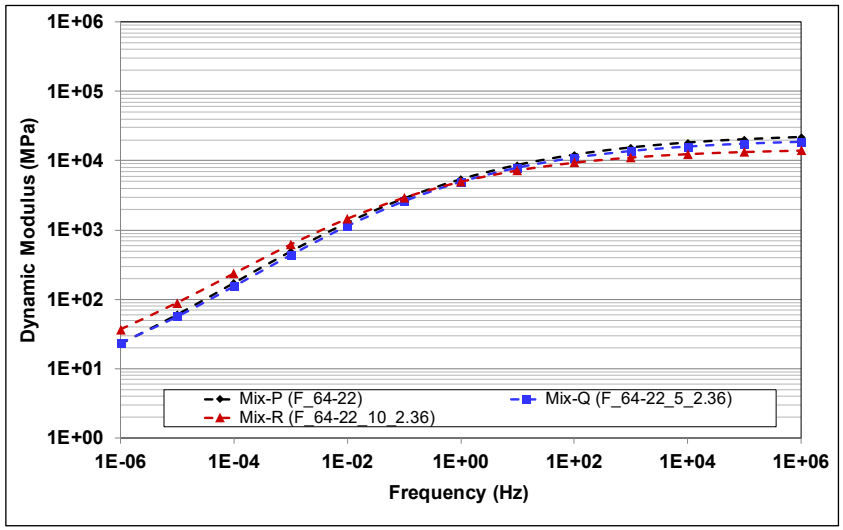

Figure 6.27: App-2/Supp-F: Dynamic modulus master curves at 20°C.

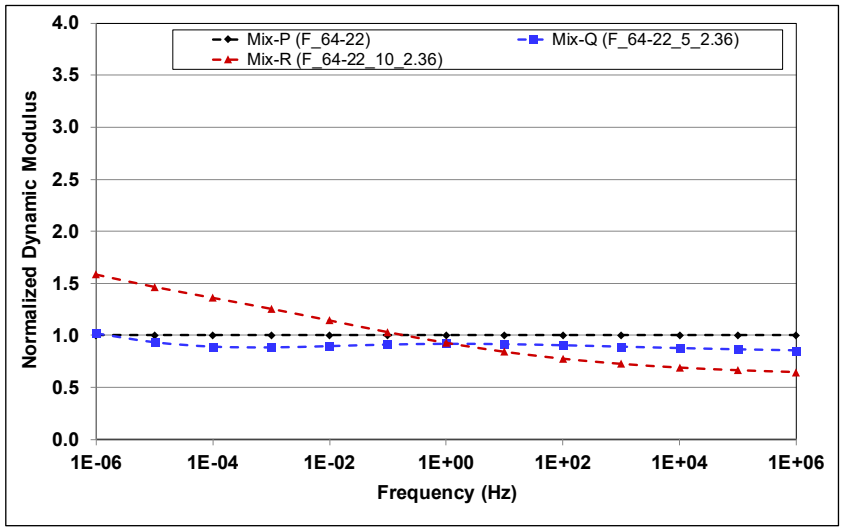

Figure 6.28: App-2/Supp-F: Normalized dynamic modulus master curves at 20°C.

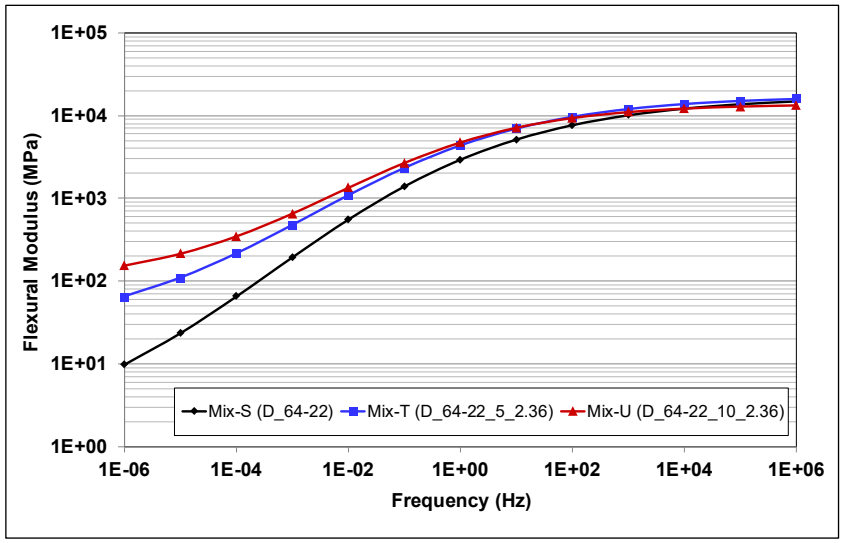

Figure 6.29: App-2/Supp-D: Flexural modulus master curves at 20°C.

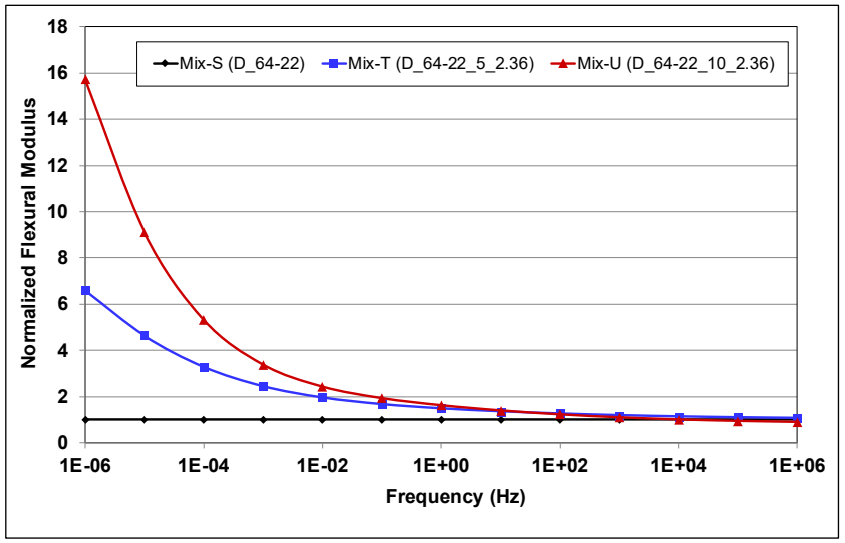

Figure 6.30: App-2/Supp-D: Normalized flexural modulus master curves at 20°C.

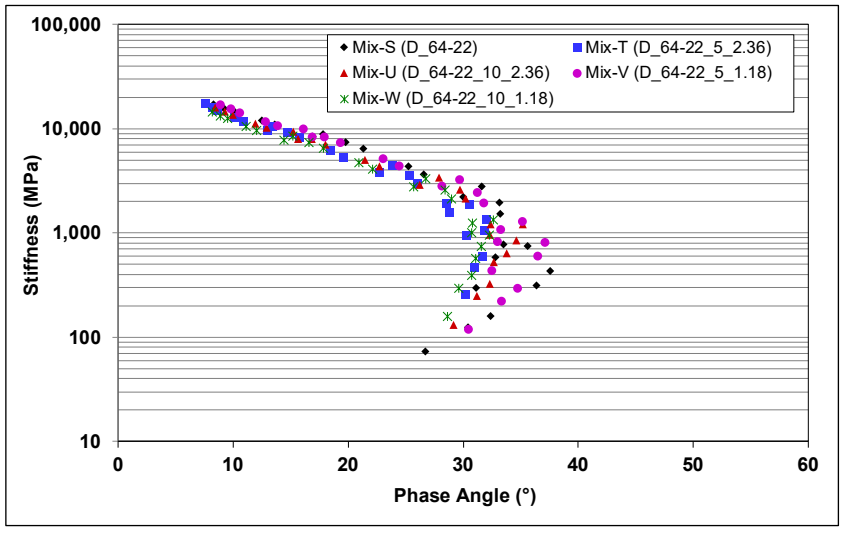

Figure 6.31: App-2/Supp-D: Black diagram of dynamic modulus results.

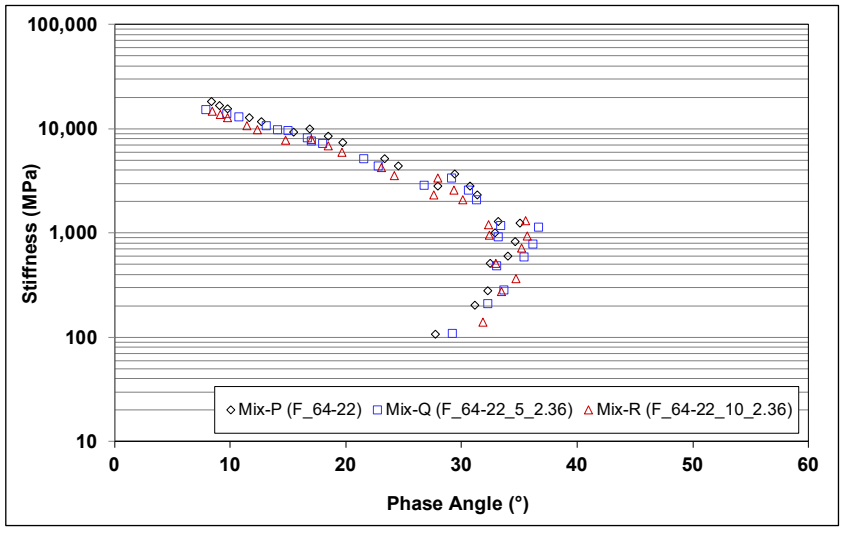

Figure 6.32: App-2/Supp-F: Black diagram of dynamic modulus results.

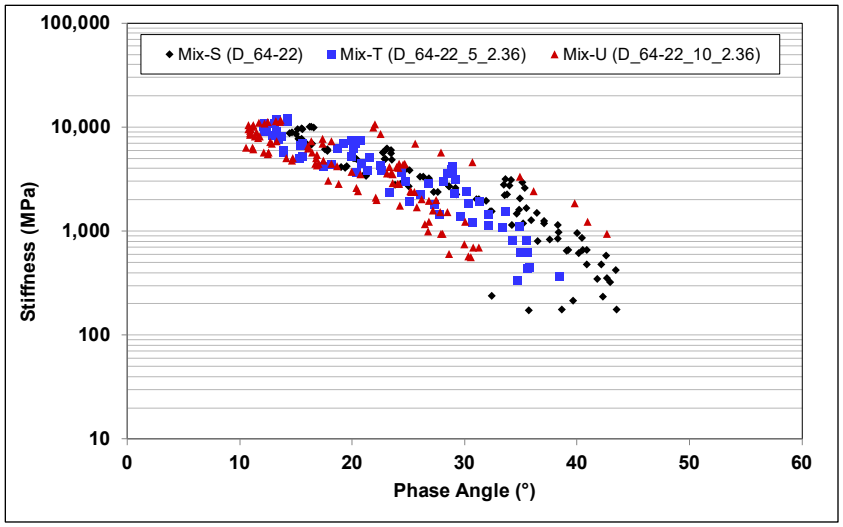

Figure 6.33: App-2/Supp-D: Black diagram of flexural modulus results.

- CRM particle size had an apparent influence on stiffness, with the mixes produced with the binders with larger particles having higher stiffnesses at lower frequencies that the mixes produced with binders with smaller particles.
- The black diagrams showed no significant differences between the mixes produced with the control binders and those produced with the CRM binders.
- The results indicate that the CRM mixes should have similar, or marginally better rutting and cracking performance than the control mixes.

6.3.3 Rutting Resistance: Unconfined Repeated Load Triaxial Test

Repeated load triaxial (RLT) test results are listed in Table B.6 in Appendix B. Figure 6.34 and Figure 6.35 plot the average unconfined RLT results for mixes produced with binders from Supplier-D and Supplier-F, respectively. Whiskers on the data indicate the lowest and highest flow numbers of the five replicates in each mix. Figure 6.36 and Figure 6.37 plot the average permanent strain against load cycle test results at 50°C. The results show that:

- There was some variability across the replicate test results, with the highest variability observed between the Mix-W results. However, the AASHTO T 378 maximum coefficient of variation for a single operator testing 19 mm (3/4 in.) NMAS mixes of 58.5% was not exceeded for any of the mixes.
- Mixes with CRM had higher flow numbers than the control mixes, and mixes with 10% CRM had higher flow numbers than mixes with 5% CRM.
- Mixes produced with CRM binders with 5% and 10% of the smaller CRM particles had higher flow numbers than those with the same CRM content but larger CRM particles. This was attributed in part to better digestion and less swelling of the smaller CRM particles.

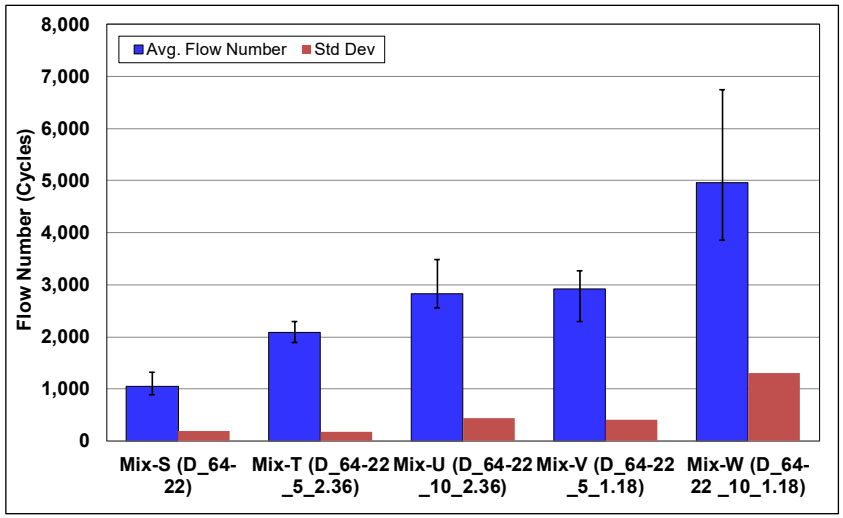

Figure 6.34: App-2/Supp-D: Flow number at 50°C.

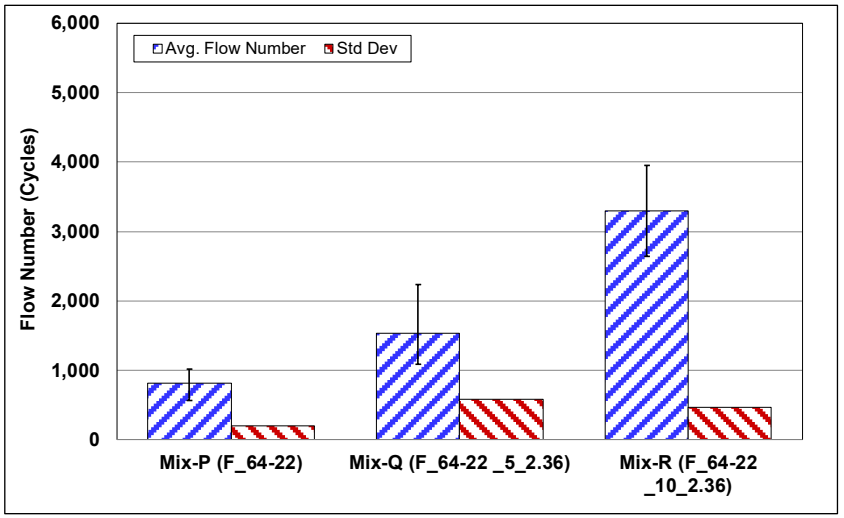

Figure 6.35: App-2/Supp-F: Flow number at 50°C.

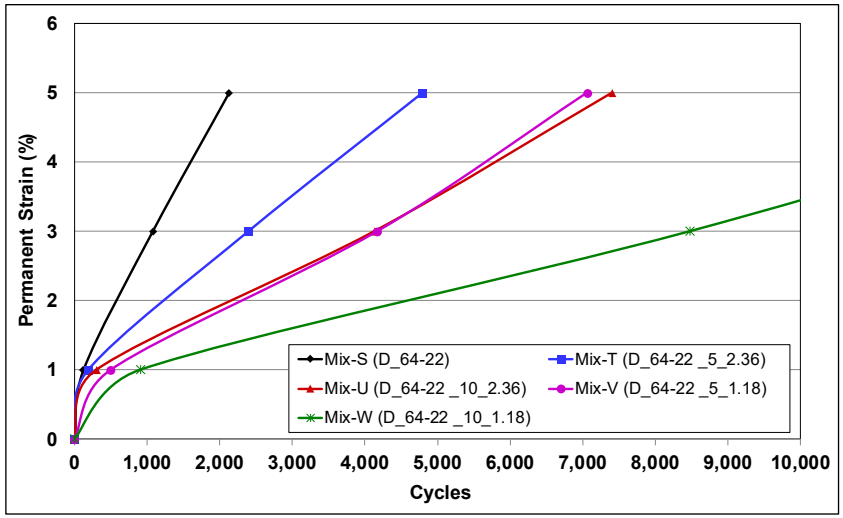

Figure 6.36: App-2/Supp-D: Average permanent strain versus load cycle at 50°C.

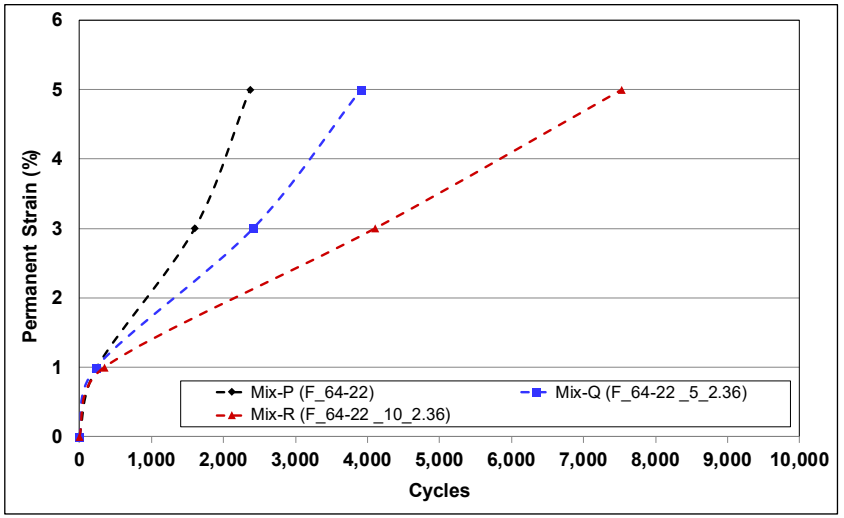

Figure 6.37: App-2/Supp-F: Average permanent strain versus load cycle at 50°C.

- Trends observed for the number of cycles to 1%, 3%, and 5% permanent axial strain were similar to those observed for the flow number results at all strain levels. At lower strain levels, the difference in the number of cycles required to reach the selected strain level was much closer between the mixes.
- These observations, together with those from the frequency sweep and multiple stress creep recovery tests, indicate that mixes produced with Approach-2 CRM binders will potentially have better rutting resistance than mixes produced with the respective control binders.

6.3.4 Rutting and Moisture Resistance: Hamburg Wheel Track Test

Hamburg wheel track test results are listed in Table B.7 in Appendix B. Figure 6.38 and Figure 6.39 show the results for all mixes at 50°C. The rut depth shown is the average of the left and right wheel track. The results show that:

- All mixes performed well within the specified limits (average maximum rut depth may not exceed 0.5 in. [≈12.5 mm] at 15,000 load cycles) and that no mixes were moisture sensitive. Inflection points indicating stripping were not observed for any of the mixes.
- The results were consistent with the RLT results discussed in Section 6.3.3, with the benefits of using CRM binders clearly evident. However, the differences between mixes with 5% and 10% CRM and with finer and coarse particles were less apparent.

6.3.5 Fatigue/Reflective Cracking Resistance: Four-Point Beam Test

Four-point beam test results for mixes produced with three of the binders from Supplier-D are listed in Table B.8 in Appendix B. No tests were conducted on mixes produced with the binders with the smaller CRM (<1.18 mm) from Supplier-D or the binders from Supplier-F. Figure 6.40 shows the flexural beam fatigue test results for the five mixes at 20°C and 10 Hz. The plots show the predicted fatigue life against the applied peak-to-peak strain in a log-log plot. Figure 6.41 shows the calculated fatigue lives at 200, 300, 400, and 600 µstrain. The results show that:

- Only the model for the control mix was considered appropriate based on the relatively high R-squared value of the model fitting and the repeatability of the test results at each strain level. The models for the CRM mixes had relatively poor correlations, indicating higher variability in the test results.

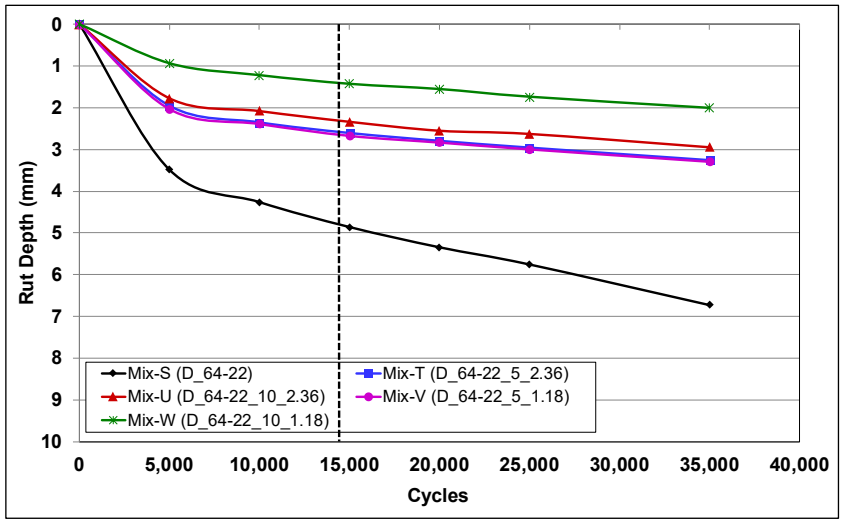

Figure 6.38: App-2/Supp-D: Hamburg Wheel Track rutting at 50°C.

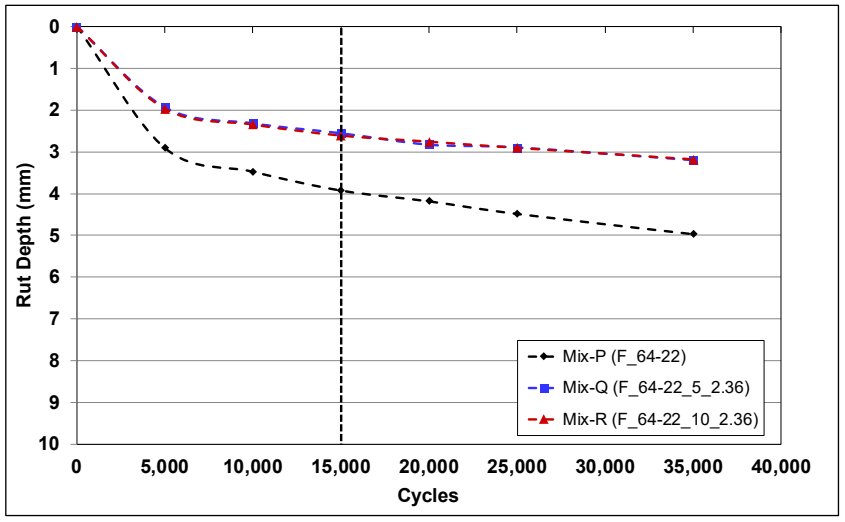

Figure 6.39: App-2/Supp-F: Hamburg Wheel Track rutting at 50°C.

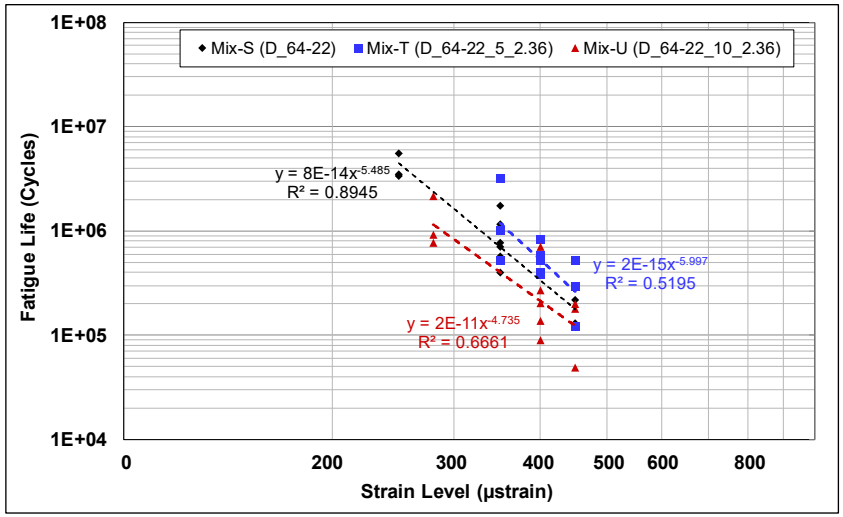

Figure 6.40: App-2/Supp-D: Beam fatigue at 20°C and 10 Hz.

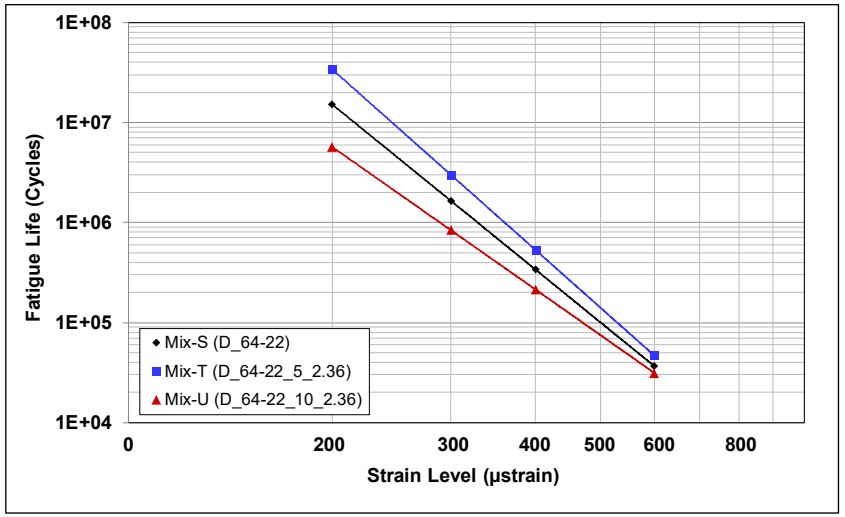

Figure 6.41: App-2/Supp-D: Calculated fatigue life.

- Taking these poor correlations into consideration, the CRM mix with 5% CRM showed potential for having a longer fatigue life than the control mixes, while the mix with 10% CRM showed potential for having a shorter fatigue life than the control. This could be an indication of potential fatigue cracking problems associated with the presence of too many incompletely digested CRM particles in a dense-graded mix. The mix with 10% CRM was also stiffer than the other mixes, based on the master curve results, and would therefore be expected to have a shorter fatigue life under strain-controlled conditions in thin overlays.
- The performance differences between the three mixes reduced with increasing strain level.

6.3.6 Fracture Cracking Resistance: Semicircular Bend Test

Semicircular bend test results are listed in Table B.9 in Appendix B. Figure 6.42 through Figure 6.45 respectively show the average fracture energy and strength, and flexibility index results.

Whiskers on the data show the lowest and highest fracture energies and flexibility indices, respectively for the four replicates tested for each mix. The results show that:

- Fracture energy and flexibility index results did not show similar trends. This was attributed in part to the high variability in the results of the replicate tests in most mixes. Table 6.5 provides a statistical analysis of the results. The coefficients of variation (CoV) for flexibility index were high in most instances, which complicated any comparisons between the different mixes and comparisons with the fatigue test results.
- The fracture energy and strength results had lower coefficients of variation than the flexibility index results, with strength results showing similar trends to the fracture index in most instances.

Table 6.5: App-2: Semicircular Bend Test Results

Mix ID	Binder ID	Fracture Energy (Jol/m^2)	CoV[a] (%)	Flexibility Index	CoV (%)	Strength (MPa)	CoV (%)
P	F_64-22	2,091	14.0	3.56	45.6	0.54	11.5
Q	F_64-22_5_2.36	2,174	20.2	2.85	93.1	0.63	15.7
R	F_64-22_10_2.36	2,138	11.8	3.54	42.6	0.51	14.3
S	D-64-22	2,339	16.0	2.98	71.0	0.59	4.9
T	D-64-22_5_2.36	2,163	10.2	2.84	32.1	0.55	6.4
U	D-64-22_10_2.36	2,322	20.1	2.38	71.5	0.59	10.7
V	D-64-22_5_1.18	2,169	18.7	1.01	76.5	0.63	6.4
W	D-64-22_10_1.18	1,897	13.7	0.93	87.1	0.61	8.2

[a] CoV: coefficient of variation

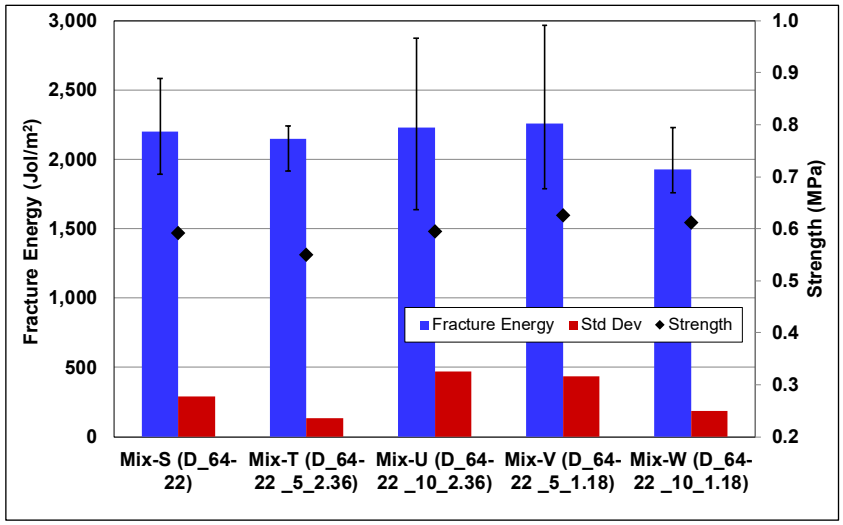

Figure 6.42: App-2/Supp-D: SCB fracture energy and tensile strength at 25°C.

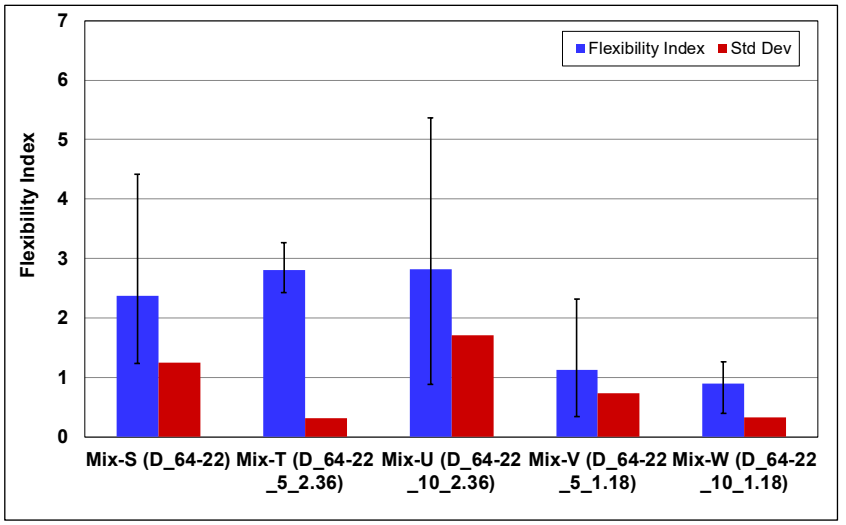

Figure 6.43: App-2/Supp-D: SCB flexibility index at 25°C.

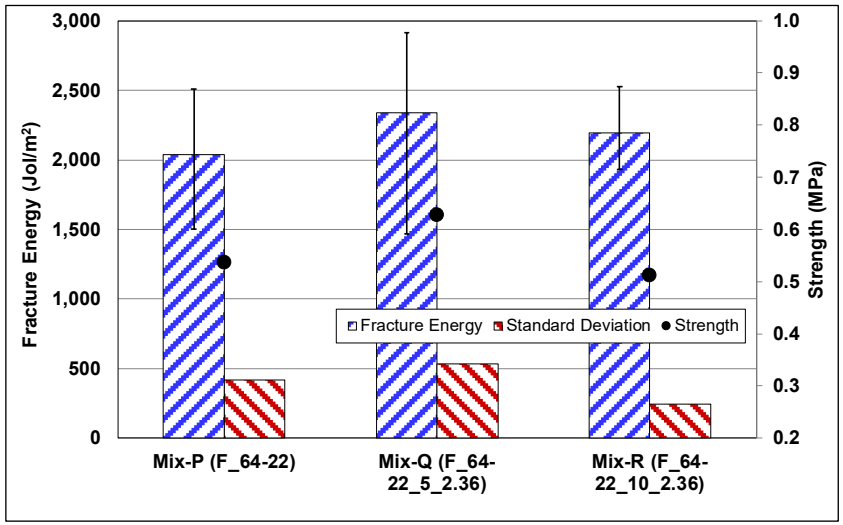

Figure 6.44: App-2/Supp-F: SCB fracture energy and tensile strength at 25°C.

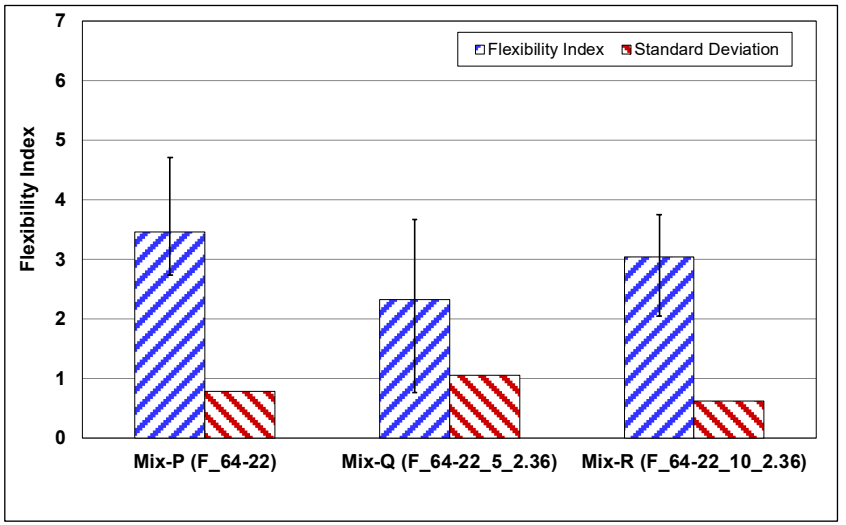

Figure 6.45: App-2/Supp-F: SCB flexibility index at 25°C.

6.3.7 Low-Temperature Cracking: Uniaxial Thermal Stress and Strain Test

Uniaxial Thermal Stress and Strain testing was not conducted on mixes produced with Approach-2 binders.

6.4 Approach-2 Test Result Summary

This chapter covers the evaluation of Approach-2 CRM binders (5% and 10% CRM by weight of the binder, with CRM particle gradations <1.18 mm and <2.36 mm) produced using a field-blending process. The following important observations were made from the test results:

- The four CRM binders (5% and 10% CRM with particles <2.36 mm and 1.18 mm, respectively) produced by Supplier-D, and the two Approach-2 CRM binders (5% and 10% CRM with particles <2.36 mm) produced by Supplier-F had higher high-performance grades at unaged and RTFO-aged conditions than the unmodified control binders. They had similar or lower intermediate-performance grades at PAV-aged conditions than their control binders.
- The low PGs of the CRM binders, determined by the BBR test, were the same as the control binders; however, the creep stiffness of the CRM binder decreased with increasing CRM content.
- The CRM binders had lower non-recoverable compliance and higher recovery than their control base binders in the multiple stress creep recovery test, indicating that modification with this type of CRM could improve the rutting resistance of the binder.
- FTIR measurements showed that the CRM binders had lower carbonyl area indices than the control binders after PAV-aging. No difference in sulfoxide area index was observed between the CRM binders and the control binders.
- The CRM binders could be accommodated in a dense-graded aggregate structure at the same binder content as the control mix, and still meet all mix design requirements. Increases in CRM content and CRM particle size required increases in the binder content to meet the volumetric design criteria (i.e., air-void content, VMA, and DP).
- The stiffness master curves indicated that the CRM mixes had higher stiffnesses than the control mixes at higher temperatures, but only slight stiffness differences at intermediate temperatures.
- Mixes produced with CRM binders had equivalent or better rutting and moisture resistance than their control mixes. Repeated load triaxial tests showed that mixes with 10% CRM performed better than mixes with 5% CRM, and that mixes with smaller CRM particles performed better than mixes with larger CRM particles. These observations were less apparent in the Hamburg Wheel Track test.

- High variability in the fatigue test results, and the limited number of mixes tested, complicated interpretation of the results. This was attributed in part to the effects of incompletely digested CRM particles in the dense gradation mix. However, the results did indicate that the CRM mix with 5% CRM (<2.36 mm) had potentially better fatigue resistance than the control mix.
- Fracture cracking test results were inconclusive because of the high variability between replicate specimens in each mix.

7. EVALUATION OF APPROACH-3 MIXES

7.1 Introduction

This chapter discusses the performance of Approach-3 CRM mixes. Given that dry CRM was added directly to the aggregate, binder testing was not required and therefore only mix test results are discussed. CRM particles (<2.36 mm) were added at 0.25% and 0.5% by dry weight of the aggregate, approximately equivalent to adding 5% and 10% CRM to the binder in mix designs with an optimum binder content of 6.0%. Summary plots are presented with the text, while tabulated test results are provided in Appendix C. Testing details are discussed in Chapter 4 and are not repeated in this chapter.

7.2 Approach-3 Mix Test Results

Mix testing was done on specimens prepared with the PG 64-16 base binder provided by Refinery-A, which is the same control binder discussed in the Approach-1 Mix-A testing in Chapter 5.

7.2.1 Volumetric Mix Design

The Superpave volumetric design method (AASHTO M 323) was followed to select the optimum binder content to meet Caltrans Type-A HMA specifications. Aggregate gradations were not adjusted to accommodate the CRM particles. Key parameters of the mix design included the following:

- Target air-void (AV) content at N_{design} (85 gyrations) of 4%±0.5%
- Voids in mineral aggregate (VMA) between 13.5% and 16.5% for 3/4 in. nominal maximum aggregate size (NMAS) mixes
- Dust proportion (DP) between 0.6 and 1.3.
- Although not specified, voids filled with asphalt (VFA) was also calculated. The recommended VFA range is between 65% and 75%.

Table 7.1 summarizes the mixing and compaction temperatures and the gyratory compaction pressures. Specimen bulging, attributed to swelling of the CRM particles when heated, was observed in several gyratory-compacted specimens and therefore all specimens were subjected

to a 30-minute hold inside the gyratory or rolling wheel compaction molds to eliminate this problem.

Table 7.1: App-3: Mixing and Compaction Settings

Mix ID	Binder ID	Mixing Temp. (°C)	Compact Temp (C)	Compact Pressure (kPa)	Hold Time (minutes)
A	A_64-16	150/165	140	600	0
G	A_64-16_5_2.36_DRY	150/165	140	600	30
H	A_64-16_10_2.36_DRY	150/165	140	600	30

Mix-A, produced with the unmodified base binder from Refinery-A, was used for the mix design confirmation (discussed in Section 5.3.1). Mix-G (0.25% CRM) and Mix-H (0.5% CRM) were verified at the Mix-A design optimum binder content (5.3%) and adjustments made to meet the volumetric requirements listed above.

Table 7.2 summarizes the verifications and adjusted optimum binder contents for Mix-G and Mix-H. The volumetric plots for the two mixes are provided in Figure C.1 and Figure C.2 in Appendix C. Both mixes failed to meet the 4.0%±0.5% air-void content requirement at the 5.3% binder content, which was attributed to the presence of the relatively large dry CRM particles. It should be noted that most dry mixes produced in the United States are now prepared with CRM particles smaller than 500 µm (passing the #30 sieve). Based on the volumetric plots, binder contents were increased to 6.0% and 6.8% for Mix-G and Mix-H, respectively. Despite these increased binder contents, and additional adjustments, Mix-G only just met, and Mix-H did not meet, the VMA or VFA criteria. This was attributed to the relatively large CRM particles not being satisfactorily accommodated in the dense gradation.

Table 7.2: App-3: Mix Design Summary

Mix ID	Binder ID	Optimum Binder Content (%)	Air-Void Content at N_{design} (%)	VMA (%)	DP	VFA (%)
A	A_64-16	5.3	4.0	13.7	1.1	71.1
G	A_64-16_5_2.36_DRY	6.0	4.1	16.1	0.9	74.3
H	A_64-16_10_2.36_DRY	6.8	4.2	18.9	0.7	77.9

7.2.2 Mix Stiffness: Dynamic and Flexural Modulus

Dynamic and flexural modulus test results are listed in Table C.1 and Table C.2 in Appendix C, respectively. Dynamic and flexural modulus master curves for the three mixes at a 20°C reference

temperature are shown in Figure 7.1 and Figure 7.3, respectively. Master curves normalized to the unmodified base binder are shown in Figure 7.2 and Figure 7.4, respectively. Dynamic modulus master curves were developed from frequency sweep testing in an AMPT at 4, 21, 38, and 54°C, while flexural frequency sweep testing was done in a beam fatigue apparatus at 10, 20, and 30°C. The results show that:

- The dynamic and flexural modulus master curves showed similar trends to each other, as expected. However, the flexural master curves show a smaller difference between the control and CRM mixes at mid and lower frequencies. The normalized curves show some erratic trends in the mix with 0.5% CRM, which was attributed to the use of relatively large CRM particles and to the mix not meeting all volumetric requirements.
- The CRM mixes had lower stiffnesses than the control mix at all frequencies, indicating the potential for lower rutting resistance at higher temperatures, but potentially better cracking performance at intermediate temperatures, than the control mix.

Figure 7.5 and Figure 7.6 show black diagrams (complex modulus versus phase angle) derived from the dynamic and flexural modulus test results. The black diagram derived from the dynamic modulus test results was consistent with the dynamic modulus master curve and does not show significant differences between the control and CRM mixes. However, the black diagram derived from the flexural modulus test results does not show any trends, which was expected given the inconsistencies observed on the flexural modulus master curves.

7.2.3 Rutting Resistance: Unconfined Repeated Load Triaxial Test

Repeated load triaxial test results are listed in Table C.3 in Appendix C. Figure 7.7 and Figure 7.8 respectively plot the average unconfined RLT and average permanent strain against load cycle test results at 50°C. Whiskers on the flow number data indicate the lowest and highest flow numbers of the five replicates in each mix. The results show that:

- There was considerable variability across the replicate test results. However, the AASHTO T 378 maximum coefficient of variation for a single operator testing 19 mm (3/4 in.) NMAS mixes of 58.5% was not exceeded for any of the mixes.
- Taking this variability into consideration, the CRM mixes had lower flow numbers and therefore less rutting resistance than the control mix, consistent with the observations from the dynamic modulus master curves.

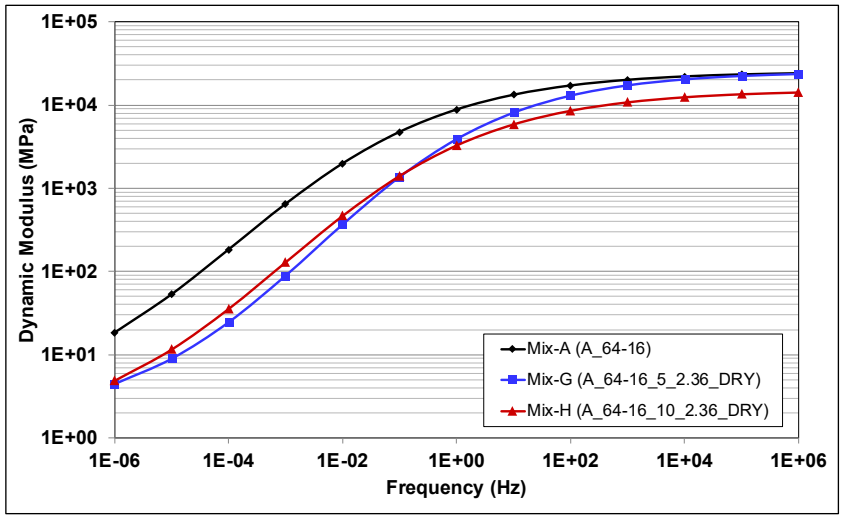

Figure 7.1: App-3: Dynamic modulus master curves at 20°C.

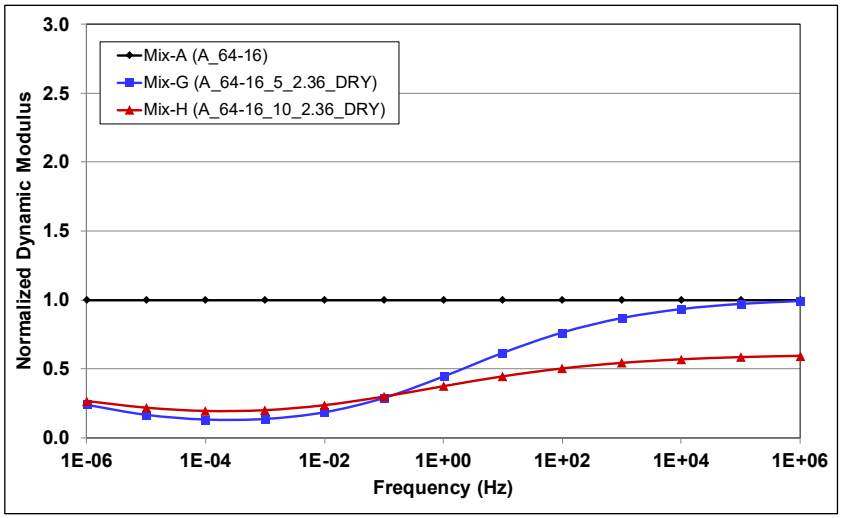

Figure 7.2: App-3: Normalized dynamic modulus master curves at 20°C.

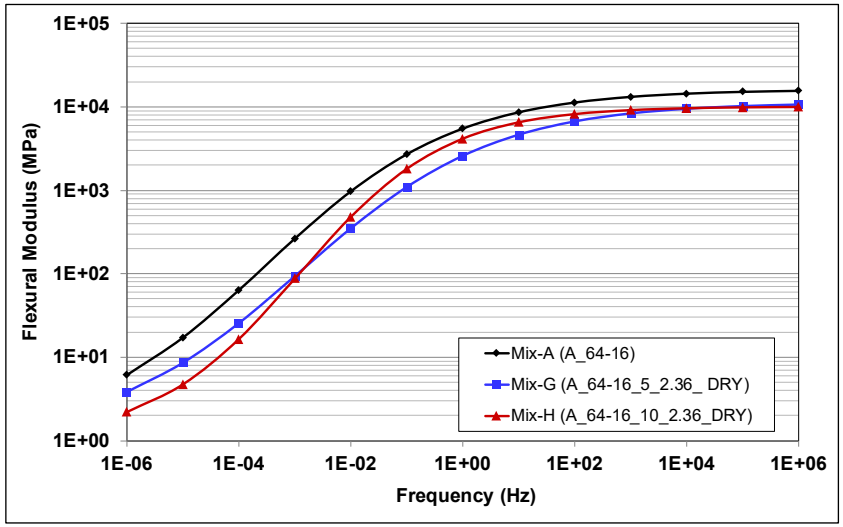

Figure 7.3: App-3: Flexural modulus master curves at 20°C.

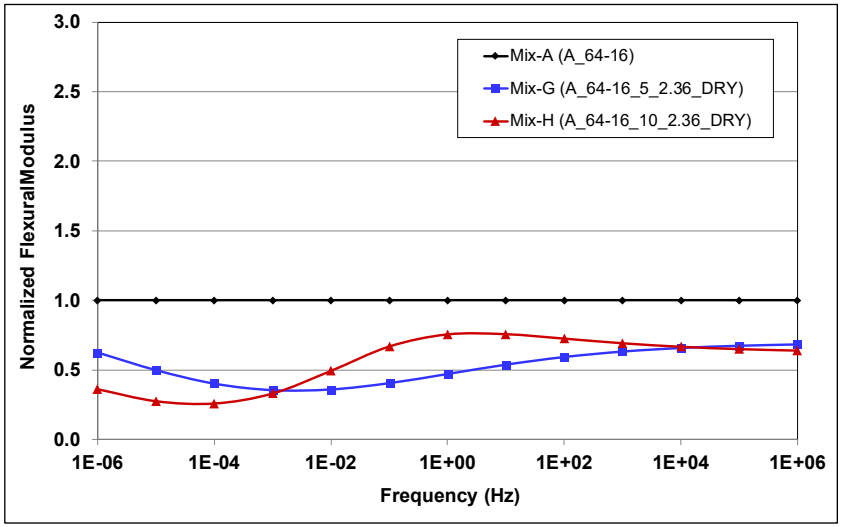

Figure 7.4: App-3: Normalized flexural modulus master curves at 20°C.

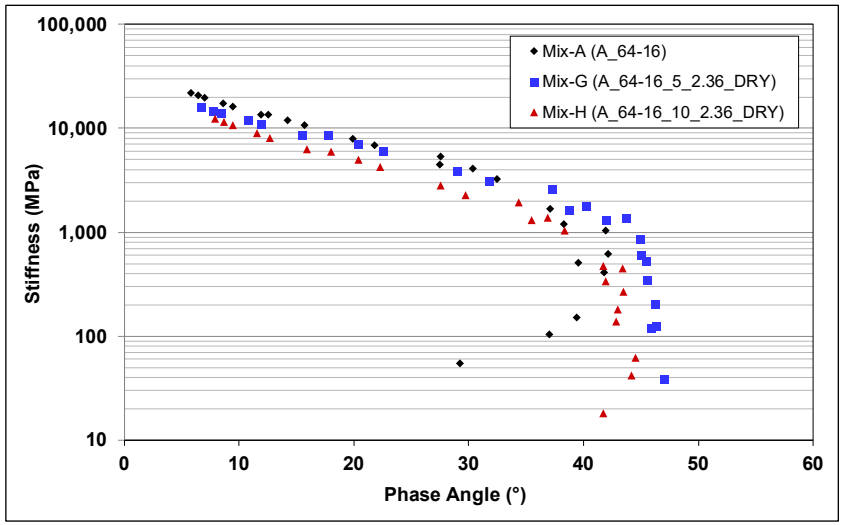

Figure 7.5: App-3: Black diagram of dynamic modulus results.

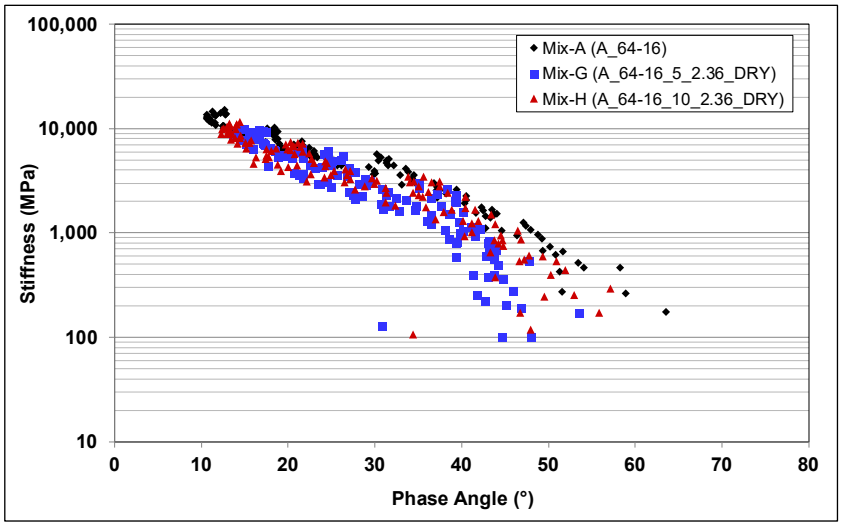

Figure 7.6: App-3: Black diagram of flexural modulus results.

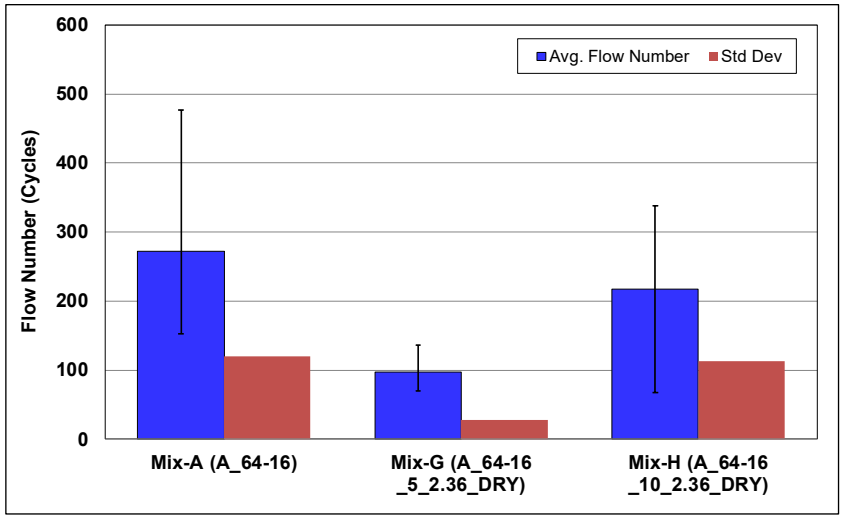

Figure 7.7: App-3: Flow number at 50°C.

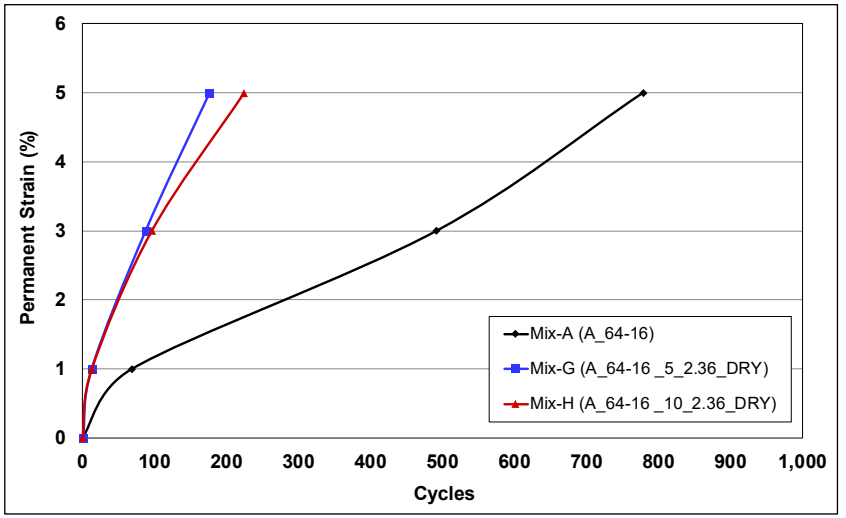

Figure 7.8: App-3: Average permanent strain vs. load cycle at 50°C.

- Trends observed for the number of cycles to 1%, 3%, and 5% permanent axial strain were similar to those observed for the flow number results, but with a more notable difference between the CRM mixes and the control mix, even at low strain levels.
- The low flow numbers and low number of cycles to 1%, 3%, and 5% permanent axial strain were attributed to problems associated with the effects of the relatively large CRM particles on the volumetric properties.

7.2.4 Rutting and Moisture Resistance: Hamburg Wheel Track Test

Hamburg wheel track test results are listed in Table C.4 in Appendix C. Figure 7.9 shows the results for the three mixes at 50°C. The rut depth shown is the average of the left and right wheel track.

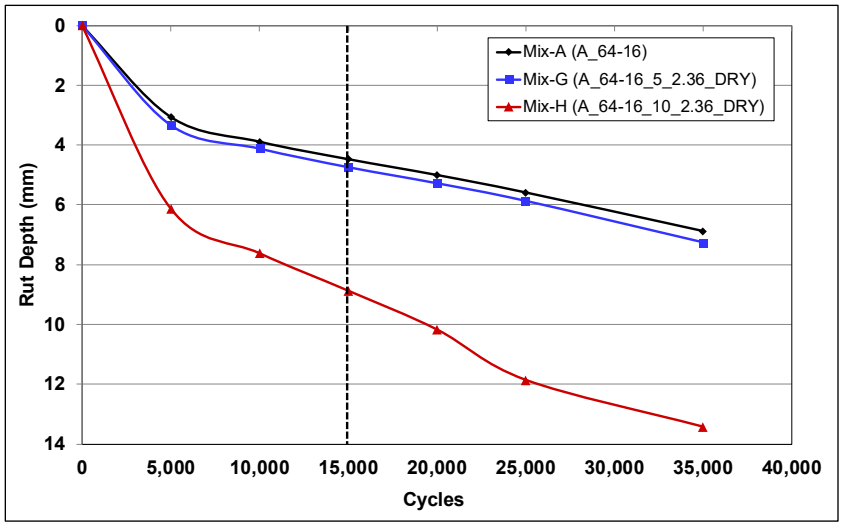

Figure 7.9: App-3: Hamburg Wheel Track rutting at 50°C.

The results show that:

- All mixes performed within the specified limits (average maximum rut depth may not exceed 0.5 in. [≈12.5 mm] at 15,000 load cycles) and that no mixes were moisture sensitive. Inflection points indicating stripping were not observed in any of the mixes.
- An embedment phase was observed in the first 3,000 load cycles for the control mix and the CRM mix with 0.25% CRM, after which the rate of rut-depth increase slowed considerably. A longer embedment phase (6,000 load cycles) and faster rate of rut-depth increase thereafter was observed on the CRM mix with 0.5% CRM.
- The Control mix had marginally better rutting resistance than the CRM mix with 0.25% CRM. Both these mixes had significantly better rutting resistance than the CRM mix with 0.5% CRM, which appeared to be more moisture sensitive than the other two mixes.

- Poorer performance in the CRM mixes was again attributed to problems associated with the effects of the relatively large CRM particles on volumetric properties.

7.2.5 Fatigue/Reflective Cracking Resistance: Four-Point Beam Test

Four-point beam test results are listed in Table C.5 in Appendix C. Figure 7.10 shows the flexural beam fatigue test results for the three mixes at 20°C and 10 Hz. The plots show the predicted fatigue life against the applied peak-to-peak strain in a log-log plot. Figure 7.11 shows the calculated fatigue lives at 200, 300, 400, and 600 µstrain. The results show that:

- The models for the control mix and CRM mix with 0.25% CRM were considered appropriate based on the high R-squared value of the model fitting and the repeatability of the test results at each strain level. The model for the CRM mix with 0.5% CRM had a relatively poor correlation, indicating higher variability in the test results.
- The CRM mixes had longer fatigue lives than the control mix, with the mix with 0.25% CRM showing better performance than the mix with 0.5% CRM. These results are consistent for strain-controlled fatigue tests with the observations from the flexural modulus master curves.
- The performance differences between the control mix and the CRM mix with 0.5% CRM reduced with increasing strain level. At 600 µstrain, the CRM mix had a marginally lower predicted fatigue life than the control mix.

7.2.6 Fracture Cracking Resistance: Semicircular Bend Test

Semicircular bend test results are listed in Table C.6 in Appendix C. Figure 7.12 and Figure 7.13 respectively show the average fracture energy and strength, and flexibility index results. Whiskers on the data show the lowest and highest fracture energies and flexibility indices, respectively for the four replicates tested for each mix. The results show that:

- Fracture energy and flexibility index results showed similar trends, as expected.
- Adding CRM resulted in a marginal strength reduction over the control mix, attributed to the CRM particle size issues discussed previously.
- The CRM mixes provided better cracking resistance and slower rates of crack propagation than the control mix, but cracking resistance decreased with increasing CRM content.
- The ranking of flexibility index results matched the ranking of fatigue life at low strain levels (<400 µstrain).

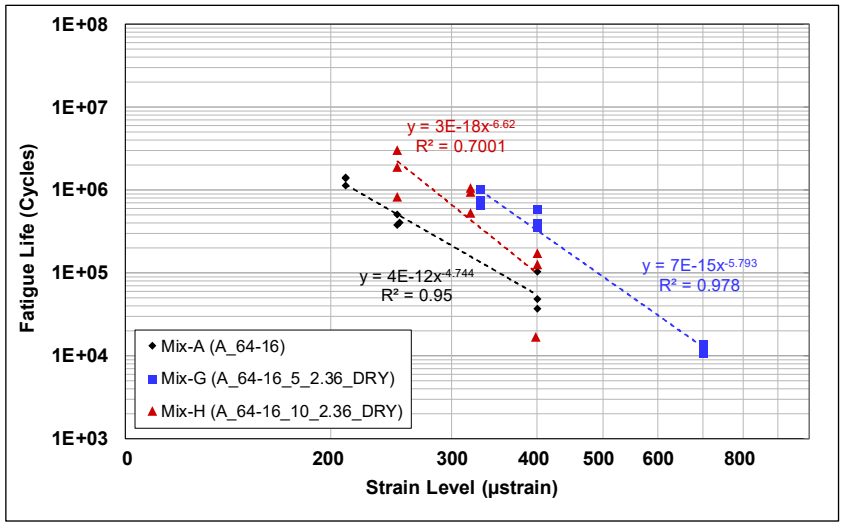

Figure 7.10: App-3: Beam fatigue at 20°C and 10 Hz.

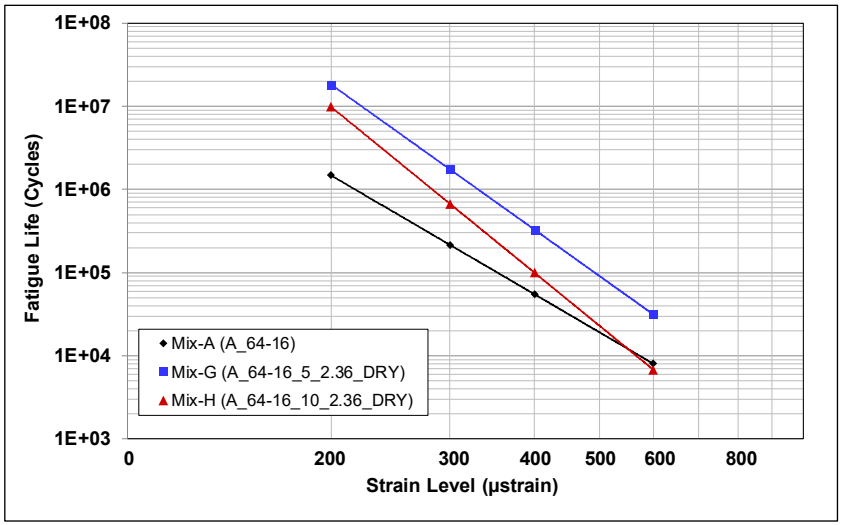

Figure 7.11: App-3: Calculated fatigue life.

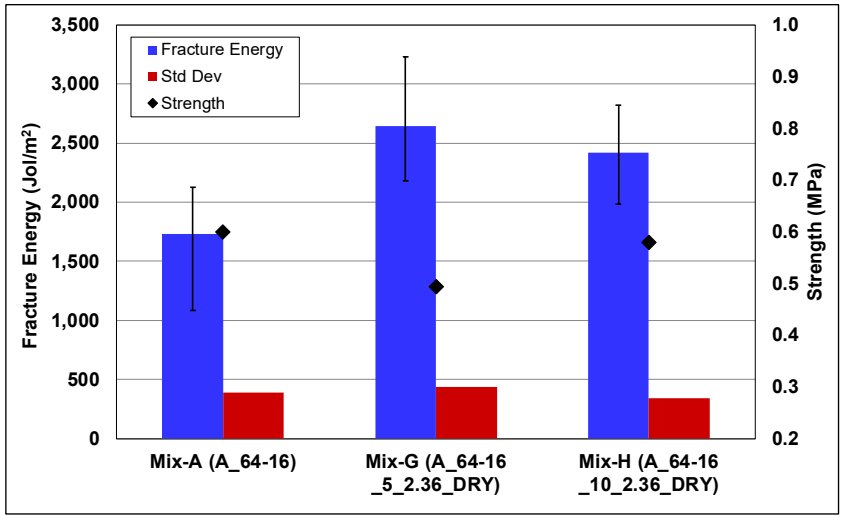

Figure 7.12: App-3: SCB fracture energy and tensile strength at 25°C.

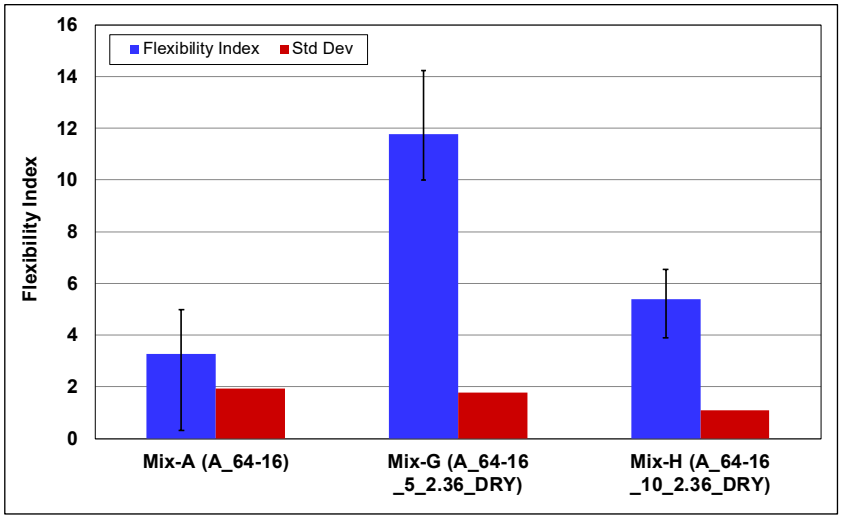

Figure 7.13: App-3: SCB flexibility index at 25°C.

- There was considerable variability in the results of the replicate tests in each mix. Table 7.3 provides a statistical analysis of the test results. The coefficients of variation (CoV) of the flexibility index values were notably higher than the fracture energy values and strength. This should be taken into consideration when interpreting the results.

Table 7.3: App-3: Semicircular Bend Test Results

Mix ID	Binder ID	Fracture Energy (Jol/m^2)	CoV[a] (%)	Flexibility Index	CoV (%)	Strength (MPa)	CoV (%)
A	A_64-16	1,714	22.7	3.27	58.8	0.60	10.8
G	A_64-16_5_2.36_DRY	2,619	16.1	11.77	15.3	0.49	13.9
H	A_64-16_10_2.36_DRY	2,377	14.4	5.39	20.4	0.58	1.6

[a] CoV: coefficient of variation

7.2.7 Low-Temperature Cracking: Uniaxial Thermal Stress and Strain Test

Uniaxial thermal stress and strain test (UTSST) results are listed in Table C.7 in Appendix C and summarized in Figure 7.14. The results show that:

- The CRM mixes had equivalent (mix with 0.5% CRM) or poorer (mix with 0.25% CRM) thermal cracking resistance than the control mix.
- The CRM mix with 0.25% CRM had a lower cracking resistance value and higher fracture temperature than the control mix, while the CRM mix with 0.5% CRM had a similar cracking resistance value and fracture temperature to the control. Given that only average results were provided by the testing laboratory, it is not clear if variability between replicate mixes would alter these observations.
- None of the mixes exceeded the recommended minimum cracking resistance index of 17°C *(66)*.

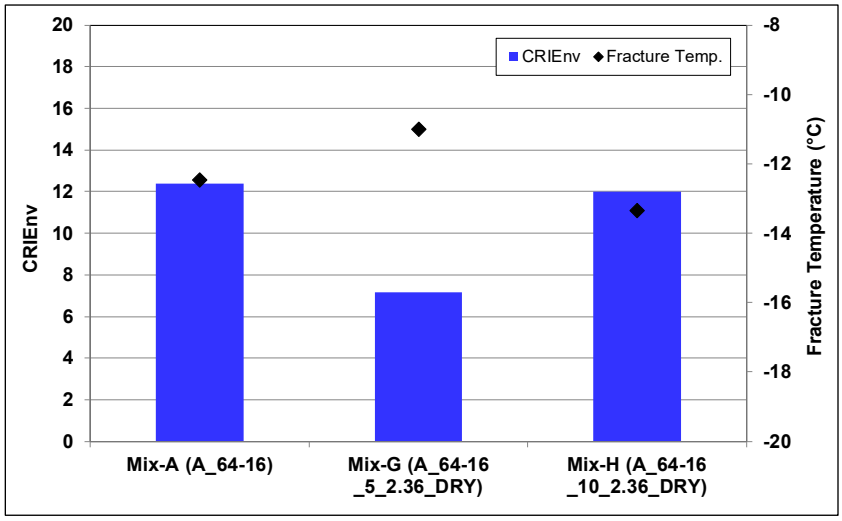

Figure 7.14: App-3: Uniaxial thermal stress and strain.

7.3 Approach-3 Test Result Summary

This chapter covers the evaluation of Approach-3 CRM mixes (0.25 and 0.5% CRM by weight of the dry aggregate, with dry CRM particles smaller than 2.36 mm added directly to the aggregate). The following important observations were made from the test results:

- Specified volumetric properties for the mixes with CRM were difficult to meet. This was attributed to accommodation of the relatively large CRM particles in the dense gradation. Swelling of these CRM particles when heated, when shearing was applied in the gyratory compactor, and when they contacted the asphalt binder also contributed to the problem. This affected all test results. It should be noted that most dry mixes produced in the United States are now prepared with CRM particles smaller than 500 µm (passing the #30 sieve), which are more easily accommodated in a dense gradation.
- The dynamic and flexural modulus master curves indicated that the CRM mixes had lower stiffnesses than the control mix at all frequencies.
- The CRM mixes had poorer rut resistance than the control mix. The CRM mix with 0.25% CRM had better moisture damage resistance than the mix with 0.5% CRM. All mixes passed the specified Hamburg Wheel Track test requirements.
- The CRM mixes had longer fatigue lives than the control mix. The mix with 0.5% CRM was more strain sensitive than the control mix at higher (600 µstrain) strain levels.
- The CRM mixes provided better fracture cracking resistance and slower rates of crack propagation than the control mix, but cracking resistance decreased with increasing CRM content.
- The CRM mixes had equivalent (mix with 0.5% CRM) or poorer (mix with 0.25% CRM) thermal cracking resistance than the control mix.
- All results in this series of tests indicate that adding relatively large dry CRM particles to dense-graded mixes will require an adjustment to the gradation to accommodate the CRM particles and thereby achieve satisfactory performance. No tests were carried out to confirm this observation.
- Further testing with CRM particles with a maximum size of 500 µm (passing the #30 sieve), and/or reviews of recent test results from other states, is recommended.

8. EVALUATION OF APPROACH-4 BINDERS AND MIXES

8.1 Introduction

This chapter discusses the test results for four Approach-4 CRM binders sourced from two suppliers (Supplier-C and Supplier-D), and for two Approach-4 mixes prepared with the CRM binders provided by Supplier-C. The PG 64-22 base binder supplied by Refinery-A was used as the control binder and to prepare the control mix, and to prepare the Approach-4 CRM binders. Binder test results are presented first, followed by mix test results. Summary plots are presented in the text, while more detailed, tabulated results are provided in Appendix D. Details on the binders tested and the binder and mix testing details are discussed in Chapter 4 and are not repeated in this chapter.

8.2 Approach-4 Binder Test Results

8.2.1 Introduction

The PG 64-22 control base binder was provided to Supplier-C and Supplier-D to produce the CRM binders with their respective crumb rubber modifiers. Given that the CRM particles from both suppliers were smaller than 250 µm, and were essentially completely digested during blending with the binder, standard Superpave PG testing methods were followed. Although the UCPRC did not witness the production of the CRM binders, both suppliers stated that no modifiers other than CRM were used during blending. It was therefore assumed that any difference between the control and CRM binder/mix could be attributed to the CRM alone. Performance parameters evaluated included binder PG, multiple stress creep recovery (MSCR), rutting resistance (frequency sweep), solubility, ductility, and aging resistance potential.

8.2.2 High-Temperature Grading

High-temperature grading results are listed in Table D.1 (unaged) and Table D.2 (RTFO-aged) in Appendix D. Figure 8.1 and Figure 8.2 show the average high temperature testing results for the unaged and RTFO-aged binders from both suppliers. Dashed lines on the plot indicate the 1.00 kPa and 2.20 kPa test thresholds for unaged and RTFO-aged binders. Figure 8.3 and Figure 8.4 show the phase angles for the unaged and RTFO-aged binders from both suppliers.

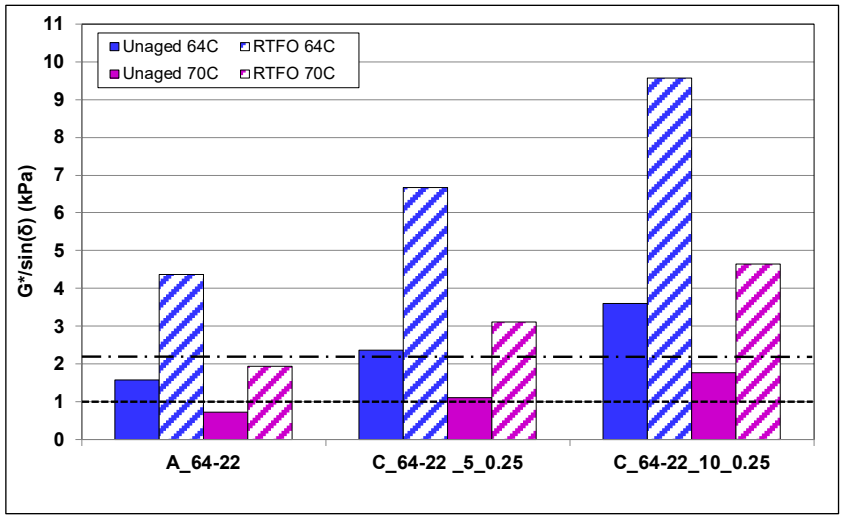

Figure 8.1: App-4/Supp-C: G*/sin(δ) of unaged and RTFO-aged binders.

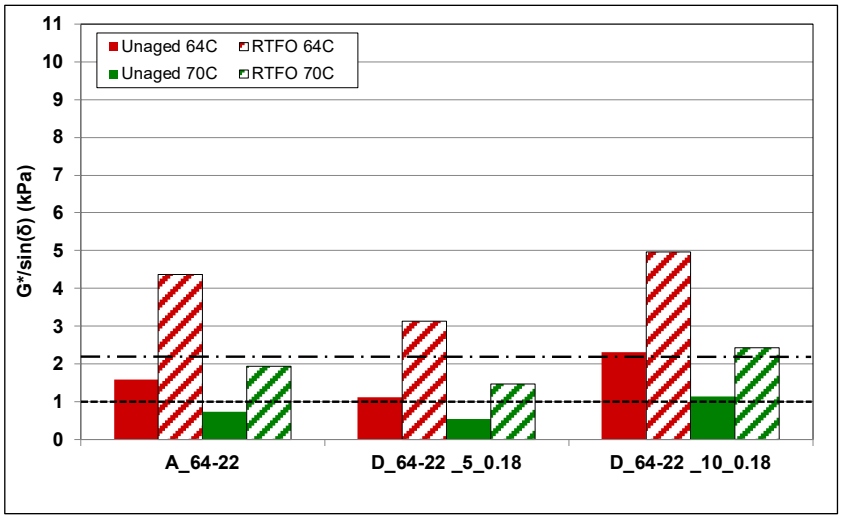

Figure 8.2: App-4/Supp-D: G*/sin(δ) of unaged and RTFO-aged binders.

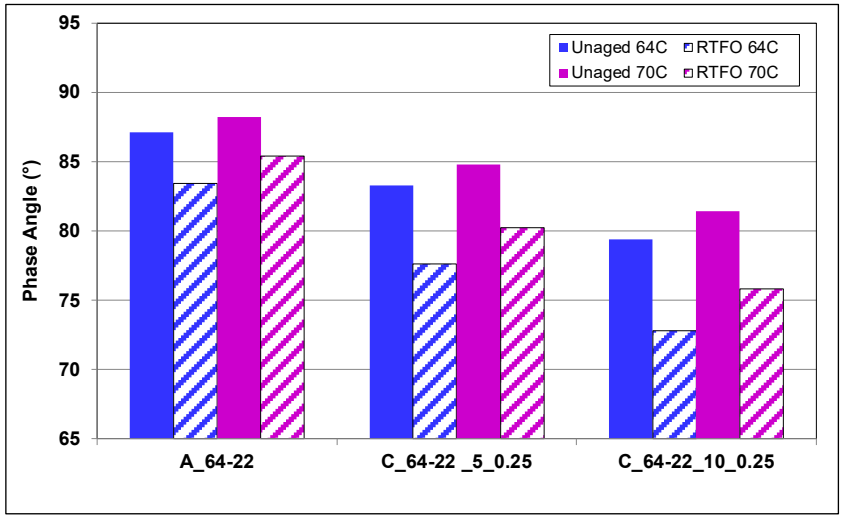

Figure 8.3: App-4/Supp-C: Phase angles of unaged and RTFO-aged binders.

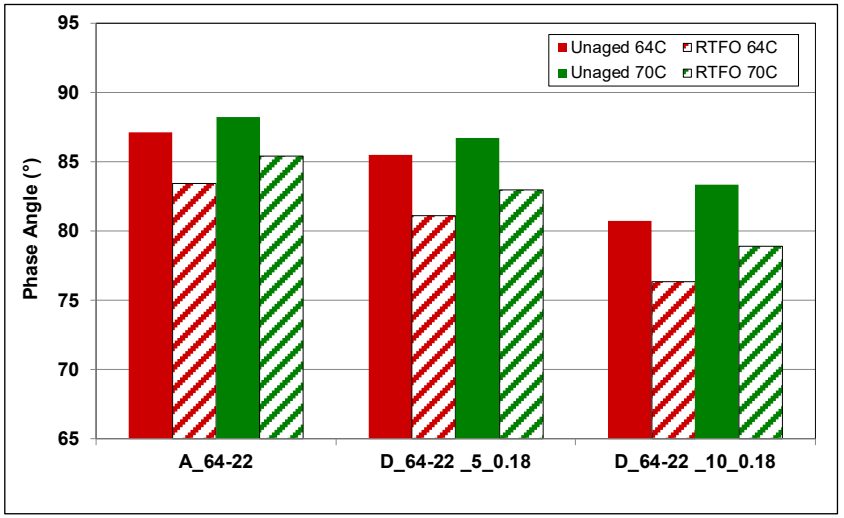

Figure 8.4: App-4/Supp-D: Phase angles of unaged and RTFO-aged binders.

The results show that:

- All binders passed the high-temperature PG criteria at 64°C. At 70°C, the control binder and the CRM binder with 5% CRM from Supplier-D did not pass. This implies that the binders with 5% and 10% CRM from Supplier-C and with 10% CRM from Supplier-D would have a high temperature PG of 70, or a one grade increase over the control binder.
- Adding devulcanized CRM with particle sizes up to 250 µm had a more notable effect on the high temperature grading (stiffness) than adding CRM with the slightly smaller 180 µm particles. This implies that the devulcanized CRM from Supplier-C modified the binder to a greater extent than the finer CRM from Supplier-D.
- The G*/sin(δ) values increased with increasing CRM content, as expected. The differences between the two CRM contents was more apparent in the binders from Supplier-C.
- The phase angles of the RTFO-aged binders were lower than those of the unaged binders, as expected, indicating that RTFO-aging made the binder more elastic at high temperatures.
- Adding 5% and 10% CRM decreased the phase angle, with the larger differences observed in the CRM binders from Supplier-C, consistent with the G*/sin(δ) results. Increasing the CRM content resulted in further lowering of the phase angle.

Table 8.1 summarizes the continuous grades for the binders. The continuous grade is defined as the temperature where the unaged binder's G*/sin(δ) value equals 1.00 kPa and the RTFO-aged binder's G*/sin(δ) value equals 2.20 kPa, respectively.

Table 8.1: App-4: Continuous Grades

Supplier	Binder ID	Unaged Binder (°C)		RTFO-Aged Binder (°C)		Hardening Ratio
		G*/sin(δ) =1.00 kPa	Grade Change	G*/sin(δ) =2.20 kPa	Grade Change	G*/sin(δ)(RTFO) / G*/sin(δ) (Unaged) at 64°C
C	A_64-22	67.7	N/A	69.1	N/A	2.75
	C_64-22_5_0.25	71.0	+3.3	72.9	+3.8	2.83
	C_64-22_10_0.25	75.4	+7.7	76.7	+7.6	2.65
D	A_64-22	67.7	N/A	69.1	N/A	2.75
	D_64-22_5_0.18	65.0	-2.7	66.8	-2.3	2.80
	D_64-22_10_0.18	71.3	+6.3	70.9	+1.8	2.14

The results show that:

- Adding 5% and 10% devulcanized CRM from Supplier-C to the binder increased the continuous grade by 3°C and 7°C, respectively. Adding the same amounts of the finer CRM from Supplier-D had a negative effect at 5% CRM, increased the grade by 6°C at 10% CRM in the unaged state, but only by 2°C after RTFO-aging.
- The age-hardening ratios calculated for each binder from Supplier-C were consistent with the continuous grade results. However, the ratios for the CRM binders from Supplier-D

were not. All binders except the one from Supplier-D with 10% CRM had an age-hardening ratio greater than 2.2.

- The binders containing 5% CRM from both suppliers had a higher age-hardening ratio than the control binder, while those with 10% CRM had lower ratios that the control. This was attributed in part to incomplete digestion of the higher quantity of CRM particles.

8.2.3 Intermediate-Temperature Grading

Intermediate-temperature grading results are listed in Table D.3 in Appendix D. Figure 8.5 shows the average intermediate-temperature test results for the PAV-aged binders from both suppliers. In the figure, the histograms represent the G*×sin(δ) values at 25°C, and the dot points show the continuous grades at the temperature where the binder G*×sin(δ) values equal 5,000 kPa, as specified in AASHTO M 320.

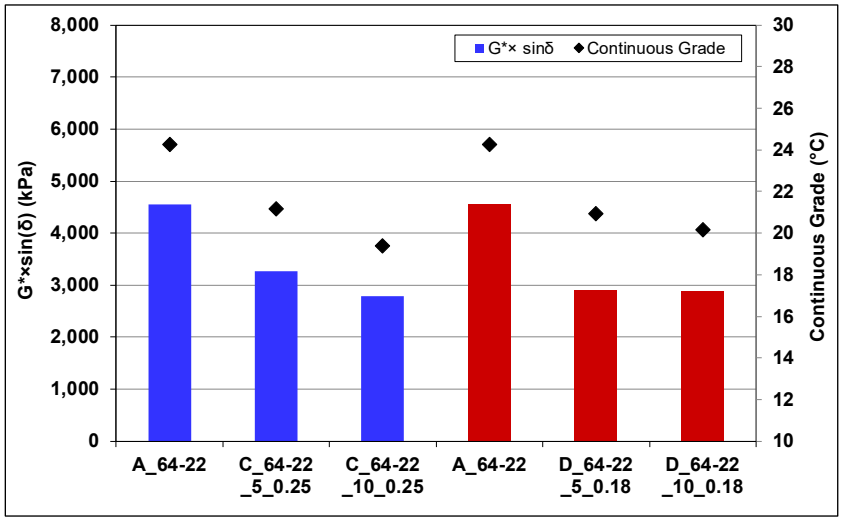

Figure 8.5: App-4: G*×sin (δ) of PAV-aged binders at 25°C.

The results show that:

- The CRM binders were softer than their control binders in each PG group after PAV-aging, which indicated potentially better fatigue cracking resistance in a thin overlay application where cracking behavior would be strain-controlled.
- The CRM binders had lower G*×sin(δ) values and lower continuous grades than the control binders.
- An increase in the CRM content in the binders from Supplier-C resulted in a decrease in G*×sin(δ) and in the continuous grade. An increase in the CRM content in the CRM binders from Supplier-D had no effect on G*×sin(δ), but resulted in a marginal decrease in the continuous grade.

- CRM particle size had a negligible effect on G*×sin(δ) and continuous grade.
- The results imply that mixes produced with the CRM binders should have marginally better fatigue cracking resistance than mixes produced with the base binders when used in thin overlays.

8.2.4 Low-Temperature Grading

Bending beam rheometer test results are listed in Table D.4 in Appendix D. Figure 8.6 shows average results for the PAV-aged binders from both suppliers at -12°C. The maximum allowable creep stiffness (300 MPa) and lowest minimum allowable m-value (0.300) limits at the selected measuring temperature are shown as dashed lines on the plots.

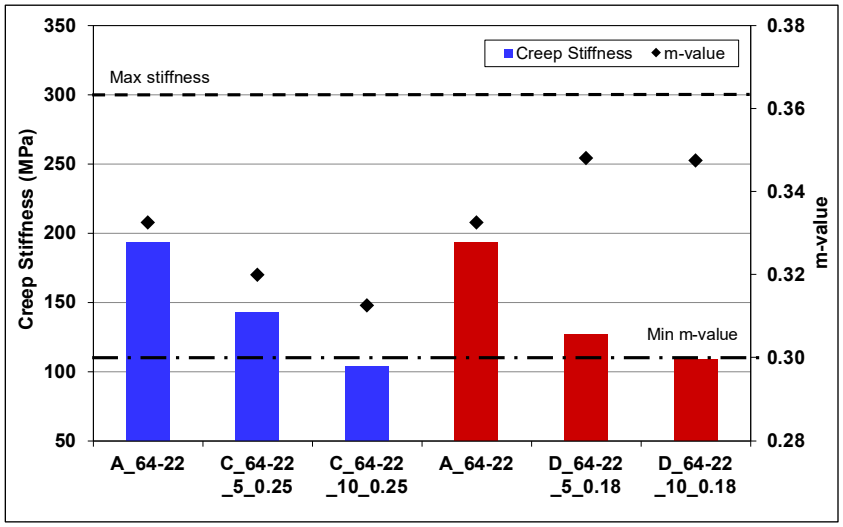

Figure 8.6: App-4: Low temperature creep stiffness and m-value.

The results show that:

- All binders passed the low-temperature stiffness and m-value criteria at the minimum measuring temperatures.
- All the CRM binders had lower creep stiffnesses than the control binders, with stiffnesses decreasing with increasing CRM content. This implies that mixes produced with Approach-2 CRM binders could have potentially better low-temperature cracking resistance than mixes produced with the control binders.
- The CRM binders from Supplier-C had lower m-values than the control, while those from Supplier-D had higher m-values than the control.
- Unlike the Approach-2 CRM binders, CRM particle size did not appear to have an influence on creep stiffness, but it did have a notable effect on m-value, with the CRM binders produced with the smaller CRM particles having much higher m-values than the binders produced with the larger binders.

A second round of BBR tests was run at -18°C to calculate the critical temperatures for these binders (i.e., where stiffness equals 300 MPa, or m-value equals 0.300). The results are summarized in Table 8.2. The difference between the critical temperatures calculated by stiffness and m-value (ΔT_C) is an indicator of the binder stress relaxation *(67)*. As noted previously, less negative or positive differences in ΔT_c indicate better resistance to thermal cracking. Less negative or positive differences in ΔT_c occur when the critical parameter for meeting the specification is the m-value, or if the critical value is stiffness then the m-value temperature is similar.

Table 8.2: App-4: Low Temperature Test Results

Supplier	Binder ID	$T_{C\text{-}stiffness}$ (°C)	$T_{C\text{-}m\text{-}value}$ (°C)	ΔT_C (°C)
C	A_64-16	-15.6	-14.8	-0.8
	C_64-22_5_0.25	-18.6	-17.3	-1.3
	C_64-22_10_0.25	-21.3	-16.6	-4.7
D	A_64-16	-15.6	-14.8	-0.8
	D_64-22_5_0.18	-19.0	-14.4	-4.6
	D_64-22_10_0.18	-20.6	-13.1	-7.4

The results show that:

- The CRM binders had the same low temperature grading as the control binders.
- The critical temperatures of the binders from both suppliers were controlled by m-value as indicated by negative ΔT_C values. However, the differences between the binders from Supplier-C were less significant than the differences between the binders from Supplier-D because of the higher m-values (lower m-value critical temperatures) recorded on the Supplier-D binders. This implies that the marginal CRM particle size change may have influenced critical temperatures.
- The CRM binders from Supplier-D had higher $T_{c\text{-}m\text{-}value}$ results than the control binder, indicating that the binder's capacity to relax the stress (m-value) was reduced by the addition of CRM.
- Adding CRM had a notable effect on the ΔT_C values, with increasing CRM content resulting in increasingly lower values.
- The CRM binders produced with 5% and 10% of the finer CRM particle sizes had lower ΔT_C values than the binders produced with 5% and 10% of the slightly larger CRM particles.
- The results are opposite to those recorded for the Approach-2 binders (i.e., the CRM binders produced with 5% and 10% finer CRM particle sizes had more positive ΔT_C values).

8.2.5 Multiple Stress Creep Recovery

Multiple stress creep recovery test results are listed in Table D.5 in Appendix D. Figure 8.7 and Figure 8.8 show the MSCR test results at 64°C for the RTFO-aged binders. The results show that:

- The CRM binders had lower non-recoverable creep compliance (Jnr) than the control binders, with 10% CRM having a notably larger effect than 5% CRM.
- The differences in Jnr between the base and CRM binders from Supplier-C were larger than those from Supplier-D.
- The CRM binders produced with finer CRM particles had higher Jnr values than those produced with the slightly larger CRM particles, which differs from the results for the Approach-2 CRM binders. This implies that mixes produced with the CRM binders from Supplier-C would potentially be more rut resistant than mixes produced with the CRM binders from Supplier-D.
- Adding CRM to binders increased the percent elastic recovery of the binder, as expected, with increasing CRM content having a corresponding increase in percent recovery. The CRM binder produced with 5% of the finer CRM particles had a higher percent recovery than the binder produced with 5% of the slightly larger CRM particles. Particle size did not appear to influence the results when 10% CRM was added.
- The differences in results between tests conducted at 0.1 kPa and 3.2 kPa were clear, but consistent across the different binders.

8.2.6 Frequency Sweep

Figure 8.9 shows the master curves for the RTFO-aged binders and Figure 8.10 shows the curves normalized to the control binders to facilitate comparison. The master curves were developed at 20°C using measured dynamic moduli and phase angles from the frequency sweep tests conducted at 20, 40, and 50°C. The results show that:

- CRM binders from Supplier-C were stiffer than the control binder at frequencies lower than 1E-02 Hz, indicating that mixes produced with these binders would likely have better rutting resistance at higher temperatures. Stiffness increased with increasing CRM content, with a notable difference between the two CRM binders at the lower frequencies. At higher frequencies, the CRM binders had marginally lower stiffnesses than the control, with essentially no difference between the binders with 5% and 10% CRM.
- Stiffnesses of the CRM binders from Supplier-D were generally close to those of the control, with the exception of the binder with 10% CRM, which was stiffer than the control at low frequencies (<1E-05 Hz) and less stiff at high frequencies (>1E+04 Hz).

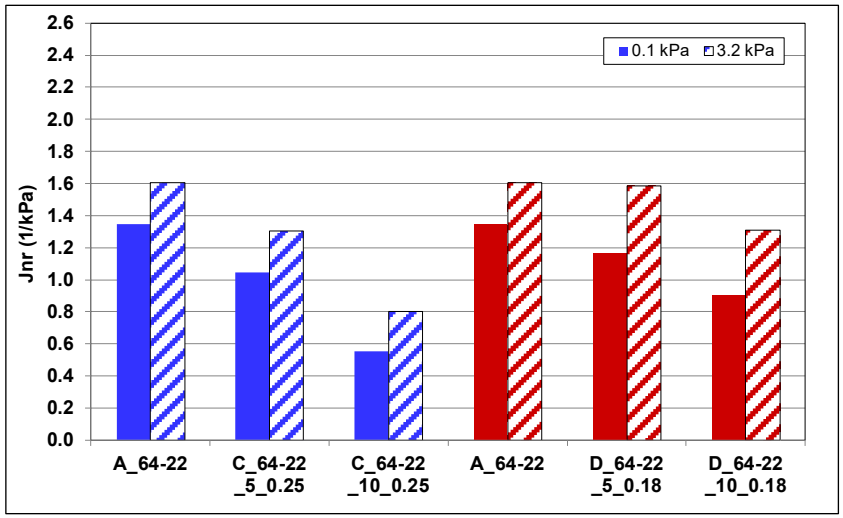

Figure 8.7: App-4: Jnr values of RTFO-aged binders at 64°C.

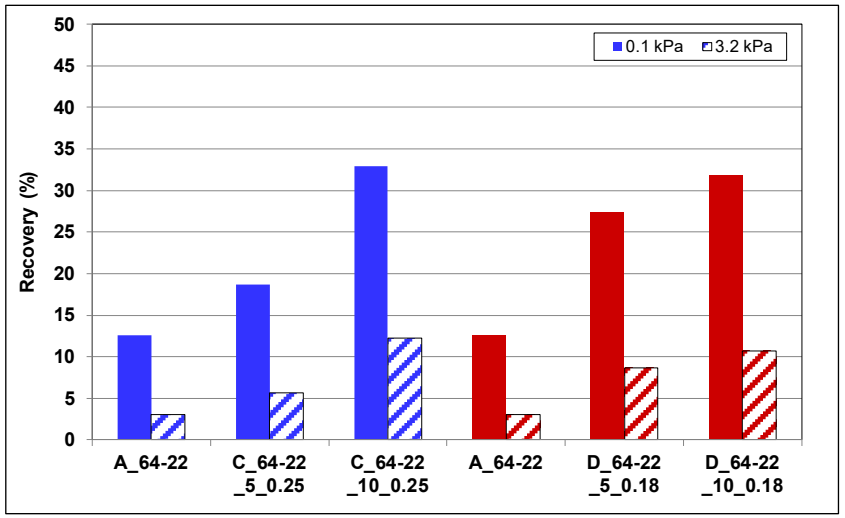

Figure 8.8: App-4: Percentage recovery of RTFO-aged binders at 64°C.

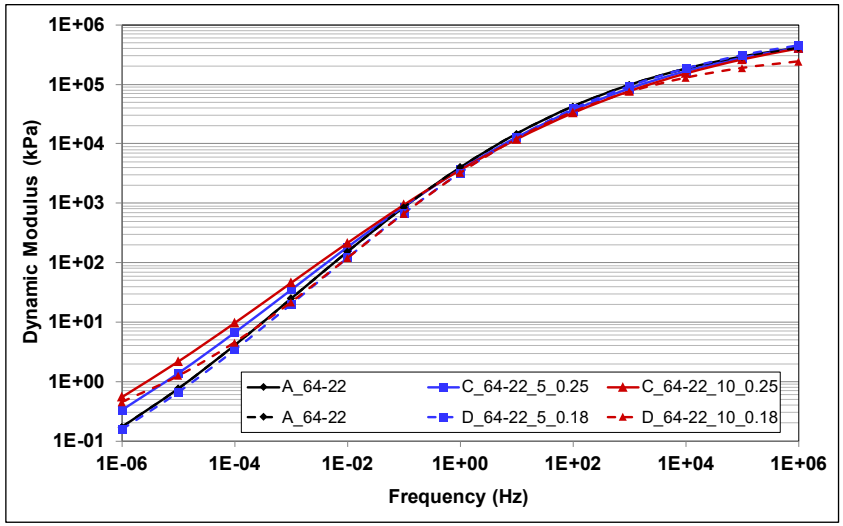

Figure 8.9: App-4: RTFO-aged binder master curves at 20°C.

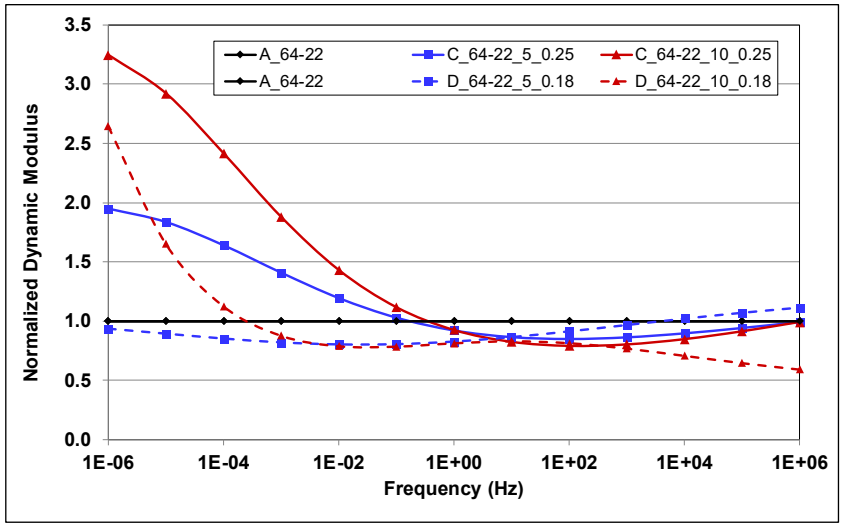

Figure 8.10: App-4: Normalized RTFO-aged binder master curves at 20°C.

- At 20°C and 10 Hz, at which beam fatigue tests were conducted, all of the CRM binders had lower stiffnesses than the control, indicating that mixes produced with them would be expected to have better fatigue performance in strain controlled fatigue tests and when used in thin overlays.
- The results were consistent with the PG tests discussed previously.

8.2.7 Solubility

Figure 8.11 shows the solubility test results for the unaged CRM binders from both suppliers. The results show that:

- Only one binder (5% CRM from Supplier-C) met the current Caltrans minimum solubility criteria for PG-M binders (97.5%). The solubilities of the other three binders were between 2.3% and 2.9% below this limit. These lower solubilities were attributed to the field blending processes followed, which may have resulted in incomplete digestion of some of the CRM particles.
- CRM content had a notable effect on the results of the Supplier-C binders, with the binder with 10% CRM having a solubility 2.3% lower than the binder with 5% CRM.
- CRM particle size and properties also had a notable effect on the results, with the binders from Supplier-D (slightly smaller CRM particle size with no devulcanization) having lower solubility. The Supplier did note difficulties with blending the fine CRM into the base binder.

8.2.8 Ductility

Figure 8.12 shows the ductility test results at 25°C for the RTFO-aged CRM binders. Caltrans specifications (Section 92) specify a minimum ductility of 75 cm for unmodified binders but do not specify any requirements for modified binders. The results show that:

- All binders had ductility well below the 75 cm limit set for unmodified binders, indicating potentially poor tensile properties. The results were notably lower than those recorded for the Approach-1 CRM binders and were inconsistent with MSCR and low temperature test results. Previous research *(71)* has suggested that ductility results are not necessarily a true representation of tensile stress and strain relationships in modified binders.
- An increase in CRM content resulted in a decrease in ductility for the binders from both suppliers.
- The binders with slightly smaller CRM particles had marginally higher ductility than the binders with larger CRM particles.

8.2.9 FTIR Testing

Binders were tested in unaged, RTFO-aged, and PAV-aged condition. Figure 8.13 and Figure 8.14 show the carbonyl area (CA) indices and sulfoxide (SUL) indices of both suppliers, respectively. The results show that:

- CA and SUL indices increased after RTFO-aging and again after PAV-aging, as expected, confirming that both indices were sensitive to the level of aging in these binders and can be used to track it.
- The unaged and RTFO-aged CRM binders from Supplier-C had similar CA indices to the control, while those from Supplier-D had notably higher CA indices than the control. The higher values for the unaged binder were attributed to additional heating of the Supplier-D CRM binders during blending, which was required to achieve satisfactory digestion.
- There were no or only minor differences in CA index between binders with 5% CRM and binders with 10% CRM in these aging conditions.
- The PAV-aged CRM binders from Supplier-C had notably lower CA indices than the control, and the binder with 10% CRM had a notably lower CA index than the binder with 5% CRM. The CRM binders from Supplier-D showed a different trend, with the binder with 5% CRM recording a slightly higher CA index than the control, and the binder with 10% CRM recording the same CA index as the control. This implies that the rate of aging of the CRM binders with larger CRM particles could potentially be slower than CRM binders with smaller CRM particles.
- The SUL area indices for the unaged, RTFO-aged, and PAV-aged CRM binders from Supplier-C were lower than those of the control.
- The SUL area indices for the binders from Supplier-D were less consistent. Both unaged CRM binders had higher SUL indices than the control, which was attributed to the longer heating during blending. The binder with 5% CRM also had higher SUL indices than the control after RTFO aging and after PAV aging. The binder with 10% CRM had notably lower SUL indices than the control and binder with 5% CRM after both RTFO and PAV aging.

8.3 Approach-4 Mix Test Results

Mix testing was done on specimens prepared with binders from Supplier-C only.

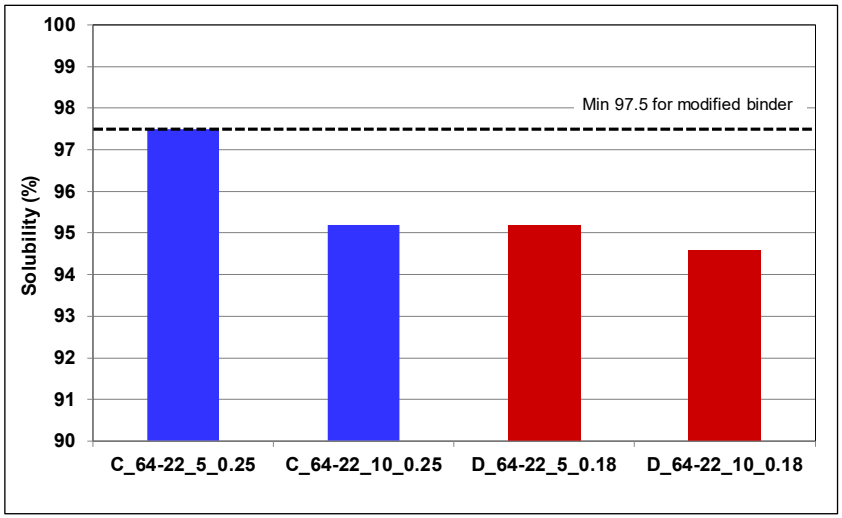

Figure 8.11: App-4: Solubility of unaged binders.

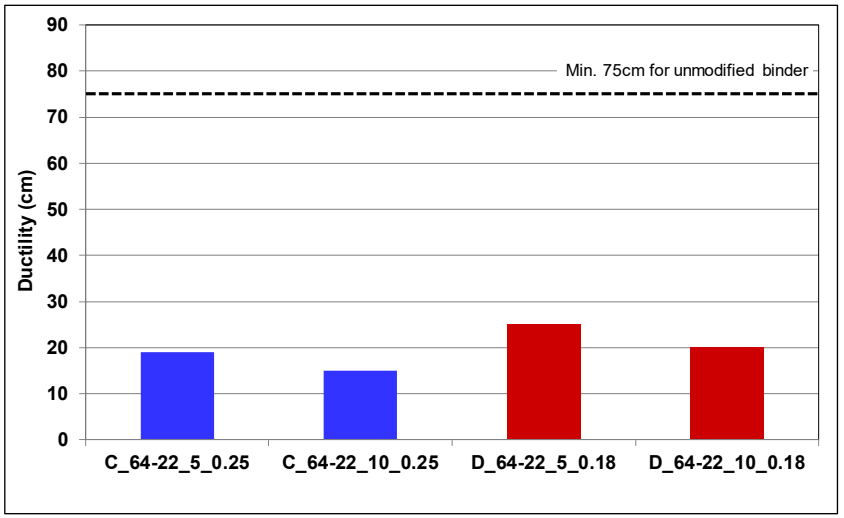

Figure 8.12: App-4: Ductility of RTFO-aged binders at 25°C.

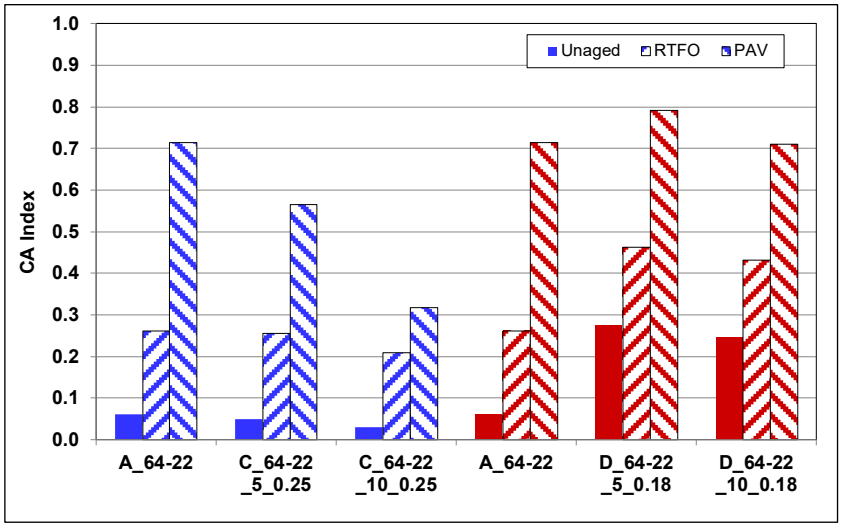

Figure 8.13: App-4: Carbonyl area index changes after aging.

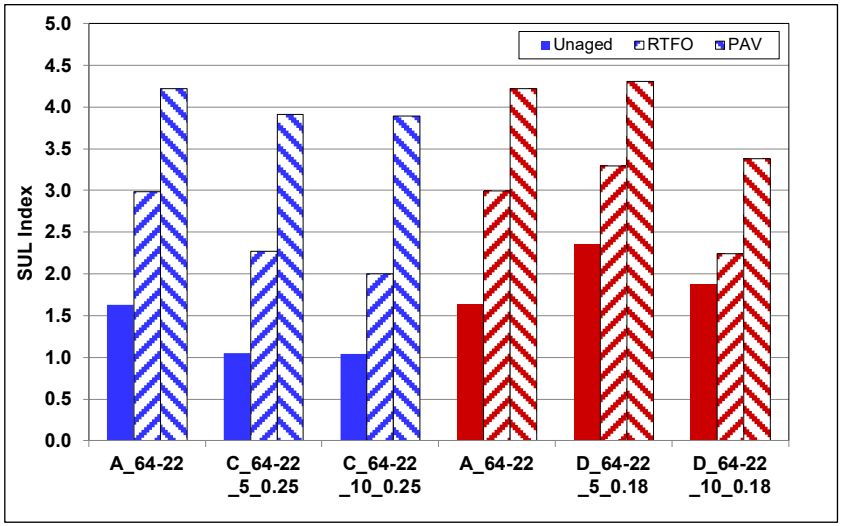

Figure 8.14: App-4: Sulfoxide area index changes after aging.

8.3.1 Volumetric Mix Design

The Superpave volumetric design method (AASHTO M 323) was followed to select the optimum binder content to meet Caltrans Type-A HMA specifications. Key parameters of the mix design include the following:

- Target air-void (AV) content at N_{design} (85 gyrations) of 4%±0.5%.
- Voids in mineral aggregate (VMA) between 13.5% and 16.5% for 3/4 in. nominal maximum aggregate size (NMAS) mixes.
- Dust proportion (DP) between 0.6 and 1.3.
- Although not specified, voids filled with asphalt (VFA) was also calculated. The recommended VFA range is between 65% and 75%.

Mixing and compaction temperatures for the CRM mixes were determined from binder temperature-viscosity curves at 135 and 165°C where the binder viscosity reached 0.17±0.02 Pa·s and 0.28±0.03 Pa·s, respectively (Figure 8.15).

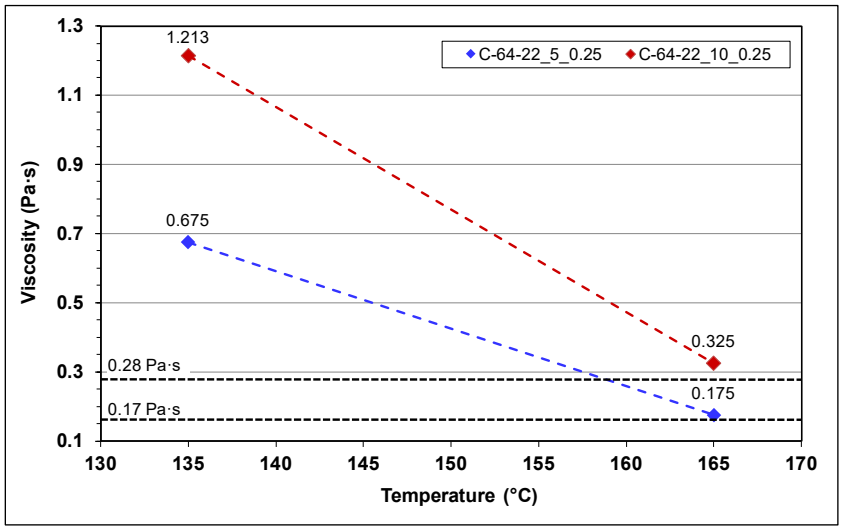

Figure 8.15: App-4: Rotational viscosity.

Table 8.3 summarizes the mixing and compaction temperatures and the gyratory compaction pressure. The required mixing and compaction temperatures increased with increasing CRM content, but were well below typical mixing temperatures (i.e., 190°C to 200°C) used for traditional RHMA-G mixes. The gyratory compactor was set to 600 kPa, which is the standard pressure used for conventional dense-graded mixes and lower than that used for RHMA-G mixes (i.e., 825 kPa). Specimens were not held after compaction because no bulging was observed in preliminary compaction trials.

Table 8.3: App-4: Mixing and Compaction Settings

Mix ID	Binder ID	Mixing Temp. (°C)	Compact Temp. (°C)	Compact Pressure (kPa)	Hold Time (Minutes)
J	A_64-22	150	140	600	0
K	C_64-22_5_0.25	165	158	600	0
L	C_64-22_10_0.25	170	166	600	0

Mix-J, produced with the unmodified base binder from Refinery-A, was used for the mix design confirmation. Once completed, the remaining two mixes (Mix-K [5% CRM] and Mix-L [10% CRM]) were verified at the design optimum binder content. No adjustments to the optimum binder content were required for Mix K and Mix L. The results are summarized in Table 8.4. Using a fixed binder content of 5.3% for all three mixes implies that adding 5% and 10% CRM would have decreased the actual base asphalt binder content in those mixes. However, the results show that this slight reduction in the actual base binder content did not appear to have any notable effect on the mix volumetric parameters.

Table 8.4: App-4: Mix Design Summary

Mix ID	Binder ID	Optimum Binder Content (%)	Air-Void Content at N_{Design} (%)	VMA (%)	DP	VFA (%)
J	A_64-22	5.3	4.0	13.7	1.1	70.3
K	C_64-22_5_0.25	5.3	4.0	13.8	1.1	70.9
L	C_64-22_10_0.25	5.3	4.0	14.1	1.1	71.9

8.3.2 Mix Stiffness: Dynamic and Flexural Modulus

Dynamic and flexural modulus test results are listed in Table D.4 and Table D.5 in Appendix D. Dynamic and flexural modulus master curves for the three mixes at a 20°C reference temperature are shown in Figure 8.16 and Figure 8.18. Master curves normalized to the unmodified base binder are shown in Figure 8.17 and Figure 8.19, respectively. Dynamic modulus master curves were developed from frequency sweep testing in an AMPT at 4, 21, 38, and 54°C, while flexural frequency sweep testing was done in a beam fatigue apparatus at 10, 20, and 30°C. The results show that:

- The dynamic modulus and flexural modulus master curve trends were different. The flexural modulus master curve showed trends consistent with the binder master curve.

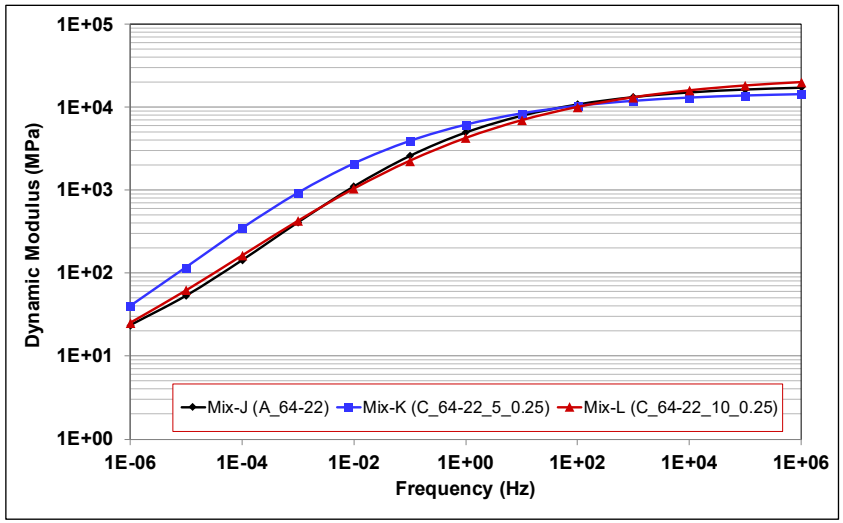

Figure 8.16: App-4/Supp-C: Dynamic modulus master curves at 20°C.

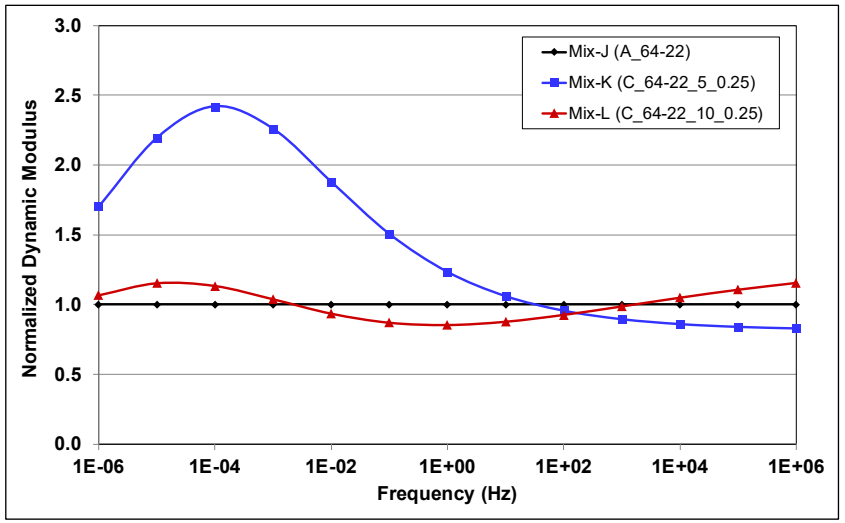

Figure 8.17: App-4/Supp-C: Normalized dynamic modulus master curves at 20°C.

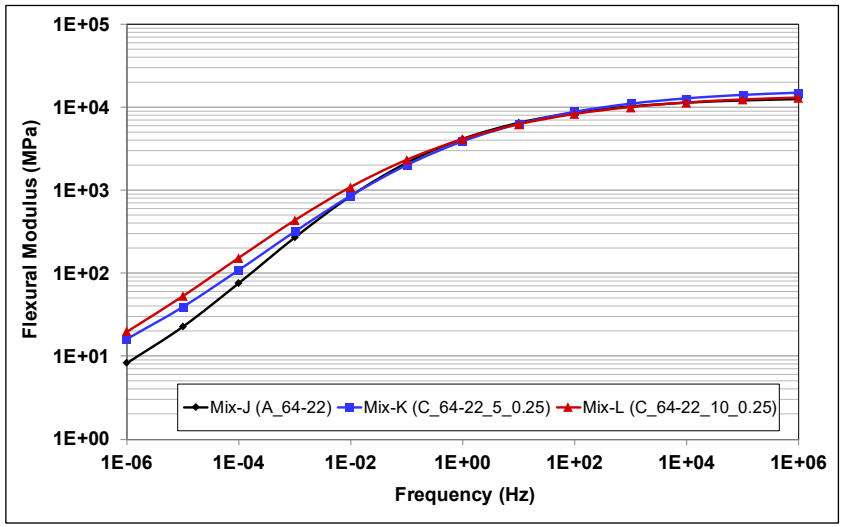

Figure 8.18: App-4/Supp-C: Flexural modulus master curves at 20°C.

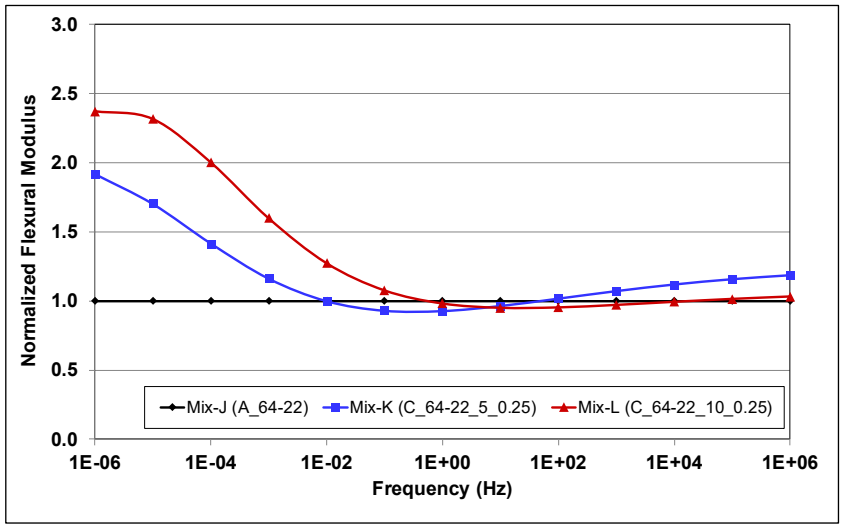

Figure 8.19: App-4/Supp-C: Normalized flexural modulus master curves at 20°C.

- The dynamic modulus master curves indicate that the CRM mix with 5% CRM had a higher stiffness at lower frequencies than the control and mix produced with the CRM binder with 10% CRM, and a lower stiffness at higher frequencies. The dynamic modulus master curve of the CRM mix with 10% CRM was similar to that of the control mix.
- The flexural modulus master curves indicate that the mixes produced with CRM binders were stiffer than the control at lower frequencies (<1E-02 Hz), with the 10% CRM mix having a proportionally higher stiffness than the 5% CRM mix, as expected. At frequencies higher than 1E-01 Hz), the CRM mixes had similar stiffnesses to the control mix.
- The CRM mixes could potentially be more resistant to rutting at higher temperatures than the control mix.

Figure 8.20 and Figure 8.21 show black diagrams (complex modulus versus phase angle) derived from the dynamic and flexural modulus test results. These black diagrams show that there were no significant differences between the control and CRM mixes. This, and the results from the dynamic and flexural modulus tests imply that mixes produced with these CRM binders should have similar, or marginally better rutting and cracking performance to the control mixes.

8.3.3 Rutting Resistance: Unconfined Repeated Load Triaxial Test

Repeated load triaxial test results are listed in Table D.6 in Appendix D. Figure 8.22 and Figure 8.23 respectively plot the average unconfined RLT and average permanent strain against load cycle test results at 50°C. Whiskers on the RLT data indicate the lowest and highest flow numbers of the five replicates in each mix. The results show that:

- There was considerable variability across the replicate test results. However, the AASHTO T 378 maximum coefficient of variation for a single operator testing 19 mm (3/4 in.) NMAS mixes of 58.5% was not exceeded for any of the mixes. The CRM mix with 5% CRM had the highest variability.
- The CRM mixes had higher flow numbers than the control mix, and the CRM mix with 10% CRM had a higher flow number than the CRM mix with 5% CRM.
- Trends observed for the number of cycles to 3% and 5% permanent axial strain were similar to those observed for the flow number results. At lower permanent strain levels, the difference in the number of cycles required to reach the selected strain level was similar between the mixes.
- These observations, together with those from the frequency sweep and multiple stress creep recovery tests, indicate that mixes produced with Approach-4 CRM binders will potentially have better rutting resistance than mixes produced with the respective control binders.

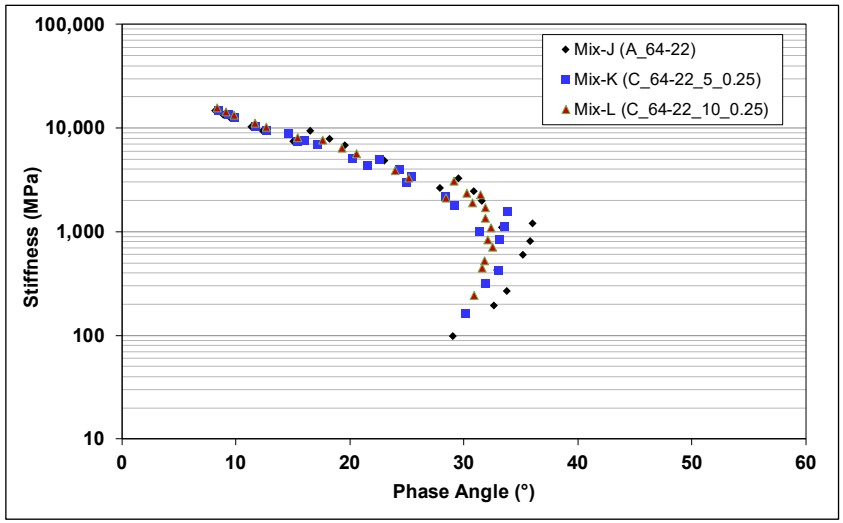

Figure 8.20: App-4/Supp-C: Black diagram of dynamic modulus results.

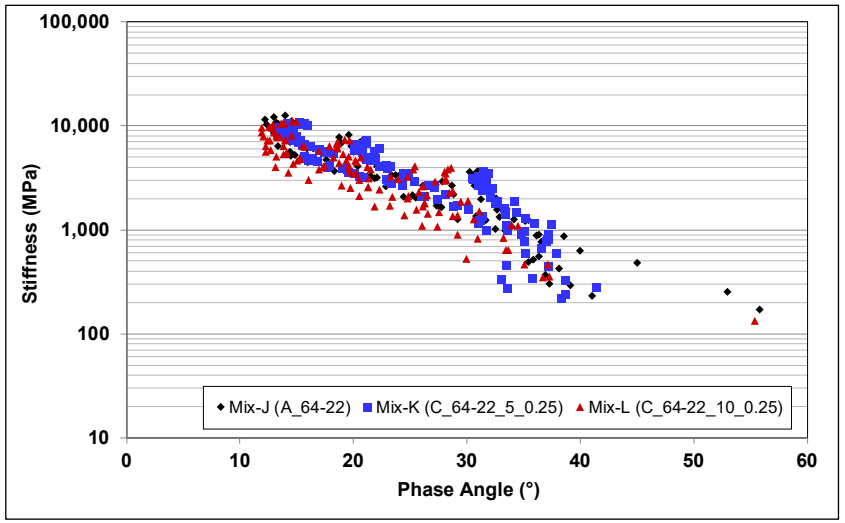

Figure 8.21: App-4/Supp-C: Black diagram of flexural modulus results.

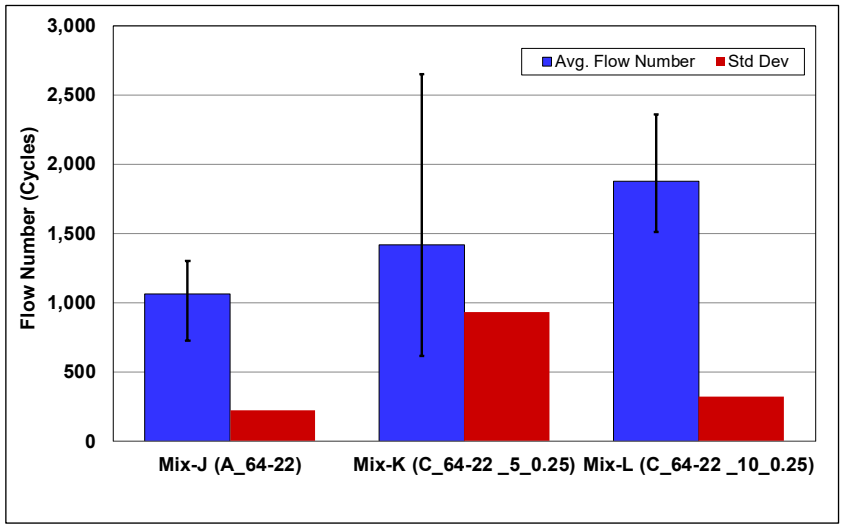

Figure 8.22: App-4/Supp-C: Flow number at 50°C.

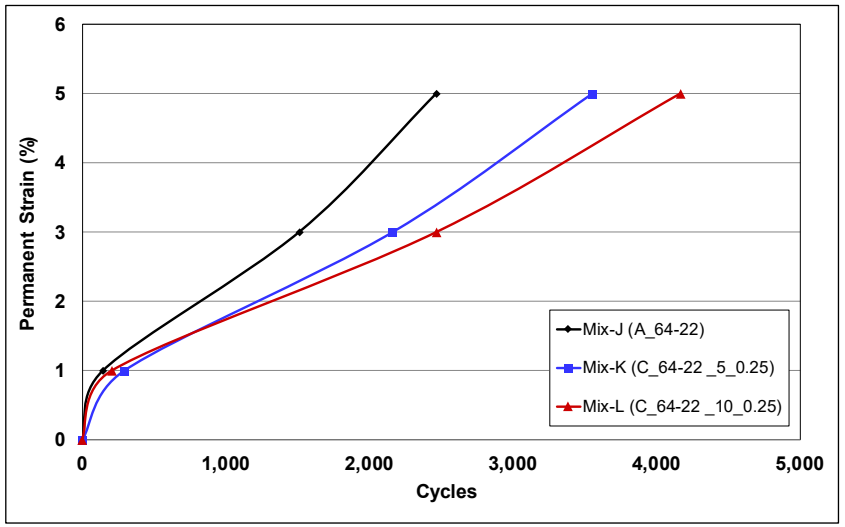

Figure 8.23: App-4/Supp-C: Average permanent strain vs. load cycles at 50°C.

8.3.4 Rutting and Moisture Resistance: Hamburg Wheel Track Test

Hamburg wheel track test results are listed in Table D.7 in Appendix D. Figure 8.24 shows the results for the three mixes at 50°C. The rut depth shown is the average of the left and right wheel track. The results show that:

- All mixes performed well within the specified limits (average maximum rut depth may not exceed 0.5 in. [≈12.5 mm] at 15,000 load cycles) and that no mixes were moisture sensitive. Inflection points indicating stripping were not observed for any of the mixes.
- The results were consistent with the RLT results discussed in Section 8.3.3, with the benefits of using CRM binders clearly evident.

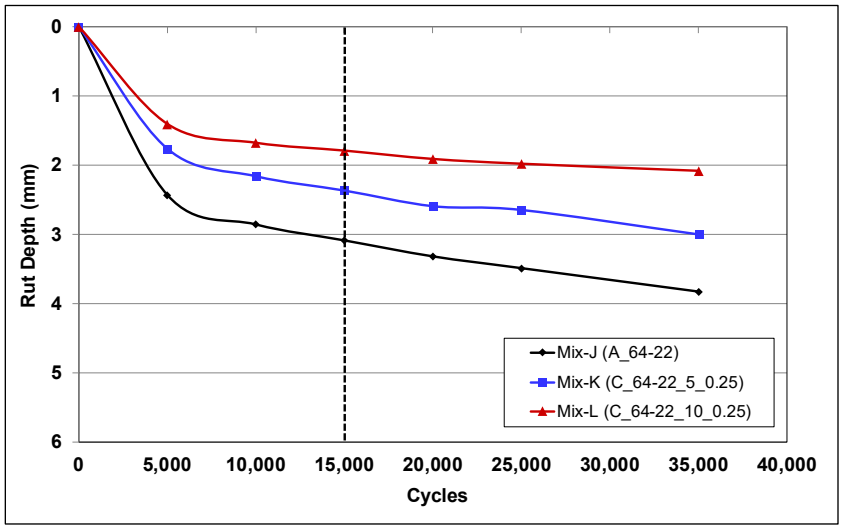

Figure 8.24: App-4/Supp-C: Hamburg wheel track rutting at 50°C.

8.3.5 Fatigue/Reflective Cracking Resistance: Four-Point Beam Test

Four-point beam test results for the three mixes are listed in Table D.8 in Appendix D. Figure 8.25 shows the flexural beam fatigue test results at 20°C and 10 Hz. The plots show the predicted fatigue life against the applied peak-to-peak strain in a log-log plot. Figure 8.26 shows the calculated fatigue lives at 200, 300, 400, and 600 µstrain. The results show that:

- The model for the CRM mix with 5% CRM was considered appropriate based on the relatively high R-squared value of the model fitting and the repeatability of the test results at each strain level. The models for the control mix and CRM mix with 10% CRM had relatively poor correlations, indicating high variability in the test results. Consequently, firm conclusions could not be drawn from the results regarding improved fatigue performance of the CRM mixes over the control mix.
- Taking these poor correlations into consideration, the calculated fatigue lives did indicate that the CRM mixes could potentially have longer fatigue lives at a given strain than the

control mix, especially at low and intermediate strains. The calculated strains did not show a difference between the CRM mixes with 5% and 10% CRM, although this is likely a consequence of the high variability in the results for the CRM mix with 10% CRM.

- Fatigue performance of the mixes produced with CRM binders was more strain-sensitive than the control mixes.

8.3.6 Fracture Cracking Resistance: Semicircular Bend Test

Semicircular bend test results are listed in Table D.9 in Appendix D. Figure 8.27 and Figure 8.28 respectively show the average fracture energy and strength, and flexibility index results. Whiskers on the data show the lowest and highest fracture energies and flexibility indices, respectively for the four replicates tested for each mix. The results show that:

- Fracture energy and flexibility index results showed similar trends, as expected.
- Trends were similar to those observed in the fatigue cracking results.
- Taking variability into consideration, the CRM mixes performed similar to the control mixes, with no apparent benefits of adding CRM, or apparent differences between the CRM mix with 5% CRM and the mix with 10% CRM. Table 8.5 provides a statistical analysis of the SCB test results. The coefficients of variation (CoV) of the flexibility index values were notably higher than the fracture energy values and strength. This should be taken into consideration when interpreting the results.

Table 8.5: App-4: SCB Test Results

Mix ID	Binder ID	Fracture Energy (Jol/m^2)	CoV[a] (%)	Flexibility Index	CoV (%)	Strength (MPa)	CoV (%)
J	A_64-22	2,575	8.1	6.3	20.8	0.58	6.3
K	C_64-22_5_0.25	2,160	6.0	4.4	48.6	0.59	5.4
L	C_64-22_10_0.25	1,889	21.5	4.7	14.1	0.56	11.5

[a] CoV: coefficient of variation

8.3.7 Low-Temperature Cracking: Uniaxial Thermal Stress and Strain

Uniaxial thermal stress and strain test (UTSST) results are listed in Table D.10 in Appendix D and summarized in Figure 8.29. The results show that:

- There were no apparent trends in the results.
- All results were below the recommended minimum cracking resistance index of 17°C *(66)*.
- The control mix had a lower CRI_{Env} value and higher fracture temperature than the CRM mix with 5% CRM and a higher CRI_{Env} value and lower fracture temperature than the CRM mix with 10% CRM.

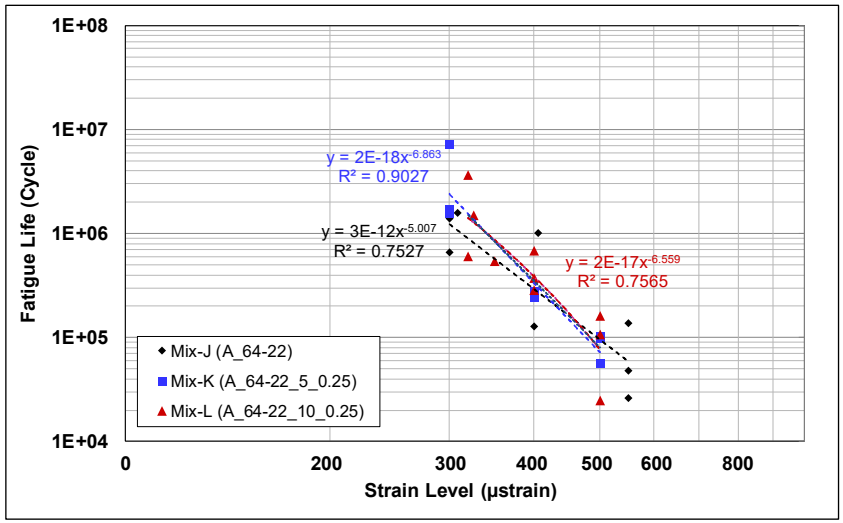

Figure 8.25: App-4/Supp-C: Beam fatigue at 20°C and 10 Hz.

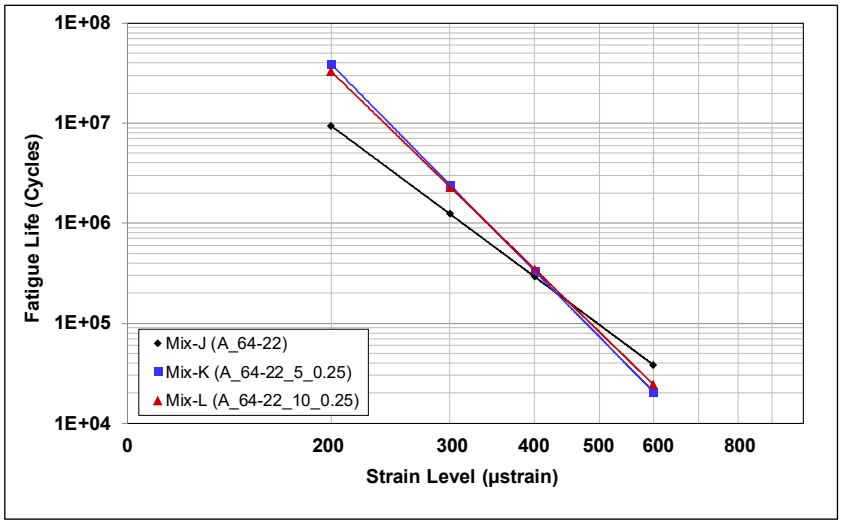

Figure 8.26: App-4/Supp-C: Calculated fatigue life.

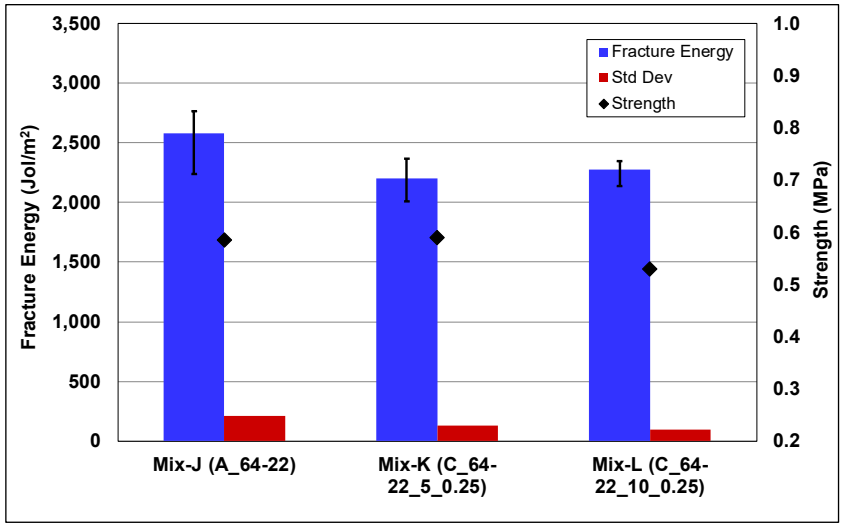

Figure 8.27: App-4/Supp-C: SCB fracture energy and tensile strength at 25°C.

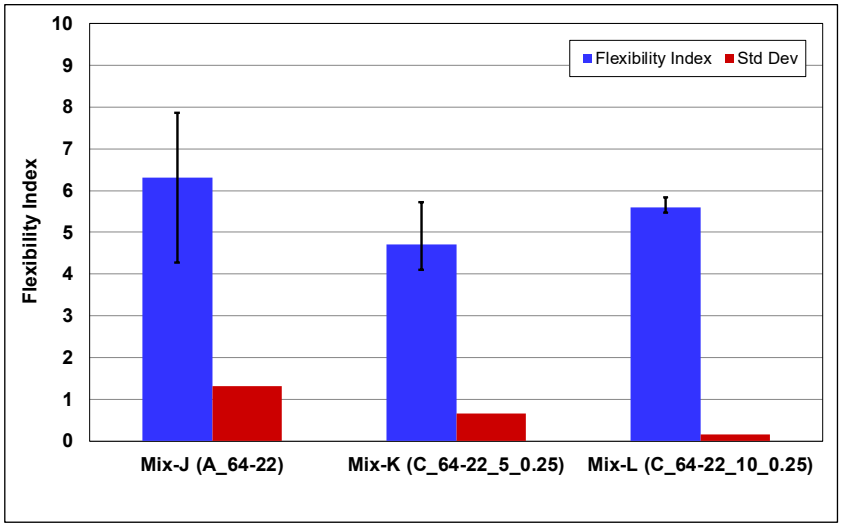

Figure 8.28: App-4/Supp-C: SCB flexibility index at 25°C.

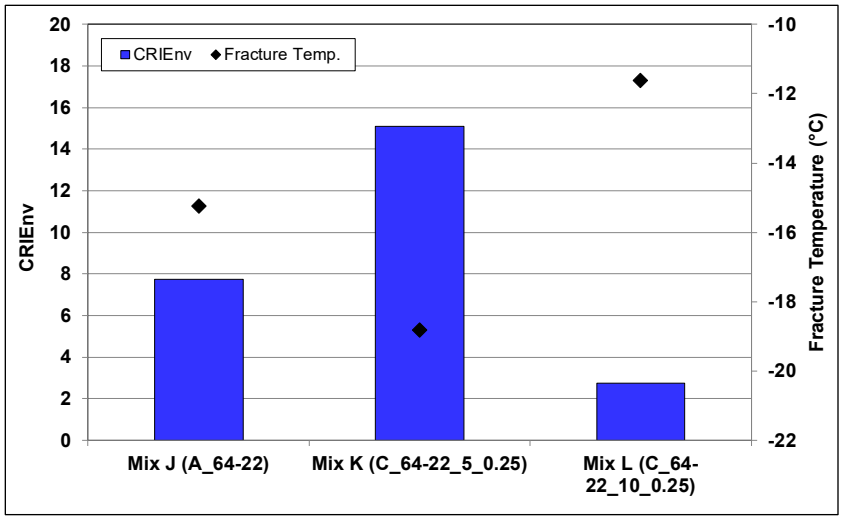

Figure 8.29: App-4/Supp-C: Uniaxial thermal stress and strain.

- The CRM mix with 5% CRM could potentially have better thermal cracking resistance than the control mix, and considerably better resistance than the CRM mix with 10% CRM.

8.4 Approach-4 Test Result Summary

This chapter covers the evaluation of Approach-4 CRM binders (5% and 10% CRM by weight of the binder, with two different CRM particle gradations [<250 µm and <180 µm]) produced using a field-blending process. The following important observations were made from the test results:

- The CRM binders tested in this part of the study met the Caltrans PG-M specifications, except for solubility, where only one CRM binder (5% CRM with <250 µm gradation) used.
- Adding CRM using this approach might result in a high temperature grade above that of the base binder, with the level of change dependent on the base binder, CRM content, and CRM particle size. Improvements were more apparent when the CRM with the <250 µm gradation was used.
- The CRM binders had higher high-temperature performance grades in the unaged and RTFO-aged condition, and lower intermediate-temperature performance grades in the PAV-aged condition, than their base binders.
- The multiple stress creep recovery test results indicated that adding CRM decreased the non-recoverable compliance and increased the percentage recovery at high temperatures (64°C in this test) when compared to the control binders with the same PG.
- The low-temperature test results indicated that adding CRM resulted in lower creep stiffnesses at low temperatures (<0°C) than the control binders with the same PG. However, the low-temperature PG of the CRM binders were the same as those of the base binders. Creep stiffnesses decreased with increasing CRM content.

- FTIR measurements indicated that the CRM binders had lower carbonyl area indices than their base binder after PAV-aging. There was no significant difference in the sulfoxide area indices.
- There did not appear to be any benefits of using an ultra-fine CRM gradation. The finer gradation was also more difficult to blend with the base binder.
- Approach-4 CRM binders could be accommodated in a dense-graded aggregate structure at the same binder content as the control mix, and still meet all mix design requirements.
- The flexural modulus master curves indicated that the CRM mixes were stiffer than the control mix at low frequencies (<1E-02 Hz), but had similar stiffnesses at intermediate and higher frequencies (>1E+01 Hz) at 20°C. Stiffnesses increased with increasing CRM content, as expected.
- The CRM mixes had better rutting and moisture resistance than the control mix. Performance improved when the CRM content was increased from 5% to 10%.
- The CRM mixes could potentially have longer fatigue lives at a given strain than the control mix, especially at low and intermediate strains. The calculated strains did not show a difference between the CRM mixes with 5% and 10% CRM, although this is likely a consequence of the high variability in the results for the CRM mix with 10% CRM. Fatigue performance of the mixes produced with CRM binders were more strain-sensitive than the control mixes.
- Taking variability into consideration, the CRM mixes had similar fracture cracking resistance to the control mixes, with no apparent benefits of adding CRM, or apparent differences between the CRM mix with 5% CRM and the mix with 10% CRM.
- The UTSST results indicated that the CRM mix with 5% CRM could potentially have better thermal cracking resistance than the control mix, and considerably better resistance than the CRM mix with 10% CRM.

Blank page

9. PRELIMINARY PAVEMENT PERFORMANCE SIMULATIONS

9.1 Introduction

The expected field performance of CRM mixes was simulated under a range of pavement structures, climate conditions, and traffic conditions using the *CalME* software program. The purpose of these simulations was to identify likely differences in performance between conventional and CRM mixes, and to determine where the use of CRM mixes would be beneficial.

Two structures were analyzed namely overlays on cracked asphalt pavements and overlays on cracked portland cement concrete pavements. Material parameters were based on flexural frequency sweep and flexural fatigue test results reported in Chapter 5 through Chapter 8. Full-depth structures were not analyzed as they typically consist of different mixes (e.g., rich bottom, intermediate, and surface) with different material properties (i.e., binder, air-void, and RAP contents) that were not tested during the laboratory evaluation of the CRM mixes. However, based on the results discussed in Chapter 5 through Chapter 8, it is clear that mixes produced with CRM binders will potentially have equal or better performance than conventional mixes in these applications.

The simulations focused on the development of reflective cracking through the overlays. Rutting performance was not analyzed because the laboratory test results indicated that the CRM mixes consistently provided equal or better rutting resistance than the control mixes.

9.2 CalME Simulation Input

Simulations using the *CalME* software take into account climate, traffic, material, and pavement structure. The estimation of pavement distress is based on changes in pavement conditions (i.e., stiffness), critical responses (stress, strain, deflection), and the number of load repetitions over time. The primary output is the pavement service life, which is the estimated time when surface cracking reaches 2.5 m/m^2 (≈0.75 $ft./ft^2$). A 20-year design life was used for all simulations.

Table 9.1 lists the climate inputs that were used in the simulations. Potentially appropriate CRM mixes were selected based on binder performance grade for four example California climate regions: north coast, inland valley, desert, and high desert. Pavement temperatures were

calculated in *CalME* using a sinusoidal function option that considers the mean yearly surface temperature, yearly temperature range, and daily temperature range.

Table 9.1: CalME Climate Inputs

Approach	Mix ID	Binder Grade	Climate Zone	Surface Temperature (°F [°C])		
				Yearly Mean	Yearly Range	Daily Range
1 and 3	A,B,C,G,H	64-16	North Coast	59 (15)	54 (12)	61 (16)
1 and 3	A,B,C,G,H	64-16	Inland Valley	70 (21)	73 (23)	75 (24)
1	D,E,F	70-10	Desert	79 (26)	82 (28)	72 (22)
2	S,T,U	64-22	High Desert	59 (15)	88 (31)	79 (26)
4	J,K,L	64-22	High Desert	59 (15)	88 (31)	79 (26)

The two different sets of pavement structures evaluated are summarized in Table 9.2 and Table 9.3. All layers were assumed to be fully bonded in the simulations.

Table 9.2: Asphalt Concrete Overlay on Cracked Asphalt Concrete

Structure	Material	Thickness		Stiffness at 20°C & 10 Hz (ksi [MPa])
		(ft.)	(mm)	
Layer 1	CRM	0.15, 0.2, 0.35, 0.5, 0.7	45, 60, 105, 150, 210	Material dependent
Layer 2	Old HMA	0.35	105	725 (5,000)
Layer 3	Aggregate base	1.0	300	44 (300)
Layer 4	Subgrade (lean clay)	Infinite	Infinite	10 (70)

Table 9.3: Asphalt Concrete Overlay on Cracked Portland Cement Concrete

Structure	Material	Thickness		Stiffness at 20°C & 10 Hz (ksi [MPa])
		(ft.)	(mm)	
Layer 1	CRM	0.15, 0.2, 0.35, 0.5	45, 60, 105, 150	Material dependent
Layer 2	PCC	0.75	225	5,076 (35,000)
Layer 3	Aggregate base	1.0	300	44 (300)
Layer 4	Subgrade (lean clay)	Infinite	Infinite	10 (70)

Two RHMA-G mixes were included in the overlay comparisons to identify the performance differences between CRM mixes and conventional RHMA-G mixes in different climates. A 60 mm (0.2 ft.) layer thickness was used for these comparisons. Table 9.4 summarizes the RHMA-G mix properties used in the simulations. It should be noted that the air-void contents of the RHMA-G mixes were 1% lower than the air-void content used in CRM mix laboratory testing (beam air-void content of 7.0%±1%). The total binder content in the RHMA-G mixes was at least 8.3% by dry weight of aggregate, which implies a base asphalt content of 6.5% if 20% CRM is added. This is higher than the base asphalt binder content used in the CRM mixes. The higher base binder content in the RHMA-G mixes would increase the binder film thickness on the aggregates, which in turn would potentially slow the rate of crack propagation.

Table 9.4: RHMA-G Mix Parameters

Mix ID	Binder Content (%)	Air-Void Content (%)	Mix Gradation	Stiffness at 20°C & 10 Hz (ksi [MPa])
RHMA-G #1	8.3	6.0	1/2 in. NMAS[a]	628 (4,329)
RHMA-G #2	8.8	6.0	3/4 in. NMAS[a]	549 (3,786)

[a] NMAS: nominal maximum aggregate size

Traffic inputs were based on the pavement structure, with higher volumes applied to stronger structures as detailed in Table 9.5.

Table 9.5: CalME Traffic Inputs

AC Overlay on AC			AC Overlay on PCC		
Thickness		Million ESALs[a]/year	Thickness		Million ESALs/year
(ft.)	(mm)		(ft.)	(mm)	
0.15	45	1	0.15	45	0.2
0.20	60	2	0.2	60	0.2
0.35	105	4	0.35	105	1
0.50	150	10	0.5	150	2
0.70	210	10	N/A	N/A	N/A

[a] ESAL: equivalent single axle load

9.3 CalME Simulation Results

9.3.1 Asphalt Concrete Overlay on Cracked Asphalt Concrete

A total of 35 cases were simulated as follows:

- Ten cases used Approach-1 PG 64-16 mixes (two climate conditions × five thicknesses).
- Five cases used the Approach-1 PG 70-10 mixes.
- Approach-2 and Approach-4 mixes were simulated in the high desert climate with five thicknesses for each approach.
- The remaining 10 cases used Approach-3 mixes (two climate conditions × five thicknesses).

Table 9.6 summarizes the rankings for reflective crack retardation performance for the asphalt concrete overlays on cracked asphalt concrete. The comparison was made within each approach according to the binder PG grouping. Given that the mixes using binders with PGs that would be used in different climate zones, no comparison was made across binder groups for a given climate zone. The best-performing mix is ranked as No.1 and the poorest as No.3 in each climate zone.

Figure 9.1 shows the *CalME* plot of simulated reflective wheelpath cracking for Approach-1 Mix-A, Mix-B, and Mix-C in inland valley and north coast climates. A complete set of plots for the remaining simulations is provided in Figure E.1 through Figure E.27 in Appendix E.

Table 9.6: Performance Ranking of Overlay Applications on Cracked Asphalt Concrete

Approach	Binder ID[a]	Mix ID	Ranking[b]			
			Inland Valley	North Coast	Desert	High Desert
1	A-64-16	A	3	3	N/A	N/A
	A-64-16-5-0.25	B	2	2		
	A-64-16-10-0.25	C	1	1		
	A-70-10	D	N/A	N/A	2	N/A
	A-70-10-5-0.25	E			1	
	A-70-10-10-0.25	F			3	
2	B-64-22	S	N/A	N/A	N/A	1
	B-64-22-5-2.36	T				2
	B-64-22-10-2.36	U				3
3	A-64-16	A	1	1	N/A	N/A
	A-64-16-5-2.36_DRY	G	2	2		
	A-64-16-10-2.36_DRY	H	3	3		
4	C-64-22	J	N/A	N/A	N/A	2
	C-64-22-5-0.25	K				3
	C-64-22-10-0.25	L				1

[a] Binder ID format: source-PG-% CRM content-maximum CRM size in mm
[b] Rankings were the same for all thicknesses evaluated

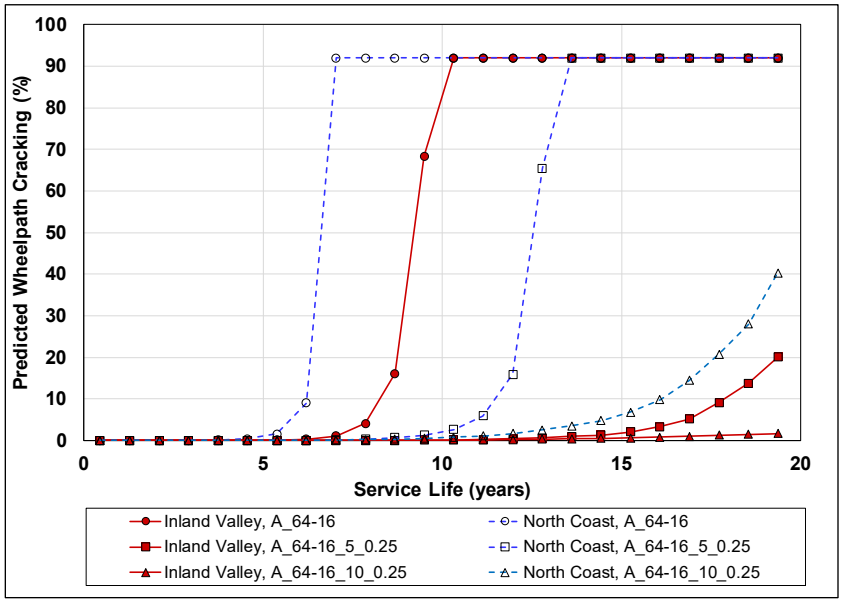

Figure 9.1: AC on AC: Simulation results for 0.15 ft. overlays of Mix-A, -B, and -C.

The results show that:

- Mix ranking depended on a number of factors, as expected, with no universal optimum CRM content across all applications. Primary influences were material, climate, and pavement structure, with tested mix properties having a secondary influence.
- Approach-1 and Approach-4 CRM mixes with an optimal CRM content for a given application had better crack retardation performance than the control mixes, indicating

that CRM mixes could be considered as an alternative to conventional mixes in these applications.

- Increasing the CRM content in the Approach-1 and Approach-4 CRM mixes slowed the development of reflective cracking in inland valley and north coast climates for all surface layer thicknesses, even though the CRM mixes had similar stiffnesses to the control mixes.
- For simulations where most strains were lower than 400 µstrain, the Approach-1 CRM mixes had longer service lives than their control mixes, which was consistent with the laboratory beam fatigue test results.
- In desert applications, the Approach-1 PG 70-10 mix with 5% CRM had the best performance and the mix with 10% CRM mix had the poorest performance. A wide range of temperature fluctuations occur in these climates, which leads to corresponding changes in the mix stiffness of the surface layer. When the temperature is high, the mix stiffness decreases and traffic loads will generate higher strains at the bottom of the layer. This resulted in a shorter service life for the mix with higher CRM content at higher strains (i.e., >400 µstrain), consistent with the laboratory beam fatigue test results.
- The Approach-2 CRM mixes had faster crack propagation rates than their control mix. Increasing the CRM content from 5% to 10% further accelerated the rate of cracking. These results are consistent with the laboratory beam fatigue results.
- The Approach-3 CRM mixes with dry-process CRM did not perform well in inland valley or north coast climate applications, with the control mix having a better cracking resistance. Under the same traffic loadings, the softer CRM mixes transferred higher strains to the underlying layer than the control mix, which accelerated the rate of reflective cracking.
- In the inland valley, north coast, and high desert climates, Approach-1 PG 64-16 mixes and Approach-4 PG 64-22 mixes with 10% CRM had the best performance.
- The RHMA-G mixes performed better than the Approach-1 and Approach-4 CRM mixes under a traffic loading of two million ESALs. This was expected given that RHMA-G mixes generally have better crack-retardation properties than dense-graded mixes. The RHMA-G mixes also had lower stiffnesses than the CRM mixes, which can be beneficial in most thin overlay applications.

9.3.2 Asphalt Concrete Overlay on Cracked Portland Cement Concrete

A total of 28 cases were simulated as follows:

- Eight cases used the Approach-1 PG 64-16 mixes (two climate conditions × four thicknesses [45, 60, 105, and 150 mm (0.15, 0.2, 0.35, and 0.5 ft.)]).
- Four cases used the Approach-1 PG 70-10 mixes in the desert climate.
- Approach-2 and Approach-4 mixes were simulated in the high desert climate with the same four thicknesses for each approach.

- The remaining eight cases used the Approach-3 mixes (two climate conditions × four thicknesses).

Table 9.7 summarizes the rankings for reflective crack retardation performance for the asphalt concrete overlays on cracked portland cement concrete.

Table 9.7: Performance Ranking of Overlays on Cracked Portland Cement Concrete

Approach	Binder ID[a]	Mix ID	Ranking[b]			
			Inland Valley	North Coast	Desert	High Desert
1	A-64-16	A	3	3	N/A	N/A
	A-64-16-5-0.25	B	1	1		
	A-64-16-10-0.25	C	2	2		
	A-70-10	D	N/A	N/A	1	N/A
	A-70-10-5-0.25	E			2	
	A-70-10-10-0.25	F			3	
2	B-64-22	S	N/A	N/A	N/A	3
	B-64-22-5-2.36	T				1
	B-64-22-10-2.36	U				2
3	A-64-16	A	1	1	N/A	N/A
	A-64-16-5-2.36_DRY	G	2	2		
	A-64-16-10-2.36_DRY	H	3	3		
4	C-64-22	J	N/A	N/A	N/A	1
	C-64-22-5-0.25	K				3
	C-64-22-10-0.25	L				2

[1] Binder ID format: source-PG-CRM content in percent-maximum CRM size in mm
[b] Rankings were the same for all thicknesses evaluated

Figure 9.2 shows the *CalME* plot of simulated reflective wheelpath cracking for Approach-1 Mix-A, Mix-B, and Mix-C in inland valley and north coast climates. A complete set of plots for the remaining simulations is provided in Figure E.28 through Figure E.49 in Appendix E. The results show that:

- Mix ranking depended on a number of factors, as expected, with no universal optimum CRM content across all applications. Primary influences were material, climate, and pavement structure, with tested mix properties having a secondary influence.
- Approach-1 PG 64-16 mixes and Approach-2 PG 64-22 mixes with 5% CRM performed well in inland valley, north coast, and high desert climates.
- The Approach-1 PG 64-16 CRM mixes with 10% CRM improved reflective cracking resistance in inland valley and north coast climates. Although these CRM mixes had similar stiffnesses to the control mix, they generally had longer fatigue lives at lower strains (<400 µstrain) in the selected climates.
- The Approach-1 PG 70-10 CRM mixes had poorer performance than the control mixes in the desert climate. The CRM mix with 10% CRM had the fastest rate of cracking, likely due

to higher temperatures leading to lower stiffnesses and consequent higher strains under traffic loading.

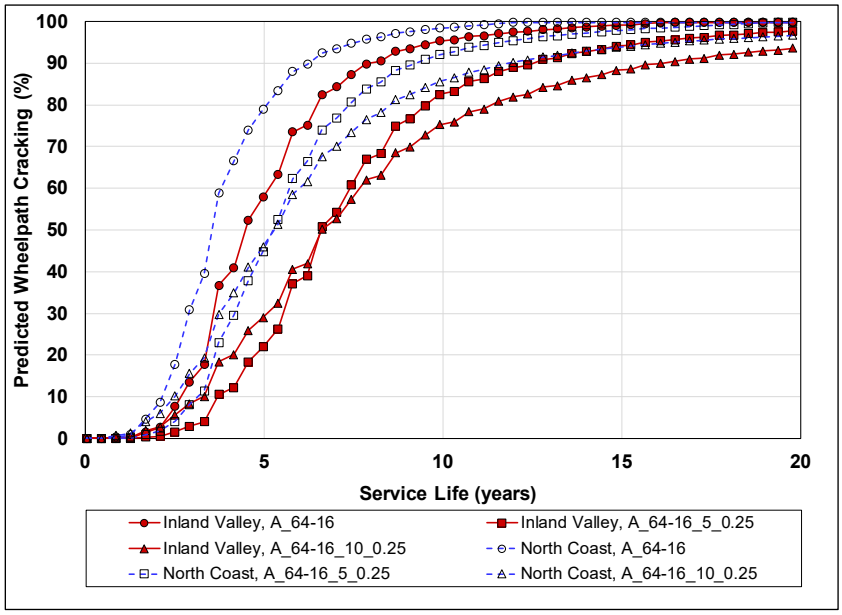

Figure 9.2: AC on PCC: Simulation results for 0.15 ft. overlays of Mix-A, -B, and -C.

- Approach-2 CRM mixes generally showed lower rates of crack propagation than the control mix. Laboratory flexural modulus results showed that the Approach-2 CRM mixes were generally stiffer than the control mix, which resulted in lower strains at the bottom of the overlay.
- The Approach-3 mixes did not perform well in AC over PCC applications. These CRM mixes had lower flexural stiffnesses than the control mix, which resulted in higher loads transferred to the underlying cracked concrete layer. This in turn resulted in faster crack initiation at the bottom of the overlay and faster crack propagation thereafter.
- The Approach-4 CRM mixes had poorer performance than the control mix in the high desert climate. The Approach-4 CRM mixes were more sensitive to stiffness fluctuations as the temperature fluctuated, with fatigue life reduced under the higher strains.
- RHMA-G mixes had similar or slower rates of crack propagation than the CRM mixes. This was attributed primarily to the gap gradation, higher binder content, higher CRM content, and lower air-void content in the RHMA-G mixes.

9.4 CalME Simulation Summary

Although most CRM mixes with wet-process binders performed better than conventional mixes in laboratory tests, simulation results indicated that field performance in different pavement structures varied on a case-by-case basis, depending on the scenario. As with any other pavement

design, appropriate applications of CRM mixes would need to be determined based on an analysis of project-specific mix properties, pavement structure, traffic, and climate.

Findings from these analyses confirmed that laboratory stiffness and fatigue tests at one specific temperature and strain condition might not necessarily represent overall field performance. Material properties, pavement structure, climate conditions, traffic, and the interaction among these factors all influence field performance. In high profile projects, a more complete series of laboratory tests and *CalME* field performance simulations would be used to ensure an optimal pavement design.

10. CONCLUSIONS AND RECOMMENDATIONS

10.1 Study Summary

In 2015, Caltrans expressed interest in studying the addition of small amounts of crumb rubber (CRM) in dense-graded asphalt mixes to increase the total amount of recycled tire rubber used. Small amounts were defined as 5% to 10% CRM by weight of the binder or approximately 0.25% to 0.5% CRM by weight of the aggregate.

The following four approaches for adding the rubber were proposed:

1. Approach-1: Addition of 5% to 10% CRM particles smaller than 250 µm to the asphalt binder, not resulting in a change to the PG of the base binder, achieved by blending softer base binders and/or polymers with the rubber at the refinery/terminal.
2. Approach-2: Addition of 5% to 10% CRM particles smaller than 2.36 mm to the asphalt binder, with allowable changes to the PG of the base binder, and produced using a field-blending process similar to that used for producing asphalt rubber binders with between 18% and 22% CRM by weight of the binder. Two gradations (passing a 2.36 mm [#8] and a 1.18 mm [#16] sieve) were assessed in this study.
3. Approach-3: Adding 0.25% to 0.5% CRM by weight of the aggregate directly into the mix using a dry-process. Particles passing a 2.36 mm (#8) sieve were used in this study; however, most dry process mixes in the United States use particles smaller than 500 µm (passing the #30 sieve).
4. Approach-4: Addition of 5% to 10% CRM with particles smaller than 250 µm to the asphalt binder, with allowable changes to the PG of the base binder, and produced using a field-blending process.

This laboratory study tested 26 binders (6 control [base] binders, 18 CRM binders, and 2 SBS binders) and 19 mixes (5 control mixes and 14 CRM mixes). Binder tests included performance grading, multiple stress creep recovery, stiffness frequency sweeps, solubility, ductility, viscosity, and Fourier-Transform Infrared Spectroscopy. Mix tests included dynamic and flexural modulus to assess stiffness, repeated load triaxial to assess rutting performance, Hamburg wheel track to assess moisture resistance, flexural beam fatigue to assess fatigue and reflective cracking resistance, semicircular bending to assess fracture cracking resistance, and uniaxial thermal stress and strain tests to assess low temperature cracking resistance.

Laboratory tests only reveal material performance under a specific set of controlled testing conditions and may not be representative of actual field performance where layer thicknesses, climate, traffic loading, and other factors all play a role, particularly for bottom-up fatigue cracking performance. Laboratory test results were therefore used as inputs in mechanistic-empirical simulations, using *CalME* software, to predict likely fatigue cracking responses.

10.2 Test Result Summary

Laboratory binder and mix test results revealed that CRM binders and mixes had equal or better performance to their control (base) binders and mixes in terms of potential rutting and cracking performance in most cases, based on the following observations:

- Approach-1 binders met project specific performance grading criteria, including solubility.
- Approach-2 binders had higher high-temperature performance gradings than their base binders in the unaged- and rolling thin film oven (RTFO)-aged conditions, and lower intermediate-temperature performance gradings after pressure vessel aging. Bending beam rheometer (BBR) tests indicated that these CRM binders had the same low-temperature performance grade as their base binders, with decreasing creep stiffness with increasing CRM content. Adding CRM also lowered the non-recoverable creep compliance and increased the percentage recovery in the multiple stress creep recovery (MSCR) test.
- Approach-4 CRM binders showed performance grade changes that were proportional to the CRM content. These binders met the Caltrans PG-M specification criteria, except for solubility, and showed better performance than their base binders at high, intermediate, and low temperatures.
- Binder test results indicate that CRM binders will potentially be more resistant to rutting and to low-temperature cracking. CRM binders generally developed fewer carbonyl components than the control binders after PAV-aging, indicating that they will potentially age at a slower rate than their base binders.
- The Approach-1, Approach-2, and Approach-4 CRM binders were found to be suitable for use in dense-graded mixes. Mixes produced with binders containing CRM particles smaller than 250 µm met volumetric design criteria at the same binder content as the control base binder. Mixes produced with binders containing larger CRM particles (up to 2.36 mm) required higher optimum binder contents than the control mix to meet volumetric criteria. Dry process mixes produced with 0.25% and 0.5% coarse CRM (<2.36 mm) by weight of the aggregate also needed higher optimum binder contents than the control mix to account for the CRM. Although no adjustments were made to aggregate gradations to accommodate the CRM, the mixes with wet-process binders (Approaches-1, 2 and 4) and the mix with

0.25% dry-process CRM all passed the volumetric criteria for Caltrans Type-A HMA. The dry process mix with 0.5% CRM failed some of the VMA criteria.

- Approach-1 and Approach-4 mixes had higher stiffnesses (determined with dynamic and flexural modulus tests) at high temperatures than the control mixes, indicating potentially better rutting performance, but only a marginal stiffness difference at intermediate temperatures, indicating potentially similar or better cracking resistance at a given tensile strain. They also showed the potential for equal or better rutting and moisture resistance than the control mixes in repeated load triaxial and Hamburg wheel track tests, and potentially longer fatigue lives than the control mixes in beam fatigue tests at strain levels below 400 µstrain. Mixes produced with binders containing 5% CRM showed potential for better low-temperature cracking performance in the uniaxial thermal stress and strain test.
- Approach-2 CRM mixes had higher stiffnesses (dynamic and flexural modulus) and better rutting and moisture resistance (repeated load triaxial and Hamburg wheel track) than the control mix. Fatigue results were inconsistent across the range of strains, with the control mix performance generally falling between the 5% CRM content mix (longer fatigue life than the control) and the 10% CRM content mix (shorter fatigue life than the control). Low-temperature cracking resistance tests were not conducted on these mixes.
- Approach-3 mixes had poorer rutting, moisture and thermal cracking resistance than the control mix, but better fatigue performance at strains higher than 600 µstrain. It should be noted that most dry mixes produced in the United States are now prepared with CRM particles smaller than 500 µm (passing the #30 sieve), considerably smaller than the 2.36 mm maximum size tested in this study. Poor performance in this round of testing was mostly attributed to the relatively large CRM particles used, which were not satisfactorily accommodated in the dense gradation.
- Semicircular bend (SCB) test results had high variability between replicate specimens. Taking this into consideration, SCB test results indicated that the CRM mixes had similar fracture resistance to their control mixes.

Mechanistic-empirical performance simulation results indicated that field performance of the CRM mixes in different pavement structures varied on a case-by-case basis, depending on the scenario. As with any other pavement design, appropriate applications of CRM mixes need to be determined based on an analysis of project-specific mix properties, pavement structure, traffic, and climate. However, general trends indicated that mixes produced with Approach-1, Approach-2, and Approach-4 binders had similar or better performance than their control binders in most of the scenarios that were assessed. The dry process mixes did not perform well,

as expected, because of the larger CRM particles used in the study. Different results are expected if finer CRM gradations are used.

10.3 Conclusions

Laboratory test results and mechanistic-empirical performance simulations both indicate that dense-graded mixes produced with binders containing between 5% and 10% CRM by weight of the binder will generally have equal or better performance to dense-graded mixes produced with unmodified binders. Finer CRM gradations (i.e., smaller than 250 µm, used in Approach-1 and Approach-4 binders) allow binder testing with standard Superpave performance grading tests and appear to provide more consistent results. Based on literature reviews, adding between 0.25% and 0.5% CRM with particles sizes smaller than 500 µm in dry process mixes will also provide equal or better performance to mixes that contain no CRM. If any of the approaches are adopted, more scrap tires would be recycled into pavement applications.

10.4 Recommendations

The following recommendations are proposed based on the findings from this study:

- Laboratory test results and mechanistic-empirical performance simulations support the use of small quantities of CRM in dense-graded mixes, both as a means of recycling more waste tires, and for improving pavement layer performance under a given set of conditions. Pilot studies should be considered to confirm these findings, to better quantify the benefits, and to expand the *CalME* materials library.
- Preliminary mechanistic-empirical performance simulation results indicate that dense-graded mixes produced with rubber-modified binders meeting the current Caltrans PG-M specification could be beneficially used in a wide range of pavement layer applications. These findings are supported by literature from other state departments of transportation that have implemented similar specifications. Additional mechanistic-empirical performance simulations should be carried out to confirm these findings and to identify the most appropriate applications in pavement structures in the different California climate zones.
- Some relaxation of the solubility requirements in the PG-M specification should be considered to allow more use of Approach-4 binders. Laboratory test results and performance simulations did not indicate that a relaxation in solubility requirements would have a detrimental effect on performance.

- Given that dry process approaches are the simplest and cheapest method of incorporating CRM into mixes, limited additional testing with finer CRM particles, along with performance simulations, should be conducted to confirm that findings from research conducted in other states and countries are applicable to California applications.

Blank page

REFERENCES

1. *Asphalt Rubber Usage Guide.* 2003. Sacramento, CA: California Department of Transportation.
2. Jones, D., Rizvi, H., Liang, Y. Hung, S., Buscheck, J., Alavi, M., and Hofko, B. 2017. *Development of Performance-Based Specifications for Asphalt Rubber Binder: Interim Report on Phase 1 and Phase 2 Testing*. Davis and Berkeley, CA: University of California Pavement Research Center. (UCPRC-RR-2017-01).
3. *2018 Crumb Rubber Report. Cost Differential Analysis Between Asphalt Containing Crumb Rubber and Conventional Asphalt*. 2020. Sacramento, CA: California Department of Transportation.
4. *Use of Scrap Tire Rubber - State of Technology and Best Practices*. 2005. Sacramento, CA: California Department of Transportation.
5. Rezaei, A. and Harvey, J. 2013. *Investigation of Noise, Ride Quality and Macrotexture Trends for Asphalt Pavement Surfaces: Summary of Six Years of Measurements*. Berkeley and Davis, CA: University of California Pavement Research Center. (UCPRC-RR-2013-11).
6. Harvey, J., Wu, R., Guada, I., Lu, Q., Ongel, A., Rezaei, A., Kohler, E. and Reyes, C. 2017. Overview of California Studies on Noise Reduction for Asphalt and Concrete Surfaces. *Proceedings of the 10th International Conference on the Bearing Capacity of Roads, Railways and Airfields (BCRRA 2017)*, Athens, Greece.
7. *Ground Rubber Applications*. 2016. U.S. Environmental Protection Agency. URL: https://archive.epa.gov/epawaste/conserve/materials/tires/web/html/ground.html.
8. Harvey, J. and Popescu, L. 2000. Accelerated Pavement Testing of Rutting Performance of two Caltrans Overlay Strategies. *Transportation Research Record: Journal of the Transportation Research Board, 1716*. pp 116-125.
9. Harvey, J. and Bejarano, M. 2001. Performance of Two Overlay Strategies Under Heavy Vehicle Simulator Trafficking. *Transportation Research Record: Journal of the Transportation Research Board, 1716*, pp. 123-133.
10. Jones, D., Harvey, J. and Monismith, C. 2007. Reflective Cracking Study: Summary Report. (UCPRC-SR-2007-01).
11. Choubane, B., Sholar, G.A., Musselman, J.A. and Page, G.C. 1998. *Long Term Performance Evaluation on Asphalt Rubber Surface Mixes*. Report No. FL/DOT/SMO/98-431, Gainesville, FL: Florida Department of Transportation.
12. Greene, J., Chun, S., Nash, T. and Choubane, B. 2015. Evaluation and Implementation of PG 76-22 Asphalt Rubber Binder in Florida. *Transportation Research Record: Journal of the Transportation Research Board, 2524*. pp 3-10.

13. Mohammad, L.N., Cooper, S.B., and Elseifi, M.A. 2011. Characterization of HMA Mixes Containing High Reclaimed Asphalt Pavement Content with Crumb Rubber Additives. *Journal of Materials in Civil Engineering, 23(11)*. pp 1560-1568.
14. Bahia, H.U. and Davies, R. 1995. Factors Controlling the Effect of Crumb Rubber on Critical Properties of Asphalt Binders (with discussion). *Journal of the Association of Asphalt Paving Technologists, 64*. pp 130-162.
15. Billiter, T.C., Davison, R.R., Glover, C.J. and Bullin, J.A. 1997. Physical Properties of Asphalt-Rubber Binder. *Petroleum Science and Technology, 15(3-4)*. pp 205-236.
16. Sebaaly, P.E., Gopal, V.T. and Epps, J.A. 2003. Low-Temperature Properties of Crumb Rubber Modified Binders. *Road Materials and Pavement Design, 4(1)*. pp 29-49.
17. Navarro, F.J., Partal, P., Martinez-Boza, F. and Gallegos, C. 2005. Influence of Crumb Rubber Concentration on the Rheological Behavior of a Crumb Rubber Modified Bitumen. *Energy and Fuels, 19(5)*. pp 1984-1990.
18. Shen, J. and Amirkhanian, S. 2005. The Influence of Crumb Rubber Modifier (CRM) Microstructures on the High-Temperature Properties of Rubber-Modified Binders. *International Journal of Pavement Engineering, 6(4)*. pp 265-271.
19. Lee, S.J., Akisetty, C.K. and Amirkhanian, S.N. 2008. The Effect of Crumb Rubber Modifier (CRM) on the Performance Properties of Rubberized Binders in HMA Pavements. *Construction and Building Materials, 22(7)*, pp 1368-1376.
20. Jeong, K.D., Lee, S.J., Amirkhanian, S.N., and Kim, K.W. 2010. Interaction Effects of Crumb Rubber Modified Asphalt Binders. *Construction and Building Materials, 24(5)*. pp 824-831.
21. Kok, B.V. and Çolak, H. 2011. Laboratory Comparison of the Crumb-Rubber and SBS Modified Bitumen and Hot-Mix Asphalt. *Construction and Building Materials, 25(8)*, pp 3204-3212.
22. Cong, P., Xun, P., Xing, M. and Chen, S. 2013. Investigation of Asphalt Binder Containing Various Crumb Rubbers and Asphalts. *Construction and Building Materials, 40*. pp 632-641.
23. Kebaïli, N., Zerzour, A. and Belabdelouhab, F. 2015. Influence of Rubber Fine Powder on the Characteristics of the Bitumens in Algeria. *Energy Procedia, 74*, pp 226-233.
24. Yousefi-Kebria, D., Moafimadani, S.R. and Goli, Y. 2015. Laboratory Investigation of the Effect of Crumb Rubber on the Characteristics and Rheological Behaviour of Asphalt Binder. *Road Materials and Pavement Design, 16(4)*, pp 946-956.
25. Bai, F., Yang, X. and Zeng, G. 2016. A Stochastic Viscoelastic–Viscoplastic Constitutive Model and its Application to Crumb Rubber Modified Asphalt Mixtures. *Materials and Design, 89*. pp 802-809.
26. Lastra-González, P., Calzada-Pérez, M.A., Castro-Fresno, D. Vega-Zamanillo, Á. and Indacoechea-Vega, I. 2016. Comparative analysis of the performance of asphalt concretes

modified by dry way with polymeric waste. *Construction and Building Materials, 112*. pp 1133-1140.

27. Rouse, M.W. 1996. *U.S. Patent No. 5,525,653*. Washington, DC: U.S. Patent and Trademark Office.
28. Abdelrahman, M. and Carpenter, S. 1999. Mechanism of Interaction of Asphalt Cement with Crumb Rubber Modifier. *Transportation Research Record: Journal of the Transportation Research Board, 1661*, pp 106-113.
29. Kim, S., Loh, S.W., Zhai, H. and Bahia, H. 2001. Advanced Characterization of Crumb Rubber-Modified Asphalts, Using Protocols Developed for Complex Binders. *Transportation Research Record: Journal of the Transportation Research Board, 1767*, pp 15-24.
30. Huang, S.C., and Pauli, A.T. 2008. Particle Size Effect of Crumb Rubber on Rheology and Morphology of Asphalt Binders with Long-Term Aging. *Road Materials and Pavement Design, 9(1)*, pp 73-95.
31. Xiao, F., Amirkhanian, S.N., Shen, J. and Putman, B. 2009. Influences of Crumb Rubber Size and Type on Reclaimed Asphalt Pavement (RAP) Mixtures. *Construction and Building Materials, 23(2)*, pp 1028-1034.
32. Wang, H., You, Z., Mills-Beale, J. and Hao, P. 2012. Laboratory Evaluation on High Temperature Viscosity and Low Temperature Stiffness of Asphalt Binder with High Percent Scrap Tire Rubber. *Construction and Building Materials, 26(1)*, pp 583-590.
33. Zanetti, M.C., Fiore, S., Ruffino, B., Santagata, E., Dalmazzo, D. and Lanotte, M. 2015. Characterization of Crumb Rubber from End-of-Life Tyres for Paving Applications. *Waste Management, 45*, pp 161-170.
34. Volle, T.H. 2000. *Performance of Rubberized Asphalt Pavements in Illinois*. Springfield, IL: Illinois Department of Transportation, (No. FHWA/IL/PRR-136).
35. Cao, W. 2007. Study on Properties of Recycled Tire Rubber Modified Asphalt Mixtures Using Dry Process. *Construction and Building Materials, 21(5)*, pp 1011-1015.
36. Moreno, F., Sol, M., Martín, J., Pérez, M. and Rubio, M.C. 2013. The Effect of Crumb Rubber Modifier on the Resistance of Asphalt Mixes to Plastic Deformation. *Materials and Design, 47*. pp 274-280.
37. Dias, J.F., Picado-Santos, L.G. and Capitao, S.D. 2014. Mechanical Performance of Dry Process Fine Crumb Rubber Asphalt Mixtures Placed on the Portuguese Road Network. *Construction and Building Materials, 73*. pp 247-254.
38. Xie, Z. and Shen, J. 2016. Performance Properties of Rubberized Stone Matrix Asphalt Mixtures Produced Through Different Processes. *Construction and Building Materials, 104*. pp 230-234.

39. Arabani, M., Tahami, S.A. and Hamedi, G.H. 2017. Performance Evaluation of Dry Process Crumb Rubber-Modified Asphalt Mixtures with Nanomaterial. *Road Materials and Pavement Design, 19*. pp 1-18.
40. Kocak, S. and Kutay, M.E. 2015. Properties of Activated Crumb Rubber Modified Binders. *Proceedings Rubberized Asphalt, Asphalt Rubber*. Las Vegas, NV.
41. Sousa, J.B., Vorobiev, A., Ishai, I. and Svechinsky. 2012. Elastomeric Asphalt Extender – A New Frontier on Asphalt Rubber Mixes. *Proceedings Asphalt Rubber Roads of the Future*. Munich, Germany.
42. Medina, J., Kaloush, K. and Underwood, S. 2015. Properties of Activated Crumb Rubber Modified Binders. *Proceedings Rubberized Asphalt, Asphalt Rubber*. Las Vegas, NV.
43. Ishai, I., Amit, M., Kesler, T. and Peled, R. 2015. New Advancements in Rubberized Asphalt Using an Elastomeric Asphalt Extender – Three Case Studies. *Proceedings Rubberized Asphalt, Asphalt Rubber*. Las Vegas, NV.
44. Xiao-Qing, Z., Can-hui, L. and Mei, L. 2009. Rheological Properties of Bitumen Modified by Mixing of Mechanochemically Devulcanized Tire Rubber Powder and SBS. *Journal of Materials in Civil Engineering, 21(11)*, pp 699-705.
45. Dong, R., Li, J. and Wang, S. 2011. Laboratory evaluation of Pre-devulcanized Crumb Rubber-Modified Asphalt as a Binder in Hot-Mix-Asphalt. *Journal of Materials in Civil Engineering, 23(8)*, pp 1138-1144.
46. Subhy, A., Lo Presti, D. and Airey, G. 2015. An Investigation on Using Pre-Treated Tyre Rubber as a Replacement of Synthetic Polymers for Bitumen Modification. *Road Materials and Pavement Design, 16*, pp 245-264.
47. Hill, R. 1963. Elastic Properties of Reinforced Solids: Some Theoretical Principles. *Journal of the Mechanics and Physics of Solids, 11(5)*. pp 357-372.
48. Hashin, Z. 1983. Analysis of Composite Materials. *Journal of Applied Mechanics, 50(2)*. pp 481-505.
49. Baumgardner, G. and D'Angleo, J. 2012. Evaluation of New Dynamic Shear Rheometer Testing Geometry for Performance Testing of Crumb Rubber-Modified Binder. *Transportation Research Record: Journal of the Transportation Research Board, 2293*. pp 73-79.
50. Houston, S., Houston, G., Shatnawi, S. and Teclemariam, S. 2017. Inter-Laboratory Study of Performance-Grade Testing of Crumb Rubber Modified Asphalt Binders. *Proceedings 54th Petersen Asphalt Research Conference.* Laramie, WY: Western Research Institute.
51. Luo, X., Gu, F. and Lytton, R.L. 2015. Prediction of Field Aging Gradient in Asphalt Pavements. *Transportation Research Record: Journal of the Transportation Research Board, 2507*. pp 19-28.

52. Liang, Y., Wu, R., Harvey, J.T., Jones, D. and Alavi, M.Z. 2019. Investigation into the Oxidative Aging of Asphalt Binders. *Transportation Research Record: Journal of the Transportation Research Board, 2673*. pp 368-378.
53. Harvey, J. and Tsai, B. 1997. Long-Term Oven-Aging Effects on Fatigue and Initial Stiffness of Asphalt Concrete. *Transportation Research Record: Journal of the Transportation Research Record, 1590*. pp. 89-98.
54. Harvey, J., Monismith, C., Bejarano, M., Tsai, B.W., and Kannekanti, V. 2004. Long-Life AC Pavements: A Discussion of Design and Construction Criteria Based on California Experience. *International Symposium on Design and Construction of Long Lasting Asphalt Pavements Auburn, AL*.
55. Huang, B., Mohammad, L., Graves, P. and Abadie, C. 2002. Louisiana Experience with Crumb Rubber-Modified Hot-Mix-Asphalt Pavement. *Transportation Research Record: Journal of the Transportation Research Board, 1789*. pp 1-13.
56. Pellinen, T.K., Witczak, M.W. and Bonaquist, R.F. 2004. Asphalt Mix Master Curve Construction using Sigmoidal Fitting Function with Non-Linear Least Squares Optimization. *Recent Advances in Materials Characterization and Modeling of Pavement Systems*. pp. 83-101.
57. Morian, N., Hajj, E. and Sebaaly, P. 2013. Significance of Mixture Parameters on Binder Aging in Hot-Mix-Asphalt Mixtures. *Transportation Research Record: Journal of the Transportation Research Board, 2370*. pp 116-127.
58. Mohammad, L.N., Cooper, S.B. and Elseifi, M.A. 2011. Characterization of HMA Mixes Containing High Reclaimed Asphalt Pavement Content with Crumb Rubber Additives. *Journal of Materials in Civil Engineering, 23(11)*. pp 1560-1568.
59. Hofko, B., Alavi, M.Z., Grothe, H., Jones, D. and Harvey, J. 2017. Repeatability and Sensitivity of FTIR ATR Spectral Analysis Methods for Bituminous Binders. *Materials and Structures, 50(3).*
60. Lamontagne. J., Dumas, P., Mouillet, V. and Kister, J. 2001. Comparison by Fourier Transform Infrared (FTIR) Spectroscopy of Different Aging Techniques: Application to Road Bitumen. *Fuel, 80(4)*. pp 483–488.
61. Williams, M.L., Landel, R.F., and Ferry, J.D. 1955. The Temperature Dependence of Relaxation Mechanisms in Amorphous Polymers and other Glass-Forming Liquids. *Journal of the American Chemical Society, 77(14)*. pp 3701-3707.
62. Harvey, J., Liu, A., Zhou, J., Signore, J., Coleri, E. and He, Y. 2016. *Superpave Implementation Phase II: Comparison of Performance-Related Test Results*. Davis and Berkeley, CA: University of California Pavement Research Center. (UCPRC-RR-2015-01).

63. He, Y. 2016. *Interaction Between New and Age-Hardened Binders in Asphalt Mixes Containing High Quantities of Reclaimed Asphalt Pavement and Reclaimed Asphalt Shingles*. Doctoral Dissertation, University of California, Davis, Davis, CA.
64. Pang, C. 2019. *Development of Shift Factors between Repeated Load Triaxial and Repeated Simple Shear Test Results*. Master's Thesis, University of California Davis, Davis, CA.
65. Ozer, H., Al-Qadi, I.L., Lambros, J., El-Khatib, A., Singhvi, P. and Doll, B. 2006. Development of the Fracture-based Flexibility Index for Asphalt Concrete Cracking Potential using Modified Semicircle Bending Test Parameters. *Construction and Building Materials, 115*. pp 390-401.
66. Alavi, M.Z., Hajj, E.Y., Morian, N.E. and Sebaaly, P.E. 2013. Low Temperature Characterization of Asphalt Mixtures by Measuring Visco-Elastic Properties under Thermal Loading. *ISCORD 2013: Planning for Sustainable Cold R*egions. pp 404-415.
67. Anderson, R.M., King, G.N., Hanson, D.I. and Blankenship, P.B. 2011. Evaluation of the Relationship Between Asphalt Binder Properties and Non-Load Related Cracking. *Journal of the Association of Asphalt Paving Technologists, 80*. pp 615-664.
68. Bonaquist, R., Pellinen, T. and Witczak, M.W. 1998. *Development of Relationship Between Binder Viscosity and Stiffness*. Superpave Support and Performance Models Management. College Park, MD: Department of Civil Engineering, University of Maryland.
69. Mateos, A. and Soares, J. 2015. Validation of a Dynamic Modulus Predictive Equation on the Basis of Spanish Asphalt Concrete Mixtures. *Materiales De Construccion. Vol.65, 317*. pp 1-11.
70. Jiao, L., Harvey, J., Elkashef, M., Jones, D. and Liang, Y. 2021. *Preliminary Study on Developing a Surrogate Performance-Related Test for Cracking of Asphalt Pavements*. Davis and Berkeley, CA: University of California Pavement Research Center. (UCPRC-RR-2021-02).
71. Tabatabaee, H.A., Clopotel, C., Arshadi, A. and Bahia, H. 2013. Critical Problems with Using the Asphalt Ductility Test as a Performance Index for Modified Binders. *Transportation Research Record, Journal of the Transportation Research Board, 2370(1)*. pp 84-91.

APPENDIX A: TEST RESULTS FOR APPROACH-1 BINDERS AND MIXES

Test results for Approach-1 (App-1) binders and mixes are summarized in the following tables:

- Table A.1: App-1: Unaged, High Temperature Performance-Grading Results
- Table A.2: App-1: RTFO-Aged, High Temperature Performance-Grading Results
- Table A.3: App-1: PAV-Aged, Intermediate Temperature Performance-Grading Results
- Table A.4: App-1: Bending Beam Rheometer Test Results
- Table A.5: App-1: Multiple Stress Creep Recovery Test Results
- Table A.6: App-1: Binder Frequency Sweep
- Table A.7: App-1: Dynamic Modulus Test Results
- Table A.8: App-1: Flexural Modulus Test Results
- Table A.9: App-1: Repeated Load Triaxial Test Results
- Table A.10: App-1: Hamburg Wheel Track Test Results
- Table A.11: App-1: Flexural Beam Fatigue Test Results
- Table A.12: App-1: Semicircular Bending Test Results
- Table A.13: App-1: Uniaxial Thermal Stress and Strain Test Results

The binder ID format used in the tables is: refinery source_CRM content in percent_maximum CRM size in mm_(3.5% SBS if used).

Table A.1: App-1: Unaged, High Temperature Performance-Grading Results

Aging Condition	Binder ID	Test Temp. (°C)	G* (kPa)	Phase Angle (°)	G*/sin (δ) (kPa)
Unaged	A_64-16	64	1.51	89.2	1.51
			1.54	89.2	1.54
		70	0.68	89.5	0.68
			0.68	89.5	0.68
	A_64-16_5_0.25	64	1.46	87.6	1.46
			1.45	87.6	1.45
		70	0.69	88.4	0.69
			0.69	88.4	0.69
	A_64-16_10_0.25	64	1.72	87.1	1.72
			1.69	87.3	1.69
		70	0.82	87.8	0.82
			0.80	87.9	0.80
	A_70-10	64	2.79	88.9	2.79
			2.77	88.9	2.78
		70	1.20	89.3	1.20
			1.19	89.3	1.19
	A_70-10_5_0.25	64	2.66	87.1	2.66
			2.66	87.1	2.66
		70	1.24	88.1	1.24
			1.25	88.1	1.25
	A_70-10_10_0.25	64	3.05	87.1	3.05
			3.03	87.2	3.04
		70	1.39	87.9	1.39
			1.38	88.0	1.38
	B_64-16	64	2.15	88.0	2.15
			2.15	88.0	2.16
		70	0.97	88.7	0.97
			0.97	88.8	0.97
	B_64-22_5_0.25	64	1.47	88.4	1.47
			1.45	88.4	1.45
		70	0.68	89.0	0.68
			0.68	89.0	0.68
	B_64-22_3.5SBS	64	1.78	70.0	1.90
			1.81	71.2	1.91
		70	1.06	64.5	1.18
			1.06	65.8	1.16
	B_64-28_5_0.25_3.5SBS	64	1.16	69.6	1.24
			1.07	72.6	1.12
		70	0.72	65.6	0.79
			0.65	68.4	0.70
	B_70-16_10_0.25	64	2.45	88.0	2.45
			2.39	88.1	2.39
		70	1.11	88.8	1.11
			1.11	88.8	1.11

Table A.2: App-1: Unaged, High Temperature Performance-Grading Results (continued)

Aging Condition	Binder ID	Test Temp. (°C)	G* (kPa)	Phase Angle (°)	G*/sin (δ) (kPa)
Unaged	B_70-22_3.5SBS	64	3.06	79.0	3.11
			3.00	79.7	3.05
		70	1.56	78.7	1.59
			1.51	79.8	1.54
	B_70-22_10_0.25_3.5SBS	64	1.99	74.2	2.07
			1.97	73.9	2.05
		70	1.13	71.1	1.20
			1.12	70.6	1.19

Table A.2: App-1: RTFO-Aged, High Temperature Performance-Grading Results

Aging Condition	Binder ID	Test Temp. (°C)	G* (kPa)	Phase Angle (°)	G*/sin (δ) (kPa)
RTFO	A_64-16	64	3.12	88.3	3.12
			3.13	88.3	3.13
		70	1.32	89.0	1.32
			1.32	89.0	1.32
	A_64-16_5_0.25	64	3.56	84.9	3.58
			3.48	85.0	3.49
		70	1.63	86.4	1.63
			1.58	86.5	1.59
	A_64-16_10_0.25	64	4.04	85.0	4.05
			3.90	85.0	3.90
		70	1.86	86.3	1.86
			1.78	86.4	1.79
	A_70-10	64	5.97	87.8	5.97
			5.78	87.8	5.79
		70	2.50	88.7	2.50
			2.39	88.7	2.39
	A_70-10_5_0.25	64	6.61	84.6	6.64
			6.62	84.6	6.62
		70	2.90	86.1	2.91
			2.90	86.1	2.91
	A_70-10_10_0.25	64	6.94	84.8	6.97
			7.02	84.8	7.05
		70	3.03	86.2	3.04
			3.06	86.2	3.07
	B_64-16	64	4.86	85.8	4.87
			4.89	85.7	4.91
		70	2.14	87.2	2.14
			2.13	87.2	2.13
	B_64-22_5_0.25	64	3.06	86.6	3.07
			3.07	86.6	3.08
		70	1.36	87.8	1.37
			1.38	87.8	1.38
	B_64-22_3.5SBS	64	2.95	77.9	3.01
			2.88	77.6	2.95
		70	1.50	78.2	1.54
			1.48	78.0	1.51
	B_64-28_5_0.25_3.5SBS	64	2.11	68.0	2.28
			2.16	69.3	2.31
		70	1.28	63.4	1.43
			1.28	65.2	1.41
	B_70-16_10_0.25	64	6.68	85.1	6.70
			6.70	85.1	6.73
		70	2.90	86.8	2.91
			2.93	86.8	2.94

Table A.2: App-1: RTFO-Aged, High Temperature Performance-Grading Results (continued)

Aging Condition	Binder ID	Test Temp. (°C)	G* (kPa)	Phase Angle (°)	G*/sin (δ) (kPa)
RTFO	B_70-22_3.5SBS	64	5.98	77.3	6.13
			6.04	77.4	6.19
		70	2.90	78.7	2.96
			2.94	79.0	2.99
	B_70-22_10_0.25_3.5SBS	64	3.60	70.8	3.81
			3.58	70.4	3.80
		70	2.02	69.8	2.15
			2.00	68.2	2.16

Table A.3: App-1: PAV-Aged, Intermediate Temperature Performance-Grading Results

Aging Condition	Binder ID	Test Temp. (°C)	G* (kPa)	Phase Angle (°)	G*×sin (δ) (kPa)
PAV	A_64-16	25	14,700	43.6	10,130
			14,900	43.6	10,280
	A_64-16_5_0.25	25	8,720	44,4	6,100
			9,640	44.3	6,315
	A_64-16_10_0.25	25	11,000	44.7	7,719
			11,800	44.4	8,282
	A_70-10	25	31,100	34.2	17,480
			29,400	34.2	16,490
	A_70-10_5_0.25	25	22,600	35.5	13,160
			24,100	35.2	13,890
	A_70-10_10_0.25	25	25,900	35.7	15,120
			25,500	35.6	14,810
	B_64-16	25	7,270	45.3	5,171
			7,410	45.3	5,260
	B_64-22_5_0.25	25	4,670	49.2	3,538
			4,580	49.3	3,470
	B_64-22_3.5SBS	25	2,600	50.6	2,011
			2,700	50.3	2,081
	B_64-28_5_0.25_3.5SBS	25	1,100	54.9	906
			1,120	55.0	919
	B_70-16_10_0.25	25	11,200	40.7	7,305
			11,200	40.5	7,292
	B_70-22_3.5SBS	25	6,680	41.1	4,397
			6,080	41.8	4,054
	B_70-22_10_0.25_3.5SBS	25	2,690	47.5	1,982
			2,880	47.2	2,110

Table A.4: App-1: Bending Beam Rheometer Test Results

Aging Condition	Binder ID	Test Temp. (°C)	Creep Stiffness (MPa)	m-value
PAV	A_64-16	-6	171.0	0.359
			172.0	0.358
	A_64-16_5_0.25	-6	90.5	0.382
			94.1	0.385
	A_64-16_10_0.25	-6	116.0	0.359
			118.0	0.342
	A_70-10	0	138.0	0.350
			134.0	0.360
	A_70-10_5_0.25	0	68.9	0.405
			67.0	0.405
	A_70-10_10_0.25	0	93.2	0.364
			83.5	0.362
	B_64-16	-6	102.0	0.352
			100.0	0.353
	B_64-22_5_0.25	-12	164.0	0.336
			153.0	0.337
	B_64-22_3.5SBS	-12	87.2	0.339
			84.8	0.345
	B_64-28_5_0.25_3.5SBS	-18	122.0	0.340
			118.0	0.349
	B_70-16_10_0.25	-6	122.0	0.318
			125.0	0.318
	B_70-22_3.5SBS	-12	145.0	0.337
			145.0	0.337
	B_70-22_10_0.25_3.5SBS	-12	94.3	0.346
			98.5	0.345

Table A.5: App-1: Multiple Stress Creep Recovery Test Results

Aging Condition	Binder ID	Average Percentage Recovery (%)		Non-Recoverable Creep Compliance (1/kPa)	
		0.1 kPa	3.2 kPa	0.1 kPa	3.2 kPa
RTFO	A_64-16	0.67	0.00	2.94	3.04
		0.15	0.00	3.08	3.17
	A_64-16_5_0.25	3.08	0.14	2.57	2.78
		3.37	0.17	2.55	2.77
	A_64-16_10_0.25	6.63	0.81	2.18	2.42
		6.19	0.77	2.15	2.38
	A_70-10	1.99	1.48	0.66	0.67
		2.48	1.50	0.66	0.67
	A_70-10_5_0.25	5.77	1.61	1.37	1.48
		7.12	1.64	1.35	1.47
	A_70-10_10_0.25	9.36	1.96	1.23	1.38
		10.05	2.06	1.24	1.39
	B_64-16	4.10	0.40	1.89	2.05
		3.05	0.26	1.99	2.11
	B_64-22_5_0.25	1.01	0.00	3.17	3.36
		1.23	0.00	3.20	3.40
	B_64-22_3.5SBS	89.69	9.90	0.24	2.76
		90.93	11.60	0.21	2.65
	B_64-28_5_0.25_3.5SBS	97.49	90.52	0.05	0.15
		97.82	95.01	0.04	0.06
	B_70-16_10_0.25	3.26	0.88	1.32	1.39
		3.06	0.73	1.44	1.52
	B_70-22_3.5SBS	69.35	28.69	0.37	0.93
		78.66	42.62	0.26	0.71
	B_70-22_10_0.25_3.5SBS	97.68	95.53	0.03	0.05
		97.08	90.69	0.04	0.11

Table A.6a: App-1: Binder Frequency Sweep Results for Refinery A (20°C)

Reduced Frequency (Hz)	A_64-16	A_64-16_5_0.25	A_64-16_10_0.25	A_70-10	A_70-10_5_0.25	A_70-10_10_0.25
1.00E-06	8.02E-02	1.50E-01	1.31E-01	5.84E-01	2.42E-01	2.76E-01
1.00E-05	4.21E-01	7.15E-01	6.26E-01	4.14E+00	1.29E+00	1.53E+00
1.00E-04	3.00E+00	4.28E+00	3.82E+00	3.43E+01	8.39E+00	1.04E+01
1.00E-03	2.55E+01	2.91E+01	2.69E+01	2.79E+02	6.00E+01	7.72E+01
1.00E-02	2.14E+02	1.98E+02	1.92E+02	1.88E+03	4.10E+02	5.36E+02
1.00E-01	1.47E+03	1.19E+03	1.21E+03	9.41E+03	2.36E+03	3.08E+03
1.00E+00	7.42E+03	5.72E+03	6.08E+03	3.35E+04	1.05E+04	1.36E+04
1.00E+01	2.62E+04	2.09E+04	2.30E+04	8.69E+04	3.51E+04	4.44E+04
1.00E+02	6.64E+04	5.80E+04	6.55E+04	1.73E+05	8.94E+04	1.10E+05
1.00E+03	1.29E+05	1.26E+05	1.44E+05	2.79E+05	1.80E+05	2.16E+05
1.00E+04	2.03E+05	2.23E+05	2.58E+05	3.88E+05	2.98E+05	3.51E+05
1.00E+05	2.76E+05	3.38E+05	3.91E+05	4.85E+05	4.29E+05	4.96E+05
1.00E+06	3.38E+05	4.53E+05	5.25E+05	5.64E+05	5.53E+05	6.31E+05

Table A.6b: App-1: Binder Frequency Sweep Results for Refinery B (20°C)

Reduced Frequency (Hz)	B_64-16	B_64-22_5_0.25	B_64-22_3.5SBS	B_64-28_ 5_0.25_3.5SBS	B_70- 16_10_0.25	B_70-22_3.5SBS	B_70-22_ 10_0.25_3.5SBS
1.00E-06	1.72E-01	2.45E-01	1.58E-01	9.39E-02	2.99E-01	2.91E-01	1.42E-01
1.00E-05	8.86E-01	7.53E-01	6.67E-01	3.22E-01	1.60E+00	1.34E+00	5.30E-01
1.00E-04	5.71E+00	3.34E+00	3.41E+00	1.34E+00	1.02E+01	7.24E+00	2.38E+00
1.00E-03	4.08E+01	2.03E+01	1.97E+01	6.48E+00	7.00E+01	4.23E+01	1.22E+01
1.00E-02	2.80E+02	1.45E+02	1.17E+02	3.43E+01	4.49E+02	2.40E+02	6.60E+01
1.00E-01	1.62E+03	9.66E+02	6.43E+02	1.84E+02	2.40E+03	1.20E+03	3.49E+02
1.00E+00	7.17E+03	4.95E+03	3.00E+03	9.22E+02	9.96E+03	4.94E+03	1.66E+03
1.00E+01	2.37E+04	1.77E+04	1.12E+04	4.02E+03	3.13E+04	1.62E+04	6.68E+03
1.00E+02	5.90E+04	4.45E+04	3.32E+04	1.46E+04	7.56E+04	4.20E+04	2.20E+04
1.00E+03	1.16E+05	8.35E+04	7.84E+04	4.33E+04	1.46E+05	8.81E+04	5.91E+04
1.00E+04	1.88E+05	1.26E+05	1.52E+05	1.05E+05	2.36E+05	1.55E+05	1.30E+05
1.00E+05	2.65E+05	1.64E+05	2.49E+05	2.12E+05	3.32E+05	2.35E+05	2.42E+05
1.00E+06	3.36E+05	1.93E+05	3.60E+05	3.68E+05	4.23E+05	3.20E+05	3.89E+05

Table A.7a: App-1: Dynamic Modulus Test Results for Mix-A (A_64-16)

Fitting Parameters	δ	α	β	γ	C1	C2
	0.27	4.13	-2.09	-0.54	117.86	955.79
Temperature (°C)	**Frequency (Hz)**	**Modulus (MPa)**	**Phase Angle (°)**	**Reduced Frequency (Hz)**	**Modeled Modulus (MPa)**	**Square of Errors**
4	25	22,063	5.8	2.61E+03	20,929	5.26E-04
	10	20,780	6.4	1.05E+03	20,052	2.40E-04
	5	19,769	7.0	5.23E+02	19,291	1.13E-04
	1	17,258	8.6	1.04E+02	17,160	6.13E-06
	0.5	16,134	9.4	5.18E+01	16,094	1.14E-06
	0.1	13,453	11.9	1.05E+01	13,322	1.80E-05
21	25	13,628	12.6	1.90E+01	14,404	5.78E-04
	10	12,029	14.2	7.60E+00	12,728	6.01E-04
	5	10,754	15.7	3.84E+00	11,421	6.83E-04
	1	7,969	19.9	7.67E-01	8,301	3.14E-04
	0.5	6,848	21.8	3.77E-01	6,976	6.51E-05
	0.1	4,506	27.5	7.46E-02	4,311	3.69E-04
38	25	5,376	27.5	1.60E-01	5,491	8.45E-05
	10	4,091	30.4	6.33E-02	4,077	2.29E-06
	5	3,241	32.5	3.14E-02	3,162	1.17E-04
	1	1,682	37.1	6.28E-03	1,610	3.65E-04
	0.5	1,205	38.3	3.31E-03	1,191	2.60E-05
	0.1	510	39.5	6.45E-04	513	5.88E-06
54	25	1,048	41.9	2.18E-03	968	1.18E-03
	10	624	42.1	8.71E-04	603	2.18E-04
	5	410	41.8	4.35E-04	415	2.45E-05
	1	152	39.4	8.63E-05	169	2.03E-03
	0.5	104	37.0	4.32E-05	115	2.00E-03
	0.1	55	29.2	8.71E-06	50	2.04E-03

Table A.7b: App-1: Dynamic Modulus Test Results for Mix-B (A_64-16_5_0.25)

Fitting Parameters	δ	α	β	γ	C1	C2
	0.00	4.31	-2.00	-0.49	49.21	400.81
Temperature (°C)	**Frequency (Hz)**	**Modulus (MPa)**	**Phase Angle ( )**	**Reduced Frequency (Hz)**	**Modeled Modulus (MPa)**	**Square of Errors**
4	25	17,911	7.6	2.70E+03	16,142	2.04E-03
	10	16,571	8.4	1.08E+03	15,342	1.12E-03
	5	15,510	9.1	5.45E+02	14,675	5.78E-04
	1	13,056	11.1	1.11E+02	12,885	3.26E-05
	0.5	11,964	12.1	5.62E+01	12,020	4.16E-06
	0.1	9,506	15.1	1.12E+01	9,800	1.76E-04
21	25	9,959	16.2	1.80E+01	10,471	4.74E-04
	10	8,358	18.2	7.20E+00	9,156	1.57E-03
	5	7,216	19.9	3.60E+00	8,143	2.75E-03
	1	4,980	24.3	7.20E-01	5,839	4.78E-03
	0.5	4,162	26.1	3.60E-01	4,915	5.23E-03
	0.1	2,572	31.0	7.20E-02	3,056	5.60E-03
38	25	4,611	29.1	1.77E-01	4,043	3.26E-03
	10	3,513	31.3	7.22E-02	3,059	3.61E-03
	5	2,822	32.8	3.61E-02	2,409	4.71E-03
	1	1,522	36.1	7.48E-03	1,296	4.87E-03
	0.5	1,125	36.6	3.77E-03	959	4.84E-03
	0.1	511	36.9	7.48E-04	440	4.16E-03
54	25	903	40.6	3.49E-03	925	1.15E-04
	10	569	40.0	1.40E-03	600	5.31E-04
	5	392	39.2	7.04E-04	427	1.40E-03
	1	156	37.7	1.41E-04	185	5.45E-03
	0.5	117	34.6	7.18E-05	129	1.90E-03
	0.1	59	29.1	1.40E-05	55	1.04E-03

Table A.7c: App-1: Dynamic Modulus Test Results for Mix-C (A_64-16_10_0.25)

Fitting Parameters	δ	α	β	γ	C1	C2
	0.00	4.39	-2.01	-0.49	41.21	340.00
Temperature (°C)	**Frequency (Hz)**	**Modulus (MPa)**	**Phase Angle (°)**	**Reduced Frequency (Hz)**	**Modeled Modulus (MPa)**	**Square of Errors**
4	25	19,910	6.9	2.42E+03	19,002	4.11E-04
	10	18,738	7.9	9.69E+02	18,026	2.83E-04
	5	17,632	8.5	4.85E+02	17,202	1.15E-04
	1	15,046	10.4	9.69E+01	15,005	1.43E-06
	0.5	13,871	11.4	4.85E+01	13,946	5.47E-06
	0.1	11,253	14.2	9.89E+00	11,326	7.88E-06
21	25	11,871	14.3	1.76E+01	12,299	2.37E-04
	10	10,283	16.2	7.03E+00	10,740	3.57E-04
	5	9,059	17.8	3.52E+00	9,543	5.11E-04
	1	6,483	22.1	7.03E-01	6,830	5.14E-04
	0.5	5,493	24.0	3.58E-01	5,773	4.66E-04
	0.1	3,487	29.0	7.23E-02	3,600	1.92E-04
38	25	4,965	27.9	1.98E-01	4,907	2.59E-05
	10	3,828	29.9	7.92E-02	3,709	1.87E-04
	5	3,067	31.4	3.96E-02	2,930	3.96E-04
	1	1,667	34.8	8.05E-03	1,575	6.02E-04
	0.5	1,234	35.7	4.13E-03	1177	4.22E-04
	0.1	575	36.2	8.05E-04	539	8.03E-04
54	25	1,242	39.6	4.41E-03	1,212	1.13E-04
	10	801	39.1	1.76E-03	792	1.93E-05
	5	558	38.5	8.82E-04	564	2.11E-05
	1	226	37.0	1.75E-04	244	1.18E-03
	0.5	155	35.5	8.82E-05	169	1.46E-03
	0.1	75	30.4	1.75E-05	72	3.58E-04

Table A.7d: App-1: Dynamic Modulus Test Results for Mix-D (A_70-10)

Fitting Parameters	δ	α	β	γ	C1	C2
	0.00	4.43	-2.32	-0.49	12.62	93.72
Temperature (°C)	**Frequency (Hz)**	**Modulus (MPa)**	**Phase Angle (°)**	**Reduced Frequency (Hz)**	**Modeled Modulus (MPa)**	**Square of Errors**
4	25	24,490	5.0	9.78E+03	23,264	4.97E-04
	10	23,338	5.4	3.91E+03	22,591	2.00E-04
	5	22,472	6.0	1.99E+03	22,019	7.80E-05
	1	20,211	7.1	4.03E+02	20,401	1.65E-05
	0.5	19,146	7.7	2.02E+02	19,568	8.95E-05
	0.1	16,604	9.2	3.97E+01	17,291	3.10E-04
21	25	15,788	10.6	1.71E+01	15,941	1.75E-05
	10	14,076	11.9	6.79E+00	14,335	6.27E-05
	5	12,807	13.0	3.39E+00	13,069	7.72E-05
	1	9,999	16.4	6.79E-01	10,022	9.39E-07
	0.5	8,822	18.0	3.46E-01	8,755	1.12E-05
	0.1	6,285	22.7	6.92E-02	5,923	6.61E-04
38	25	7,460	22.0	2.10E-01	7,840	4.65E-04
	10	6,016	24.5	8.48E-02	6,256	2.88E-04
	5	5,048	26.4	4.30E-02	5,172	1.11E-04
	1	3,082	31.5	8.79E-03	3,066	5.25E-06
	0.5	2,393	33.3	4.46E-03	2,369	1.92E-05
	0.1	1,193	36.7	8.85E-04	1,182	1.40E-05
54	25	3,295	33.0	1.08E-02	3,306	1.86E-06
	10	2,411	34.7	4.31E-03	2,337	1.80E-04
	5	1,831	35.9	2.14E-03	1,753	3.62E-04
	1	858	38.5	4.31E-04	839	8.95E-05
	0.5	591	38.8	2.17E-04	595	9.97E-06
	0.1	241	37.6	4.31E-05	254	4.67E-04

Table A.7e: App-1: Dynamic Modulus Test Results for Mix-E (A_70-10_5_0.25)

Fitting Parameters	δ	α	β	γ	C1	C2
	0.42	3.89	-2.22	-0.52	8.23	44.45
Temperature (°C)	**Frequency (Hz)**	**Modulus (MPa)**	**Phase Angle (°)**	**Reduced Frequency (Hz)**	**Modeled Modulus (MPa)**	**Square of Errors**
4	25	21,998	5.8	9.96E+05	19,426	2.92E-03
	10	20,835	6.0	4.12E+05	19,243	1.19E-03
	5	19,909	6.5	2.14E+05	19,082	3.39E-04
	1	17,646	7.7	4.42E+04	18,597	5.20E-04
	0.5	16,603	8.4	2.14E+04	18,315	1.82E-03
	0.1	14,138	10.3	4.27E+03	17,529	8.72E-03
21	25	13,254	11.7	1.56E+01	12,360	9.18E-04
	10	11,711	13.1	6.41E+00	11,158	4.41E-04
	5	10,556	14.4	3.21E+00	10,167	2.67E-04
	1	8,040	17.9	6.50E-01	7,790	1.89E-04
	0.5	7,040	19.6	3.25E-01	6,761	3.07E-04
	0.1	4,911	24.2	6.33E-02	4,502	1.42E-03
38	25	4,696	27.6	1.03E-01	5,138	1.52E-03
	10	3,650	30.0	4.11E-02	3,973	1.36E-03
	5	2,977	31.5	2.07E-02	3,202	1.00E-03
	1	1,687	35.0	4.14E-03	1,781	5.55E-04
	0.5	1,290	35.6	2.09E-03	1,343	2.98E-04
	0.1	640	36.3	4.11E-04	644	4.93E-06
54	25	2,224	35.7	6.69E-03	2,146	2.43E-04
	10	1,576	36.6	2.68E-03	1,491	5.84E-04
	5	1,176	36.8	1.35E-03	1,112	5.84E-04
	1	534	37.2	2.73E-04	528	2.29E-05
	0.5	373	36.6	1.34E-04	373	6.37E-07
	0.1	164	34.5	2.66E-05	165	1.78E-05

Table A.7f: App-1: Dynamic Modulus Test Results for Mix-F (A_70-10_10_0.25)

Fitting Parameters	δ	α	β	γ	C1	C2
	0.00	4.37	-2.18	-0.51	13.08	96.02
Temperature (°C)	**Frequency (Hz)**	**Modulus (MPa)**	**Phase Angle (°)**	**Reduced Frequency (Hz)**	**Modeled Modulus (MPa)**	**Square of Errors**
4	25	21,910	5.4	1.06E+04	20,483	8.55E-04
	10	20,688	5.8	4.25E+03	19,842	3.29E-04
	5	19,756	6.2	2.22E+03	19,322	9.34E-05
	1	17,469	7.6	4.51E+02	17,776	5.73E-05
	0.5	16,412	8.3	2.16E+02	16,922	1.77E-04
	0.1	13,926	10.4	4.38E+01	14,775	6.60E-04
21	25	13,134	11.7	1.80E+01	13,405	7.85E-05
	10	11,656	13.1	7.26E+00	11,911	8.84E-05
	5	10,522	14.5	3.67E+00	10,738	7.82E-05
	1	8,014	18.2	7.41E-01	7,948	1.31E-05
	0.5	6,984	20.1	3.74E-01	6,794	1.43E-04
	0.1	4,801	25.1	7.41E-02	4,331	2.00E-03
38	25	5,455	25.6	2.09E-01	5,856	9.48E-04
	10	4,226	28.4	8.24E-02	4,478	6.34E-04
	5	3,424	30.2	4.15E-02	3,583	3.89E-04
	1	1,927	34.7	8.49E-03	1,962	6.00E-05
	0.5	1,450	35.7	4.40E-03	1,477	6.76E-05
	0.1	692	37.0	8.62E-04	673	1.32E-04
54	25	2,120	36.9	9.34E-03	2,042	2.66E-04
	10	1,441	38.0	3.69E-03	1,365	5.54E-04
	5	1,034	38.5	1.83E-03	980	5.53E-04
	1	429	39.4	3.61E-04	426	4.59E-06
	0.5	284	39.3	1.81E-04	292	1.50E-04
	0.1	114	40.0	3.61E-05	119	3.96E-04

Table A.8a: App-1: Flexural Modulus Test Results for Mix-A (A_64-16)

Fitting Parameters	δ	α	β	γ	C1	C2
	0.00	4.21	-2.08	-0.59	8.03	53.76
Temp. (°C)	**Frequency (Hz)**	**Modulus (MPa)**	**Phase Angle (°)**	**Reduced Frequency (Hz)**	**Modeled Modulus (MPa)**	**Square of Errors**
10	15	14,150	12.6	1.15E+03	13,388	8.74E-04
	10	13,715	11.5	7.68E+02	13,110	6.70E-04
	5	12,945	10.7	3.89E+02	12,594	4.60E-04
	2	11,773	11.1	1.57E+02	11,803	3.84E-04
	1	10,891	12.0	7.79E+01	11,107	5.12E-04
	0.5	9,972	12.8	3.84E+01	10,331	6.94E-04
	0.2	8,713	14.9	1.51E+01	9,203	1.05E-03
	0.1	7,694	17.0	7.21E+00	8,249	1.27E-03
	0.05	6,719	19.2	3.76E+00	7,363	1.88E-03
	0.02	5,508	22.7	1.51E+00	6,106	2.42E-03
	0.01	4,624	25.6	7.38E-01	5,124	2.39E-03
20	15	9,729	18.6	1.81E+01	9,442	4.27E-04
	10	9,292	18.1	1.19E+01	8,906	8.09E-04
	5	8,318	18.5	5.95E+00	7,991	9.11E-04
	2	6,984	21.3	2.35E+00	6,717	9.87E-04
	1	6,013	22.8	1.18E+00	5,759	1.29E-03
	0.5	5,051	25.2	5.91E-01	4,828	1.42E-03
	0.2	3,893	29.8	2.33E-01	3,658	2.16E-03
	0.1	3,052	34.2	1.13E-01	2,848	2.01E-03
	0.05	2,358	37.3	5.62E-02	2,172	1.81E-03
	0.02	1,613	42.5	2.42E-02	1,505	1.70E-03
	0.01	1,149	45.5	1.14E-02	4,108	2.42E-03
30	15	5,195	30.6	7.94E-01	5,223	6.47E-04
	10	4,670	31.7	5.23E-01	4,670	6.17E-04
	5	3,781	33.7	2.62E-01	3,798	6.20E-04
	2	2,728	37.7	1.05E-01	2,775	8.01E-04
	1	2,057	40.2	5.32E-02	2,122	1.06E-03
	0.5	1,511	43.4	2.68E-02	1,576	1.13E-03
	0.2	962	48.1	1.06E-02	1,008	1.43E-03
	0.1	675	50.5	5.32E-03	700	1.40E-03
	0.05	468	54.3	2.69E-03	477	8.39E-04
	0.02	267	42.9	3.97E-01	272	1.87E-04
	0.01	175	42.2	3.53E-01	182	2.29E-04

Table A.8b: App-1: Flexural Modulus Test Results for Mix-B (A_64-16_5_0.25)

Fitting Parameters	δ	α	β	γ	C1	C2
	0.05	4.18	-1.75	-0.51	7.69	53.15
Temp. (°C)	**Frequency (Hz)**	**Modulus (MPa)**	**Phase Angle (°)**	**Reduced Frequency (Hz)**	**Modeled Modulus (MPa)**	**Square of Errors**
10	15	12,562	14.5	1.11E+03	12,200	2.43E-04
	10	12,100	13.4	7.65E+02	11,867	1.33E-04
	5	11,245	12.7	3.89E+02	11,215	6.63E-05
	2	10,068	13.4	1.56E+02	10,249	1.04E-04
	1	9,160	14.3	7.90E+01	9,469	2.38E-04
	0.5	8,249	15.2	3.93E+01	8,629	4.37E-04
	0.2	7,054	17.5	1.43E+01	7,380	4.11E-04
	0.1	6,092	19.6	7.10E+00	6,495	8.10E-04
	0.05	5,234	21.8	3.59E+00	5,643	1.12E-03
	0.02	4,180	25.0	1.34E+00	4,465	8.68E-04
	0.01	3,440	27.6	6.94E-01	3,731	1.31E-03
20	15	8,114	16.1	8.86E+02	11,114	3.91E-04
	10	7,587	15.3	6.07E+02	10,730	3.35E-04
	5	6,641	14.9	3.08E+02	10,021	2.53E-04
	2	5,425	15.9	1.23E+02	9,017	2.89E-04
	1	4,562	17.1	6.35E+01	8,249	4.26E-04
	0.5	3,764	18.3	3.19E+01	7,446	6.62E-04
	0.2	2,832	21.0	1.14E+01	6,260	6.65E-04
	0.1	2,199	23.3	5.53E+00	5,427	9.01E-04
	0.05	1,694	25.9	2.70E+00	4,627	1.10E-03
	0.02	1,164	28.6	1.02E+00	3,618	1.26E-03
	0.01	864	31.4	5.37E-01	3,020	1.68E-03
30	15	3,987	33.5	8.86E-01	3,997	1.31E-04
	10	3,547	34.2	5.77E-01	3,537	1.60E-04
	5	2,815	35.6	2.86E-01	2,846	2.39E-04
	2	2,013	39.0	1.13E-01	2,063	5.69E-04
	1	1,512	39.3	5.64E-02	1,578	8.44E-04
	0.5	1,123	42.0	2.82E-02	1,182	1.19E-03
	0.2	738	42.8	1.18E-02	799	2.37E-03
	0.1	541	46.2	5.83E-03	570	1.07E-03
	0.05	383	46.4	2.90E-03	402	2.30E-03
	0.02	256	47.0	1.20E-03	253	1.16E-03
	0.01	181	46.9	5.79E-04	172	2.10E-03

Table A.8c: App-1: Flexural Modulus Test Results for Mix-C (A_64-16_10_0.25)

Fitting Parameters	δ	α	β	γ	C1	C2
	0.00	4.23	-1.92	-0.53	7.96	53.14
Temp. (°C)	**Frequency (Hz)**	**Modulus (MPa)**	**Phase Angle (°)**	**Reduced Frequency (Hz)**	**Modeled Modulus (MPa)**	**Square of Errors**
10	15	13,203	14.0	1.11E+03	12,786	3.77E-04
	10	12,761	13.3	7.27E+02	12,446	3.03E-04
	5	11,967	12.1	3.67E+02	11,843	2.26E-04
	2	10,823	12.8	1.47E+02	10,946	2.60E-04
	1	9,943	13.5	7.39E+01	10,201	3.82E-04
	0.5	9,054	14.4	3.62E+01	9,374	5.39E-04
	0.2	7,860	16.5	1.46E+01	8,250	8.39E-04
	0.1	6,907	18.4	7.55E+00	7,420	1.44E-03
	0.05	6,020	20.5	3.87E+00	6,555	1.95E-03
	0.02	4,915	23.7	1.45E+00	5,309	1.91E-03
	0.01	4,110	26.4	7.53E-01	4,506	2.40E-03
20	15	8,863	15.5	8.43E+02	11,697	5.54E-04
	10	8,354	14.8	5.56E+02	11,310	5.36E-04
	5	7,408	14.1	2.80E+02	10,620	4.92E-04
	2	6,141	15.2	1.11E+02	9,645	4.64E-04
	1	5,246	15.9	5.57E+01	8,876	5.29E-04
	0.5	4,381	17.3	2.70E+01	8,036	6.62E-04
	0.2	3,350	20.0	1.09E+01	6,941	8.93E-04
	0.1	2,638	22.0	5.65E+00	6,166	1.11E-03
	0.05	2,053	24.6	2.90E+00	5,392	1.37E-03
	0.02	1,412	27.7	1.08E+00	4,300	1.32E-03
	0.01	1,051	30.5	5.69E-01	3,618	2.02E-03
30	15	4,580	31.8	7.96E-01	4,573	5.54E-05
	10	4,103	32.7	5.24E-01	4,083	7.38E-05
	5	3,321	33.9	2.63E-01	3,328	6.03E-05
	2	2,393	36.2	1.06E-01	2,459	2.30E-04
	1	1,830	39.3	5.32E-02	1,897	3.27E-04
	0.5	1,353	41.6	2.70E-02	1,438	8.12E-04
	0.2	890	44.8	1.06E-02	948	9.68E-04
	0.1	639	48.7	5.39E-03	682	1.06E-03
	0.05	455	48.5	2.61E-03	471	4.40E-04
	0.02	287	48.8	1.07E-03	292	1.30E-04
	0.01	206	49.5	5.30E-04	198	9.33E-04

Table A.8d: App-1: Flexural Modulus Test Results for Mix-D (A_70-10)

Fitting Parameters	δ	α	β	γ	C1	C2
	0.80	3.45	-1.97	-0.49	5.86	46.58
Temp. (°C)	**Frequency (Hz)**	**Modulus (MPa)**	**Phase Angle (°)**	**Reduced Frequency (Hz)**	**Modeled Modulus (MPa)**	**Square of Errors**
10	15	14,304	11.8	5.54E+02	12,844	9.62E-03
	10	13,977	10.4	3.65E+02	12,485	1.06E-02
	5	13,258	9.3	1.85E+02	11,854	1.25E-02
	2	12,252	9.6	7.39E+01	10,941	1.56E-02
	1	11,489	10.2	3.65E+01	10,190	1.90E-02
	0.5	10,676	10.4	1.87E+01	9,450	2.24E-02
	0.2	9,580	11.9	7.55E+00	8,407	2.90E-02
	0.1	8,688	13.2	3.79E+00	7,600	3.49E-02
	0.05	7,844	14.6	1.88E+00	6,782	4.21E-02
	0.02	6,779	16.9	7.73E-01	5,754	5.44E-02
	0.01	5,984	19.0	3.77E-01	4,968	6.59E-02
20	15	9,975	12.9	3.97E+02	11,966	9.58E-03
	10	9,556	11.7	2.60E+02	11,570	1.06E-02
	5	8,727	10.8	1.32E+02	10,876	1.25E-02
	2	7,576	11.4	5.27E+01	9,892	1.56E-02
	1	6,701	11.9	2.61E+01	9,110	1.90E-02
	0.5	5,873	12.6	1.32E+01	8,330	2.25E-02
	0.2	4,816	14.4	5.33E+00	7,278	2.91E-02
	0.1	4,018	15.9	2.67E+00	6,486	3.49E-02
	0.05	3,319	17.7	1.33E+00	5,712	4.21E-02
	0.02	2,533	20.2	5.35E-01	4,740	5.44E-02
	0.01	2,012	22.5	2.65E-01	4,047	6.58E-02
30	15	6,935	22.5	4.18E+00	8,023	1.43E-02
	10	6,477	22.6	2.66E+00	7,496	1.59E-02
	5	5,657	22.7	1.31E+00	6,649	1.95E-02
	2	4,610	24.9	5.21E-01	5,561	2.67E-02
	1	3,865	27.1	2.53E-01	4,763	3.33E-02
	0.5	3,192	29.2	1.24E-01	4,029	4.17E-02
	0.2	2,426	32.0	4.81E-02	3,141	5.42E-02
	0.1	1,894	34.8	2.14E-02	2,511	6.45E-02
	0.05	1,472	38.2	7.78E-03	1,873	7.33E-02
	0.02	1,029	39.7	2.79E-03	1,310	8.43E-02
	0.01	737	43.8	1.15E-03	938	9.00E-02

Table A.8e: App-1: Flexural Modulus Test Results for Mix-E (A_70-10_5_0.25)

Fitting Parameters	δ	α	β	γ	C1	C2
	0.00	4.26	-2.08	-0.49	1.28	18.19
Temp. (°C)	**Frequency (Hz)**	**Modulus (MPa)**	**Phase Angle (°)**	**Reduced Frequency (Hz)**	**Modeled Modulus (MPa)**	**Square of Errors**
10	15	14,278	11.9	1.14E+03	13,834	1.62E-03
	10	13,943	10.7	7.63E+02	13,520	1.66E-03
	5	13,239	9.5	3.76E+02	12,919	1.91E-03
	2	12,236	9.8	1.52E+02	12,062	2.66E-03
	1	11,481	10.4	7.56E+01	11,344	3.65E-03
	0.5	10,717	10.4	3.79E+01	10,583	4.88E-03
	0.2	9,659	12.1	1.59E+01	9,562	7.19E-03
	0.1	8,766	13.5	7.72E+00	8,672	9.43E-03
	0.05	7,935	15.1	3.76E+00	7,765	1.17E-02
	0.02	6,869	17.7	1.55E+00	6,637	1.83E-02
	0.01	6,051	19.9	7.80E-01	5,777	2.32E-02
20	15	9,792	12.9	8.77E+02	12,765	1.85E-03
	10	9,388	11.8	5.87E+02	12,404	2.02E-03
	5	8,607	10.7	2.88E+02	11,735	2.51E-03
	2	7,533	11.4	1.16E+02	10,802	3.64E-03
	1	6,725	12.1	5.69E+01	10,030	5.16E-03
	0.5	5,915	12.5	2.87E+01	9,251	6.96E-03
	0.2	4,899	14.5	1.20E+01	8,223	1.02E-02
	0.1	4,101	16.4	5.79E+00	7,365	1.31E-02
	0.05	3,428	18.3	2.85E+00	6,533	1.63E-02
	0.02	2,625	21.3	1.20E+00	5,521	2.40E-02
	0.01	2,089	24.2	5.97E-01	4,742	3.06E-02
30	15	7,916	20.7	9.03E+00	8,749	9.20E-03
	10	7,432	20.6	5.87E+00	8,214	1.01E-02
	5	6,565	20.9	2.87E+00	7,315	1.25E-02
	2	5,426	23.0	1.14E+00	6,154	1.67E-02
	1	4,602	24.8	5.63E-01	5,291	2.05E-02
	0.5	3,839	27.3	2.79E-01	4,474	2.53E-02
	0.2	2,942	30.8	1.09E-01	3,477	3.12E-02
	0.1	2,307	33.8	5.20E-02	2,782	3.75E-02
	0.05	1,800	37.9	2.12E-02	2,076	3.66E-02
	0.02	1,245	41.5	7.95E-03	1,435	4.21E-02
	0.01	886	43.7	3.61E-03	1,037	4.23E-02

Table A.8f: App-1: Flexural Modulus Test Results for Mix-F (A_70-10_10_0.25)

Fitting Parameters	δ	α	β	γ	C1	C2
	0.00	4.21	-2.26	-0.51	40.26	269.60
Temp. (°C)	**Frequency (Hz)**	**Modulus (MPa)**	**Phase Angle (°)**	**Reduced Frequency (Hz)**	**Modeled Modulus (MPa)**	**Square of Errors**
10	15	13,281	11.7	7.51E+02	12,975	5.36E-04
	10	12,997	10.4	4.96E+02	12,701	5.28E-04
	5	12,362	9.1	2.47E+02	12,198	4.80E-04
	2	11,482	9.3	9.87E+01	11,451	5.15E-04
	1	10,801	9.7	4.84E+01	10,805	5.13E-04
	0.5	10,090	9.9	2.48E+01	10,149	5.89E-04
	0.2	9,097	11.4	9.83E+00	9,165	6.64E-04
	0.1	8,264	12.7	5.01E+00	8,402	7.67E-04
	0.05	7,480	14.2	2.50E+00	7,587	8.11E-04
	0.02	6,479	16.5	9.88E-01	6,469	8.95E-04
	0.01	5,733	18.6	4.92E-01	5,633	9.76E-04
20	15	9,643	12.8	5.66E+02	12,158	4.09E-04
	10	9,244	11.6	3.74E+02	11,840	4.25E-04
	5	8,472	10.5	1.86E+02	11,263	4.40E-04
	2	7,375	11.1	7.43E+01	10,427	5.28E-04
	1	6,574	11.9	3.63E+01	9,730	5.70E-04
	0.5	5,761	12.0	1.87E+01	9,033	6.70E-04
	0.2	4,719	14.2	7.44E+00	8,032	7.99E-04
	0.1	3,936	15.7	3.79E+00	7,269	9.10E-04
	0.05	3,242	17.5	1.89E+00	6,487	9.73E-04
	0.02	2,447	20.3	7.50E-01	5,449	1.04E-03
	0.01	1,932	22.4	3.72E-01	4,686	1.24E-03
30	15	5,833	24.4	5.73E-01	5,814	7.81E-04
	10	5,386	24.4	3.78E-01	5,320	8.42E-04
	5	4,600	25.8	1.89E-01	4,519	9.12E-04
	2	3,595	28.6	7.57E-02	3,540	1.06E-03
	1	2,898	30.6	3.82E-02	2,880	1.15E-03
	0.5	2,301	33.2	1.93E-02	2,291	1.20E-03
	0.2	1,634	38.3	7.66E-03	1,627	1.37E-03
	0.1	1,219	41.3	3.83E-03	1,226	1.56E-03
	0.05	905	43.6	2.01E-03	924	2.18E-03
	0.02	595	45.5	7.66E-04	588	3.10E-03
	0.01	420	47.7	3.89E-04	419	2.75E-03

Table A.9: App-1: Repeated Load Triaxial Test Results

Specimen ID	AV Content (%)	Flow Number (Cycles)	Average (Cycles)	Std. Dev. (Cycles)	Std. Dev./Average (%)
Mix-A-1	6.5	254	272	120	44.0
Mix-A-2	6.9	158			
Mix-A-3	7.3	153			
Mix-A-4	6.9	320			
Mix-B-1	6.5	700	670	289	43.2
Mix-B-2	6.9	692			
Mix-B-3	6.9	429			
Mix-B-4	7.2	985			
Mix-C-1	6.7	722	589	217	40.4
Mix-C-2	7.0	781			
Mix-C-3	7.2	277			
Mix-C-4	7.4	493			
Mix-D-1	6.5	1,510	844	398	47.2
Mix-D-2	6.7	788			
Mix-D-3	7.1	559			
Mix-D-4	7.1	519			
Mix-E-1	6.7	660	891	269	30.1
Mix-E-2	6.7	604			
Mix-E-3	7.0	1,247			
Mix-E-4	7.2	1,052			
Mix-F-1	6.5	2,267	1,415	582	41.2
Mix-F-2	6.6	953			
Mix-F-3	6.7	1,935			
Mix-F-4	7.0	1,149			
Mix-F-5	6.9	770			

Table A.10: App-1: Hamburg Wheel Track Test Results

Specimen ID	AV Content (%)	Left Wheel Rutting (mm)			Right Wheel Rutting (mm)		
		@5k Passes	@15k Passes	@25k Passes	@5k Passes	@15k Passes	@25k Passes
Mix-A-1	7.1	3.51	5.05	6.20	Not tested	Not tested	Not tested
Mix-A-2	8.0						
Mix-A-3	7.4	Not tested	Not tested	Not tested	2.61	3.89	4.98
Mix-A-4	7.2						
Mix-B-1	7.1	2.52	3.30	3.82	Not tested	Not tested	Not tested
Mix-B-2	7.3						
Mix-B-3	7.2	Not tested	Not tested	Not tested	1.90	2.44	2.75
Mix-B-4	6.6						
Mix-C-1	7.4	2.30	2.81	3.11	Not tested	Not tested	Not tested
Mix-C-2	6.8						
Mix-C-3	7.3	Not tested	Not tested	Not tested	2.06	2.76	3.08
Mix-C-4	7.0						
Mix-D-1	6.8	1.80	2.38	2.69	Not tested	Not tested	Not tested
Mix-D-2	6.9						
Mix-D-3	6.7	Not tested	Not tested	Not tested	1.65	2.22	2.52
Mix-D-4	6.4						
Mix-E-1	6.8	2.02	2.58	2.89	Not tested	Not tested	Not tested
Mix-E-2	6.8						
Mix-E-3	7.1	Not tested	Not tested	Not tested	1.68	2.23	2.51
Mix-E-4	6.9						
Mix-F-1	6.8	2.10	2.66	2.91	Not tested	Not tested	Not tested
Mix-F-2	7.0						
Mix-F-3	6.6	Not tested	Not tested	Not tested	1.84	2.40	2.71
Mix-F-4	7.1						

Table A.11a: App-1: Flexural Beam Fatigue Test Results for Mix-A (A_64-16)

Specimen ID	Air-Void Content (%)	Test Strain (µstrain)	Fatigue Life (Cycles)
MixA-B#3-2-B8	7.5	210	1,397,500
MixA-B#3-3-B1	7.7	210	1,130,000
MixA-B#3-2-B6	6.3	210	1,440,000
MixA-B#3-2-B2	6.4	250	382,500
MixA-B#3-3-B4	7.3	252	405,000
MixA-B#3-3-B7	7.6	250	512,500
MixA-B#3-2-B7	6.5	400	49,000
MixA-B#3-3-B3	7.4	400	37,000
MixA-B#3-3-B6	7.5	400	105,000

Table A.11b: App-1: Flexural Beam Fatigue Test Results for Mix-B (A_64-16_5_0.25)

Specimen ID	Air-Void Content (%)	Test Strain (µstrain)	Fatigue Life (Cycles)
MixB-B#3-2-B1	6.7	250	1,057,500
MixB-B#3-2-B2	6.3	250	1,335,000
MixB-B#3-2-B3	6.3	250	2,750,000
MixB-B#3-2-B4	6.6	400	152,500
MixB-B#3-2-B7	6.6	400	130,000
MixB-B#3-2-B8	6.6	400	227,500
MixB-B#3-3-B2	6.2	500	38,000
MixB-B#3-3-B3	6.2	500	18,000
MixB-B#3-3-B6	6.5	500	41,000

Table A.11c: App-1: Flexural Beam Fatigue Test Results for Mix-C (A_64-16_10_0.25)

Specimen ID	Air-Void Content (%)	Test Strain (µstrain)	Fatigue Life (Cycles)
MixC-B#3-2-B1	6.6	250	972,500
MixC-B#3-2-B4	6.8	250	1,410,000
MixC-B#3-2-B3	6.5	250	1,962,500
MixC-B#3-2-B5	6.6	304	855,000
MixC-B#3-1-B3	6.5	300	152,500
MixC-B#3-1-B4	6.3	300	475,000
MixC-B#3-1-B5	6.4	400	60,000
MixC-B#3-1-B6	6.5	400	90,000
MixC-B#3-1-B7	6.7	400	20,000

Table A.11d: App-1: Flexural Beam Fatigue Test Results for Mix-D (A_70-10)

Specimen ID	Air-Void Content (%)	Test Strain (µstrain)	Fatigue Life (Cycles)
MixD-B#3-1-B1	6.3	210	1,365,000
MixD-B#3-1-B7	6.1	210	665,000
MixD-B#3-2-B1	7.0	210	497,500
MixD-B#3-1-B6	6.2	250	757,500
MixD-B#3-2-B3	6.9	251	165,000
MixD-B#3-2-B4	7.1	250	712,500
MixD-B#3-1-B5	6.0	400	57,000
MixD-B#3-1-B8	6.7	400	29,000
MixD-B#3-2-B2	7.0	400	36,000

Table A.11e: App-1: Flexural Beam Fatigue Test Results for Mix-E (A_70-10_5_0.25)

Specimen ID	Air-Void Content (%)	Test Strain (µstrain)	Fatigue Life (Cycles)
MixE-B#3-1-B2	7.9	250	1,957,500
MixE-B#3-2-B1	6.9	256	860,000
MixE-B#3-2-B6	7.1	250	1,117,500
MixE-B#3-1-B3	7.4	290	392,500
MixE-B#3-1-B4	7.6	290	705,000
MixE-B#3-1-B5	7.6	290	1,555,000
MixE-B#3-1-B6	7.9	400	94,000
MixE-B#3-2-B3	6.8	400	147,500
MixE-B#3-2-B8	7.7	400	23,000

Table A.11f: App-1: Flexural Beam Fatigue Test Results for Mix-F (A_70-10_10_0.25)

Specimen ID	Air-Void Content (%)	Test Strain (µstrain)	Fatigue Life (Cycles)
MixF-B#3-1-B1	6.8	250	1,210,000
MixF-B#3-2-B2	6.8	250	490,000
MixF-B#3-2-B4	6.8	250	977,500
MixF-B#3-1-B5	7.8	280	695,000
MixF-B#3-1-B7	7.8	280	370,000
MixF-B#3-2-B7	6.7	280	217,500
MixF-B#3-1-B3	6.8	400	147,500
MixF-B#3-2-B1	6.8	400	20,000
MixF-B#3-2-B5	6.7	400	102,500

Table A.12: App-1: Semicircular Bending Test Results

Specimen ID	Air-Void Content (%)	Fracture Energy (Jol/m^2)	Flexibility Index	Strength (MPa)
Mix-A	6.9	2,125	4.99	0.59
	6.9	1,837	4.99	0.50
	7.2	1,871	2.78	0.65
	7.2	1,084	0.33	0.66
Mix-B	6.6	1,418	0.56	0.78
	6.5	3,167	6.45	0.69
	6.8	2,325	5.86	0.57
	6.4	2,116	4.62	0.54
Mix-C	7.1	2,030	1.27	0.80
	7.3	3,441	6.61	0.70
	7.2	2,858	6.75	0.62
	7.2	3,169	8.59	0.66
Mix-D	7.1	1,093	0.37	0.76
	6.9	1,395	0.46	0.79
	7.0	1,298	1.00	0.70
	6.8	1,513	1.71	0.69
Mix-E	7.8	1,660	0.94	0.81
	7.2	1,740	0.95	0.80
	7.4	1,773	0.73	0.81
	7.4	1,741	0.73	0.91
Mix-F	6.4	1,740	0.49	0.88
	7.1	1,252	0.36	0.86
	6.3	2,096	1.60	0.78
	6.4	1,961	0.74	0.81

Table A.13: App-1: Uniaxial Thermal Stress and Strain Test Results

Specimen ID	Air-Void Content (%)	Average UTSST Air-Void Content (%)[1]	Average CRI_{Env}[1]	Average Fracture Temperature (°C)[1]
Mix-A	7.2	6.0	12	-12.5
	7.6			
Mix-B	7.6	5.6	31	-16.4
	7.5			
Mix-C	8.8	7.8	12	-13.6
	7.2			
Mix-D	7.8	6.2	6	-6.3
	7.9			
Mix-E	7.5	5.9	21	-11.5
	7.4			
Mix-F	7.6	6.6	6	-8.0
	8.4			

[1] Only the average results were received by UCPRC

APPENDIX B: TEST RESULTS FOR APPROACH-2 BINDERS AND MIXES

Test results for Approach-2 (App-2) binders and mixes are summarized in the following tables and figures:

- Table B.1: App-2: Unaged, High Temperature Performance-Grading Results
- Table B.2: App-2: RTFO-Aged, High Temperature Performance-Grading Results
- Table B.3: App-2: PAV-Aged, Intermediate Temperature Performance-Grading Results
- Table B.4: App-2: Bending Beam Rheometer Test Results
- Table B.5: App-2: Multiple Stress Creep Recovery Test Results
- Table B.6: App-2: Binder Frequency Sweep Results
- Table B.7: App-2: Dynamic Modulus Test Results
- Table B.8: App-2: Flexural Modulus Test Results
- Table B.9: App-2: Repeated Load Triaxial Test Results
- Table B.10: App-2: Hamburg Wheel Track Test Results
- Table B.11: App-2: Flexural Beam Fatigue Test Results
- Table B.12: App-2: Semicircular Bending Test Results
- Figure B.1: App-2: Mix-Q Volumetric Design Results
- Figure B.2: App-2: Mix-R Volumetric Design Results
- Figure B.3: App-2: Mix-T Volumetric Design Results
- Figure B.4: App-2: Mix-U Volumetric Design Results
- Figure B.5: App-2: Mix-V Volumetric Design Results
- Figure B.6: App-2: Mix-W Volumetric Design Results

The binder ID format used in the tables is: refinery source_CRM content in percent_maximum CRM size in mm.

Table B.1: App-2: Unaged, High Temperature Performance-Grading Results

Aging Condition	Binder ID	Test Temp. (°C)	G* (kPa)	Phase Angle (°)	G*/sin (δ) (kPa)
Unaged	D_64-22	64	1.61	85.1	1.61
			1.60	85.1	1.60
		70	0.74	96.7	0.74
			0.75	86.6	0.75
	D_64-22_5_2.36	70	1.42	82.2	1.44
			1.52	82.0	1.53
		76	0.76	84.4	0.76
			0.77	84.5	0.77
	D_64-22_10_2.36	70	3.71	73.1	3.87
			4.39	70.6	4.65
		76	2.03	76.9	2.09
			2.45	74.7	2.54
	D_64-22_5_1.18	70	1.45	82.5	1.46
			2.03	80.1	2.06
		76	0.76	84.9	0.77
			0.94	83.0	0.95
	D_64-22_10_1.18	70	2.67	76.1	2.75
			2.88	78.6	2.98
		76	1.43	79.4	1.45
			1.57	78.6	1.60
	F_64-22	64	1.45	86.7	1.45
			1.36	86.7	1.36
		70	0.69	87.7	0.69
			0.64	87.7	0.64
	F_64-22_5_2.36	70	1.95	83.1	1.96
			1.63	84.8	1.64
		76	0.97	85.3	0.97
			0.80	86.6	0.80
	F_64-22_10_2.36	70	2.00	79.8	2.03
			1.93	79.8	1.96
		76	1.08	82.4	1.09
			1.05	82.2	1.06

Table B.2: App-2: RTFO-Aged, High Temperature Performance-Grading Results

Aging Condition	Binder ID	Test Temp. (°C)	G* (kPa)	Phase Angle (°)	G*/sin (δ) (kPa)
RTFO	D_64-22	64	4.74	79.3	4.82
			4.67	79.3	4.60
		70	2.21	81.8	2.23
			2.19	81.8	2.21
	D_64-22_5_2.36	70	11.12	62.4	12.55
			10.97	63.2	12.30
		76	6.06	66.0	6.63
			6.50	66.5	6.60
	D_64-22_10_2.36	70	14.76	58.1	17.29
			14.38	58.7	16.82
		76	8.30	61.2	9.48
			8.19	61.7	9.30
	D_64-22_5_1.18	70	10.03	65.6	11.01
			10.43	65.4	11.48
		76	5.40	68.9	5.79
			5.51	68.8	5.91
	D_64-22_10_1.18	70	18.58	51.2	23.85
			16.23	56.0	19.59
		76	11.32	53.9	14.00
			9.37	59.0	10.93
	F_64-22	64	3.67	82.9	3.70
			3.69	83.0	3.72
		70	1.69	85.0	1.70
			1.67	84.9	1.68
	F_64-22_5_2.36	70	4.22	76.6	4.34
			4.15	77.7	4.24
		76	2.17	79.3	2.21
			2.03	80.4	2.06
	F_64-22_10_2.36	70	8.43	66.9	9.17
			9.11	66.0	9.98
		76	4.55	70.4	4.83
			4.89	69.7	5.21

Table B.3: App-2: PAV-Aged, Intermediate Temperature Performance-Grading Results

Aging Condition	Binder ID	Test Temp. (°C)	G* (kPa)	Phase Angle (°)	G*×sin (δ) (kPa)
PAV	D_64-22	25	5,223	45.8	3,742
			5,391	45.3	3,832
	D_64-22_5_2.36	25	4,560	38.7	2,854
			5,238	37.9	3,215
	D_64-22_10_2.36	25	4,407	38.5	2,746
			4,872	37.9	2,990
	D_64-22_5_1.18	25	5,462	35.1	3,143
			6,572	35.4	3,806
	D_64-22_10_1.18	25	5,711	37.5	3,480
			6,712	35.5	3,891
	F_64-22	25	5,305	45.0	3,748
			5,127	45.5	3,653
	F_64-22_5_2.36	25	4,710	42.5	3,184
			5,316	41.8	3,541
	F_64-22_10_2.36	25	5,748	39.8	3,193
			5,795	40.0	3,722

Table B.4: App-2: Bending Beam Rheometer Test Results

Aging Condition	Binder ID	Test Temp. (°C)	Creep Stiffness (MPa)	m-value
PAV	D_64-22	-12	154	0.322
			178	0.323
	D_64-22_5_2.36	-12	139	0.307
			110	0.297
	D_64-22_10_2.36	-12	112	0.302
			102	0.307
	D_64-22_5_1.18	-12	162	0.302
			148	0.303
	D_64-22_10_1.18	-12	129	0.293
			100	0.312
	F_64-22	-12	158	0.335
			169	0.323
	F_64-22_5_2.36	-12	159	0.324
			143	0.317
	F_64-22_10_2.36	-12	120	0.312
			121	0.299

Table B.5: App-2: Multiple Stress Creep Recovery Test Results

Aging Condition	Binder ID	Average Percentage Recovery (%)		Non-Recoverable Creep Compliance (1/kPa)	
		0.1 kPa	3.2 kPa	0.1 kPa	3.2 kPa
RTFO	D_64-22	12.77	1.61	1.48	2.00
		11.66	1.69	1.54	1.97
	D_64-22_5_2.36	57.24	50.42	0.12	0.13
		57.71	51.17	0.10	0.12
	D_64-22_10_2.36	69.28	63.10	0.06	0.07
		68.56	62.97	0.06	0.07
	D_64-22_5_1.18	52.24	46.27	0.14	0.16
		50.84	44.81	0.15	0.17
	D_64-22_10_1.18	80.91	75.18	0.02	0.03
		72.96	67.46	0.04	0.05
	F_64-22	5.05	0.04	2.53	2.95
		4.14	0.08	2.49	2.86
	F_64-22_5_2.36	25.07	16.88	0.60	0.70
		22.02	14.20	0.73	0.82
	F_64-22_10_2.36	47.32	38.71	0.18	0.23
		52.64	40.76	0.23	0.16

Table B.6a: App-2: Binder Frequency Sweep Results for Refinery D (40°C)

Reduced Frequency (Hz)	D_64-22	D_64-22_5_2.36	D_64-22_10_2.36	D_64-22_10_1.18	D_64-22_10_1.18
1.00E-06	8.02E-02	1.50E-01	1.31E-01	2.47E-01	6.35E-01
1.00E-05	4.21E-01	7.15E-01	6.26E-01	7.73E-01	1.75E+00
1.00E-04	3.00E+00	4.28E+00	3.82E+00	2.69E+00	5.15E+00
1.00E-03	2.55E+01	2.91E+01	2.69E+01	1.00E+01	1.58E+01
1.00E-02	2.14E+02	1.98E+02	1.92E+02	3.82E+01	4.93E+01
1.00E-01	1.47E+03	1.19E+03	1.21E+03	1.42E+02	1.52E+02
1.00E+00	7.42E+03	5.72E+03	6.08E+03	4.92E+02	4.53E+02
1.00E+01	2.62E+04	2.09E+04	2.30E+04	1.53E+03	1.27E+03
1.00E+02	6.64E+04	5.80E+04	6.55E+04	4.20E+03	3.30E+03
1.00E+03	1.29E+05	1.26E+05	1.44E+05	1.00E+04	7.84E+03
1.00E+04	2.03E+05	2.23E+05	2.58E+05	2.08E+04	1.69E+04
1.00E+05	2.76E+05	3.38E+05	3.91E+05	3.80E+04	3.32E+04
1.00E+06	3.38E+05	4.53E+05	5.25E+05	6.20E+04	5.95E+04

Table B.6b: App-2: Binder Frequency Sweep Results for Refinery F (40°C)

Reduced Frequency (Hz)	F_64-22	F_64-22_5_2.36	F_64-22_10_2.36
1.00E-06	7.16E-03	7.55E-02	3.92E-01
1.00E-05	1.78E-02	2.35E-01	1.18E+00
1.00E-04	6.11E-02	8.57E-01	3.86E+00
1.00E-03	2.98E-01	3.53E+00	1.34E+01
1.00E-02	1.99E+00	1.55E+01	4.71E+01
1.00E-01	1.62E+01	6.75E+01	1.63E+02
1.00E+00	1.34E+02	2.72E+02	5.31E+02
1.00E+01	9.35E+02	9.62E+02	1.59E+03
1.00E+02	4.85E+03	2.88E+03	4.27E+03
1.00E+03	1.77E+04	7.23E+03	1.02E+04
1.00E+04	4.65E+04	1.53E+04	2.16E+04
1.00E+05	9.25E+04	2.76E+04	4.07E+04
1.00E+06	1.49E+05	4.37E+04	6.91E+04

Table B.7a: App-2: Dynamic Modulus Test Results for Mix-S (D_64-22)

Fitting Parameters	δ	α	β	γ	C1	C2
	1.02	3.40	-1.24	-0.52	107.42	956.99
Temperature (°C)	**Frequency (Hz)**	**Modulus (MPa)**	**Phase Angle (°)**	**Reduced Frequency (Hz)**	**Modeled Modulus (MPa)**	**Square of Errors**
4	25	17,739	8.8	1.61E+03	17,706	2.28E-04
	10	16,173	9.7	6.46E+02	16,229	2.33E-04
	5	14,991	10.6	3.24E+02	15,026	2.28E-04
	1	12,240	13.1	6.55E+01	12,019	2.71E-04
	0.5	11,056	14.3	3.26E+01	10,659	4.66E-04
	0.1	8,402	17.7	6.63E+00	7,631	1.99E-03
21	25	9,043	18.3	1.93E+01	9,646	1.45E-03
	10	7,539	20.4	7.75E+00	7,916	1.17E-03
	5	6,484	21.9	3.88E+00	6,683	8.63E-04
	1	4,343	26.0	7.70E-01	4,183	1.13E-03
	0.5	3,593	27.4	3.88E-01	3,329	2.29E-03
	0.1	2,144	30.9	7.69E-02	1,814	6.92E-03
38	25	2,674	32.6	2.46E-01	2,832	3.72E-03
	10	1,880	34.4	9.85E-02	2,001	5.38E-03
	5	1,441	34.6	4.93E-02	1,513	6.07E-03
	1	718	35.1	9.88E-03	759	7.64E-03
	0.5	530	34.6	4.97E-03	559	8.09E-03
	0.1	260	33.3	1.00E-03	275	8.81E-03
54	25	718	36.9	5.11E-03	566	1.19E-02
	10	413	39.2	2.04E-03	377	3.45E-03
	5	299	38.0	1.02E-03	278	3.01E-03
	1	150	34.1	2.07E-04	143	2.83E-03
	0.5	114	32.1	1.03E-04	109	3.00E-03
	0.1	66	27.9	2.07E-05	63	2.79E-03

Table B.7b: App-2: Dynamic Modulus Test Results for Mix-T (D_64-22_5_2.36)

Fitting Parameters	**δ**	**α**	**β**	**γ**	**C1**	**C2**
	0.33	4.02	-1.80	-0.40	50.80	402.29
Temperature (°C)	**Frequency (Hz)**	**Modulus (MPa)**	**Phase Angle ( )**	**Reduced Frequency (Hz)**	**Modeled Modulus (MPa)**	**Square of Errors**
4	25	17,739	8.8	1.61E+03	17,706	2.28E-04
	10	16,173	9.7	6.46E+02	16,229	2.33E-04
	5	14,991	10.6	3.24E+02	15,026	2.28E-04
	1	12,240	13.1	6.55E+01	12,019	2.71E-04
	0.5	11,056	14.3	3.26E+01	10,659	4.66E-04
	0.1	8,402	17.7	6.63E+00	7,631	1.99E-03
21	25	9,043	18.3	1.93E+01	9,646	1.45E-03
	10	7,539	20.4	7.75E+00	7,916	1.17E-03
	5	6,484	21.9	3.88E+00	6,683	8.63E-04
	1	4,343	26.0	7.70E-01	4,183	1.13E-03
	0.5	3,593	27.4	3.88E-01	3,329	2.29E-03
	0.1	2,144	30.9	7.69E-02	1,814	6.92E-03
38	25	2,674	32.6	2.46E-01	2,832	3.72E-03
	10	1,880	34.4	9.85E-02	2,001	5.38E-03
	5	1,441	34.6	4.93E-02	1,513	6.07E-03
	1	718	35.1	9.88E-03	759	7.64E-03
	0.5	530	34.6	4.97E-03	559	8.09E-03
	0.1	260	33.3	1.00E-03	275	8.81E-03
54	25	718	36.9	5.11E-03	566	1.19E-02
	10	413	39.2	2.04E-03	377	3.45E-03
	5	299	38.0	1.02E-03	278	3.01E-03
	1	150	34.1	2.07E-04	143	2.83E-03
	0.5	114	32.1	1.03E-04	109	3.00E-03
	0.1	66	27.9	2.07E-05	63	2.79E-03

Table B.7c: App-2: Dynamic Modulus Test Results for Mix-U (D_64-22_10_2.36)

Fitting Parameters	δ	α	β	γ	C1	C2
	0.46	3.90	-1.66	-0.42	40.62	339.79
Temperature (°C)	**Frequency (Hz)**	**Modulus (MPa)**	**Phase Angle (°)**	**Reduced Frequency (Hz)**	**Modeled Modulus (MPa)**	**Square of Errors**
4	25	15,807	8.1	2.45E+03	15,508	2.58E-04
	10	14,571	8.9	9.85E+02	14,492	1.45E-04
	5	13,628	9.6	4.95E+02	13,674	1.13E-04
	1	11,432	11.3	1.00E+02	11,629	1.62E-04
	0.5	10,487	12.3	5.01E+01	10,691	1.87E-04
	0.1	8,376	14.8	1.01E+01	8,487	1.92E-04
21	25	9,437	14.8	1.91E+01	9,366	2.04E-04
	10	8,147	16.3	7.68E+00	8,119	1.64E-04
	5	7,228	17.5	3.86E+00	7,197	1.77E-04
	1	5,273	20.8	7.73E-01	5,181	2.85E-04
	0.5	4,541	22.1	3.82E-01	4,388	4.14E-04
	0.1	3,044	25.6	7.62E-02	2,850	1.10E-03
38	25	3,713	26.9	2.24E-01	3,835	1.10E-03
	10	2,877	28.6	8.97E-02	2,987	1.47E-03
	5	2,381	29.3	4.49E-02	2,435	1.51E-03
	1	1,397	31.8	9.03E-03	1,441	2.13E-03
	0.5	1,115	31.9	4.52E-03	1,127	2.02E-03
	0.1	607	32.8	9.09E-04	614	2.44E-03
54	25	1,264	34.3	5.15E-03	1,182	9.17E-04
	10	848	35.4	2.06E-03	842	3.32E-05
	5	646	34.8	1.03E-03	645	4.63E-06
	1	336	33.4	2.07E-04	340	1.69E-04
	0.5	258	32.4	1.03E-04	256	4.12E-04
	0.1	135	31.2	2.04E-05	133	3.08E-03

Table B.7d: App-2: Dynamic Modulus Test Results for Mix-V (D_64-22_5_1.18)

Fitting Parameters	δ	α	β	γ	C1	C2
	0.49	3.90	-1.55	-0.44	20.04	168.42
Temperature (°C)	**Frequency (Hz)**	**Modulus (MPa)**	**Phase Angle (°)**	**Reduced Frequency (Hz)**	**Modeled Modulus (MPa)**	**Square of Errors**
4	25	17,276	8.8	3.28E+03	16,749	5.66E-04
	10	15,803	9.6	1.30E+03	15,589	4.01E-04
	5	14,654	10.4	6.49E+02	14,658	3.45E-04
	1	12,065	12.6	1.31E+02	12,340	4.31E-04
	0.5	10,965	13.6	6.56E+01	11,282	4.76E-04
	0.1	8,574	16.5	1.30E+01	8,776	4.70E-04
21	25	9,570	16.7	2.05E+01	9,479	1.00E-03
	10	8,104	18.5	8.26E+00	8,091	1.01E-03
	5	7,074	19.9	4.10E+00	7,052	1.09E-03
	1	4,944	23.5	8.27E-01	4,891	1.33E-03
	0.5	4,178	24.8	4.18E-01	4,086	1.28E-03
	0.1	2,672	28.4	8.07E-02	2,497	2.19E-03
38	25	3,575	28.8	4.17E+03	8,535	1.16E-03
	10	2,710	30.4	1.67E+03	7,614	1.48E-03
	5	2,184	31.0	8.35E+02	6,964	1.55E-03
	1	1,222	32.7	1.67E+02	5,605	2.55E-03
	0.5	951	32.5	8.35E+01	5,076	2.59E-03
	0.1	507	32.2	1.67E+01	3,958	3.39E-03
54	25	1,330	35.1	1.08E-02	1,228	1.44E-03
	10	858	36.8	4.31E-03	859	3.85E-04
	5	642	36.0	2.16E-03	648	4.94E-04
	1	322	34.2	4.37E-04	331	6.84E-04
	0.5	243	32.8	2.18E-04	247	6.13E-04
	0.1	129	30.1	4.37E-05	125	6.70E-04

Table B.7e: App-2: Dynamic Modulus Test Results for Mix-W (D_64-22_10_1.18)

Fitting Parameters	δ	α	β	γ	C1	C2
	0.57	3.73	-1.67	-0.43	31.37	263.49
Temperature (°C)	**Frequency (Hz)**	**Modulus (MPa)**	**Phase Angle (°)**	**Reduced Frequency (Hz)**	**Modeled Modulus (MPa)**	**Square of Errors**
4	25	14,634	8.8	2.72E+03	14,134	6.68E-04
	10	13,422	9.6	1.09E+03	13,278	4.26E-04
	5	12,475	10.3	5.44E+02	12,577	4.43E-04
	1	10,341	12.2	1.09E+02	10,797	8.76E-04
	0.5	9,449	13.1	5.44E+01	9,976	1.14E-03
	0.1	7,557	15.7	1.08E+01	7,994	1.16E-03
21	25	9,176	14.8	2.05E+01	8,785	8.58E-04
	10	7,942	16.2	8.21E+00	7,656	7.17E-04
	5	7,051	17.4	4.19E+00	6,834	6.52E-04
	1	5,183	20.6	8.37E-01	4,973	8.16E-04
	0.5	4,478	21.8	4.30E-01	4,271	9.93E-04
	0.1	3,044	25.4	8.35E-02	2,783	2.40E-03
38	25	3,513	26.8	2.37E-01	3,691	8.92E-04
	10	2,730	28.5	9.49E-02	2,887	1.13E-03
	5	2,257	29.2	4.74E-02	2,359	8.75E-04
	1	1,344	31.5	9.64E-03	1,409	9.98E-04
	0.5	1,080	31.6	4.82E-03	1,104	7.87E-04
	0.1	605	32.4	9.95E-04	610	1.03E-03
54	25	1,300	33.8	6.50E-03	1,228	6.96E-04
	10	910	34.1	2.60E-03	880	7.51E-04
	5	702	33.3	1.30E-03	677	9.18E-04
	1	358	32.7	2.60E-04	359	1.58E-03
	0.5	272	31.6	1.30E-04	271	1.66E-03
	0.1	143	30.5	2.60E-05	143	1.74E-03

Table B.7f: App-2: Dynamic Modulus Test Results for Mix-P (F_64-22)

Fitting Parameters	δ	α	β	γ	C1	C2
	0.03	4.37	-1.71	-0.42	24.69	199.82
Temperature (°C)	**Frequency (Hz)**	**Modulus (MPa)**	**Phase Angle (°)**	**Reduced Frequency (Hz)**	**Modeled Modulus (MPa)**	**Square of Errors**
4	25	17,478	8.5	3.43E+03	16,910	3.20E-04
	10	16,066	9.3	1.37E+03	15,787	1.76E-04
	5	14,950	10.0	6.86E+02	14,879	1.26E-04
	1	12,349	12.0	1.39E+02	12,616	2.56E-04
	0.5	11,208	13.0	6.95E+01	11,575	3.92E-04
	0.1	8,759	15.9	1.39E+01	9,114	5.83E-04
21	25	9,738	16.7	1.90E+01	9,591	1.74E-04
	10	8,199	18.4	7.58E+00	8,205	1.68E-04
	5	7,145	19.7	3.79E+00	7,184	1.91E-04
	1	4,999	23.3	7.54E-01	5,007	1.90E-04
	0.5	4,239	24.7	3.78E-01	4,189	2.82E-04
	0.1	2,720	28.0	7.54E-02	2,602	6.83E-04
38	25	3,509	29.9	2.13E-01	3,569	3.73E-04
	10	2,679	31.1	8.52E-02	2,705	4.29E-04
	5	2,155	31.7	4.27E-02	2,155	4.79E-04
	1	1,193	33.4	8.56E-03	1,199	7.42E-04
	0.5	918	33.0	4.28E-03	910	9.22E-04
	0.1	470	32.5	8.72E-04	463	1.02E-03
54	25	1,126	35.4	6.34E-03	1,066	1.55E-03
	10	747	34.8	2.55E-03	735	1.29E-03
	5	542	34.0	1.28E-03	548	1.19E-03
	1	255	31.9	2.60E-04	268	1.81E-03
	0.5	186	30.6	1.28E-04	194	1.76E-03
	0.1	98	27.2	2.58E-05	93	3.98E-03

Table B.7g: App-2: Dynamic Modulus Test Results for Mix-Q (F_64-22_5_2.36)

Fitting Parameters	δ	α	β	γ	C1	C2
	0.35	3.96	-1.68	-0.46	31.39	261.30
Temperature (°C)	**Frequency (Hz)**	**Modulus (MPa)**	**Phase Angle (°)**	**Reduced Frequency (Hz)**	**Modeled Modulus (MPa)**	**Square of Errors**
4	25	15,289	8.6	2.75E+03	14,729	3.22E-04
	10	14,024	9.8	1.09E+03	13,797	9.17E-05
	5	13,008	10.7	5.43E+02	13,025	3.74E-05
	1	10,640	12.9	1.09E+02	11,072	3.47E-04
	0.5	9,645	14.0	5.56E+01	10,198	6.44E-04
	0.1	7,494	16.9	1.10E+01	8,014	9.44E-04
21	25	9,113	15.9	1.92E+01	8,772	5.43E-04
	10	7,720	17.7	7.69E+00	7,533	4.92E-04
	5	6,746	19.1	3.84E+00	6,611	5.18E-04
	1	4,772	22.7	7.58E-01	4,603	9.15E-04
	0.5	4,049	24.1	3.83E-01	3,852	1.14E-03
	0.1	2,614	27.8	7.62E-02	2,375	2.68E-03
38	25	3,044	30.4	2.03E-01	3,219	1.60E-03
	10	2,310	31.7	8.13E-02	2,425	1.58E-03
	5	1,854	32.4	4.07E-02	1,921	1.56E-03
	1	1,020	34.3	8.19E-03	1,054	2.34E-03
	0.5	787	34.0	4.12E-03	797	2.48E-03
	0.1	402	33.5	8.42E-04	402	3.83E-03
54	25	984	37.0	5.98E-03	929	3.36E-03
	10	664	36.3	2.40E-03	636	3.82E-03
	5	487	35.4	1.21E-03	472	4.29E-03
	1	229	33.5	2.45E-04	231	5.73E-03
	0.5	167	32.1	1.21E-04	168	6.16E-03
	0.1	86	29.0	2.45E-05	83	6.45E-03

Table B.7h: App-2: Dynamic Modulus Test Results for Mix-R (F_64-22_10_2.36)

Fitting Parameters	δ	α	β	γ	C1	C2
	0.47	3.71	-1.89	-0.46	10.31	67.34
Temperature (°C)	**Frequency (Hz)**	**Modulus (MPa)**	**Phase Angle (°)**	**Reduced Frequency (Hz)**	**Modeled Modulus (MPa)**	**Square of Errors**
4	25	14,748	8.5	3.88E+04	13,076	2.79E-03
	10	13,572	9.2	1.57E+04	12,693	9.06E-04
	5	12,671	9.8	7.91E+03	12,367	1.81E-04
	1	10,607	11.5	1.61E+03	11,468	1.29E-03
	0.5	9,739	12.4	7.66E+02	10,976	2.89E-03
	0.1	7,795	14.9	1.59E+02	9,787	1.01E-02
21	25	8,483	15.9	1.77E+01	7,812	1.74E-03
	10	7,283	17.4	7.07E+00	6,915	1.05E-03
	5	6,439	18.6	3.54E+00	6,224	8.86E-04
	1	4,631	21.9	7.00E-01	4,633	9.75E-04
	0.5	3,974	23.2	3.54E-01	4,001	1.29E-03
	0.1	2,633	26.6	7.01E-02	2,662	1.72E-03
38	25	3,333	27.8	1.63E-01	3,325	3.08E-04
	10	2,590	29.3	6.51E-02	2,608	4.63E-04
	5	2,123	30.0	3.26E-02	2,131	5.68E-04
	1	1,239	32.2	6.55E-03	1,257	7.98E-04
	0.5	986	32.3	3.31E-03	981	8.50E-04
	0.1	543	32.7	6.63E-04	522	1.17E-03
54	25	1,345	35.3	8.71E-03	1,389	2.59E-03
	10	960	35.4	3.47E-03	999	3.50E-03
	5	742	34.9	1.73E-03	766	3.84E-03
	1	377	34.5	3.46E-04	399	5.52E-03
	0.5	285	33.4	1.75E-04	299	5.65E-03
	0.1	141	34.1	3.47E-05	150	9.30E-03

Table B.8a: App-2: Flexural Modulus Test Results for Mix-S (D_64-22)

Fitting Parameters	δ	α	β	γ	C1	C2
	0.00	4.24	-1.51	-0.45	7.29	53.83
Temp. (°C)	**Frequency (Hz)**	**Modulus (MPa)**	**Phase Angle (°)**	**Reduced Frequency (Hz)**	**Modeled Modulus (MPa)**	**Square of Errors**
10	15	10,027	16.4	8.49E+02	9,961	8.29E-05
	10	9,579	15.4	5.62E+02	9,537	1.16E-04
	5	8,733	14.7	2.76E+02	8,790	1.35E-04
	2	7,640	15.3	1.10E+02	7,787	1.94E-04
	1	6,818	16.3	5.56E+01	7,026	3.37E-04
	0.5	6,027	17.7	2.72E+01	6,233	3.63E-04
	0.2	5,018	20.2	1.05E+01	5,194	3.93E-04
	0.1	4,120	19.3	5.13E+00	4,453	1.42E-03
	0.05	3,486	21.2	2.67E+00	3,814	1.67E-03
	0.02	2,780	24.4	1.11E+00	3,030	1.58E-03
	0.01	2,335	28.0	5.64E-01	2,488	1.01E-03
20	15	6,121	23.2	1.68E+01	5,707	9.72E-04
	10	5,685	23.0	1.09E+01	5,241	1.29E-03
	5	4,906	23.1	5.42E+00	4,512	1.36E-03
	2	3,932	24.8	2.17E+00	3,618	1.38E-03
	1	3,272	26.4	1.08E+00	3,006	1.44E-03
	0.5	2,675	28.8	5.37E-01	2,450	1.53E-03
	0.2	1,999	31.4	2.10E-01	1,814	1.80E-03
	0.1	1,514	33.1	1.06E-01	1,429	6.36E-04
	0.05	1,172	35.5	5.39E-02	1,110	7.81E-04
	0.02	829	37.4	2.18E-02	774	9.30E-04
	0.01	637	39.5	1.12E-02	585	1.55E-03
30	15	3,057	34.3	1.25E+00	3,134	3.16E-04
	10	2,720	34.3	8.31E-01	2,791	3.40E-04
	5	2,181	34.1	4.13E-01	2,261	4.91E-04
	2	1,585	35.6	1.65E-01	1,671	9.36E-04
	1	1,218	37.1	8.32E-02	1,308	1.40E-03
	0.5	929	39.6	4.11E-02	999	1.69E-03
	0.2	632	41.3	1.60E-02	681	1.94E-03
	0.1	460	42.2	7.55E-03	492	1.70E-03
	0.05	341	42.5	3.48E-03	347	4.58E-04
	0.02	229	38.1	1.48E-03	234	8.59E-04
	0.01	176	39.3	7.35E-04	168	4.46E-04

Table B.8b: App-2: Flexural Modulus Test Results for Mix-T (D_64-22_5_2.36)

Fitting Parameters	δ	α	β	γ	C1	C2
	1.36	2.88	-1.34	-0.50	24.18	163.92
Temp. (°C)	**Frequency (Hz)**	**Modulus (MPa)**	**Phase Angle (°)**	**Reduced Frequency (Hz)**	**Modeled Modulus (MPa)**	**Square of Errors**
10	15	11,880	14.2	7.79E+02	11,766	3.05E-04
	10	11,494	13.1	5.11E+02	11,366	3.04E-04
	5	10,663	12.1	2.50E+02	10,646	2.97E-04
	2	9,609	12.3	1.01E+02	9,666	3.41E-04
	1	8,760	13.0	4.96E+01	8,854	3.15E-04
	0.5	7,968	13.6	2.48E+01	8,039	3.51E-04
	0.2	6,899	15.5	9.44E+00	6,889	3.41E-04
	0.1	5,900	13.9	4.63E+00	6,050	3.91E-04
	0.05	5,142	15.4	2.19E+00	5,195	2.40E-04
	0.02	4,324	17.8	9.51E-01	4,301	3.15E-05
	0.01	3,769	20.8	4.92E-01	3,650	2.98E-04
20	15	7,475	20.3	1.58E+01	7,508	1.63E-05
	10	7,025	19.7	1.04E+01	7,006	8.01E-06
	5	6,208	19.4	5.14E+00	6,174	5.73E-06
	2	5,197	20.7	2.04E+00	5,119	5.21E-05
	1	4,449	21.7	1.07E+00	4,420	1.09E-05
	0.5	3,781	23.5	5.39E-01	3,736	3.59E-05
	0.2	2,980	25.7	2.18E-01	2,927	1.85E-04
	0.1	2,334	24.6	1.14E-01	2,420	5.43E-04
	0.05	1,887	26.2	5.77E-02	1,959	1.17E-03
	0.02	1,431	28.7	2.23E-02	1,432	9.48E-04
	0.01	1,178	31.4	1.15E-02	1,142	3.05E-04
30	15	4,074	28.9	7.82E-01	4,103	2.54E-04
	10	3,696	28.7	5.11E-01	3,686	2.89E-04
	5	3,076	28.6	2.54E-01	3,056	2.67E-04
	2	2,356	29.6	1.02E-01	2,340	1.37E-04
	1	1,900	30.8	5.14E-02	1,889	1.66E-04
	0.5	1,506	32.8	2.59E-02	1,508	9.84E-05
	0.2	1,093	34.1	1.01E-02	1,090	3.67E-05
	0.1	812	34.8	4.80E-03	836	3.04E-04
	0.05	626	35.3	2.06E-03	616	4.40E-04
	0.02	448	35.6	8.69E-04	452	2.60E-04
	0.01	353	36.6	4.30E-04	352	1.37E-04

Table B.8c: App-2: Flexural Modulus Test Results for Mix-U (D_64-22_10_2.36)

Fitting Parameters	δ	α	β	γ	C1	C2
	1.97	2.17	-1.30	-0.58	7.56	53.36
Temp. (°C)	**Frequency (Hz)**	**Modulus (MPa)**	**Phase Angle (°)**	**Reduced Frequency (Hz)**	**Modeled Modulus (MPa)**	**Square of Errors**
10	15	11,391	13.5	1.06E+03	11,139	1.57E-04
	10	11,016	12.1	6.96E+02	10,873	8.92E-05
	5	10,317	11.0	3.42E+02	10,385	6.40E-05
	2	9,416	10.9	1.36E+02	9,669	1.95E-04
	1	8,712	11.1	6.87E+01	9,075	3.68E-04
	0.5	8,067	11.6	3.47E+01	8,439	4.54E-04
	0.2	7,161	12.9	1.39E+01	7,521	5.04E-04
	0.1	6,286	10.9	7.10E+00	6,823	1.31E-03
	0.05	5,659	12.4	3.64E+00	6,116	1.20E-03
	0.02	4,928	14.5	1.38E+00	5,096	2.64E-04
	0.01	4,396	16.9	7.27E-01	4,442	8.26E-05
20	15	8,547	19.2	1.50E+01	7,595	8.34E-03
	10	8,052	18.5	9.64E+00	7,138	7.58E-03
	5	7,159	18.2	4.82E+00	6,405	6.14E-03
	2	6,022	19.6	1.91E+00	5,424	4.45E-03
	1	5,194	20.7	9.60E-01	4,712	3.06E-03
	0.5	4,431	22.5	4.72E-01	4,016	2.45E-03
	0.2	3,530	25.2	1.93E-01	3,209	3.22E-03
	0.1	2,776	24.3	1.08E-01	2,741	4.74E-03
	0.05	2,293	26.9	5.40E-02	2,259	4.86E-03
	0.02	1,773	28.4	2.14E-02	1,710	8.76E-03
	0.01	1,463	30.9	1.06E-02	1,372	1.80E-02
30	15	4,434	24.5	1.14E+00	4,895	1.86E-03
	10	4,110	23.8	7.59E-01	4,485	1.46E-03
	5	3,546	23.4	3.87E-01	3,837	1.21E-03
	2	2,857	24.0	1.55E-01	3,036	7.31E-04
	1	2,393	25.3	7.73E-02	2,506	4.41E-04
	0.5	1,994	26.8	3.85E-02	2,045	1.33E-04
	0.2	1,533	27.8	1.51E-02	1,534	6.14E-05
	0.1	1,210	27.8	7.27E-03	1,220	4.79E-05
	0.05	953	27.6	3.29E-03	950	1.81E-04
	0.02	714	30.6	1.29E-03	711	2.06E-04
	0.01	579	29.8	6.78E-04	586	2.07E-04

Table B.9: App-2: Repeated Load Triaxial Test Results

Specimen ID	AV Content (%)	Flow Number (Cycles)	Average (Cycles)	Std. Dev. (Cycles)	Std. Dev./Average (%)
Mix-S-1	7.0	1,326	1,055	192	18.2
Mix-S-2	7.0	882			
Mix-S-3	6.6	1,042			
Mix-S-4	6.6	969			
Mix-T-1	7.0	2,010	2,090	173	8.3
Mix-T-2	6.5	2,295			
Mix-T-3	6.8	2,155			
Mix-T-4	7.3	1,898			
Mix-U-1	6.7	3,485	2,831	442	15.6
Mix-U-2	7.2	2,718			
Mix-U-3	7.3	2,570			
Mix-U-4	7.1	2,552			
Mix-V-1	6.9	3,261	2,914	406	13.9
Mix-V-2	6.7	2,292			
Mix-V-3	7.5	3,210			
Mix-V-4	7.1	2,723			
Mix-W-1	7.3	6,748	4,965	1,301	26.2
Mix-W-2	7.0	3,862			
Mix-W-3	6.5	5,101			
Mix-W-4	7.1	4,150			
Mix-P-1	7.3	648	820	202	24.6
Mix-P-2	7.5	1,024			
Mix-P-3	7.2	572			
Mix-P-4	6.5	872			
Mix-Q-1	6.7	2,079	1,529	578	37.8
Mix-Q-2	6.9	2,239			
Mix-Q-3	7.0	1,140			
Mix-Q-4	6.6	1,091			
Mix-R-1	7.1	2,639	3,298	465	14.1
Mix-R-2	7.2	3,299			
Mix-R-3	7.0	3,945			
Mix-R-4	6.9	3,382			

Table B.10: App-2: Hamburg Wheel Track Test Results

Specimen ID	AV Content (%)	Left Wheel Rutting (mm)			Right Wheel Rutting (mm)		
		@5k Passes	@15k Passes	@25k Passes	@5k Passes	@15k Passes	@25k Passes
Mix-S-1	7.2	4.25	6.03	7.29	Not Tested	Not Tested	Not Tested
Mix-S-2	7.0						
Mix-S-3	7.1	Not Tested	Not Tested	Not Tested	2.73	3.69	4.23
Mix-S-4	6.6						
Mix-T-1	6.9	1.87	2.37	2.63	Not Tested	Not Tested	Not Tested
Mix-T-2	6.2						
Mix-T-3	6.3	Not Tested	Not Tested	Not Tested	2.04	2.85	3.30
Mix-T-4	6.4						
Mix-U-1	6.7	1.60	2.05	2.23	Not Tested	Not Tested	Not Tested
Mix-U-2	6.2						
Mix-U-3	6.9	Not Tested	Not Tested	Not Tested	1.95	2.62	3.02
Mix-U-4	7.1						
Mix-V-1	6.6	1.92	2.51	2.84	Not Tested	Not Tested	Not Tested
Mix-V-2	7.0						
Mix-V-3	6.7	Not Tested	Not Tested	Not Tested	2.14	2.83	3.14
Mix-V-4	6.8						
Mix-W-1	6.2	0.62	1.14	1.51	Not Tested	Not Tested	Not Tested
Mix-W-2	6.2						
Mix-W-3	7.6	Not Tested	Not Tested	Not Tested	1.26	1.73	1.98
Mix-W-4	7.2						
Mix-P-1	7.3	2.88	3.74	4.19	Not Tested	Not Tested	Not Tested
Mix-P-2	7.3						
Mix-P-3	7.7	Not Tested	Not Tested	Not Tested	2.93	4.11	4.78
Mix-P-4	6.1						
Mix-Q-1	7.6	2.09	2.79	3.21	Not Tested	Not Tested	Not Tested
Mix-Q-2	6.8						
Mix-Q-3	7.0	Not Tested	Not Tested	Not Tested	1.79	2.33	2.58
Mix-Q-4	6.6						
Mix-R-1	7.3	2.04	2.61	2.87	Not Tested	Not Tested	Not Tested
Mix-R-2	7.0						
Mix-R-3	6.7	Not Tested	Not Tested	Not Tested	1.91	2.61	2.95
Mix-R-4	7.0						

Table B.11a: App-2: Flexural Beam Fatigue Test Results for Mix-S (D_64-22)

Specimen ID	Air-Void Content (%)	Test Strain (µstrain)	Fatigue Life (Cycles)
MixS-B#3-B4	7.5	250	5,582,620
MixS-B#5-B1	7.5	250	3,487,727
MixS-B#5-B3	6.0	250	3,339,704
MixS-B#3-B2	8.0	350	773,208
MixS-B#3-B3	7.8	350	1,150,000
MixS-B#3-B5	7.9	350	1,741,816
MixS-B#4-B2	7.2	350	402,062
MixS-B#4-B7	7.8	350	573,662
MixS-B#4-B8	7.8	350	700,046
MixS-B#4-B1	7.6	450	128,800
MixS-B#4-B3	7.2	450	218,881
MixS-B#4-B6	7.8	450	130,896

Table B.11b: App-2: Flexural Beam Fatigue Test Results for Mix-T (D_64-22_5_2.36)

Specimen ID	Air-Void Content (%)	Test Strain (µstrain)	Fatigue Life (Cycles)
MIXT-B#4-B1	7.1	350	1,021,554
MIXT-B#4-B6	7.1	350	519,951
MIXT-B#4-B7	7.0	350	3,211,359
MIXT-B#3-B1	7.0	400	529,306
MIXT-B#3-B7	6.3	400	830,639
MIXT-B#3-B8	7.5	400	385,760
MIXT-B#4-B2	7.0	450	121,436
MIXT-B#4-B3	7.1	450	520,031
MIXT-B#4-B8	7.8	450	294,703

Table B.11c: App-2: Flexural Beam Fatigue Test Results for Mix-U (D_64-22_10_2.36)

Specimen ID	Air-Void Content (%)	Test Strain (µstrain)	Fatigue Life (Cycles)
MixU-B#2-B8	8.0	280	920,670
MixU-B#3-B6	7.6	280	2,152,070
MixU-B#3-B7	7.5	280	774,419
MixU-B#1-B8	6.2	400	700,133
MixU-B#2-B3	7.6	400	268,430
MixU-B#2-B4	7.8	400	204,181
MixU-B#2-B6	6.8	400	89,078
MixU-B#2-B7	7.4	400	137,033
MixU-B#4-B1	6.9	450	199,504
MixU-B#4-B2	6.6	450	49,433
MixU-B#4-B3	6.9	450	179,828

Table B.12: App-2: Semicircular Bending Test Results

Specimen ID	Air-Void Content (%)	Fracture Energy (Jol/m^2)	Flexibility Index	Strength (MPa)
Mix-S	7.4	2,371	1.24	0.63
	7.2	1,891	4.41	0.55
	7.5	1,947	1.50	0.57
	7.5	2,580	2.34	0.62
Mix-T	7.2	2,193	3.26	0.54
	7.5	2,243	2.64	0.56
	7.0	1,915	2.90	0.56
	7.0	2,242	2.42	0.57
Mix-U	6.9	2,872	3.32	0.62
	7.0	2,449	5.36	0.52
	6.9	1,639	1.73	0.52
	6.5	1,952	0.88	0.58
Mix-V	7.1	2,964	2.32	0.69
	7.1	2,226	1.00	0.59
	7.2	1,790	0.34	0.62
	7.2	2,045	0.84	0.59
Mix-W	7.6	1,800	0.83	0.61
	7.7	1,920	1.09	0.59
	7.5	1,760	0.40	0.59
	6.8	2,229	1.26	0.62
Mix-P	7.0	1,503	2.74	0.88
	6.4	2,377	2.85	0.86
	7.3	1,753	3.53	0.78
	7.5	2,512	4.71	0.81
Mix-Q	7.4	2,455	3.67	0.60
	7.4	1,468	2.09	0.55
	6.9	2,530	0.77	0.72
	6.9	2,911	2.77	0.68
Mix-R	7.6	2,000	3.75	0.43
	8.0	2,321	3.09	0.56
	8.0	1,928	3.26	0.52
	8.0	2,527	2.05	0.59

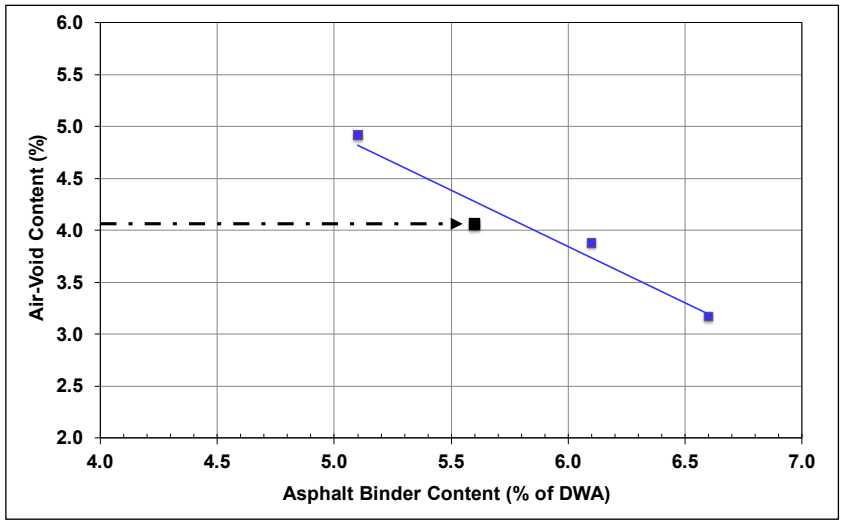

Figure B.1a: App-2/Mix-Q: Air-void content vs. asphalt binder content.

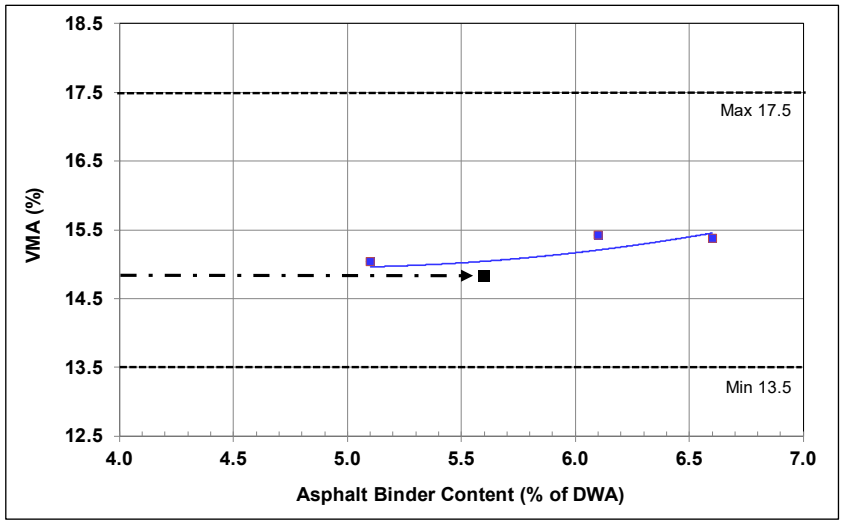

Figure B.1b: App-2/Mix-Q: VMA vs. asphalt binder content.

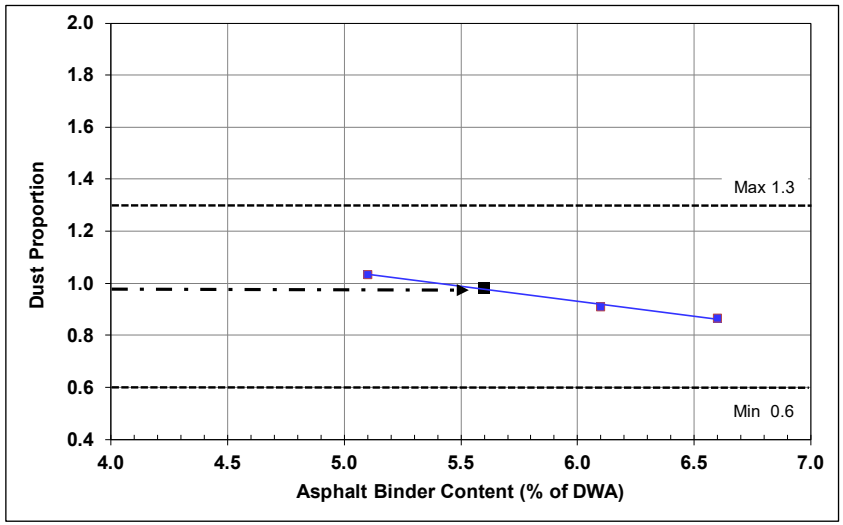

Figure B.1c: App-2/Mix-Q: Dust proportion vs. asphalt binder content.

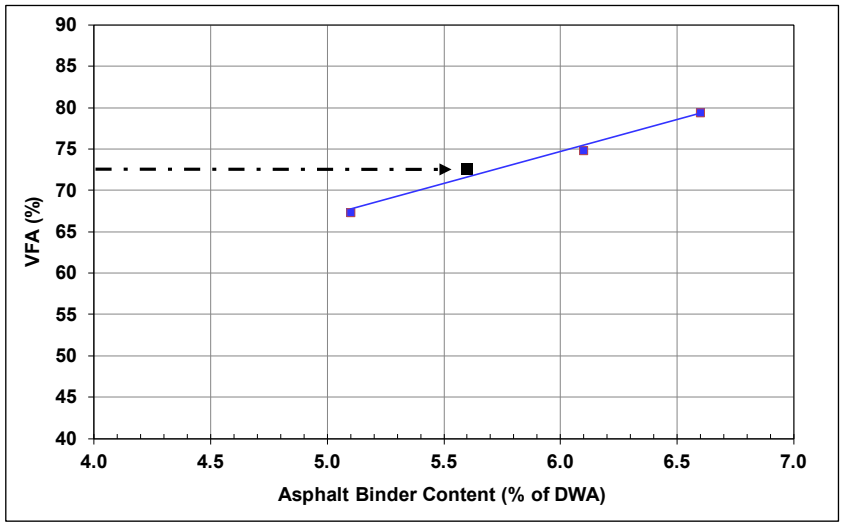

Figure B.1d: App-2/Mix-Q: VFA vs. asphalt binder content.

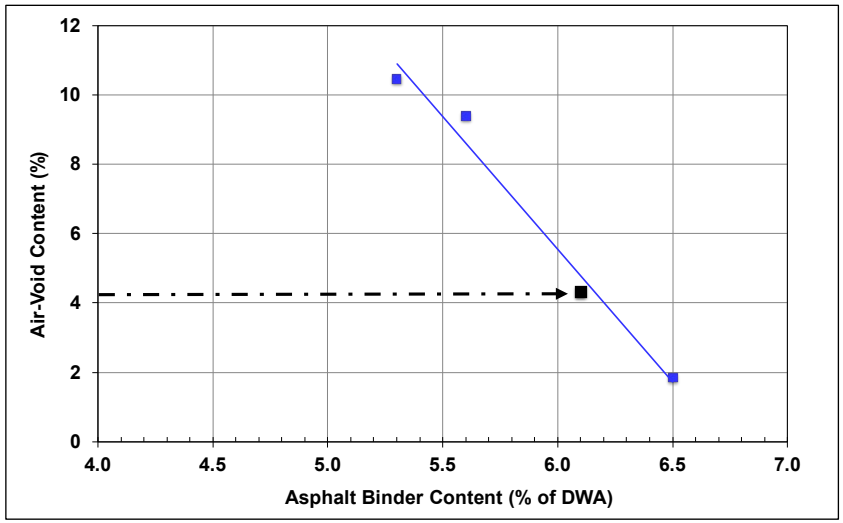

Figure B.2a: App-2/Mix-R: Air-void content vs. asphalt binder content.

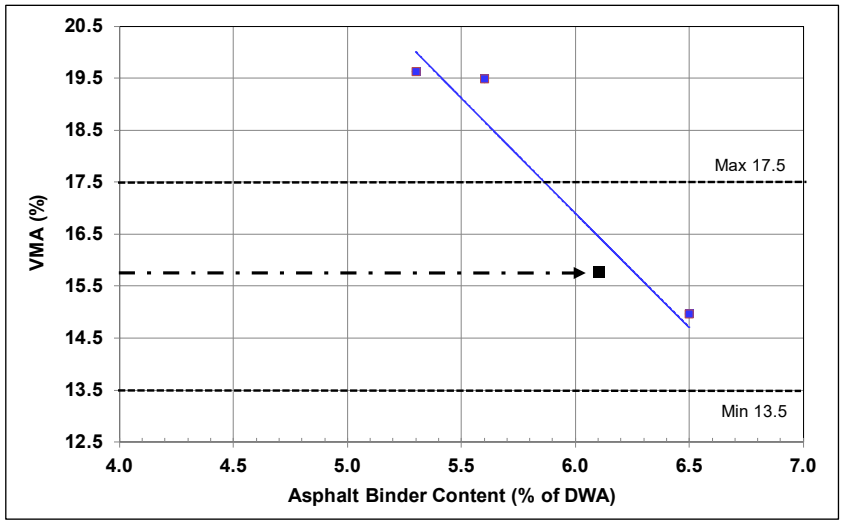

Figure B.2b: App-2/Mix-R: VMA vs. asphalt binder content.

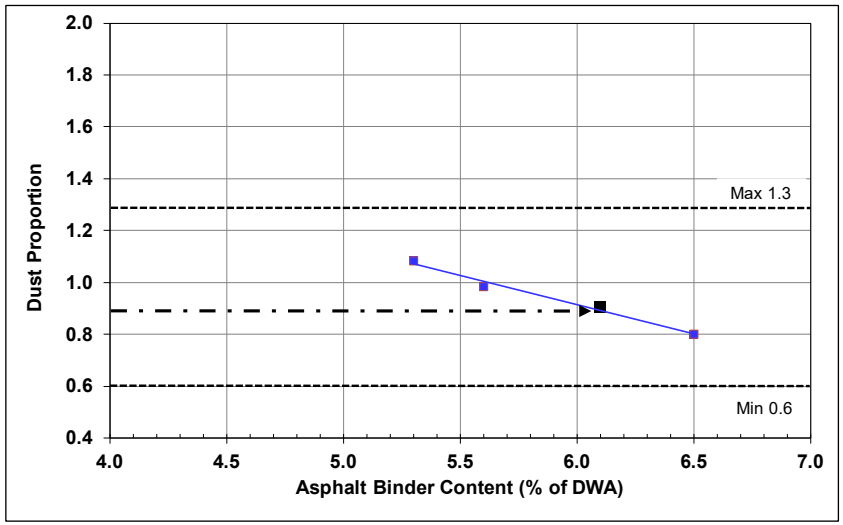

Figure B.2c: App-2/Mix-R: Dust proportion vs. asphalt binder content.

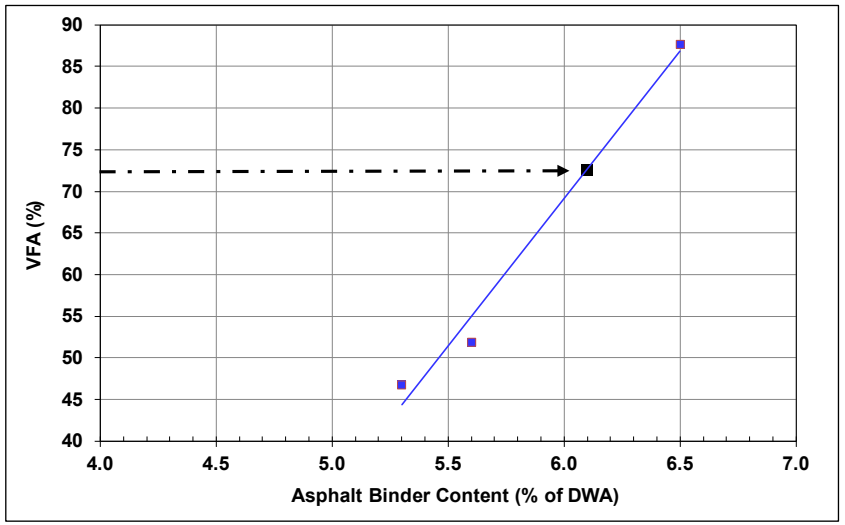

Figure B.2d: App-2/Mix-R: VFA vs. asphalt binder content.

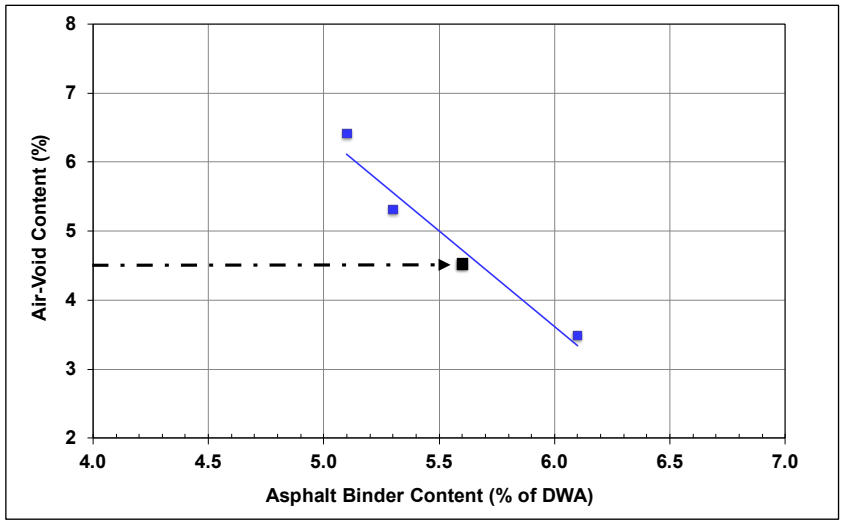

Figure B.3a: App-2/Mix-T: Air-void content vs. asphalt binder content.

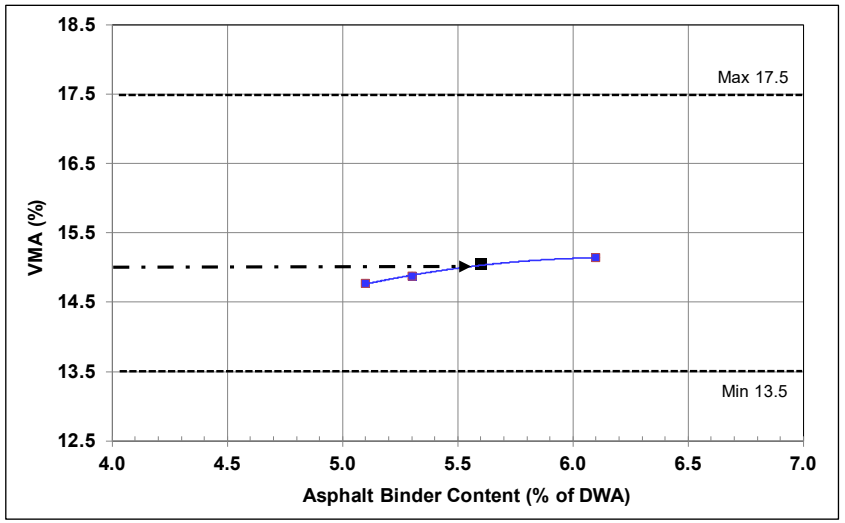

Figure B.3b: App-2/Mix-T: VMA vs. asphalt binder content.

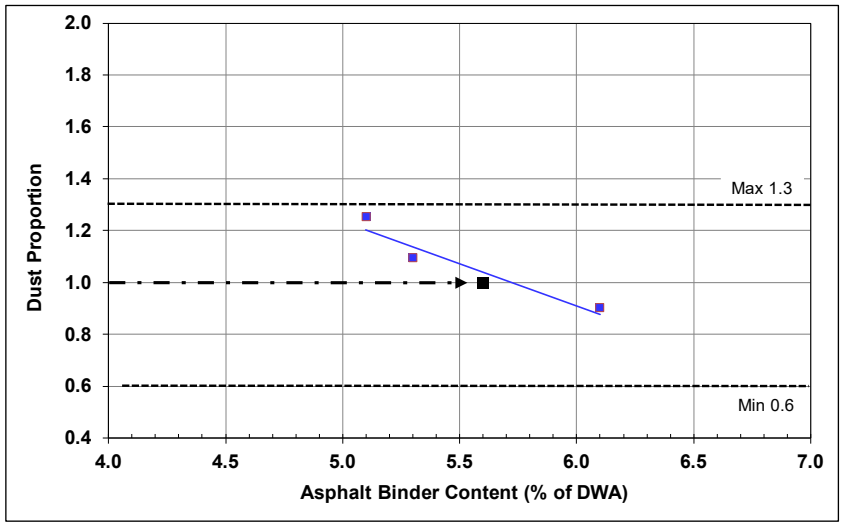

Figure B.3c: App-2/Mix-T: Dust proportion vs. asphalt binder content.

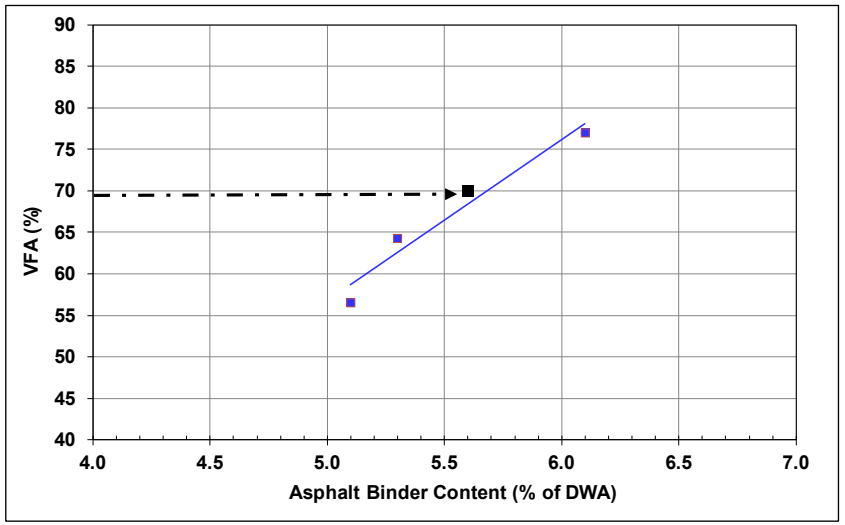

Figure B.3d: App-2/Mix-T: VFA vs. asphalt binder content.

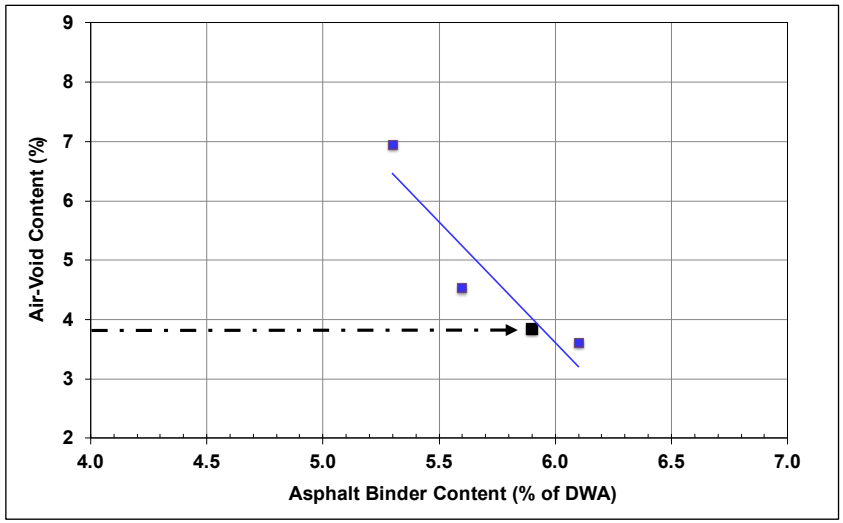

Figure B.4a: App-2/Mix-U: Air-void content vs. asphalt binder content.

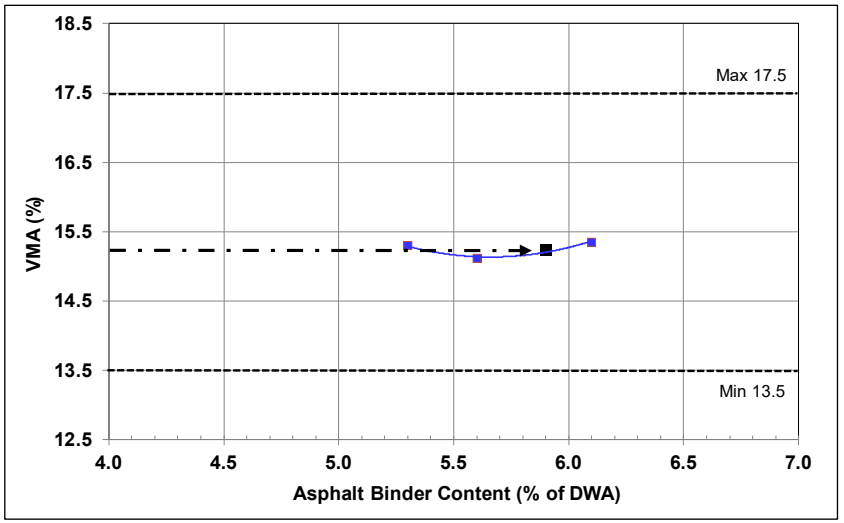

Figure B.4b: App-2/Mix-U: VMA vs. asphalt binder content.

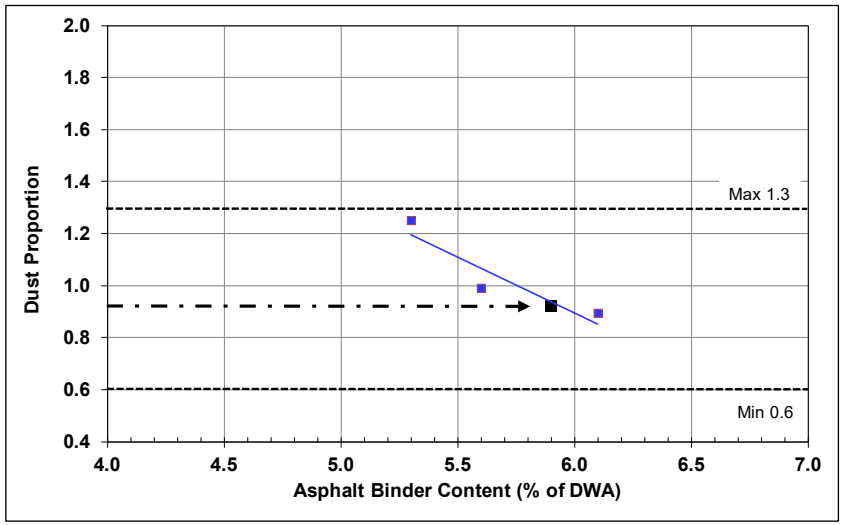

Figure B.4c: App-2/Mix-U: Dust proportion vs. asphalt binder content.

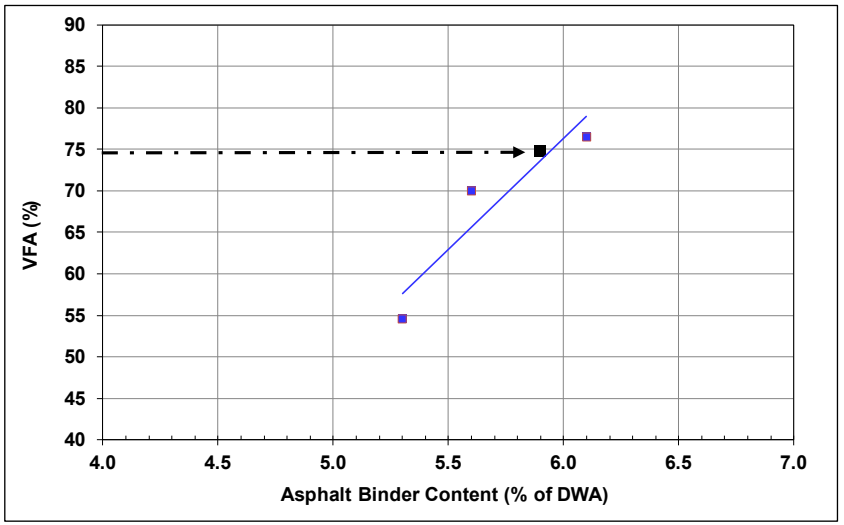

Figure B.4d: App-2/Mix-U: VFA vs. asphalt binder content.

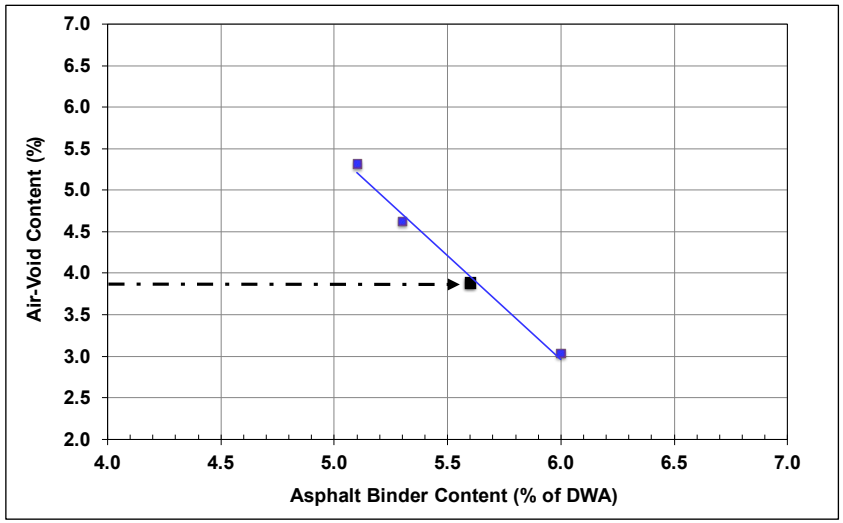

Figure B.5a: App-2/Mix-V: Air-void content vs. asphalt binder content.

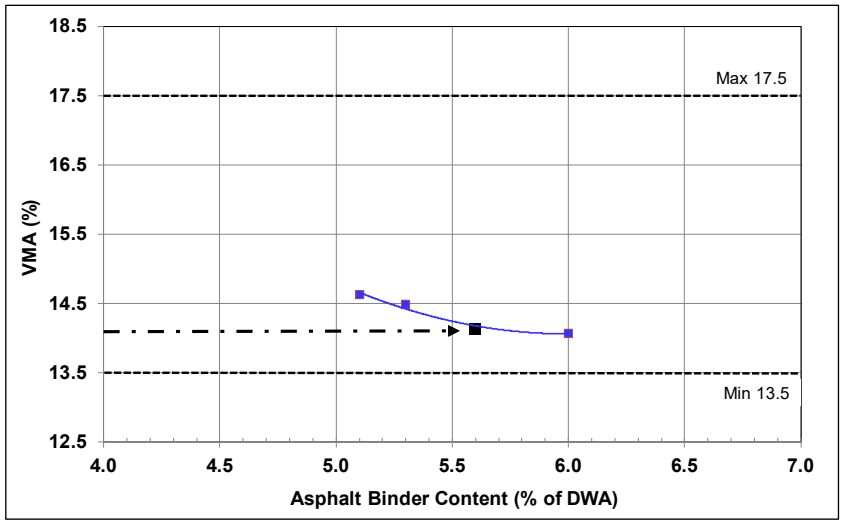

Figure B.5b: App-2/Mix-V: VMA vs. asphalt binder content.

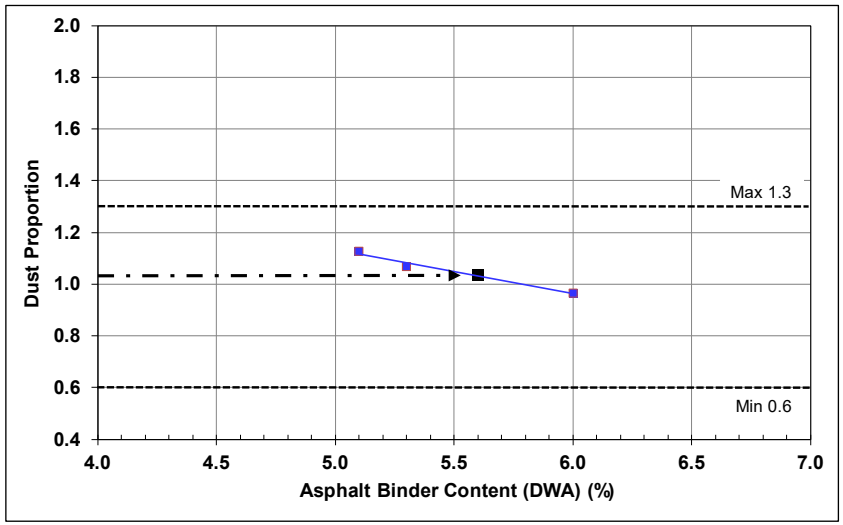

Figure B.5c: App-2/Mix-V: Dust proportion vs. asphalt binder content.

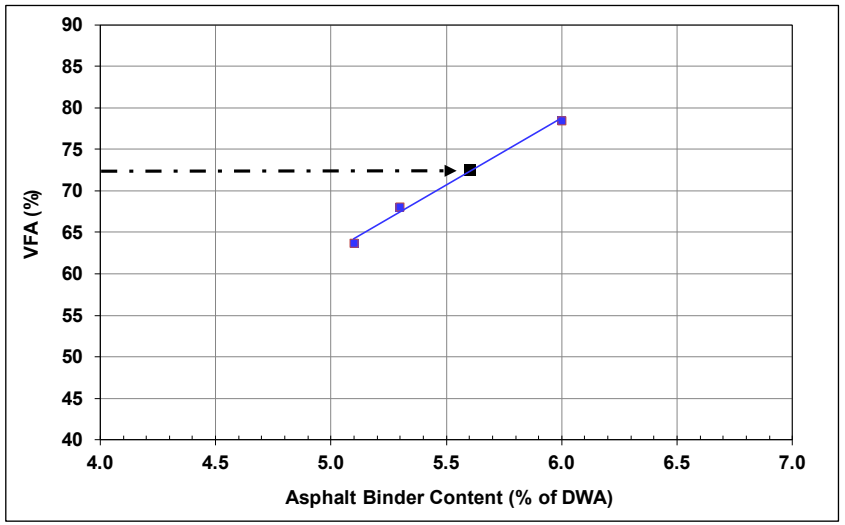

Figure B.5d: App-2/Mix-V: VFA vs. asphalt binder content.

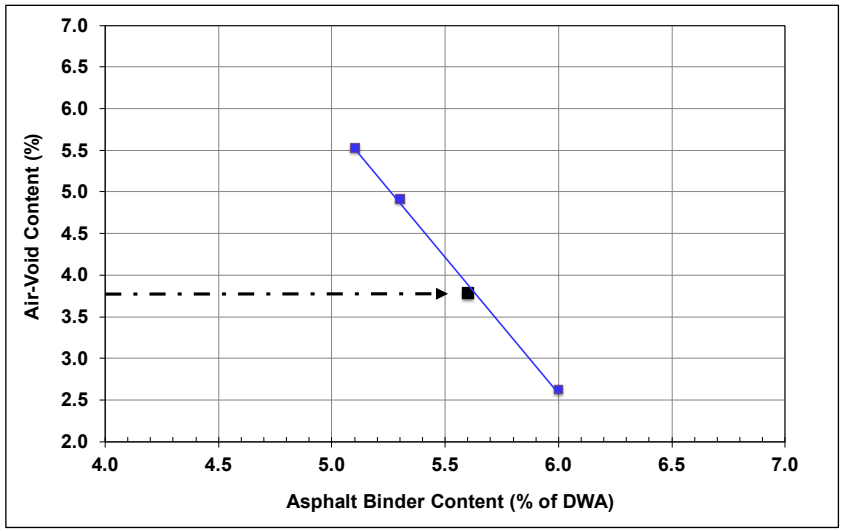

Figure B.6a: App-2/Mix-W: Air-void content vs. asphalt binder content.

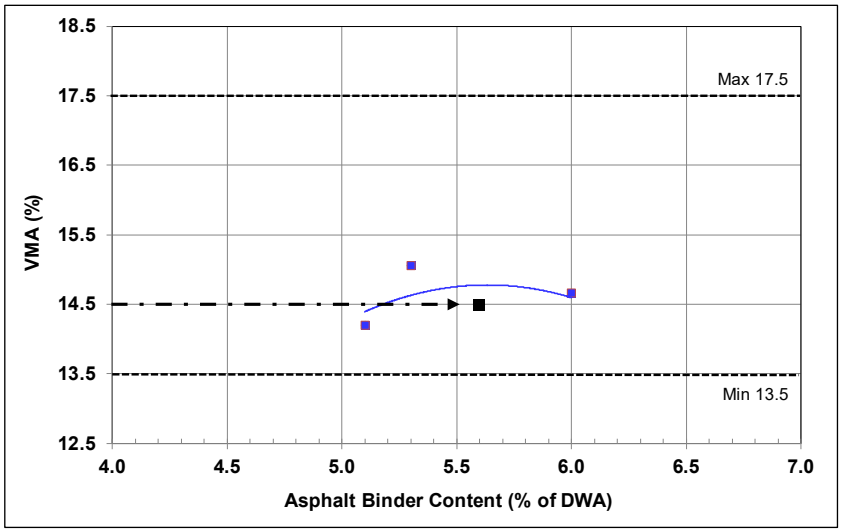

Figure B.6b: App-2/Mix-W: VMA vs. asphalt binder content.

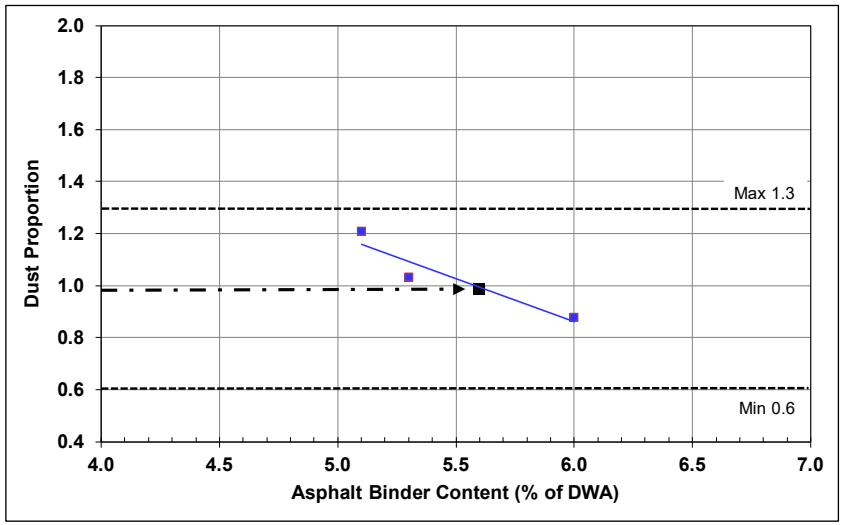

Figure B.6c: App-2/Mix-W: Dust proportion vs. asphalt binder content.

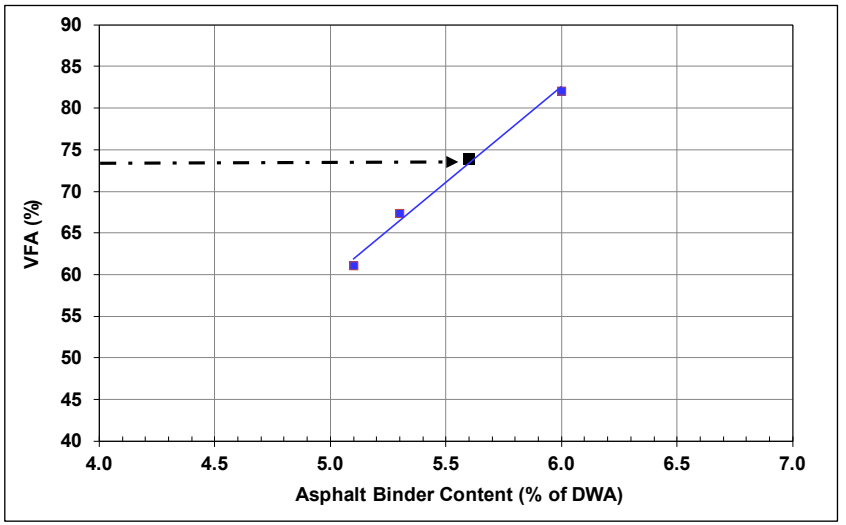

Figure B.6d: App-2/Mix-W: VFA vs. asphalt binder content.

APPENDIX C: TEST RESULTS FOR APPROACH-3 MIXES

Test results for Approach-3 (App-3) mixes are summarized in the following figures and tables:

- Table C.1: App-3: Dynamic Modulus Test Results
- Table C.2: App-3: Flexural Modulus Test Results
- Table C.3: App-3: Repeated Load Triaxial Test Results
- Table C.4: App-3: Hamburg Wheel Track Test Results
- Table C.5: App-3: Flexural Beam Fatigue Test Results
- Table C.6: App-3: Semicircular Bending Test Results
- Table C.7: App-3: Uniaxial Thermal Stress and Strain Test Results
- Figure C.1: App-3: Mix-G Volumetric Design Results
- Figure C.2: App-3: Mix-H Volumetric Design Results

The binder ID format used in the tables is: refinery source_CRM content in percent_maximum CRM size in mm.

Table C.1a: App-3: Dynamic Modulus Test Results for Mix-A (A_64-16)

Fitting Parameters	δ	α	β	γ	C1	C2
	0.27	4.13	-2.09	-0.54	117.86	955.79
Temperature (°C)	**Frequency (Hz)**	**Modulus (MPa)**	**Phase Angle (°)**	**Reduced Frequency (Hz)**	**Modeled Modulus (MPa)**	**Square of Errors**
4	25	22,063	5.8	2.61E+03	20,929	5.26E-04
	10	20,780	6.4	1.05E+03	20,052	2.40E-04
	5	19,769	7.0	5.23E+02	19,291	1.13E-04
	1	17,258	8.6	1.04E+02	17,160	6.13E-06
	0.5	16,134	9.4	5.18E+01	16,094	1.14E-06
	0.1	13,453	11.9	1.05E+01	13,322	1.80E-05
21	25	13,628	12.6	1.90E+01	14,404	5.78E-04
	10	12,029	14.2	7.60E+00	12,728	6.01E-04
	5	10,754	15.7	3.84E+00	11,421	6.83E-04
	1	7,969	19.9	7.67E-01	8,301	3.14E-04
	0.5	6,848	21.8	3.77E-01	6,976	6.51E-05
	0.1	4,506	27.5	7.46E-02	4,311	3.69E-04
38	25	5,376	27.5	1.60E-01	5,491	8.45E-05
	10	4,091	30.4	6.33E-02	4,077	2.29E-06
	5	3,241	32.5	3.14E-02	3,162	1.17E-04
	1	1,682	37.1	6.28E-03	1,610	3.65E-04
	0.5	1,205	38.3	3.31E-03	1,191	2.60E-05
	0.1	510	39.5	6.45E-04	513	5.88E-06
54	25	1,048	41.9	2.18E-03	968	1.18E-03
	10	624	42.1	8.71E-04	603	2.18E-04
	5	410	41.8	4.35E-04	415	2.45E-05
	1	152	39.4	8.63E-05	169	2.03E-03
	0.5	104	37.0	4.32E-05	115	2.00E-03
	0.1	55	29.2	8.71E-06	50	2.04E-03

Table C.1b: App-3: Dynamic Modulus Test Results for Mix-G (A_64-16_5_2.36_DRY)

Fitting Parameters	δ	α	β	γ	C1	C2
	0.18	4.23	-1.43	-0.59	17.73	199.99
Temperature (°C)	**Frequency (Hz)**	**Modulus (MPa)**	**Phase Angle ( )**	**Reduced Frequency (Hz)**	**Modeled Modulus (MPa)**	**Square of Errors**
4	25	15,922	6.8	8.16E+02	17,046	8.78E-04
	10	14,883	7.7	3.26E+02	15,417	2.34E-04
	5	14,049	8.5	1.63E+02	14,072	5.13E-07
	1	11,930	10.8	3.26E+01	10,693	2.26E-03
	0.5	10,982	11.9	1.63E+01	9,201	5.91E-03
	0.1	8,701	15.5	3.29E+00	5,944	2.74E-02
21	25	8,527	17.7	1.97E+01	9,608	2.69E-03
	10	7,074	20.4	7.89E+00	7,672	1.24E-03
	5	6,032	22.6	3.97E+00	6,302	3.63E-04
	1	3,874	29.0	7.95E-01	3,579	1.19E-03
	0.5	3,091	31.8	4.00E-01	2,682	3.82E-03
	0.1	1,635	38.8	8.00E-02	1,222	1.60E-02
38	25	2,571	37.3	8.30E-01	3,642	2.29E-02
	10	1,789	40.3	3.26E-01	2,449	1.86E-02
	5	1,308	41.9	1.60E-01	1,748	1.58E-02
	1	528	45.5	3.08E-02	720	1.80E-02
	0.5	344	45.6	1.52E-02	475	1.98E-02
	0.1	120	45.9	3.38E-03	189	3.84E-02
54	25	1,389	43.7	6.57E-02	1,100	1.03E-02
	10	875	44.9	2.62E-02	654	1.60E-02
	5	594	45.0	1.30E-02	431	1.94E-02
	1	205	46.2	2.56E-03	159	1.23E-02
	0.5	124	46.4	1.31E-03	105	5.45E-03
	0.1	38	47.0	2.60E-04	41	8.04E-04

Table C.1c: App-3: Dynamic Modulus Test Results for Mix-H (A_64-16_10_2.36_DRY)

Fitting Parameters	δ	α	β	γ	C1	C2
	0.00	4.18	-1.66	-0.55	23.98	199.77
Temperature (°C)	**Frequency (Hz)**	**Modulus (MPa)**	**Phase Angle (°)**	**Reduced Frequency (Hz)**	**Modeled Modulus (MPa)**	**Square of Errors**
4	25	12,395	7.9	2.44E+03	11,573	8.89E-04
	10	11,434	8.7	9.74E+02	10,843	5.31E-04
	5	10,669	9.5	4.87E+02	10,224	3.42E-04
	1	8,904	11.5	9.74E+01	8,576	2.65E-04
	0.5	8,118	12.7	4.92E+01	7,802	2.96E-04
	0.1	6,329	15.9	1.02E+01	5,923	8.27E-04
21	25	5,956	18.1	1.86E+01	6,653	2.30E-03
	10	4,962	20.4	7.46E+00	5,551	2.37E-03
	5	4,257	22.3	3.80E+00	4,754	2.31E-03
	1	2,799	27.6	7.53E-01	3,015	1.04E-03
	0.5	2,286	29.7	3.80E-01	2,392	3.86E-04
	0.1	1,301	35.5	7.67E-02	1,265	1.45E-04
38	25	1,939	34.3	2.45E-01	2,036	4.52E-04
	10	1,380	36.9	9.80E-02	1,407	7.47E-05
	5	1,043	38.3	4.82E-02	1,027	4.61E-05
	1	477	41.7	9.50E-03	457	3.45E-04
	0.5	336	41.9	4.75E-03	314	8.63E-04
	0.1	138	42.8	9.58E-04	127	1.38E-03
54	25	453	43.4	8.03E-03	418	1.24E-03
	10	269	43.5	3.21E-03	253	7.55E-04
	5	180	43.0	1.61E-03	171	4.99E-04
	1	62	44.5	3.19E-04	68	1.30E-03
	0.5	42	44.2	1.57E-04	46	1.57E-03
	0.1	18	41.8	3.15E-05	20	1.14E-03

Table C.2a: App-3: Flexural Modulus Test Results for Mix-A (A_64-16)

Fitting Parameters	δ	α	β	γ	C1	C2
	0.00	4.21	-2.08	-0.59	8.03	53.76
Temp. (°C)	**Frequency (Hz)**	**Modulus (MPa)**	**Phase Angle (°)**	**Reduced Frequency (Hz)**	**Modeled Modulus (MPa)**	**Square of Errors**
10	15	14,150	12.6	1.15E+03	13,388	8.74E-04
	10	13,715	11.5	7.68E+02	13,110	6.70E-04
	5	12,945	10.7	3.89E+02	12,594	4.60E-04
	2	11,773	11.1	1.57E+02	11,803	3.84E-04
	1	10,891	12.0	7.79E+01	11,107	5.12E-04
	0.5	9,972	12.8	3.84E+01	10,331	6.94E-04
	0.2	8,713	14.9	1.51E+01	9,203	1.05E-03
	0.1	7,694	17.0	7.21E+00	8,249	1.27E-03
	0.05	6,719	19.2	3.76E+00	7,363	1.88E-03
	0.02	5,508	22.7	1.51E+00	6,106	2.42E-03
	0.01	4,624	25.6	7.38E-01	5,124	2.39E-03
20	15	9,729	18.6	1.81E+01	9,442	4.27E-04
	10	9,292	18.1	1.19E+01	8,906	8.09E-04
	5	8,318	18.5	5.95E+00	7,991	9.11E-04
	2	6,984	21.3	2.35E+00	6,717	9.87E-04
	1	6,013	22.8	1.18E+00	5,759	1.29E-03
	0.5	5,051	25.2	5.91E-01	4,828	1.42E-03
	0.2	3,893	29.8	2.33E-01	3,658	2.16E-03
	0.1	3,052	34.2	1.13E-01	2,848	2.01E-03
	0.05	2,358	37.3	5.62E-02	2,172	1.81E-03
	0.02	1,613	42.5	2.42E-02	1,505	1.70E-03
	0.01	1,149	45.5	1.14E-02	4,108	2.42E-03
30	15	5,195	30.6	7.94E-01	5,223	6.47E-04
	10	4,670	31.7	5.23E-01	4,670	6.17E-04
	5	3,781	33.7	2.62E-01	3,798	6.20E-04
	2	2,728	37.7	1.05E-01	2,775	8.01E-04
	1	2,057	40.2	5.32E-02	2,122	1.06E-03
	0.5	1,511	43.4	2.68E-02	1,576	1.13E-03
	0.2	962	48.1	1.06E-02	1,008	1.43E-03
	0.1	675	50.5	5.32E-03	700	1.40E-03
	0.05	468	54.3	2.69E-03	477	8.39E-04
	0.02	267	42.9	3.97E-01	272	1.87E-04
	0.01	175	42.2	3.53E-01	182	2.29E-04

Table C.2b: App-3: Flexural Modulus Test Results for Mix-G (A_64-16_5_2.36_DRY)

Fitting Parameters	δ	α	β	γ	C1	C2
	0.00	4.05	-1.68	-0.58	8.65	54.57
Temp. (°C)	**Frequency (Hz)**	**Modulus (MPa)**	**Phase Angle (°)**	**Reduced Frequency (Hz)**	**Modeled Modulus (MPa)**	**Square of Errors**
10	15	9,541	16.5	1.42E+03	8,611	2.06E-03
	10	9,133	15.8	9.08E+02	8,342	1.65E-03
	5	8,328	15.4	4.63E+02	7,903	7.69E-04
	2	7,260	16.5	1.84E+02	7,229	4.65E-04
	1	6,446	17.5	9.13E+01	6,662	9.16E-04
	0.5	5,648	18.9	4.71E+01	6,091	2.26E-03
	0.2	4,641	21.7	1.88E+01	5,255	4.48E-03
	0.1	3,754	20.6	9.00E+00	4,567	9.60E-03
	0.05	3,101	23.4	4.28E+00	3,869	1.26E-02
	0.02	2,411	26.8	1.85E+00	3,122	1.73E-02
	0.01	1,967	30.0	8.98E-01	2,517	1.69E-02
20	15	5,900	24.2	1.61E+01	5,106	4.32E-03
	10	5,444	24.0	1.06E+01	4,717	4.29E-03
	5	4,686	24.7	5.26E+00	4,062	4.40E-03
	2	3,716	26.8	2.07E+00	3,216	4.87E-03
	1	3,040	28.7	1.02E+00	2,619	5.65E-03
	0.5	2,449	31.1	5.15E-01	2,095	6.67E-03
	0.2	1,786	34.6	2.08E-01	1,495	9.30E-03
	0.1	1,295	35.9	1.07E-01	1,130	7.29E-03
	0.05	972	38.5	5.13E-02	810	1.08E-02
	0.02	613	40.9	1.78E-02	473	1.48E-02
	0.01	494	42.8	1.04E-02	358	2.21E-02
30	15	6,049	23.5	1.66E+01	5,137	5.31E-03
	10	4,687	27.3	8.34E+00	4,049	4.00E-03
	5	4,004	27.6	4.12E+00	3,443	4.21E-03
	2	3,154	29.6	1.62E+00	2,685	4.79E-03
	1	2,575	31.9	7.95E-01	2,165	5.66E-03
	0.5	2,070	33.7	3.98E-01	1,709	6.95E-03
	0.2	1,509	36.2	1.55E-01	1,192	1.05E-02
	0.1	1,092	36.8	7.84E-02	891	7.53E-03
	0.05	819	40.4	3.73E-02	631	1.48E-02
	0.02	518	40.7	1.55E-02	403	1.14E-01
	0.01	394	45.0	7.17E-03	260	4.12E-02

Table C.2c: App-3: Flexural Modulus Test Results for Mix-H (A_64-16_10_2.36_DRY)

Fitting Parameters	δ	α	β	γ	C1	C2
	0.00	4.01	-2.24	-0.77	12.98	89.61
Temp. (°C)	**Frequency (Hz)**	**Modulus (MPa)**	**Phase Angle (°)**	**Reduced Frequency (Hz)**	**Modeled Modulus (MPa)**	**Square of Errors**
10	15	10,881	14.1	6.90E+02	9,086	6.68E-03
	10	10,497	13.2	4.47E+02	8,935	5.47E-03
	5	9,812	12.6	2.23E+02	8,649	3.66E-03
	2	8,783	13.3	8.84E+01	8,178	1.68E-03
	1	7,987	14.2	4.45E+01	7,751	9.14E-04
	0.5	7,185	15.4	2.16E+01	7,224	8.76E-04
	0.2	6,109	17.9	8.36E+00	6,408	1.36E-03
	0.1	5,077	16.9	4.08E+00	5,697	3.79E-03
	0.05	4,296	19.7	2.33E+00	5,110	6.81E-03
	0.02	3,443	23.5	8.71E-01	4,026	5.59E-03
	0.01	2,846	28.2	4.42E-01	3,279	5.03E-03
20	15	7,179	20.9	1.53E+01	6,943	4.48E-04
	10	6,736	20.4	9.94E+00	6,563	3.94E-04
	5	5,925	21.3	4.97E+00	5,903	2.11E-04
	2	4,841	23.6	1.97E+00	4,930	2.52E-04
	1	4,079	25.8	9.87E-01	4,165	2.72E-04
	0.5	3,344	28.4	4.92E-01	3,395	2.18E-04
	0.2	2,476	33.0	1.97E-01	2,445	4.62E-04
	0.1	1,801	34.6	1.01E-01	1,826	8.80E-04
	0.05	1,229	39.9	4.23E-02	1,151	5.27E-03
	0.02	831	43.3	1.74E-02	690	9.41E-03
	0.01	635	46.0	1.04E-02	495	1.30E-02
30	15	3,293	35.4	6.84E-01	3,759	3.93E-03
	10	2,929	35.8	4.57E-01	3,316	3.34E-03
	5	2,340	37.7	2.29E-01	2,592	2.50E-03
	2	1,622	40.8	9.20E-02	1,752	1.90E-03
	1	1,106	44.2	3.94E-02	1,119	1.31E-03
	0.5	702	47.6	1.59E-02	637	2.80E-03
	0.2	451	49.9	6.83E-03	364	1.06E-02
	0.05	230	50.9	2.55E-03	174	9.43E-02
	0.02	121	51.3	8.58E-04	78	1.64E-01
	0.01	79	48.4	3.48E-04	39	1.38E-01

Table C.3: App-3: Repeated Load Triaxial Test Results

Specimen ID	AV Content (%)	Flow Number (Cycles)	Average (Cycles)	Std. Dev. (Cycles)	Std. Dev./Average (%)
Mix-A-1	6.5	254	272	120	44.0
Mix-A-2	6.9	158			
Mix-A-3	7.3	153			
Mix-A-4	6.9	320			
Mix-G-1	6.9	136	97	28	29.2
Mix-G-2	6.6	70			
Mix-G-3	7.0	70			
Mix-G-4	7.2	112			
Mix-H-1	7.3	67	217	113	51.9
Mix-H-2	6.6	246			
Mix-H-3	6.6	338			
Mix-H-4	-	-			

Table C.4: App-3: Hamburg Wheel Track Test Results

Specimen ID	AV Content (%)	Left Wheel Rutting (mm)			Right Wheel Rutting (mm)		
		@5k Passes	@15k Passes	@25k Passes	@5k Passes	@15k Passes	@25k Passes
Mix-A-1	7.1	3.51	5.05	6.20	Not tested	Not tested	Not tested
Mix-A-2	8.0						
Mix-A-3	7.4	Not tested	Not tested	Not tested	2.61	3.89	4.98
Mix-A-4	7.2						
Mix-G-1	7.9	4.00	5.43	6.53	Not tested	Not tested	Not tested
Mix-G-2	7.3						
Mix-G-3	7.9	Not tested	Not tested	Not tested	2.67	4.05	5.22
Mix-G-4	6.3						
Mix-H-1	7.7	7.00	9.21	10.63	Not tested	Not tested	Not tested
Mix-H-2	8.0						
Mix-H-3	7.3	Not tested	Not tested	Not tested	5.30	8.54	13.1
Mix-H-4	7.8						

Table C.5a: App-4: Flexural Beam Fatigue Test Results for Mix-A (A_64-16)

Specimen ID	Air-Void Content (%)	Test Strain (µstrain)	Fatigue Life (Cycles)
MixA-B#3-2-B8	7.5	210	1,397,500
MixA-B#3-3-B1	7.7	210	1,130,000
MixA-B#3-2-B6	6.3	210	1,440,000
MixA-B#3-2-B2	6.4	250	382,500
MixA-B#3-3-B4	7.3	252	405,000
MixA-B#3-3-B7	7.6	250	512,500
MixA-B#3-2-B7	6.5	400	49,000
MixA-B#3-3-B3	7.4	400	37,000
MixA-B#3-3-B6	7.5	400	105,000

Table C.5b: App-3: Flexural Beam Fatigue Test Results for Mix-G (A_64-16_5_2.36_DRY)

Specimen ID	Air-Void Content (%)	Test Strain (µstrain)	Fatigue Life (Cycles)
MixG-B#3-1-B3	7.6	330	667,500
MixG-B#3-2-B3	7.5	330	765,000
MixG-B#3-2-B5	8.0	330	1,027,500
MixG-B#3-1-B2	8.0	400	360,000
MixG-B#3-1-B4	7.5	400	400,000
MixG-B#3-1-B7	7.8	400	595,000
MixG-B#3-2-B4	7.0	700	11,000
MixG-B#3-1-B8	8.0	700	14,000
MixG-B#3-2-B4	7.0	700	11,000

Table C.5c: App-3: Flexural Beam Fatigue Test Results for Mix-H (A_64-16_10_2.36_DRY)

Specimen ID	Air-Void Content (%)	Test Strain (µstrain)	Fatigue Life (Cycles)
MixH-B#3-2-B1	6.0	250	1,887,500
MixH-B#3-2-B8	6.9	250	3,022,500
MixH-B#3-3-B4	7.0	250	832,500
MixH-B#3-3-B1	7.0	320	530,000
MixH-B#3-3-B5	6.7	320	957,500
MixH-B#3-3-B6	7.5	320	1,065,000
MixH-B#3-2-B3	6.4	400	175,000
MixH-B#3-2-B6	6.5	398	17,000
MixH-B#3-3-B2	7.3	400	127,500

Table C.6: App-3: Semicircular Bending Test Results

Specimen ID	Air-Void Content (%)	Fracture Energy (Jol/m^2)	Flexibility Index	Strength (MPa)
Mix-A	6.9	2,125	4.99	0.59
	6.9	1,837	4.99	0.50
	7.2	1,871	2.78	0.65
	7.2	1,084	0.33	0.66
Mix-G	6.9	2,125	4.99	0.59
	6.9	1,837	4.99	0.50
	7.2	1,871	2.78	0.65
	7.2	1,084	0.33	0.66
Mix-H	6.1	2,535	14.23	0.44
	7.0	3,228	11.08	0.59
	6.5	2,177	10.00	0.45
	7.1	1,982	3.90	0.57

Table C.7: App-3: Uniaxial Thermal Stress and Strain Test Results

Specimen ID	Air-Void Content (%)	Average UTSST Air-Void Content (%)[1]	Average CRI_{Env}[1]	Average Fracture Temperature (°C)[1]
Mix-A	7.2	6.0	12	-12.5
	7.6			
Mix-G	6.6	5.8	7	-11.0
	7.0			
Mix-H	5.9	5.4	12	-11.3
	6.0			

[1] Only the average results were received by UCPRC

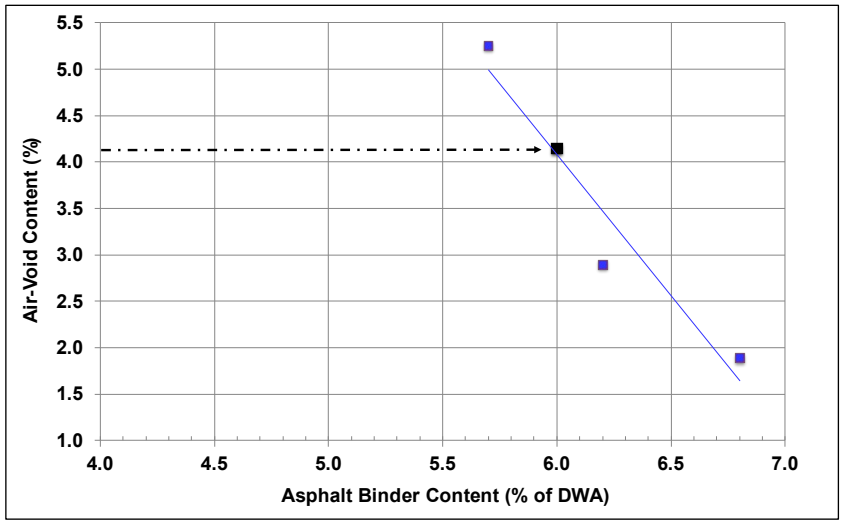

Figure C.1a: App-3/Mix-G: Air-void content vs. asphalt binder content.

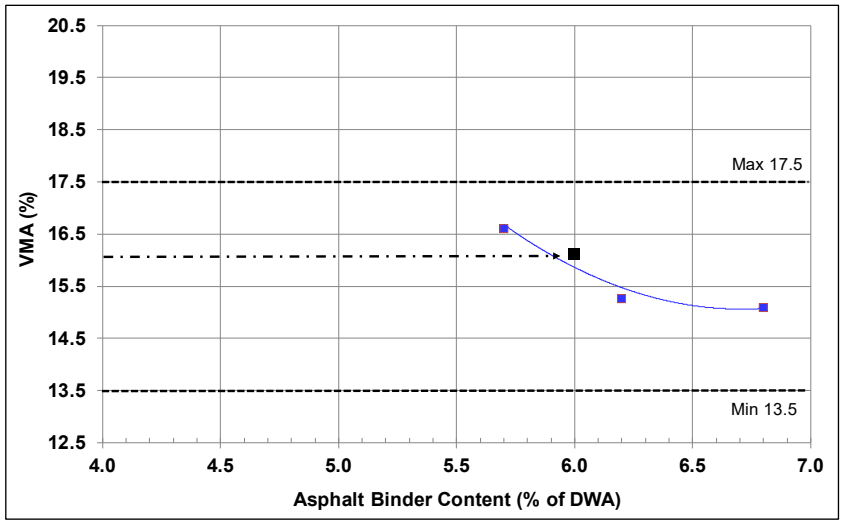

Figure C.1b: App-3/Mix-G: VMA vs. asphalt binder content.

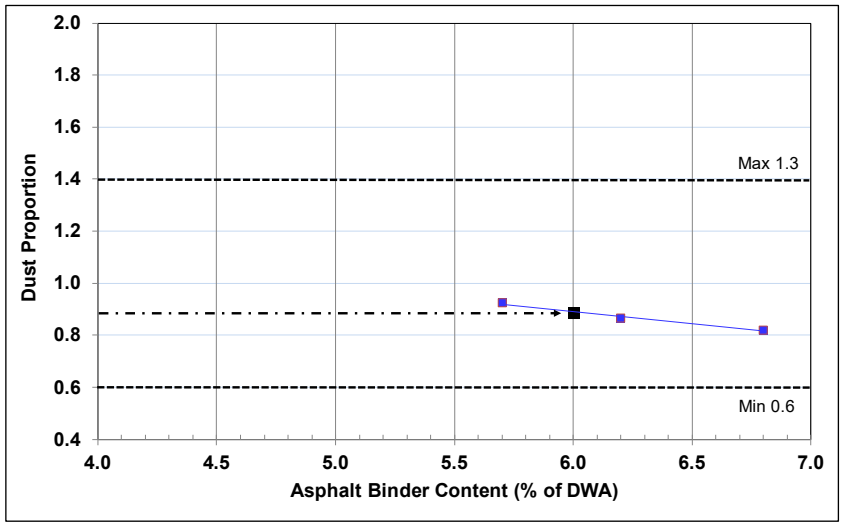

Figure C.1c: App-3/Mix-G: Dust proportion vs. asphalt binder content.

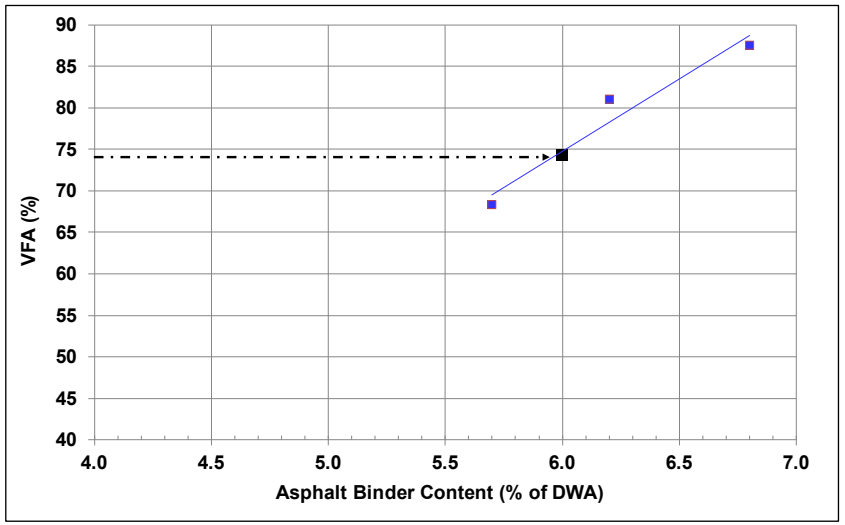

Figure C.1d: App-3/Mix-G: VFA vs. asphalt binder content.

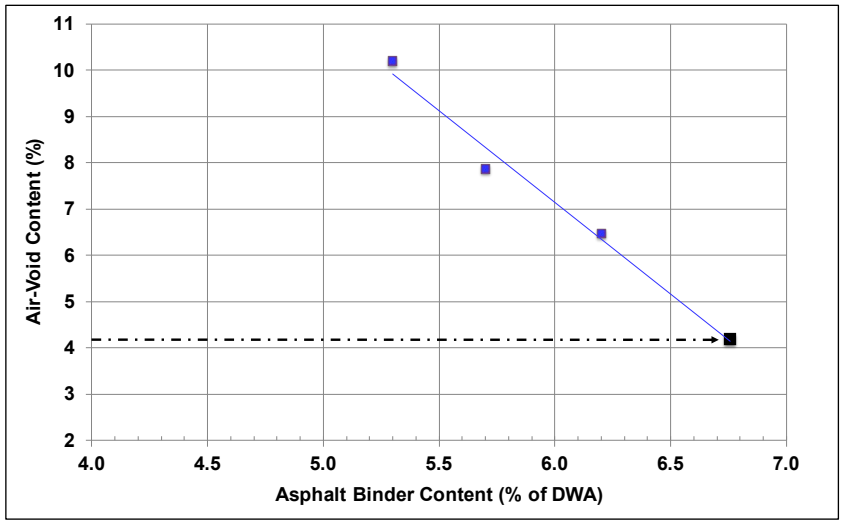

Figure C.2a: App-3/Mix-H: Air-void content vs. asphalt binder content.

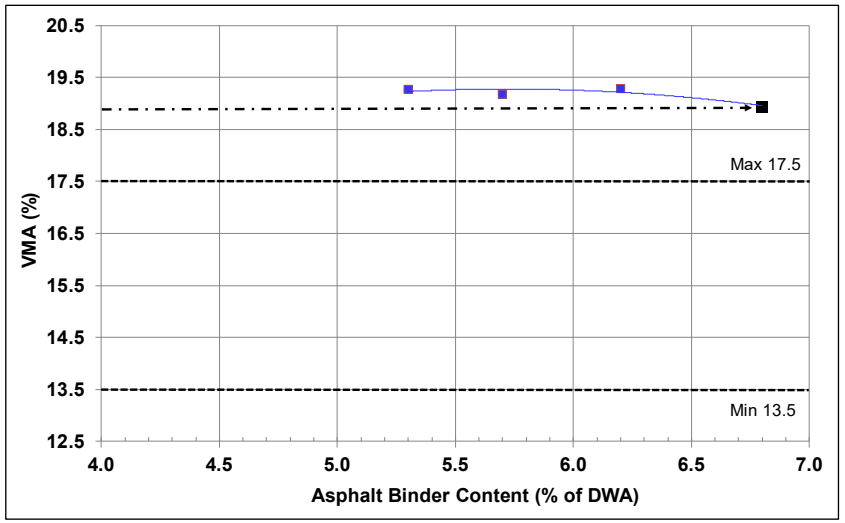

Figure C.2b: App-3/Mix-H: VMA vs. asphalt binder content.

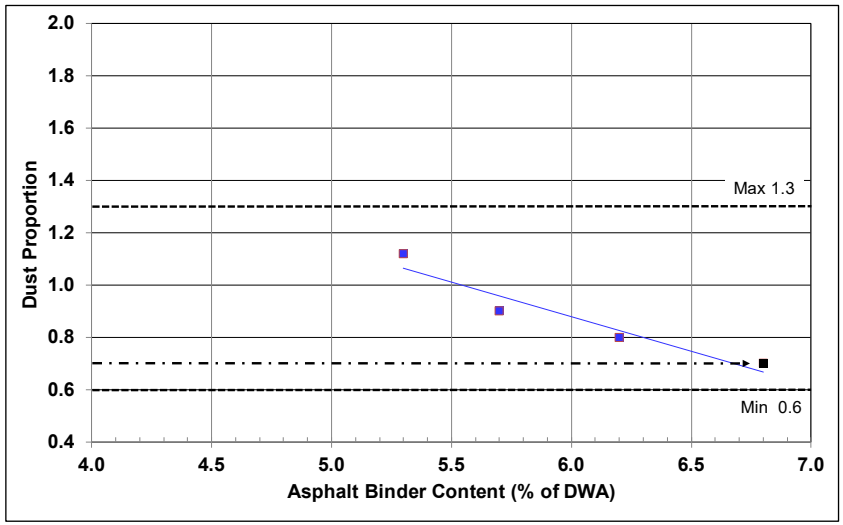

Figure C.2c: App-3/Mix-H: Dust proportion vs. asphalt binder content.

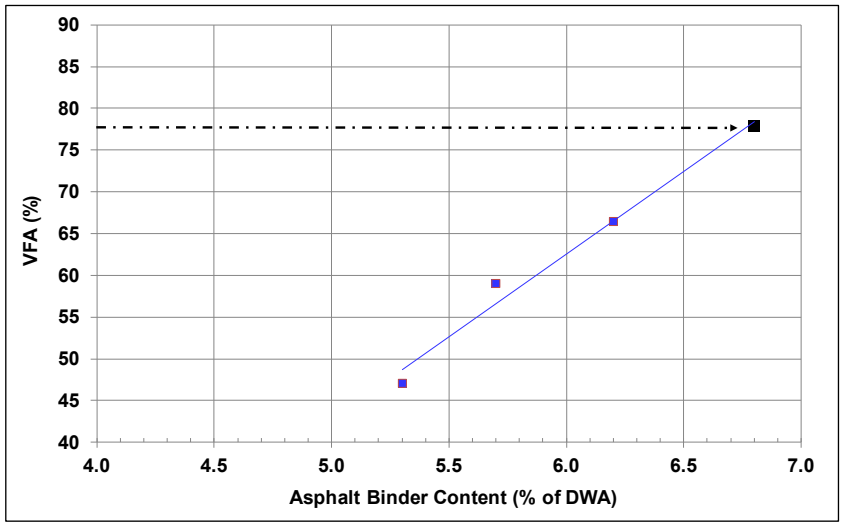

Figure C.2d: App-3/Mix-H: VFA vs. asphalt binder content.

APPENDIX D: TEST RESULTS FOR APPROACH-4 BINDERS AND MIXES

Test results for Approach-4 (App-4) binders and mixes are summarized in the following tables:

- Table D.1: App-4: Unaged, High Temperature Performance-Grading Results
- Table D.2: App-4: RTFO-Aged, High Temperature Performance-Grading Results
- Table D.3: App-4: PAV-Aged, Intermediate Temperature Performance-Grading Results
- Table D.4: App-4: Bending Beam Rheometer Test Results
- Table D.5: App-4: Multiple Stress Creep Recovery Test Results
- Table D.6: App-4: Binder Frequency Sweep Results
- Table D.7: App-4: Dynamic Modulus Test Results
- Table D.8: App-4: Flexural Modulus Test Results
- Table D.9: App-4: Repeated Load Triaxial Test Results
- Table D.10: App-4: Hamburg Wheel Track Test Results
- Table D.11: App-4: Flexural Beam Fatigue Test Results
- Table D.12: App-4: Semicircular Bending Test Results
- Table D.13: App-4: Uniaxial Thermal Stress and Strain Test Results

The binder ID format used in the tables is: refinery source_CRM content in percent_maximum CRM size in mm.

Supplier-C and Supplier-D used PG 64-22 binder from Refinery-A as the base binder to produce Approach-4 CRM binder.

Table D.1: App-4: Unaged, High Temperature Performance-Grading Results

Aging Condition	Binder ID	Test Temp. (°C)	G* (kPa)	Phase Angle (°)	G*/sin (δ) (kPa)
Unaged	A_64-22	64	1.62	87.1	1.62
			1.55	87.1	1.55
		70	0.75	88.2	0.75
			0.73	88.2	0.73
	C_64-22_5_0.25	64	2.35	83.2	2.37
			2.23	83.3	2.35
		70	1.13	84.7	1.14
			1.07	84.9	1.08
	C_64-22_10_0.25	64	3.55	79.3	3.61
			3.54	79.5	3.60
		70	1.76	81.3	1.78
			1.75	81.5	1.77
	A_64-22	64	1.62	87.1	1.62
			1.55	87.1	1.55
		70	0.75	88.2	0.75
			0.73	88.2	0.73
	D_64-22_5_0.18	64	1.13	85.4	1.13
			1.11	85.6	1.11
		70	0.56	86.6	0.56
			0.55	86.8	0.55
	D_64-22_10_0.18	64	2.34	80.5	2.37
			2.23	80.9	2.26
		70	1.16	83.2	1.17
			1.11	83.5	1.11

Table D.2: App-4: RTFO-Aged, High Temperature Performance-Grading Results

Aging Condition	Binder ID	Test Temp. (°C)	G* (kPa)	Phase Angle (°)	G*/sin (δ) (kPa)
RTFO	A_64-22	64	4.28	83.4	4.31
			4.40	83.4	4.42
		70	1.93	85.4	1.93
			1.96	85.4	1.97
	C_64-22_5_0.25	64	6.53	77.6	6.69
			6.50	77.6	6.66
		70	3.07	80.3	3.12
			3.04	80.2	3.09
	C_64-22_10_0.25	64	9.36	72.7	9.80
			8.90	72.9	9.31
		70	4.64	75.7	4.79
			4.36	75.9	4.50
	A_64-22	64	4.28	83.4	4.31
			4.40	83.4	4.42
		70	1.93	85.4	1.93
			1.96	85.4	1.97
	D_64-22_5_0.18	64	3.12	80.4	3.16
			3.08	81.8	3.11
		70	1.49	82.2	1.51
			1.45	83.7	1.46
	D_64-22_10_0.18	64	4.81	76.6	4.95
			4.84	76.1	4.98
		70	2.37	79.2	2.41
			2.40	78.6	2.45

Table D.3: App-4: PAV-Aged, Intermediate Temperature Performance-Grading Results

Aging Condition	Binder ID	Test Temp. (°C)	G* (kPa)	Phase Angle (°)	G*×sin (δ) (kPa)
PAV	A_64-22	25	6,210	47.1	4,547
			6,200	47.1	4,542
	C_64-22_5_0.25	25	5,130	41.9	3,424
			4,640	42.0	3,104
	C_64-22_10_0.25	25	4,010	40.4	2,595
			4,610	40.3	2,982
	A_64-22	25	6,210	47.1	4,547
			6,200	47.1	4,542
	D_64-22_5_0.18	25	3,830	50.2	2,945
			3,730	50.1	2,860
	D_64-22_10_0.18	25	4,160	43.1	2,844
			4,230	43.7	2,922

Table D.4: App-4: Bending Beam Rheometer Test Results

Aging Condition	Binder ID	Test Temp. (°C)	Creep Stiffness (MPa)	m-value
PAV	A_64-22	-12	191	0.330
			195	0.335
	C_64-22_5_0.25	-12	148	0.323
			137	0.317
	C_64-22_10_0.25	-12	99	0.312
			108	0.313
	A_64-22	-12	191	0.330
			195	0.335
	D_64-22_5_0.18	-12	128	0.345
			126	0.351
	D_64-22_10_0.18	-12	109	0.348
			108	0.347

Table D.5: App-4: Multiple Stress Creep Recovery Test Results

Aging Condition	Binder ID	Average Percentage Recovery (%)		Non-Recoverable Creep Compliance (1/kPa)	
		0.1 kPa	3.2 kPa	0.1 kPa	3.2 kPa
RTFO	A_64-22	13.80	3.76	1.15	1.37
		11.35	2.27	1.54	1.84
	C_64-22_5_0.25	18.04	5.66	1.05	1.30
		19.40	5.61	1.04	1.31
	C_64-22_10_0.25	26.43	12.29	0.58	0.78
		39.43	12.12	0.52	0.82
	A_64-22	13.80	3.76	1.15	1.37
		11.35	2.27	1.54	1.84
	D_64-22_5_0.18	27.13	8.86	1.16	1.56
		27.39	8.43	1.17	1.61
	D_64-22_10_0.18	31.00	10.22	0.93	1.34
		32.58	11.24	0.88	1.28

Table D.6: App-4: Binder Frequency Sweep Results (20°C)

Reduced Frequency (Hz)	A_64-22	C_64-22_5_0.25	C_64-22_10_0.25	A_64-22	D_64-22_5_0.18	D_64-22_10_0.18
1.00E-06	1.71E-01	3.33E-01	5.54E-01	1.71E-01	1.60E-01	4.52E-01
1.00E-05	7.54E-01	1.38E+00	2.20E+00	7.54E-01	6.74E-01	1.25E+00
1.00E-04	4.06E+00	6.66E+00	9.81E+00	4.06E+00	3.47E+00	4.57E+00
1.00E-03	2.47E+01	3.48E+01	4.64E+01	2.47E+01	2.03E+01	2.17E+01
1.00E-02	1.52E+02	1.82E+02	2.18E+02	1.52E+02	1.22E+02	1.20E+02
1.00E-01	8.54E+02	8.80E+02	9.53E+02	8.54E+02	6.88E+02	6.70E+02
1.00E+00	3.98E+03	3.68E+03	3.68E+03	3.98E+03	3.30E+03	3.24E+03
1.00E+01	1.47E+04	1.28E+04	1.21E+04	1.47E+04	1.27E+04	1.22E+04
1.00E+02	4.25E+04	3.61E+04	3.36E+04	4.25E+04	3.88E+04	3.46E+04
1.00E+03	9.73E+04	8.42E+04	7.81E+04	9.73E+04	9.40E+04	7.48E+04
1.00E+04	1.83E+05	1.64E+05	1.55E+05	1.83E+05	1.86E+05	1.29E+05
1.00E+05	2.92E+05	2.76E+05	2.67E+05	2.92E+05	3.12E+05	1.89E+05
1.00E+06	4.12E+05	4.09E+05	4.08E+05	4.12E+05	4.58E+05	2.43E+05

Table D.7a: App-4: Dynamic Modulus Test Results for Mix-J (A_64-22)

Fitting Parameters	δ	α	β	γ	C1	C2
	0.56	3.71	-1.70	-0.49	23.24	199.71
Temperature (°C)	**Frequency (Hz)**	**Modulus (MPa)**	**Phase Angle (°)**	**Reduced Frequency (Hz)**	**Modeled Modulus (MPa)**	**Square of Errors**
4	25	14,672	8.2	2.61E+03	14,097	3.01E-04
	10	13,361	8.9	1.06E+03	13,306	3.15E-06
	5	12,442	9.5	5.40E+02	12,657	5.52E-05
	1	10,369	11.4	1.09E+02	10,907	4.83E-04
	0.5	9,475	12.3	5.40E+01	10,056	6.69E-04
	0.1	7,512	15.0	1.09E+01	8,006	7.67E-04
21	25	9,337	16.5	1.86E+01	8,706	9.25E-04
	10	7,862	18.2	7.39E+00	7,496	4.28E-04
	5	6,856	19.5	3.70E+00	6,593	2.88E-04
	1	4,824	23.0	7.33E-01	4,595	4.47E-04
	0.5	4,093	24.2	3.66E-01	3,826	8.60E-04
	0.1	2,638	27.9	7.33E-02	2,333	2.86E-03
38	25	3,254	29.5	2.84E-01	3,561	1.54E-03
	10	2,473	30.8	1.15E-01	2,702	1.49E-03
	5	1,980	31.6	5.77E-02	2,150	1.27E-03
	1	1,095	33.3	1.16E-02	1,179	1.03E-03
	0.5	839	33.1	5.77E-03	884	5.03E-04
	0.1	426	32.9	1.13E-03	432	3.19E-05
54	25	1,207	36.0	1.05E-02	1,133	7.41E-04
	10	816	35.8	4.16E-03	769	6.70E-04
	5	596	35.2	2.07E-03	567	4.78E-04
	1	271	33.8	4.13E-04	273	1.76E-05
	0.5	194	32.6	2.05E-04	198	7.24E-05
	0.1	98	29.0	4.16E-05	97	9.87E-06

Table D.7b: App-4: Dynamic Modulus Test Results for Mix-K (C_64-22_5_0.25)

Fitting Parameters	δ	α	β	γ	C1	C2
	0.00	4.18	-2.26	-0.46	21.66	166.57
Temperature (°C)	**Frequency (Hz)**	**Modulus (MPa)**	**Phase Angle ( )**	**Reduced Frequency (Hz)**	**Modeled Modulus (MPa)**	**Square of Errors**
4	25	14,873	8.5	5.01E+03	12,684	4.78E-03
	10	13,616	9.3	2.00E+03	12,240	2.14E-03
	5	12,677	9.9	1.00E+03	11,863	8.31E-04
	1	10,534	11.8	2.00E+02	10,837	1.52E-04
	0.5	9,620	12.7	1.00E+02	10,329	9.53E-04
	0.1	7,507	15.4	2.00E+01	9,000	6.20E-03
21	25	8,992	14.6	1.78E+01	8,896	2.17E-05
	10	7,784	16.0	7.21E+00	8,060	2.29E-04
	5	6,927	17.1	3.68E+00	7,411	8.61E-04
	1	5,086	20.2	7.57E-01	5,841	3.62E-03
	0.5	4,400	21.4	3.68E-01	5,125	4.39E-03
	0.1	2,975	24.9	7.21E-02	3,603	6.92E-03
38	25	5,041	22.6	1.81E-01	4,441	3.03E-03
	10	4,080	24.3	7.29E-02	3,612	2.79E-03
	5	3,465	25.4	3.58E-02	3,016	3.63E-03
	1	2,228	28.3	7.35E-03	1,890	5.11E-03
	0.5	1,812	29.2	3.83E-03	1,519	5.87E-03
	0.1	1,022	31.3	7.41E-04	820	9.14E-03
54	25	1,572	33.8	5.14E-03	1,679	8.24E-04
	10	1,113	33.6	2.05E-03	1,216	1.46E-03
	5	864	33.1	1.03E-03	934	1.12E-03
	1	427	33.0	2.07E-04	479	2.44E-03
	0.5	322	31.9	1.04E-04	352	1.56E-03
	0.1	165	30.1	2.04E-05	165	7.07E-07

Table D.7c: App-4: Dynamic Modulus Test Results for Mix-L (C_64-22_10_0.25)

Fitting Parameters	δ	α	β	γ	C1	C2
	0.70	3.59	-1.42	-0.47	5.28	45.20
Temperature (°C)	**Frequency (Hz)**	**Modulus (MPa)**	**Phase Angle (°)**	**Reduced Frequency (Hz)**	**Modeled Modulus (MPa)**	**Square of Errors**
4	25	15,633	8.4	1.68E+04	14,714	6.93E-04
	10	14,373	9.1	6.71E+03	13,957	1.63E-04
	5	13,390	9.8	3.36E+03	13,323	4.75E-06
	1	11,173	11.7	6.85E+02	11,680	3.71E-04
	0.5	10,214	12.7	3.50E+02	10,912	8.24E-04
	0.1	8,059	15.4	7.31E+01	8,995	2.28E-03
21	25	7,709	17.6	1.84E+01	7,243	7.33E-04
	10	6,460	19.3	7.37E+00	6,097	6.30E-04
	5	5,603	20.6	3.71E+00	5,276	6.82E-04
	1	3,897	24.0	7.49E-01	3,552	1.62E-03
	0.5	3,288	25.2	3.68E-01	2,902	2.94E-03
	0.1	2,098	28.4	7.49E-02	1,739	6.65E-03
38	25	3,060	29.1	7.75E-01	3,585	4.71E-03
	10	2,339	30.3	3.10E-01	2,756	5.06E-03
	5	1,901	30.8	1.56E-01	2,221	4.58E-03
	1	1,082	32.4	3.11E-02	1,269	4.78E-03
	0.5	837	32.1	1.55E-02	974	4.29E-03
	0.1	447	31.6	3.10E-03	510	3.33E-03
54	25	2,273	31.4	1.34E-01	2,114	9.93E-04
	10	1,697	31.9	5.35E-02	1,545	1.66E-03
	5	1,345	31.9	2.67E-02	1,198	2.55E-03
	1	705	32.5	5.40E-03	640	1.73E-03
	0.5	524	31.8	2.71E-03	482	1.32E-03
	0.1	244	30.9	5.37E-04	245	1.78E-06

Table D.8a: App-4: Flexural Modulus Test Results for Mix-A (A_64-22)

Fitting Parameters	δ	α	β	γ	C1	C2
	0.00	4.12	-1.98	-0.54	13.93	90.07
Temp. (°C)	**Frequency (Hz)**	**Modulus (MPa)**	**Phase Angle (°)**	**Reduced Frequency (Hz)**	**Modeled Modulus (MPa)**	**Square of Errors**
10	15	11,308	14.5	9.09E+02	10,273	2.46E-03
	10	10,909	13.4	6.03E+02	10,015	2.20E-03
	5	10,148	12.7	3.01E+02	9,541	1.63E-03
	2	9,092	13.0	1.21E+02	8,844	1.16E-03
	1	8,293	13.6	6.04E+01	8,257	1.21E-03
	0.5	7,508	14.1	3.01E+01	7,626	1.36E-03
	0.2	6,470	15.9	1.21E+01	6,741	1.82E-03
	0.1	5,531	14.3	6.09E+00	6,048	3.28E-03
	0.05	4,800	15.8	2.83E+00	5,258	3.43E-03
	0.02	3,979	18.5	1.09E+00	4,284	3.26E-03
	0.01	3,435	21.4	5.93E-01	3,691	3.31E-03
20	15	7,229	20.4	1.57E+01	7,001	1.23E-03
	10	6,788	19.8	1.04E+01	6,592	1.29E-03
	5	6,002	19.8	5.15E+00	5,876	1.32E-03
	2	4,983	21.0	2.05E+00	4,930	1.43E-03
	1	4,259	22.1	1.03E+00	4,230	1.58E-03
	0.5	3,604	23.4	5.21E-01	3,567	1.89E-03
	0.2	2,840	26.1	2.11E-01	2,757	2.31E-03
	0.1	2,115	25.0	9.27E-02	2,084	2.39E-03
	0.05	1,692	28.0	4.38E-02	1,574	2.97E-03
	0.01	1,143	32.0	1.29E-02	949	1.03E-02
30	15	3,432	29.9	6.30E-01	3,749	3.48E-03
	10	3,098	30.1	4.13E-01	3,350	3.00E-03
	5	2,550	30.6	2.05E-01	2,732	2.53E-03
	2	1,933	31.5	8.13E-02	2,011	1.69E-03
	1	1,533	32.6	4.05E-02	1,554	1.15E-03
	0.5	1,199	34.7	2.01E-02	1,170	1.03E-03
	0.2	855	36.9	8.11E-03	782	2.47E-03
	0.1	549	36.9	3.06E-03	480	5.88E-03
	0.02	282	43.3	8.21E-04	245	1.92E-02
	0.01	179	47.7	3.62E-04	156	3.51E-01

Table D.8b: App-4: Flexural Modulus Test Results for Mix-K (C_64-22_5_0.25)

Fitting Parameters	δ	α	β	γ	C1	C2
	0.20	4.02	-1.68	-0.46	54.07	382.01
Temp. (°C)	**Frequency (Hz)**	**Modulus (MPa)**	**Phase Angle (°)**	**Reduced Frequency (Hz)**	**Modeled Modulus (MPa)**	**Square of Errors**
10	15	10,464	15.5	4.25E+02	10,286	1.68E-04
	10	10,060	14.3	2.80E+02	9,882	1.96E-04
	5	9,303	13.8	1.41E+02	9,190	1.84E-04
	2	8,251	14.1	5.70E+01	8,231	1.93E-04
	1	7,457	14.8	2.83E+01	7,467	2.16E-04
	0.5	6,684	15.6	1.40E+01	6,685	2.20E-04
	0.2	5,599	17.7	5.55E+00	5,665	1.28E-04
	0.1	5,039	16.5	3.42E+00	5,088	4.30E-04
	0.05	4,317	17.5	1.78E+00	4,417	3.74E-04
	0.02	3,404	20.2	5.99E-01	3,415	6.43E-04
	0.01	2,879	23.3	2.83E-01	2,773	6.28E-04
20	15	6,805	17.0	3.23E+02	9,470	3.54E-05
	10	6,368	15.8	2.13E+02	9,040	5.86E-05
	5	5,602	15.4	1.08E+02	8,328	6.33E-05
	2	4,628	15.9	4.36E+01	7,357	1.17E-04
	1	3,929	16.7	2.16E+01	6,607	1.38E-04
	0.5	3,315	17.9	1.07E+01	5,856	1.75E-04
	0.2	2,568	19.9	4.21E+00	4,891	2.55E-04
	0.1	1,943	16.3	2.69E+00	4,891	3.81E-04
	0.05	1,688	20.1	1.09E+00	3,687	3.86E-04
	0.02	1,165	23.1	4.69E-01	2,868	7.19E-04
	0.01	918	25.6	2.14E-01	2,300	7.55E-04
30	15	3,452	31.6	6.23E-01	3,446	1.63E-04
	10	3,107	30.9	4.09E-01	3,074	2.16E-04
	5	2,553	31.6	2.02E-01	2,506	2.69E-04
	2	1,914	32.8	8.08E-02	1,869	3.80E-04
	1	1,514	33.6	4.00E-02	1,463	3.46E-04
	0.5	1,174	35.5	2.01E-02	1,132	4.61E-04
	0.2	836	37.1	7.99E-03	784	1.13E-03
	0.1	622	36.5	3.98E-03	585	1.08E-03
	0.05	324	74.5	1.76E-03	407	1.85E-01
	0.02	322	37.2	7.86E-04	283	3.94E-03
	0.01	246	38.1	3.87E-04	204	7.46E-03

Table D.8c: App-4: Flexural Modulus Test Results for Mix-L (C_64-22_10_0.25)

Fitting Parameters	δ	α	β	γ	C1	C2
	0.00	4.16	-1.90	-0.45	18.71	129.44
Temp. (°C)	Frequency (Hz)	Modulus (MPa)	Phase Angle (°)	Reduced Frequency (Hz)	Modeled Modulus (MPa)	Square of Errors
10	15	10,152	14.5	5.48E+02	9,608	3.47E-03
	10	9,754	13.4	3.69E+02	9,315	3.28E-03
	5	9,086	12.5	1.87E+02	8,787	3.28E-03
	2	8,168	12.6	7.50E+01	8,032	3.24E-03
	1	7,486	12.9	3.80E+01	7,440	3.29E-03
	0.5	6,809	13.6	1.94E+01	6,832	3.35E-03
	0.2	5,944	15.0	7.80E+00	5,993	3.35E-03
	0.1	5,158	13.4	3.93E+00	5,356	3.81E-03
	0.05	4,559	14.5	1.88E+00	4,681	4.10E-03
	0.02	3,871	16.4	7.78E-01	3,905	3.37E-03
	0.01	3,395	19.0	3.83E-01	3,318	3.83E-03
20	15	6,601	15.7	4.14E+02	8,871	3.03E-03
	10	6,207	14.6	2.75E+02	8,538	3.00E-03
	5	5,560	13.9	1.39E+02	7,979	3.16E-03
	2	4,725	14.2	5.60E+01	7,203	3.22E-03
	1	4,118	14.6	2.85E+01	6,600	3.40E-03
	0.5	3,554	15.4	1.45E+01	5,998	3.53E-03
	0.2	2,878	17.1	5.79E+00	5,181	3.66E-03
	0.1	2,312	15.5	3.01E+00	4,599	4.00E-03
	0.05	1,919	16.9	1.41E+00	3,998	4.11E-03
	0.02	1,509	18.4	5.89E-01	3,286	3.66E-03
	0.01	1,241	21.6	2.89E-01	2,767	4.43E-03
30	15	3,702	27.4	6.31E-01	3,727	4.16E-03
	10	3,397	26.9	4.12E-01	3,376	3.93E-03
	5	2,880	26.7	2.05E-01	2,834	3.68E-03
	2	2,261	27.4	8.13E-02	2,190	4.00E-03
	1	1,859	28.4	4.10E-02	1,777	4.27E-03
	0.5	1,516	29.1	2.11E-02	1,426	4.14E-03
	0.2	1,130	32.1	8.56E-03	1,035	4.26E-03
	0.1	868	30.5	4.22E-03	790	4.99E-03
	0.05	497	64.8	1.97E-03	579	9.88E-02
	0.02	376	40.2	8.86E-04	413	6.43E-02
	0.01	322	56.3	3.83E-04	283	1.47E-01

Table D.9: App-4: Repeated Load Triaxial Test Results

Specimen ID	AV Content (%)	Flow Number (Cycles)	Average (Cycles)	Std. Dev. (Cycles)	Std. Dev./Average (%)
Mix-J-1	6.9	724	929	333	35.9
Mix-J-2	6.6	1,214			
Mix-J-3	6.9	1,303			
Mix-J-4	7.4	1,009			
Mix-J-5	7.1	394			
Mix-K-1	7.3	2,461	1,594	930	58.3
Mix-K-2	7.5	2,648			
Mix-K-3	6.5	614			
Mix-K-4	6.6	653			
Mix-K-5	7.0	716			
Mix-L-1	7.0	1,970	1,879	323	17.2
Mix-L-2	6.6	1,673			
Mix-L-3	6.5	1,512			
Mix-L-4	7.1	2,360			

Table D.10: App-4: Hamburg Wheel Track Test Results

Specimen ID	AV Content (%)	Left Wheel Rutting (mm)			Right Wheel Rutting (mm)		
		@5k Passes	@15k Passes	@25k Passes	@5k Passes	@15k Passes	@25k Passes
Mix-J-1	7.6	2.44	2.94	3.23	Not tested	Not tested	Not tested
Mix-J-2	7.9						
Mix-J-3	7.8	Not tested	Not tested	Not tested	2.43	3.24	4.18
Mix-J-4	7.2						
Mix-K-1	7.8	2.00	2.48	2.73	Not tested	Not tested	Not tested
Mix-K-2	8.0						
Mix-K-3	7.1	Not tested	Not tested	Not tested	1.52	2.25	2.56
Mix-K-4	7.8						
Mix-L-1	7.8	1.70	2.12	2.32	Not tested	Not tested	Not tested
Mix-L-2	7.0						
Mix-L-3	8.0	Not tested	Not tested	Not tested	1.11	1.46	1.64
Mix-L-4	7.2						

Table D.11a: App-4: Flexural Beam Fatigue Test Results for Mix-J (A_64-22)

Specimen ID	Air-Void Content (%)	Test Strain (µstrain)	Fatigue Life (Cycles)
MixJ-B#3-1-B6	7.3	300	1,392,500
MixJ-B#3-2-B6	6.7	300	655,000
MixJ-B#3-2-B7	7.2	309	1,585,000
MixJ-B#3-1-B1	7.5	400	127,500
MixJ-B#3-1-B5	7.1	400	247,500
MixJ-B#3-2-B4	6.5	405	1,008,995
MixJ-B#3-1-B7	7.4	550	137,500
MixJ-B#3-2-B5	6.5	550	48,000
MixJ-B#3-2-B8	6.8	550	26,000

Table D.11b: App-4: Flexural Beam Fatigue Test Results for Mix-K (C_64-22_5_0.25)

Specimen ID	Air-Void Content (%)	Test Strain (µstrain)	Fatigue Life (Cycles)
MixK-B#3-1-B5	7.8	300	1,570,000
MixK-B#3-2-B1	7.8	300	1,715,000
MixK-B#3-2-B3	7.9	300	7,222,500
MixK-B#3-1-B1	8.0	400	280,000
MixK-B#3-1-B2	7.9	400	245,000
MixK-B#3-1-B4	7.4	400	247,500
MixK-B#3-1-B3	7.5	500	102,500
MixK-B#3-1-B6	7.7	500	99,000
MixK-B#3-1-B8	7.8	500	57,000

Table D.11c: App-4: Flexural Beam Fatigue Test Results for Mix-L (C_64-22_10_0.25)

Specimen ID	Air-Void Content (%)	Test Strain (µstrain)	Fatigue Life (Cycles)
MixL-B#3-1-B7	6.4	320	600,000
MixL-B#3-1-B8	6.9	320	3,632,500
MixL-B#3-2-B4	7.4	326	1,500,000
MixL-B#3-1-B2	6.4	400	287,500
MixL-B#3-1-B3	6.1	400	682,500
MixL-B#3-2-B7	7.3	400	370,000
MixL-B#3-1-B1	6.7	500	25,000
MixL-B#3-2-B5	7.3	500	107,500
MixL-B#3-2-B8	7.9	500	162,500

Table D.12: App-4: Semicircular Bending Test Results

Specimen ID	Air-Void Content (%)	Fracture Energy (Jol/m^2)	Flexibility Index	Strength (MPa)
Mix-J	7.2	2,242	4.27	0.64
	6.8	2,740	7.87	0.53
	6.9	2,764	6.22	0.59
	7.2	2,566	6.85	0.58
Mix-K	7.2	2,237	5.72	0.54
	7.6	2,007	4.10	0.60
	7.0	2,368	4.92	0.59
	6.4	2,205	4.13	0.63
Mix-L	7.1	1,355	0.70	0.67
	6.9	2,343	5.47	0.57
	6.9	2,136	5.84	0.51
	6.6	2,344	5.50	0.51

Table D.13: App-4: Uniaxial Thermal Stress and Strain Test Results

Specimen ID	Air-Void Content (%)	Average UTSST Air-Void Content (%)[1]	Average CRI_{Env}[1]	Average Fracture Temperature (°C)[1]
Mix-J	8.1	6.3	8	-15.2
	8.0			
Mix-K	8.3	7.0	15	-18.8
	8.3			
Mix-L	7.7	5.7	3	-11.6
	7.4			

[1] Only the average results were received by UCPRC

APPENDIX E: CalME SIMULATION RESULTS

CalME simulation results are summarized in the following figures:

- Figure E.1 through Figure E.27: Asphalt concrete (AC) overlays on cracked asphalt concrete
- Figure E.28 through Figure E.49: Asphalt concrete overlays on cracked portland cement concrete (PCC)

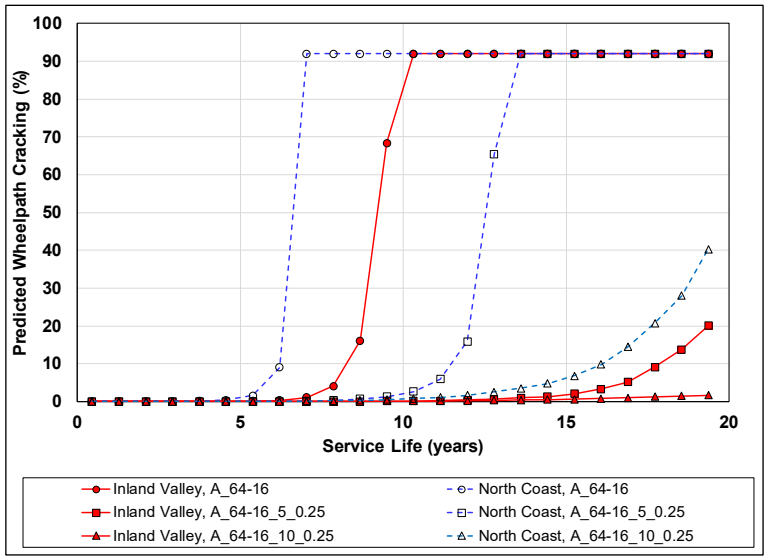

Figure E.1: AC on AC: 0.15 ft. overlays of Mix-A, -B, and -C.

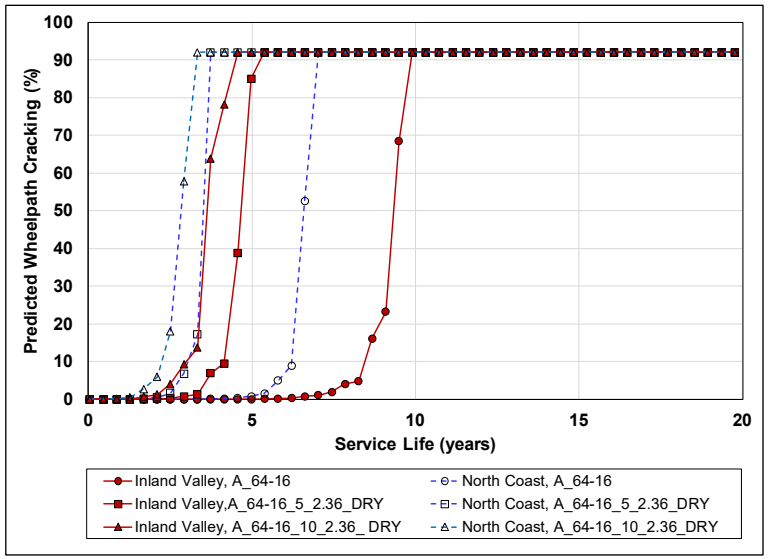

Figure E.2: AC on AC: 0.15 ft. overlays of Mix- D, -E, and -F.

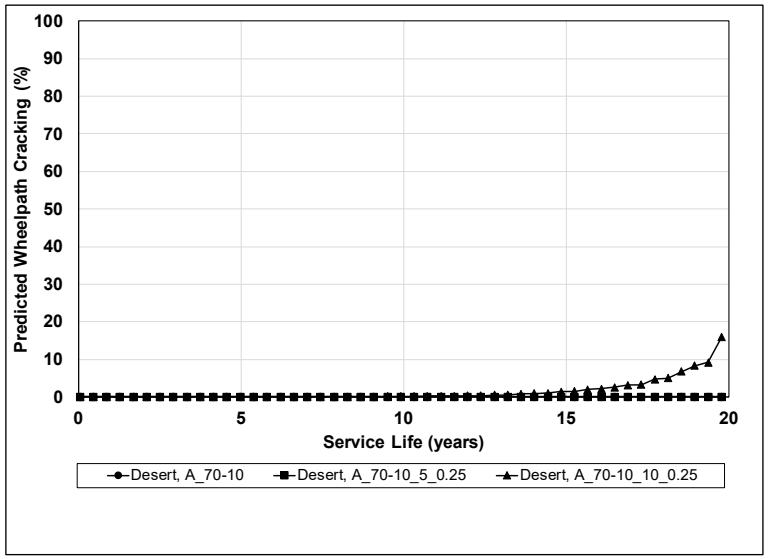

Figure E.3: AC on AC: 0.15 ft. overlays of Mix-A, -G, and -H.

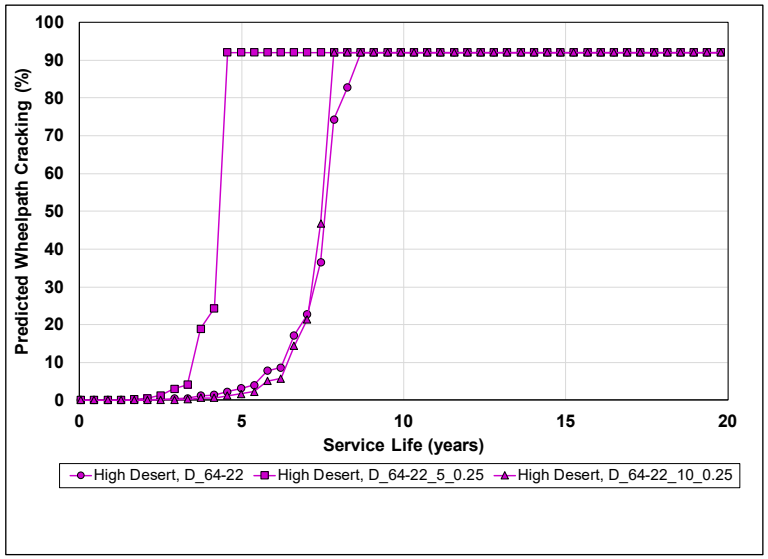

Figure E.4: AC on AC: 0.15 ft. overlays of Mix-J, -K, and -L.

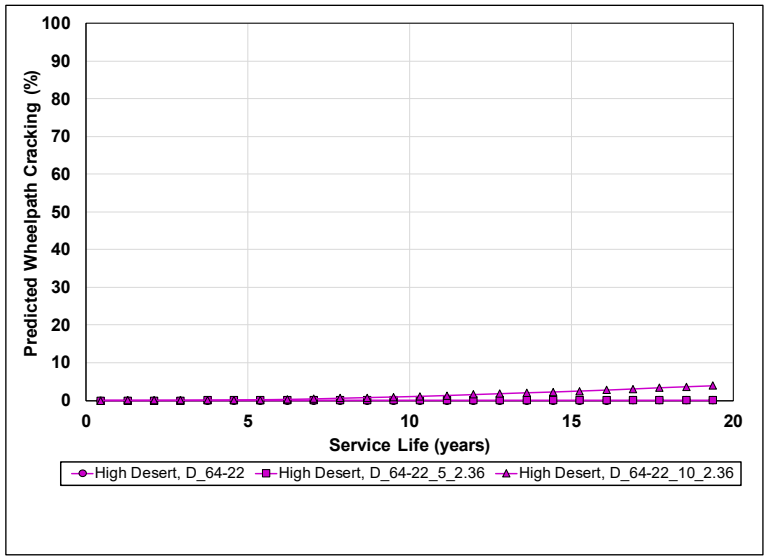

Figure E.5: AC on AC: 0.15 ft. overlays of Mix-S, -T, and -U.

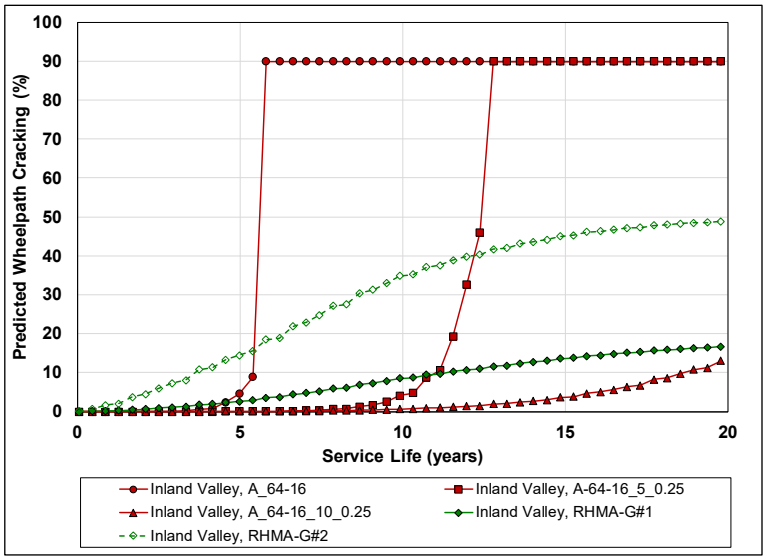

Figure E.6: AC on AC: 0.2 ft. overlays of Mix-A, -B, -C, and RHMA-G (inland valley).

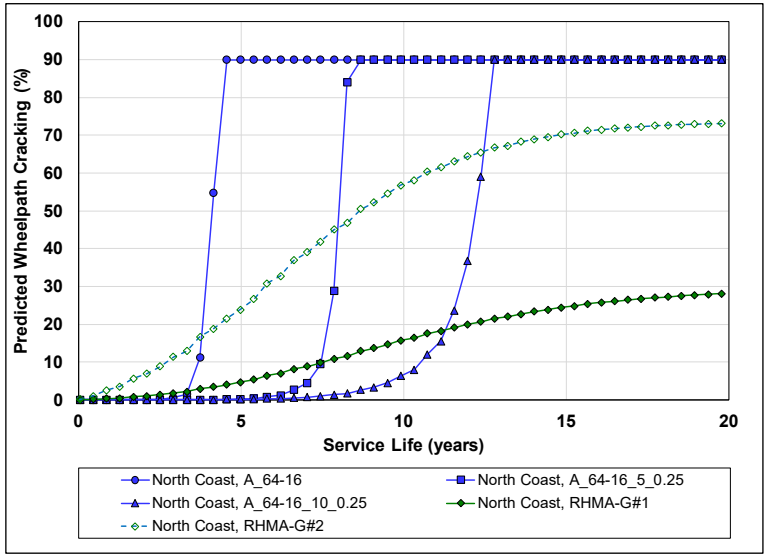

Figure E.7: AC on AC: 0.2 ft. overlays of Mix-A, -B, -C, and RHMA-G (north coast).

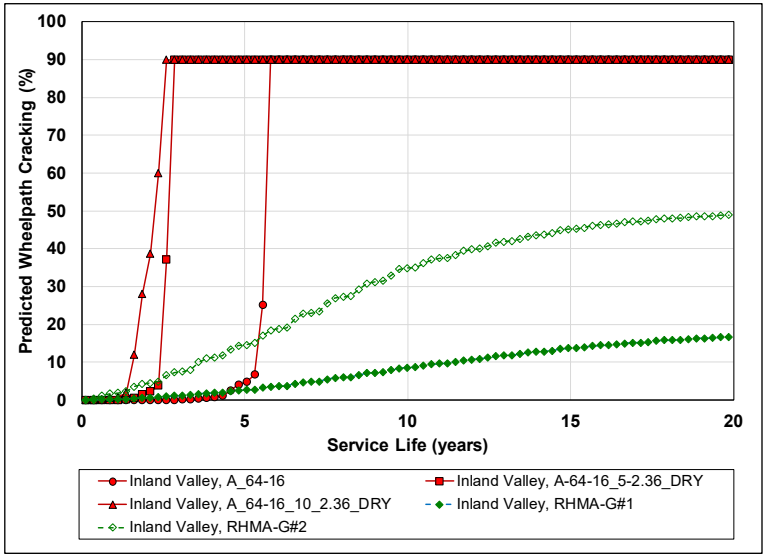

Figure E.8: AC on AC: 0.2 ft. overlays of Mix-A, -G, -H, and RHMA-G (inland valley).

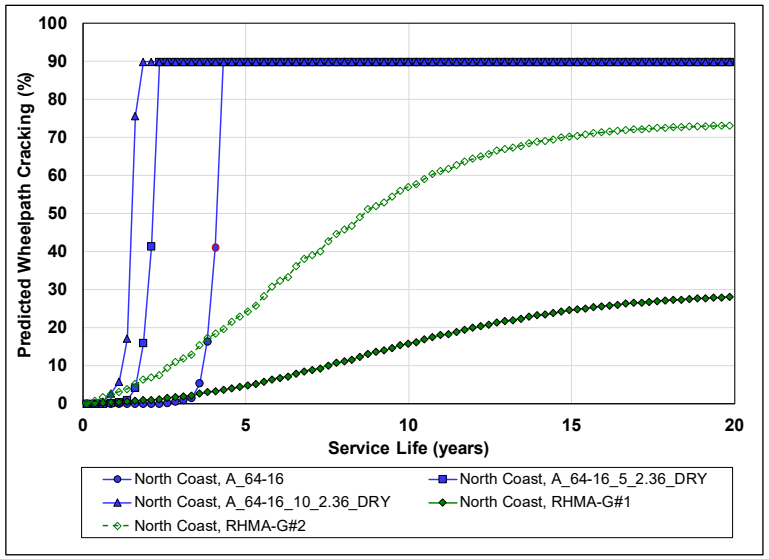

Figure E.9: AC on AC: 0.2 ft. overlays of Mix-A, -G, -H, and RHMA-G (north coast).

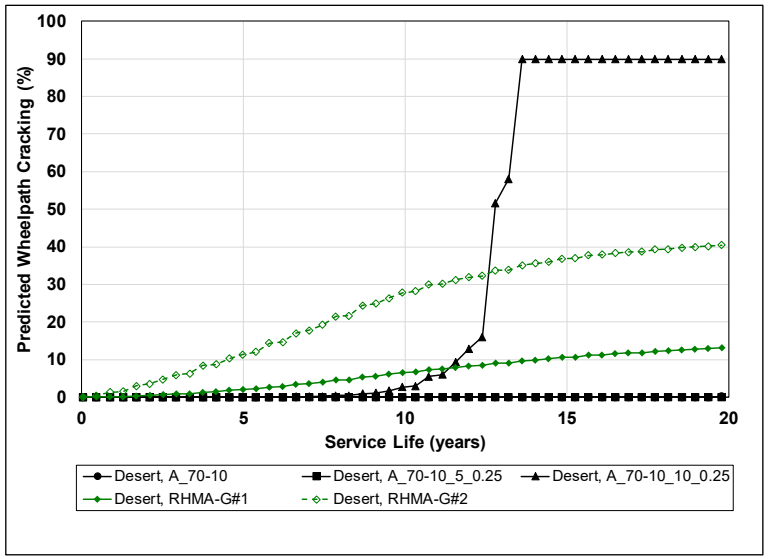

Figure E.10: AC on AC: 0.2 ft. overlays of Mix-D, -E, -F, and RHMA-G (high desert).

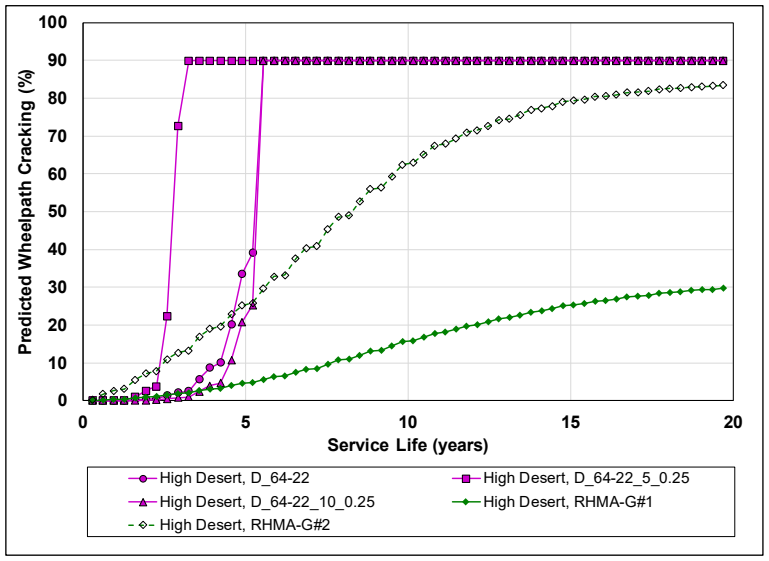

Figure E.11: AC on AC: 0.2 ft. overlays of Mix-J, -K, -L, and RHMA-G (high desert).

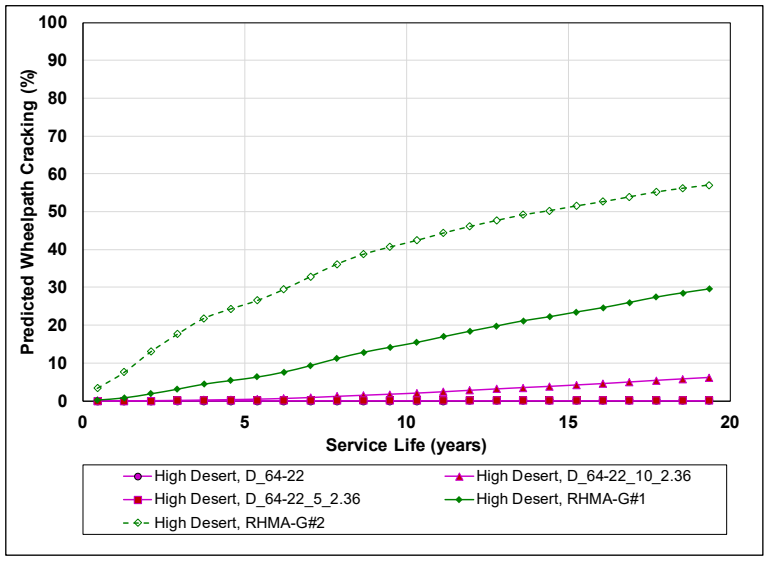

Figure E.12: AC on AC: 0.2 ft. overlays of Mix-S, -T, -U, and RHMA-G (high desert).

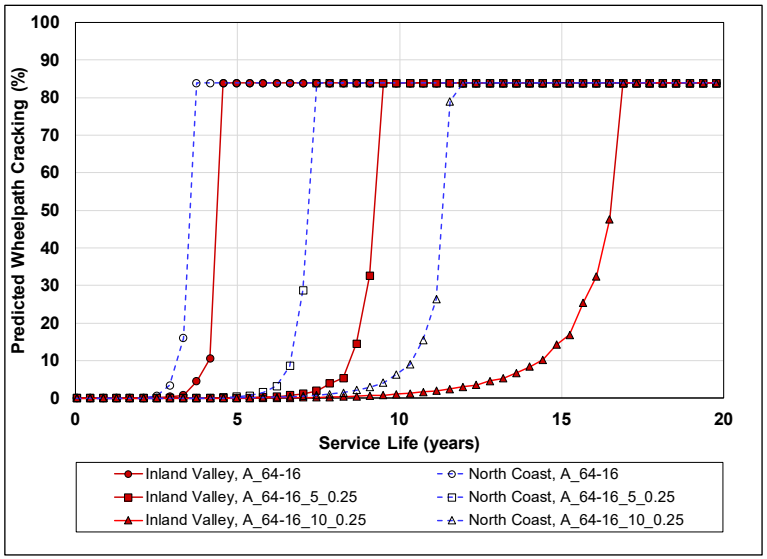

Figure E.13: AC on AC: 0.35 ft. overlays of Mix-A, -B, and -C.

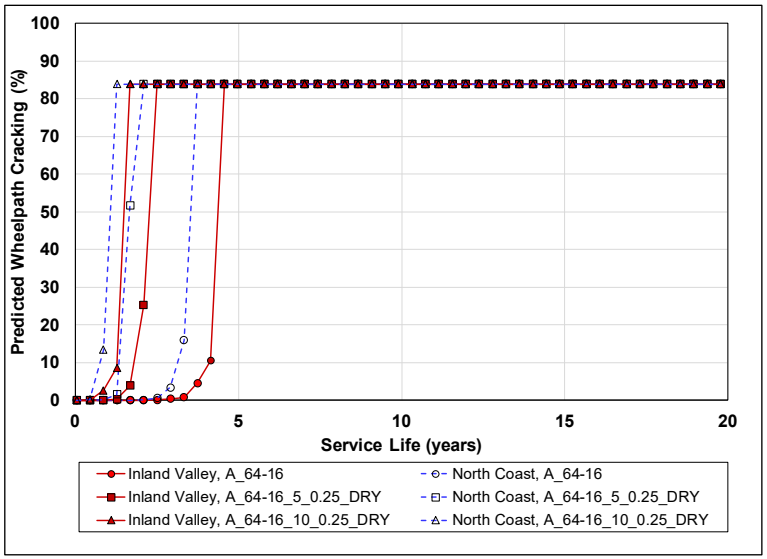

Figure E.14: AC on AC: 0.35 ft. overlays of Mix-A, -G, and -H.

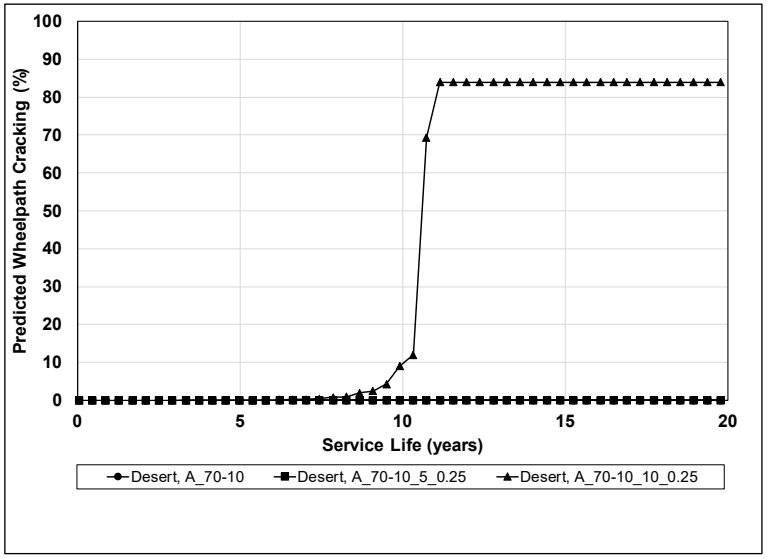

Figure E.15: AC on AC: 0.35 ft. overlays of Mix-D, -E, and -F.

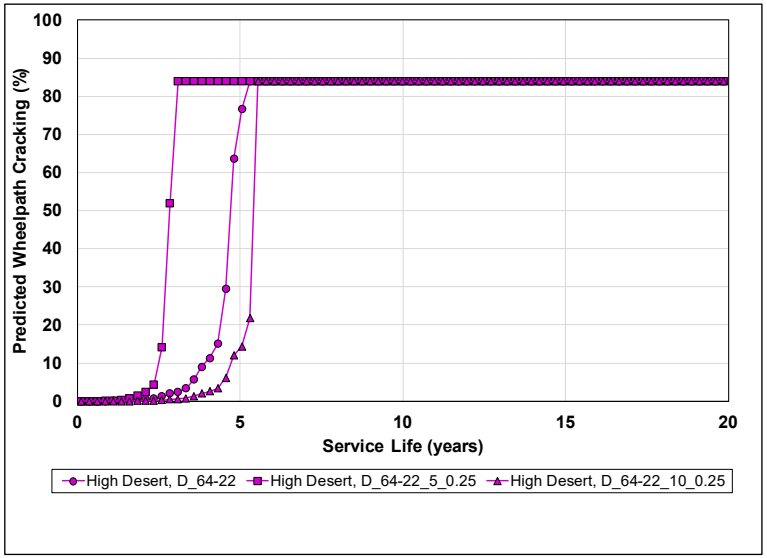

Figure E.16: AC on AC: 0.35 ft. overlays of Mix-J, -K, and -L.

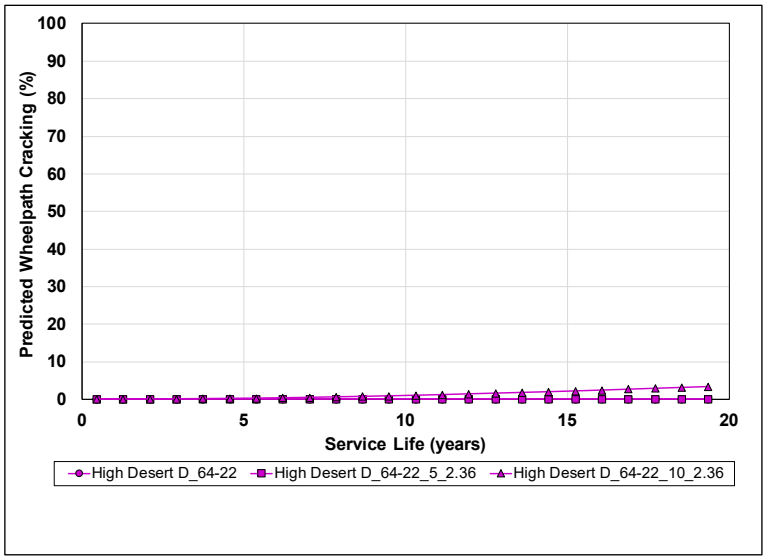

Figure E.17: AC on AC: 0.35 ft. overlays of Mix-S, -T, and -U.

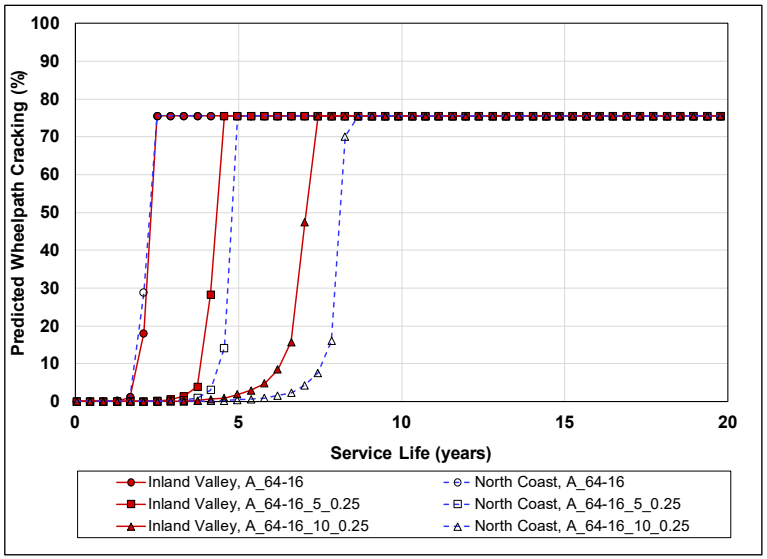

Figure E.18: AC on AC: 0.5 ft. overlays of Mix-A, -B, and -C.

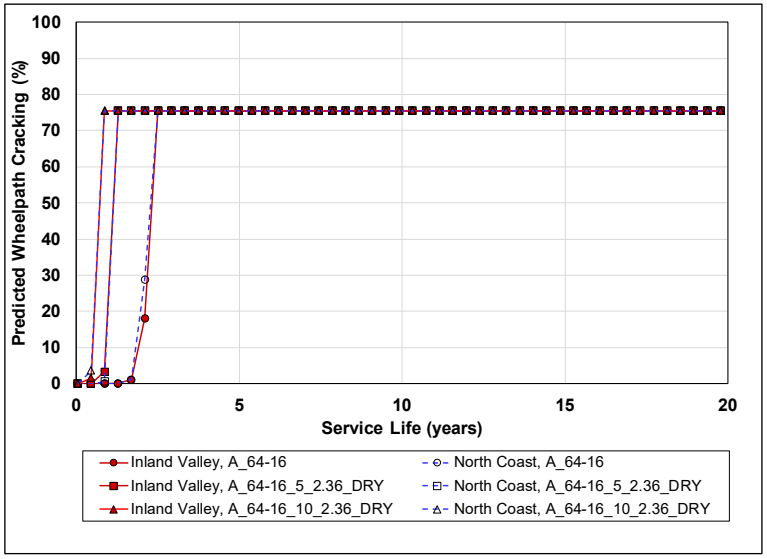

Figure E.19: AC on AC: 0.5 ft. overlays of Mix-A, -G, and -H.

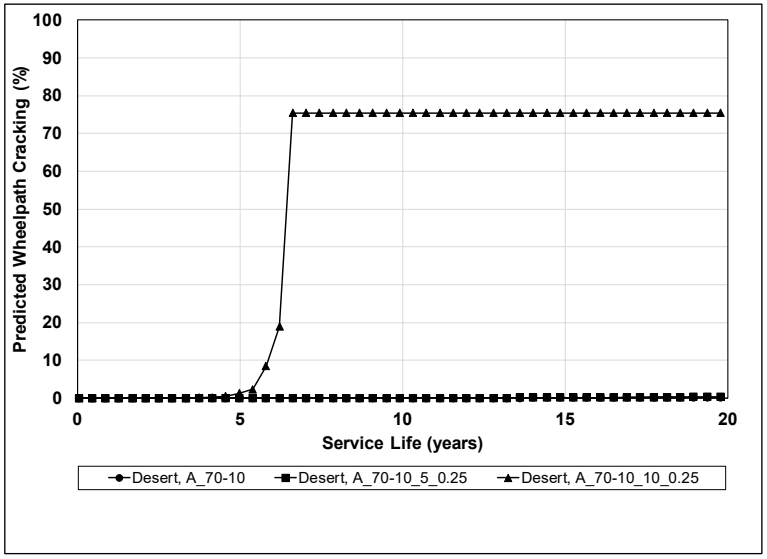

Figure E.20: AC on AC: 0.5 ft. overlays of Mix-D, -E, and -F.

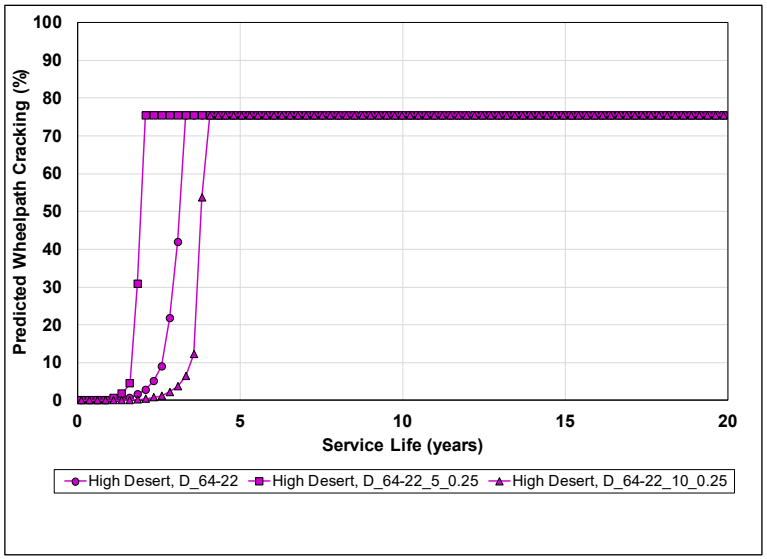

Figure E.21: AC on AC: 0.5 ft. overlays of Mix-J, -K, and- L.

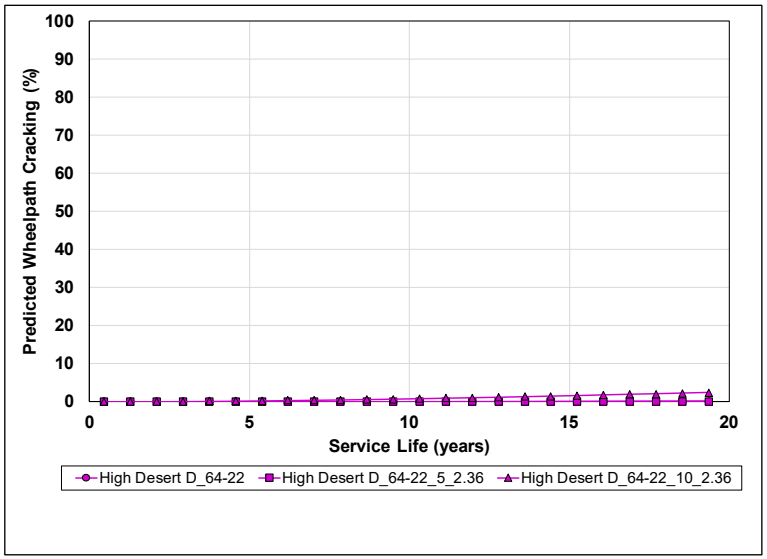

Figure E.22: AC on AC: 0.5 ft. overlays of Mix-S, -T, and -U.

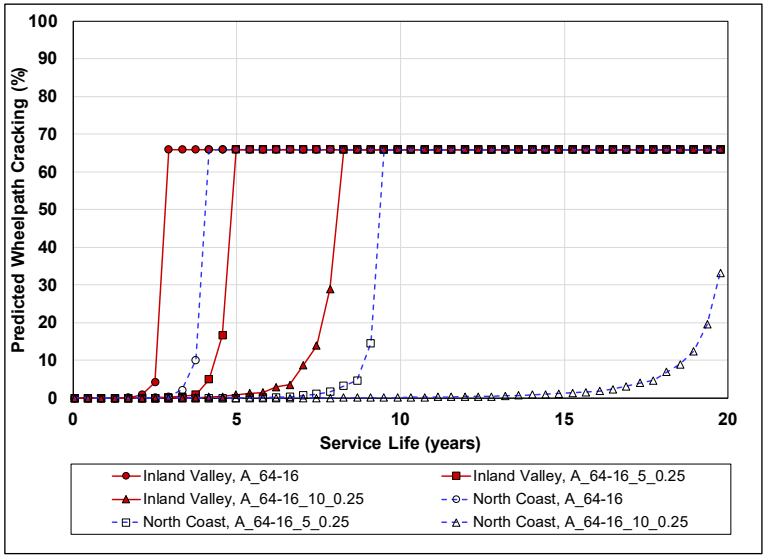

Figure E.23: AC on AC: 0.7 ft. overlays of Mix-A, -B, and -C.

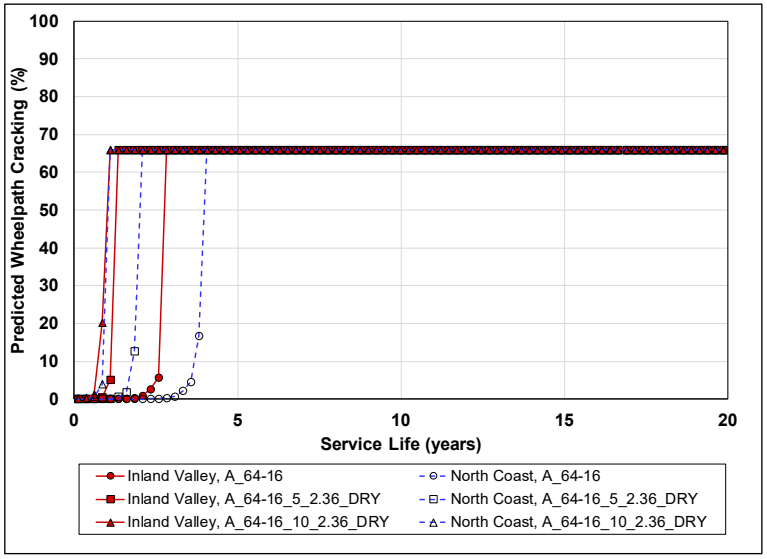

Figure E.24: AC on AC: 0.7 ft. overlays of Mix-A, -G, and -H.

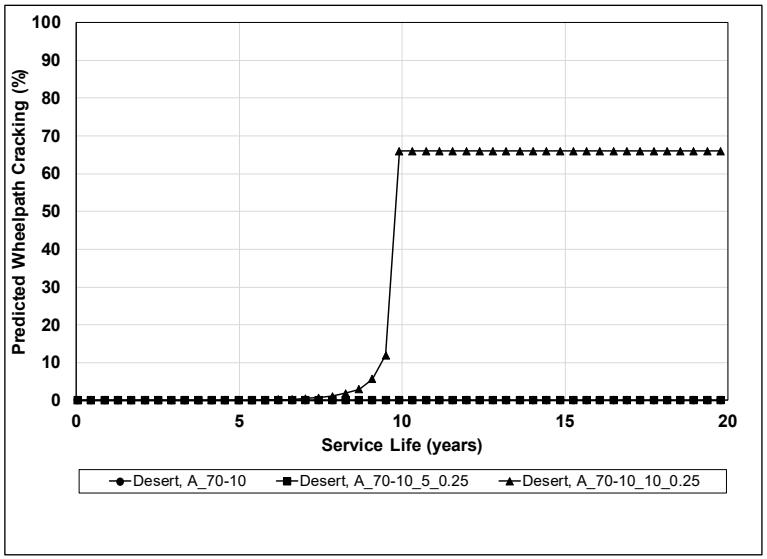

Figure E.25: AC on AC: 0.7 ft. overlays of Mix-D, -E, and -F.

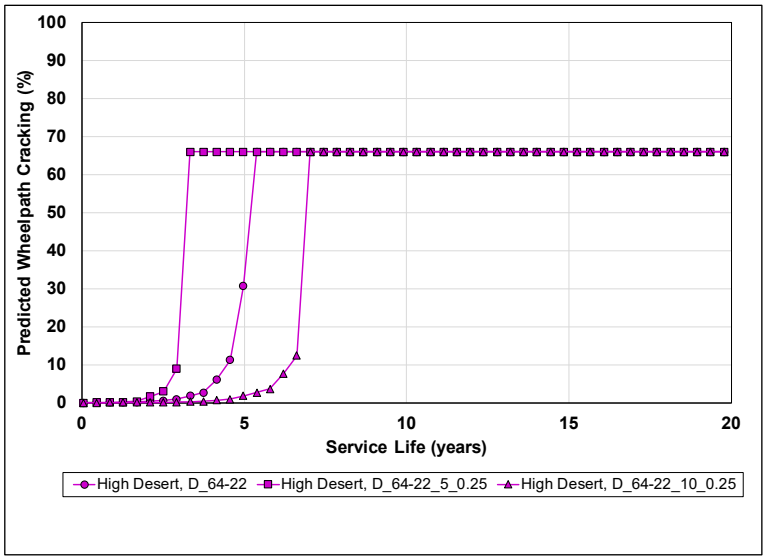

Figure E.26: AC on AC: 0.7 ft. overlays of Mix-J, -K, and -L.

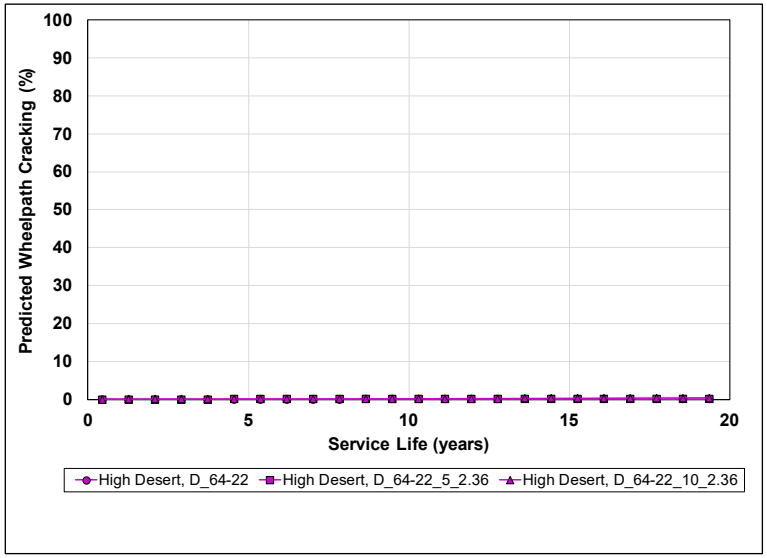

Figure E.27: AC on AC: 0.7 ft. overlays of Mix-S, -T, and -U.

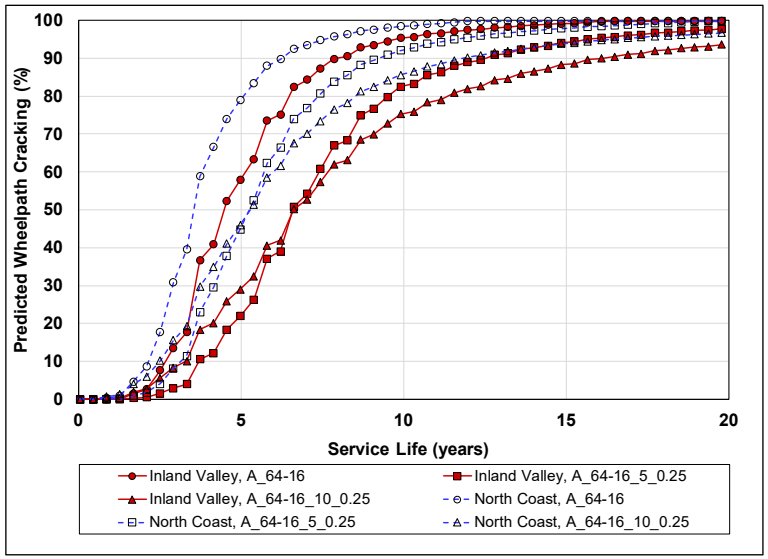

Figure E.28: AC on PCC: 0.15 ft. overlays of Mix-A, -B, and -C.

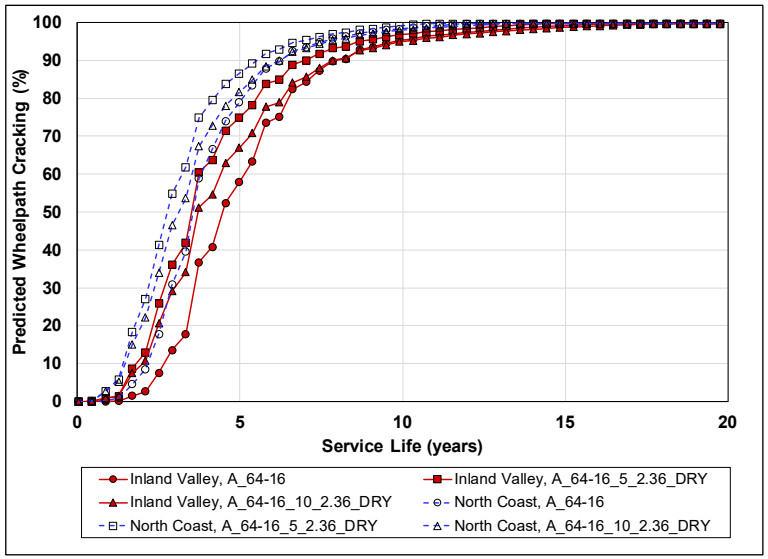

Figure E.29: AC on PCC: 0.15 ft. overlays of Mix-A, -G, and -H.

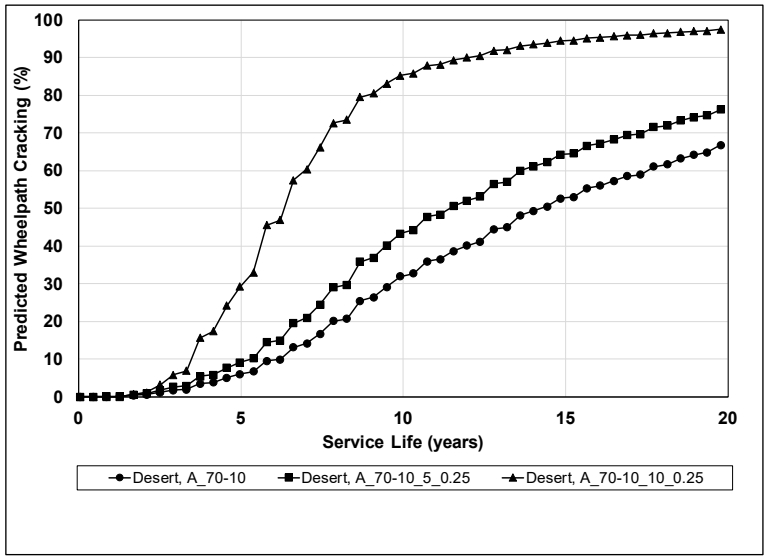

Figure E.30: AC on PCC: 0.15 ft. overlays of Mix- D, -E, and -F.

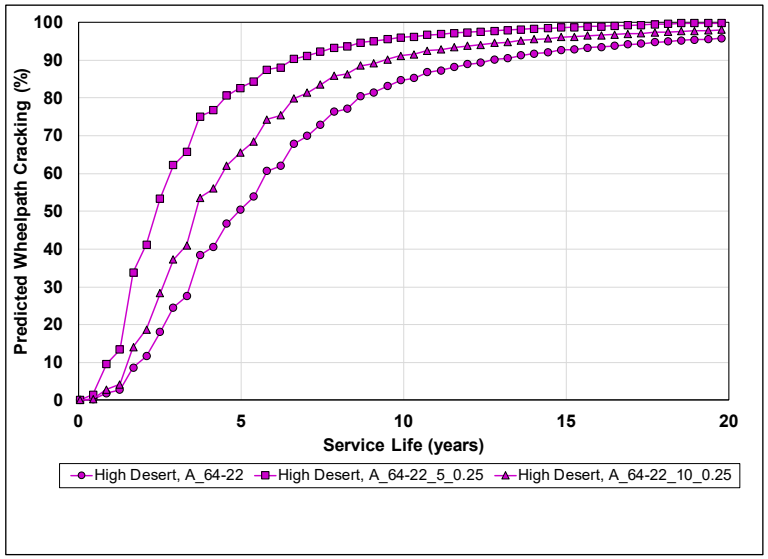

Figure E.31: AC on PCC: 0.15 ft. overlays of Mix-J, K, and -L.

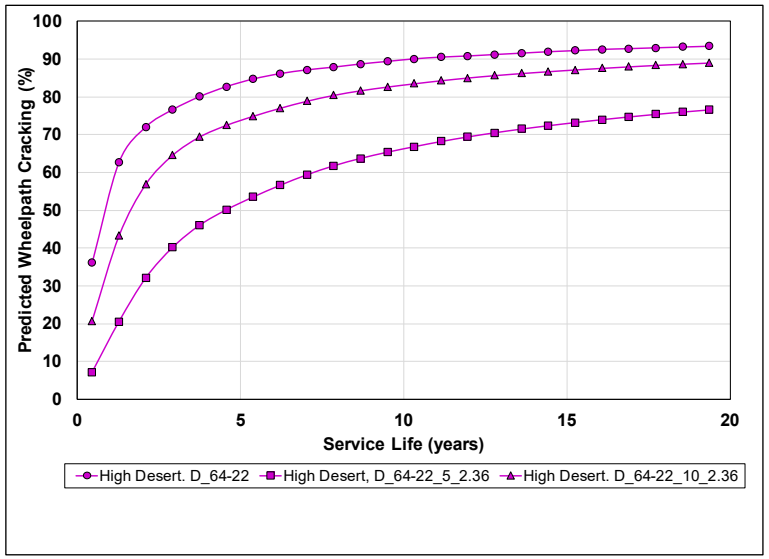

Figure E.32: AC on PCC: 0.15 ft. overlays of Mix-S, -T, and -U.

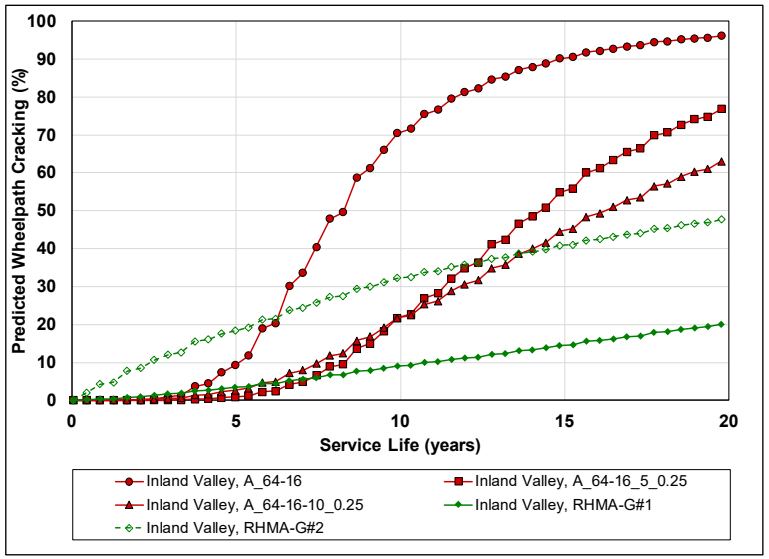

Figure E.33: AC on PCC: 0.2 ft. overlays of Mix-A, -B, -C, and RHMA-G (inland valley).

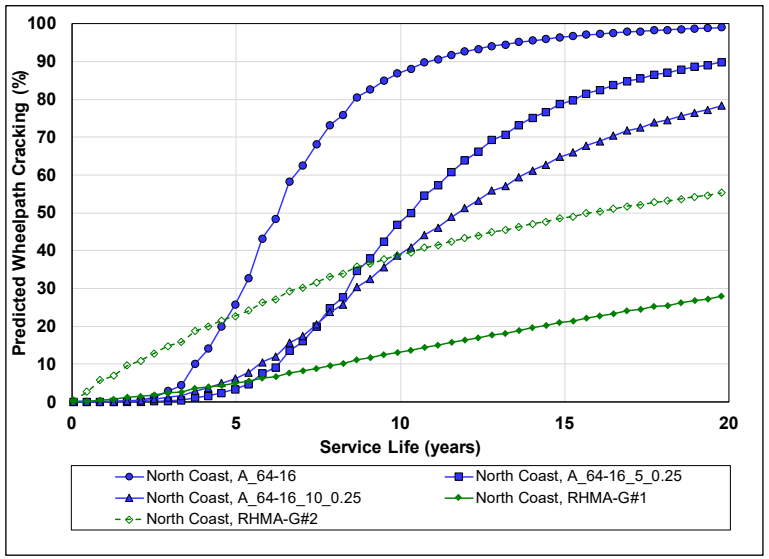

Figure E.34: AC on PCC: 0.2 ft. overlays of Mix-A, -B, -C, and RHMA-G (north coast).

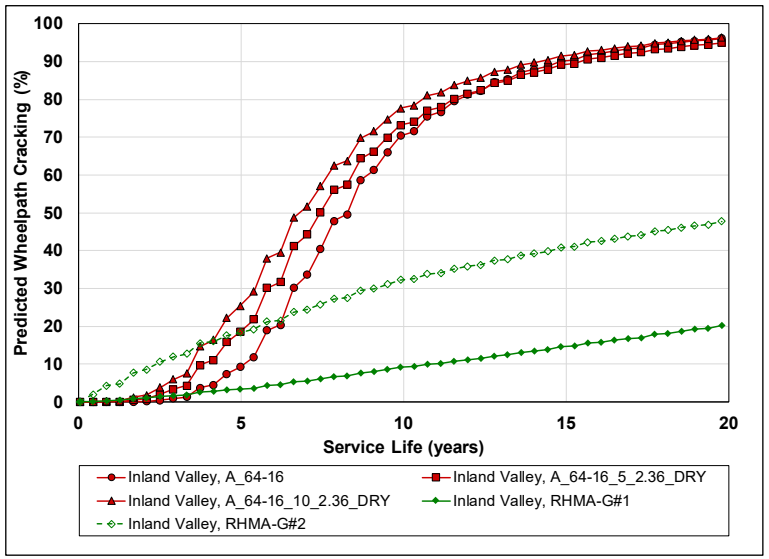

Figure E.35: AC on PCC: 0.2 ft. overlays of Mix-A, -G, -H, and RHMA-G (inland valley).

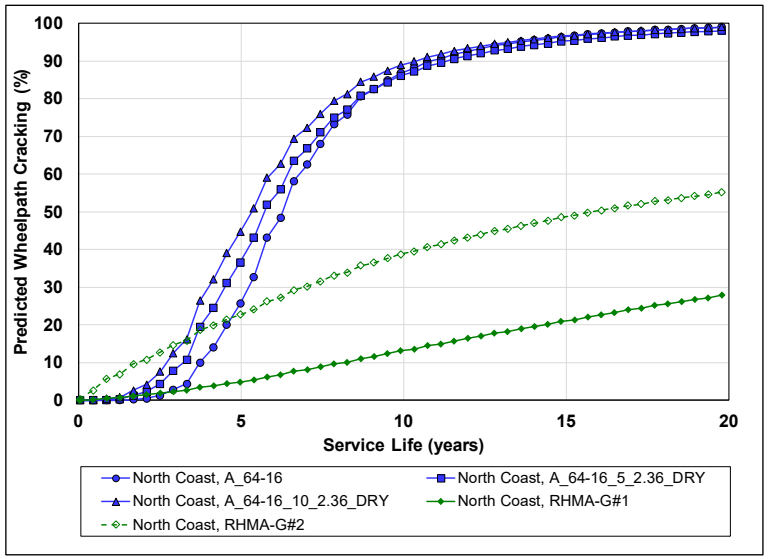

Figure E.36: AC on PCC: 0.2 ft. overlays of Mix-A, -G, -H, and RHMA-G (north coast).

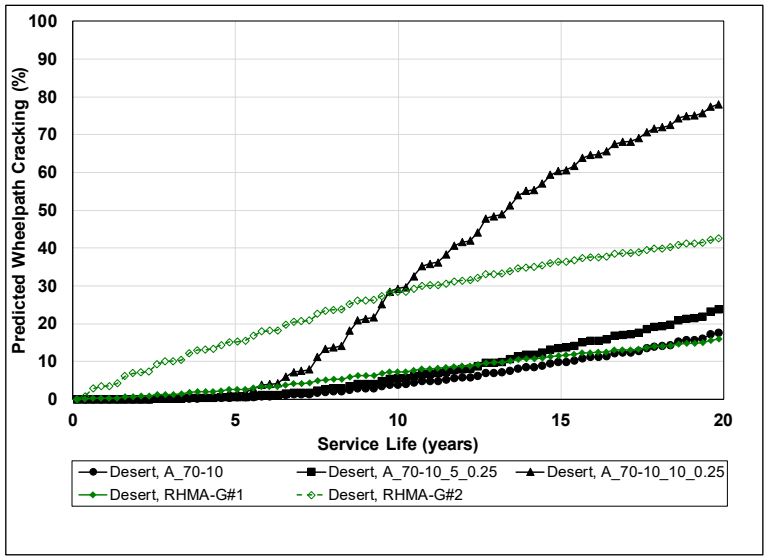

Figure E.37: AC on PCC: 0.2 ft. overlays of Mix-D, -E, -F, and RHMA-G.

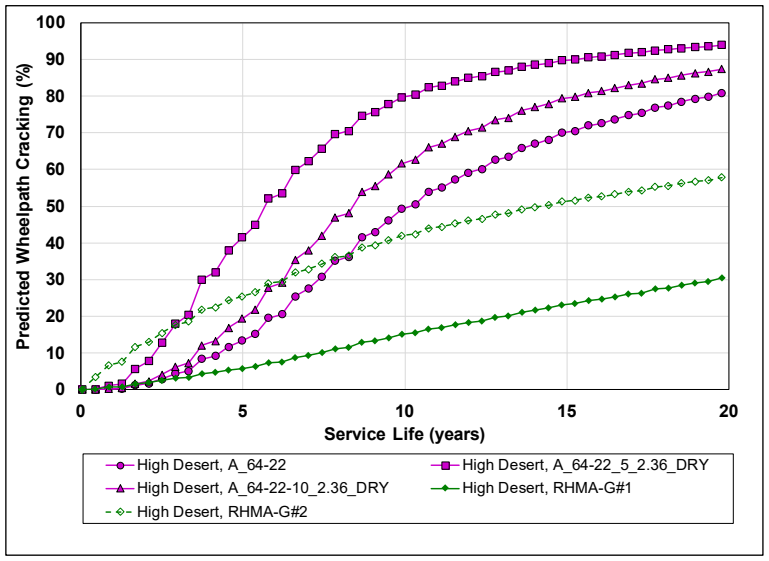

Figure E.38: AC on PCC: 0.2 ft. overlays of Mix-J, -K, -L, and RHMA-G.

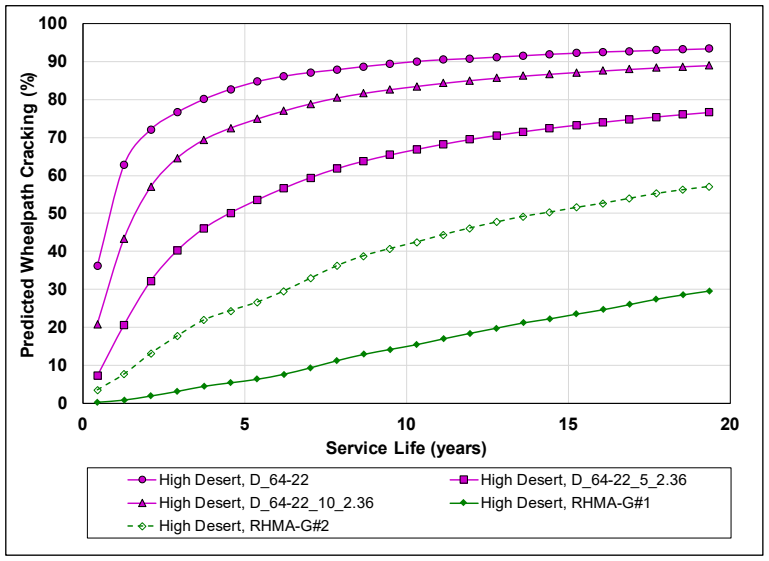

Figure E.39: AC on PCC: 0.2 ft. overlays of Mix-S, -T, -U, and RHMA-G.

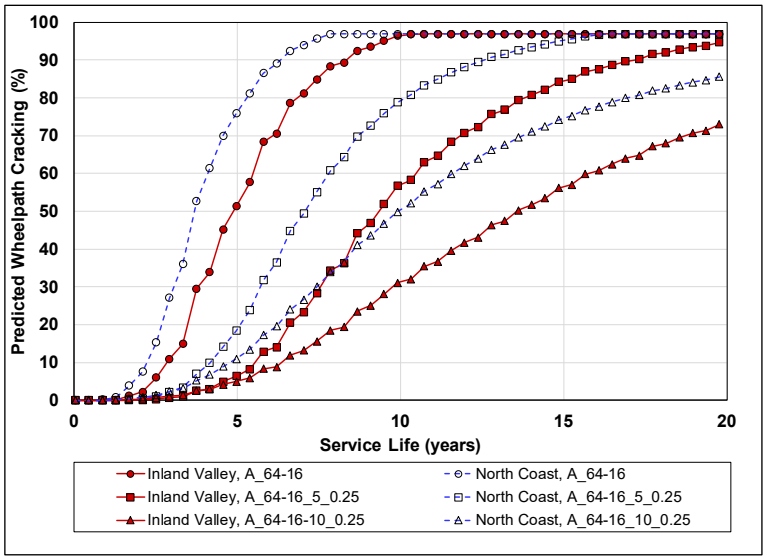

Figure E.40: AC on PCC: 0.35 ft. overlays of Mix-A, -B, and -C.

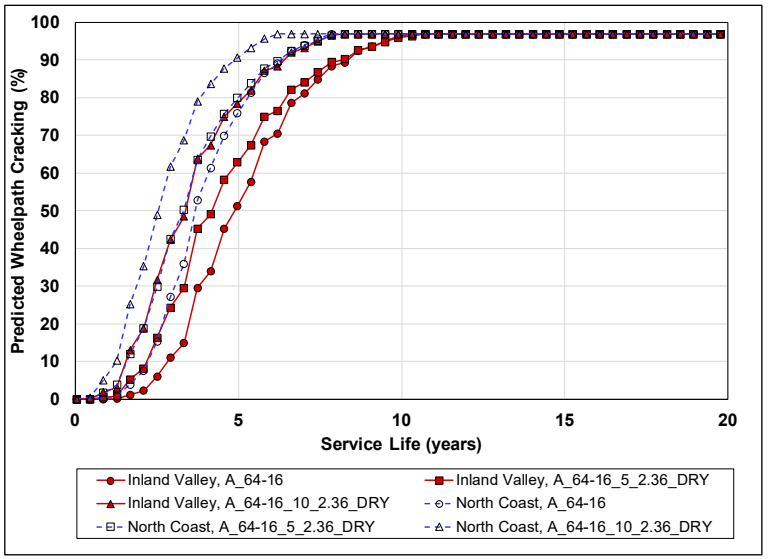

Figure E.41: AC on PCC: 0.35 ft. overlays of Mix-A, -G, and -H.

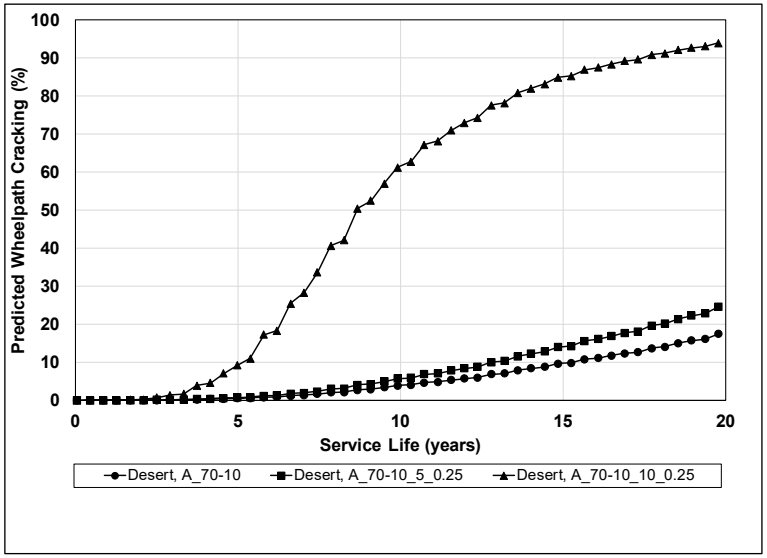

Figure E.42: AC on PCC: 0.35 ft. overlays of Mix-D, -E, and -F.

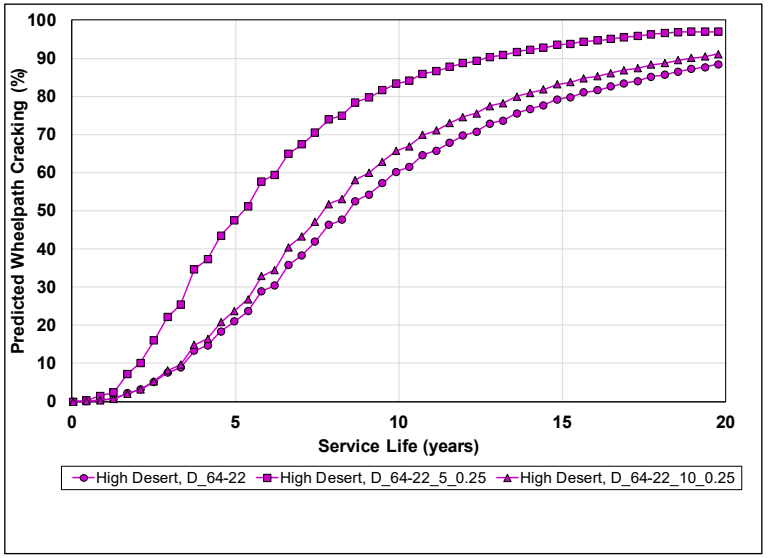

Figure E.43: AC on PCC: 0.35 ft. overlays of Mix-J, -K, and -L.

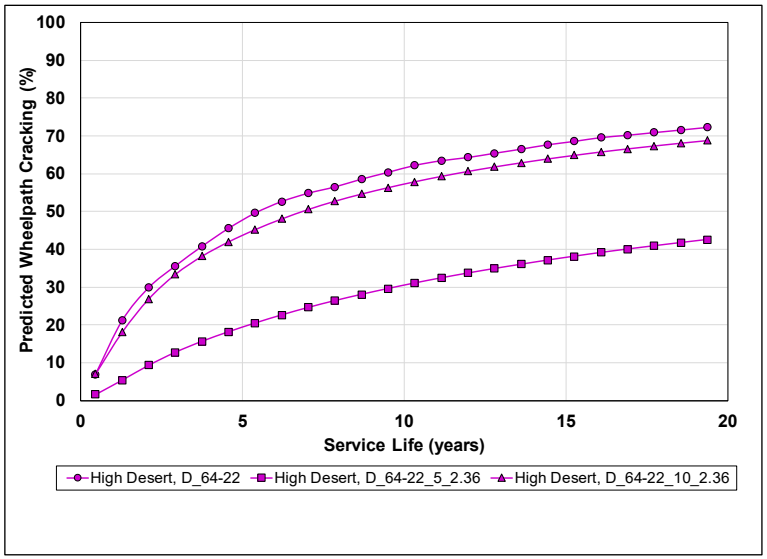

Figure E.44: AC on PCC: 0.35 ft. overlays of Mix-S, -T, and -U.

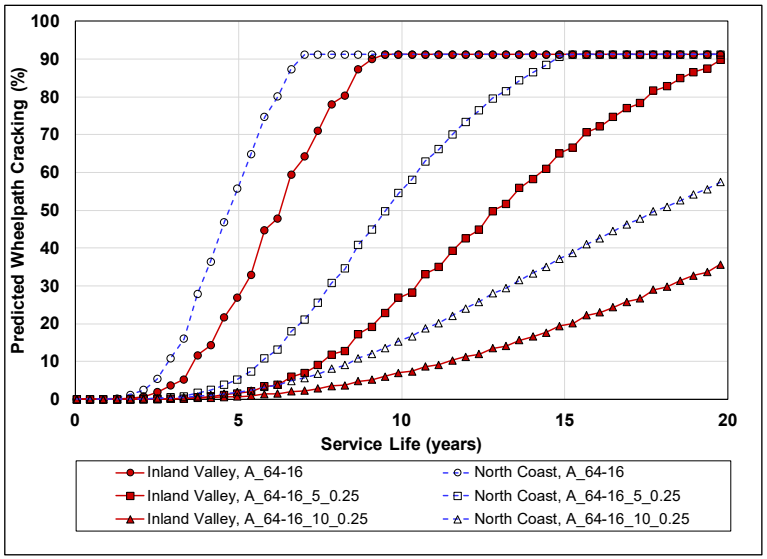

Figure E.45: AC on PCC: 0.5 ft. overlays of Mix-A, -B, and -C.

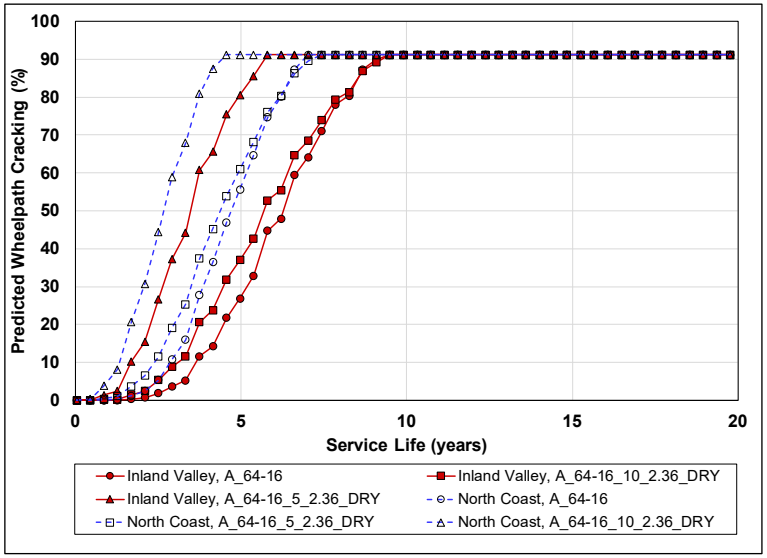

Figure E.46: AC on PCC: 0.5 ft. overlays of Mix-A, -G, and -H.

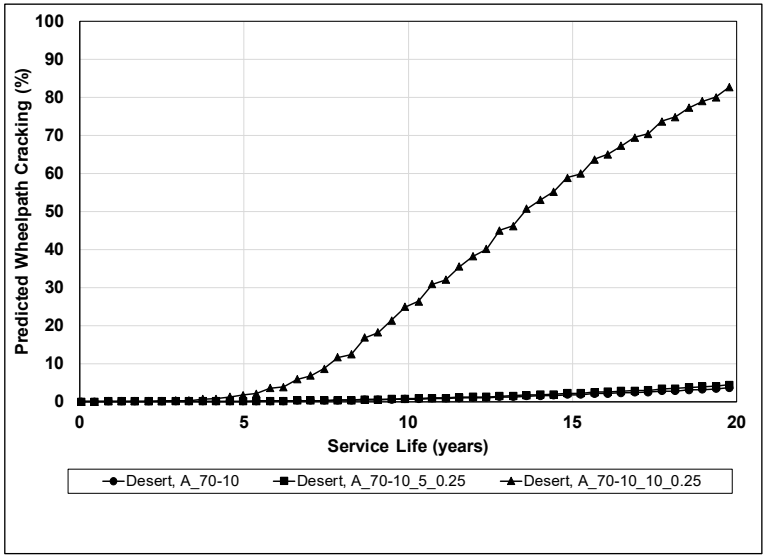

Figure E.47: AC on PCC: 0.5 ft. overlays of Mix-D, -E, and -F.

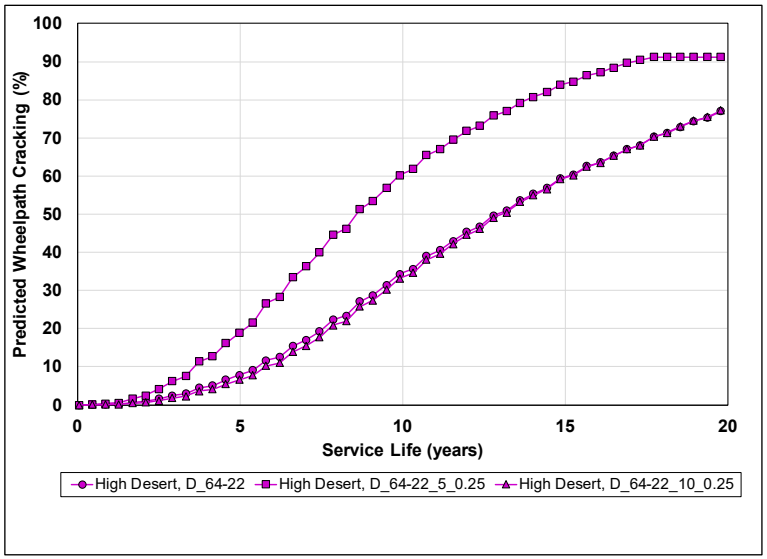

Figure E.48: AC on PCC: 0.5 ft. overlays of Mix-J, -K, and -L.

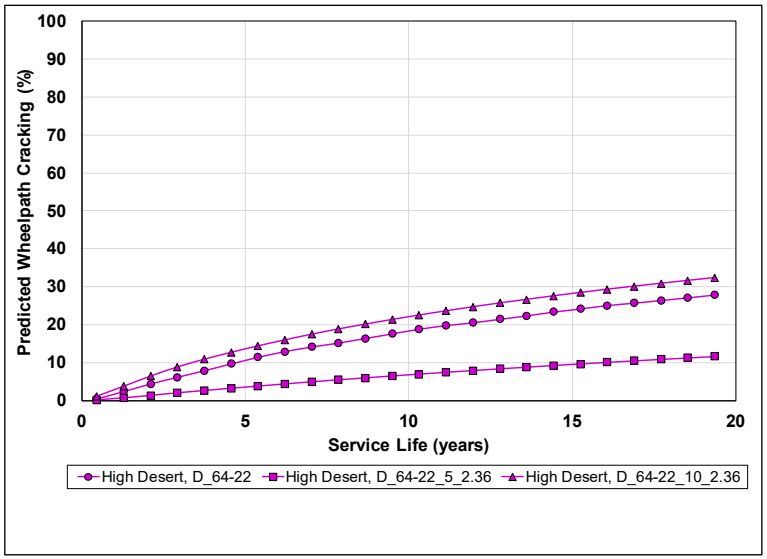

Figure E.49: AC on PCC: 0.5 ft. overlays of Mix-S, -T, and -U.